Defining the molecular mechanisms mediating class IA phosphoinositide 3-kinase (PI3K) regulation and their role in human disease

by

Gillian Leigh Dornan
BSc Honours, University of Leicester, 2009
MSc, University of Leicester, 2011

A Dissertation Submitted in Partial Fulfillment
of the Requirements for the Degree of

DOCTOR OF PHILOSOPHY

in the Department of Biochemistry and Microbiology

Supervisory Committee

Defining the molecular mechanisms mediating class IA phosphoinositide 3-kinase (PI3K) regulation and their role in human disease

by

Gillian Leigh Dornan
BSc Honours, University of Leicester, 2009
MSc, University of Leicester, 2011

Supervisory Committee

Dr. John E. Burke, Department of Biochemistry and Microbiology
Supervisor

Dr. Martin J. Boulanger, Department of Biochemistry and Microbiology
Departmental Member

Dr. Perry Howard, Department of Biochemistry and Microbiology
Departmental Member

Dr. Leigh Anne Swayne, Division of Medical Sciences
Outside Member

Abstract

Supervisory Committee
Dr. John E. Burke, Department of Biochemistry and Microbiology
Supervisor
Dr. Martin J. Boulanger, Department of Biochemistry and Microbiology
Departmental Member
Dr. Perry Howard, Department of Biochemistry and Microbiology
Departmental Member
Dr. Leigh Anne Swayne, Division of Medical Sciences
Outside Member

The phosphoinositide species phosphatidylinositol 3,4,5, trisphosphate (PIP_3) is an essential mediator of many vital cellular processes involved in cell growth, survival, and metabolism. The class I PI3Ks are responsible for production of PIP_3, and their activity is tightly controlled through interactions with regulatory proteins and activating stimuli. The class IA PI3Ks are composed of three distinct p110 catalytic subunits (p110α, p110β, p110δ) and they play different roles in specific tissues due to disparities in both expression and engagement downstream of cell surface receptors. Disruption of PI3K regulation is a frequent driver of numerous human diseases. Growth of all cell types is dependent on PI3K signalling, and development of immune cells relies on a precise balance of PIP_3 production. Activating mutations in the genes encoding the catalytic and regulatory subunits of PI3K lead to cancer and immunodeficiencies. The *PIK3CA* gene encoding the p110α catalytic subunit of class IA PI3K is one of the most frequently mutated genes in cancer, and mutations in the *PIK3CD* gene encoding the p110δ catalytic subunit lead to primary immunodeficiency. All class IA p110 subunits interact with p85 regulatory subunits, and mutations/deletions in different p85 regulatory subunits (PIK3R1, PIK3R2, PIK3R3) have been identified in both cancer and primary immunodeficiencies. By asking how these mutations mediate activation and disease phenotypes, we can identify the natural regulatory molecular mechanisms of class IA PI3Ks. Fundamentally understanding how mutations in PI3K subunits mediate human disease will expand our knowledge of PI3K biology and is essential to the development of novel therapeutics.

To identify the molecular mechanisms of class IA PI3K activating mutations, I employed a sophisticated combination of hydrogen-deuterium eXchange mass spectrometry (HDX-MS) with biochemical activity assays to probe the regulatory mechanisms of PI3Ks. HDX-MS measures the exchange rate of amide hydrogens in solution, which in turn can provide information on protein conformation and conformational changes between different states. By comparing PI3K mutants identified in primary immunodeficiency and cancer patients to wild-type enzymes, I have identified dynamic conformational changes induced by activating mutations. Biochemical and biophysical analysis of these mutants led us to generate a panel of engineered mutations to further characterise molecular mechanisms by which class IA PI3Ks are regulated. This thesis will consist of an introduction to class IA PI3K signalling and an introduction to the method of HDX-MS, followed by two data chapters wherein I investigate the mechanisms of activating mutations in PIK3CD followed by an investigation into activating mutations in PIK3R1. A conclusion and discussion of future directions will be presented in the final chapter. This work provides novel insight into the complex regulatory mechanisms of the class IA PI3Ks, which may lead to better understanding of human diseases that activate these enzymes.

Table of Contents

List of Tables

List of Figures

List of Abbreviations

aa	Amino acid
ADP	Adenosine di-phosphate
APDS	Activated PI3K Delta Syndrome
ATP	Adenosine tri-phosphate
Bacmid	Bacterial artificial chromosome containing the baculovirus genome
BEVS	Baculovirus Expression Vector system
bMe	beta mercaptoethanol
CHAPS	3-[(3-Cholamidopropyl)dimethylammonio]-1-propanesulfonate
DMSO	Dimethyl sulfoxide
DNA	Deoxyribonucleic acid
ER	Endoplasmic reticulum
EtOH	Ethanol
FBS	Feotal Bovine Serum
GPCR	G protein coupled receptor
HDX-MS	Hydrogen Deuterium Exchange
kDa	Kilo Dalton
Lip-TEV	A tobacco etch virus protease with a lipoyl tag
MS	Mass spectrometry
MS/MS	Tandem mass spectrometry
MWCO	Molecular weight cut-off
Ni-NTA	Nickel nitrilotriacetic acid
P1, P2	Primary, and secondary amplified baculovirus
PBS	Phosphate-buffered saline
PC	Phosphatidylcholine
PCR	Poymerase chain reaction
PDB	Protein data bank
PDGFR	Platelet derived growth factor receptor
PE	Phosphatidylethanolamine
PI	Phosphatidylinositol
PI(3,4)P	Phosphatidylinositol 3,4-bisphosphate
PI(3,4,5)P	Phosphatidylinositol 3,4,5-trisphosphate
PI(4,5)P	Phosphatidylinositol 4,5-bisphosphate
PI3K	Phosphatidylinositol 3-kinase
PI3P	Phosphatidylinositol 3-phosphate
PI4P	Phosphatidylinositol 4-phosphate
PIP2	Phosphatidylinositol 4,5-bisphosphate
PIP3	Phosphatidylinositol 3,4,5-trisphosphate
PM	Plasma membrane

PS	Phosphatidylserine
pY	Phosphorylated tyrosine
RTK	Receptor tyrosine kinase
SDS-PAGE	Sodium dodecyl sulfate polyacrylamide gel electrophoresis
Sf9	*Spodoptera frugiperda 9*
SFM	Serum-free media
SHORT	Short Stature, Hyperextensibility, Hernia, Occular depression, Rieger anaomaly and teething delay
Strep	Streptavidin
TCEP	Tris(2-carboxyethyl)phosphine
WT	Wildtype

Acknowledgments

This pursuit would not have been possible without the support and mentorship I have received throughout my academic career, and thus, I have many amazing people to whom I am eternally grateful.

First and foremost, I must thank my supervisor and mentor John Burke, who provided the opportunity to pursue this PhD and who has continually encouraged and supported my growth as a researcher throughout my time in his group. I only hope that as your first student (guinea pig) I was able to provide you with countless learning opportunities. A huge thank you as well for your support of my career as a whole and not just the time spent between the walls of your lab. It has been your persistence and patience in pushing me to be the best scientist/researcher along with your academic advice (and ALL those reference letters) that have promoted my success in this PhD and in my next stage. ☺

I would also like to thank my committee members, Leigh Anne Swayne, Marty Boulanger, and Perry Howard. Your breadth of knowledge and insight have helped me to steer my research and to think about the bigger picture.

Björn, for caring for and supporting me in the best and worst of times. My housemates Jennifer Reeve and Aharon Fleury, for supporting me through all those dark days with whiskey, fire, and so many good times. My lab mates in the Burke lab: Bay Buddy Jacob McPhail, Whiz Kid Braden Siempelkamp, Mass Spec master Meredith Jenkins, Manoj "John Burkes post doc" Rathinaswamy, Jordan Stariha, and Reece Hoffman. You have provided scientific support, engagement, and endless chortles, making time in the lab seem more like play than work. I will remember my time with you lot FOREVER!!! Also, to my many colleagues in the Biochemistry and Microbiology department as well as throughout UVic: Nick Brodie, Kevin Yongblah, Neda Savic, Teesha Lueher (Baker) Karen Lithgow, Dr. Jo Hobbs, Dr. Geoff Gudavicius, Dr. Craig Robb, Dr. Melissa Cid, Brigette Church, Stacy Chappel, Susan Kim, and all my other colleagues at the GSS. As well, my research heavily benefited from the assistance of all the support staff at the University of Victoria, especially those in the Biochemistry and Microbiology department.

My mentors and supporters prior to UVic: Dr. Lori Passmore, Dr. Andrew Carter, Dr. Eeson Rajendra, Dr. Max Schlager, Dr. Helgo Schmidt, Dr. Soledad Baños Mateos, Dr. John Shin, Dr. Ashley Easter, Dr. James Stowell, Dr. Ruta Zalyte, Dr. Aristides Diamant, Dr. Seth Thomas Scanlon, Dr. Tim Halim, Dr. Olga Persic, Dr. Roger Williams, Dr. Mirko Pegoraro, Dr. Eamonn Mallon, Dr. Josh Pemberton, Dr. Crisenthiya Clayton, Dr. Kate Beaumont, Dr. Lewis Collins, Dr. Helen Turrell, Emma Paterson, Rebecca Forsythe, Caitlin Bennett, Mark Patrick Wellstead, David Jordan, Dr. Dean Hallam, Esra Özerkman, Dilavar Rana, Kimiko Foster, and all my UoL/SFU/fun-employment friends. All of these people have provided me with supportive guidance throughout my career, from kind words the first time I cried over an experimental mistake, to encouraging me to pursue this PhD and pushing me to be my best self. From telling me that everything will turn out O.K. when this PhD seemed to be a proper mess, to supporting my future career choices and fellowship applications. And most importantly, many of these people have supported me in times of profound crisis. I would not have made it to this level without their support.

Finally, I acknowledge the unwavering support of my friends and family. My mother and father, for always thinking I'm cool and clever, and supporting me throughout my academic career (and life). The rest of my family, brother (Bryan), sisters (Nicole, Marie, Sarah), extended family on both sides, and the Brady Bunch. You can all rest easy knowing you don't have to ask me when I'll be finished school ever again.

Research can be incredibly challenging, and research does not occur in a bubble insulated from the world outside the ivory tower. One of the most striking aspects of my journey through academia has been the importance of a supportive and compassionate community. It truly takes a village to raise a scientist.

Dedication

For Max William Hurren and Jean Audrey Hurren (Wells).

Partners, adventurers, and life-long learners who championed education above all and provided the privilege to pursue this dream.

Sunset and evening star,
And one clear call for me!
And may there be no moaning of the bar,
When I put out to sea,

But such a tide as moving seems asleep,
Too full for sound and foam,
When that which drew from out the boundless deep
Turns again home.

Twilight and evening bell,
And after that the dark!
And may there be no sadness of farewell,
When I embark;

For tho' from out our bourne of Time and Place
The flood may bear me far,
I hope to see my Pilot face to face
When I have crost the bar.

- Crossing the Bar; Alfred, Lord Tennyson

Chapter 1:
Introduction

Adapted from:

Dornan, G.L., & Burke, J.E. (2018). Molecular Mechanisms of Human Disease Mediated by Oncogenic and Primary Immunodeficiency Mutations in Class IA Phosphoinositide 3-Kinases. Front. Immunol. 9. *575*.

Contributions:

GLD and JEB wrote the manuscript.

1.1 Phosphoinositides

Phosphoinositides are minor membrane lipid species that play diverse roles in the cell. These lipid species act not only as structural components to membranes, but as signalling molecules that mediate membrane trafficking, cell growth, and development. There are seven different phosphoinositide species derived from the precursor lipid phosphatidylinositol (PI). PI consists of an inositol head group connected via a phosphodiester linkage to a diacylglycerol backbone, where the acyl chains are most commonly a stearoyl and arachidoyl (Fig. 1A). Phosphoinositides are produced by the action of phosphoinositide kinases or phosphatases, which alter the phosphorylation status of one of three different positions on the inositol head group (3', 4', or 5'). The seven different phosphoinositides produced can be visualised in figure 1B and include: Phosphoinositide 3-phosphate (PI3P), phosphoinositide 4-phosphate (PI4P), phosphoinositide 5-phosphate (PI5P), phosphoinositide 3,4-bisphosphate [$PI(3,4)P_2$], phosphoinositide 3,5-bisphosphate [$PI(3,5)P_2$], phosphoinositide 4,5-bisphosphate [$PI(4,5)P_2$], and phosphoinositide 3,4,5-trisphosphate [$PI(3,4,5)P_3$ but referred to primarily

as PIP_3]. The plethora of roles these lipid species are responsible for are dependent on their cellular localisation, and the proteins which can bind them.

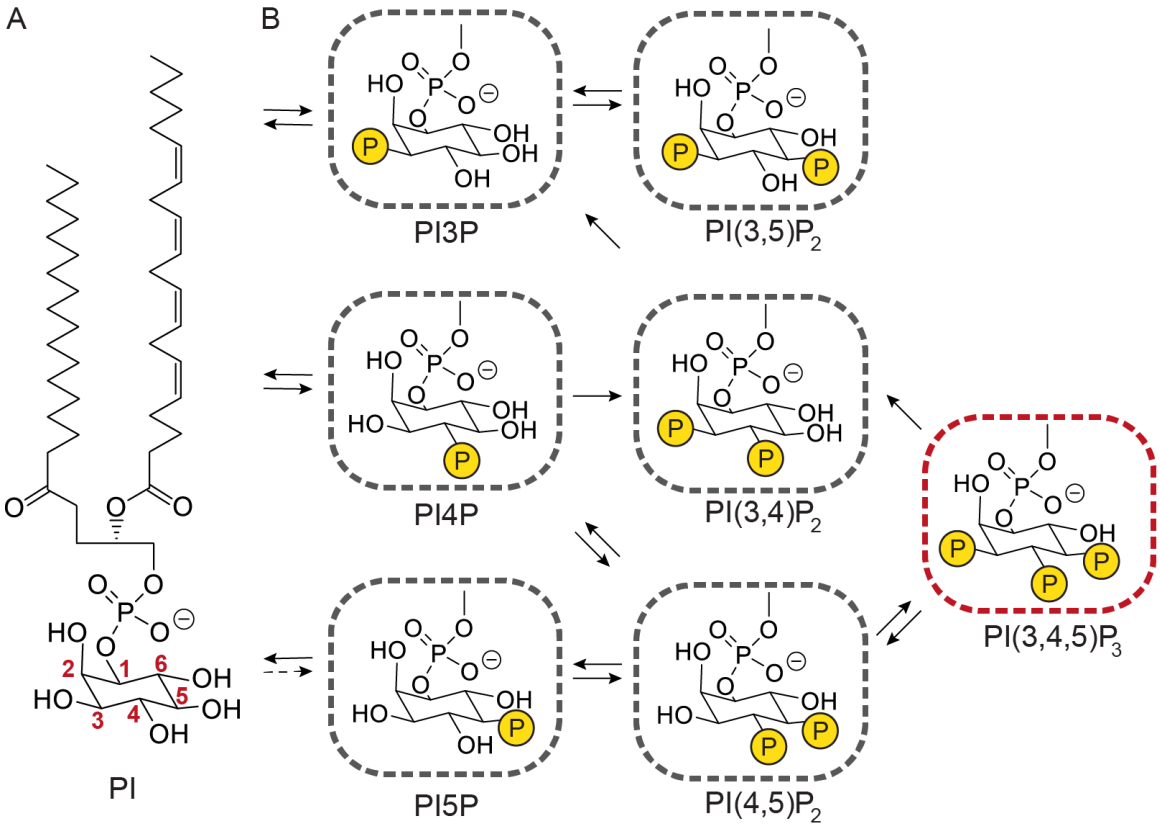

Figure 1: Phosphoinositide species.
(A) Phosphatidylinositol is the precursor to (B) the seven different phosphoinositide species that are determined by differential phosphorylation states of the inositol head group at 3', 4', or 5' hydroxyl positions. (Adapted from Burke, 2018).

Phosphoinositides act as docking modules, allowing for the localisation and activation of downstream proteins at specific cellular membranes. The interaction of phosphoinositide binding proteins with their target lipid(s) is mediated through specialised binding domains. Many phospholipid binding domains have been identified, with varying degrees of affinity and specificity that is determined by the structure of their phosphoinositide binding pocket (Lemmon, 2008). For example, some Pleckstrin homology (PH) domains can bind polyphosphoinositides with high affinity and specificity, as is the case for GRP1-PH, BTK-PH, and DAPP1-PH. These specific PH domains bind

with high affinity to PIP_3; however, DAPP1-PH can also bind $PI(3,4)P_2$, revealing different levels of specificity within similar domains (Ferguson et al., 2000; Lemmon, 2007). At the other end of the spectrum, PH domains can have low affinity and specificity for a lipid substrate alone, requiring the presence of another protein or molecule to bind simultaneously. This mechanism is known as coincidence detection and is important for the spatiotemporal localisation or activation of proteins. An example of this mechanism is the Oxysterol Binding Protein (OSBP) PH domain, which binds PI4P but is primarily Golgi localised despite the presence of PI4P at different cellular membranes. This localisation was identified as being dependent on the small GTPase Arf1p in conjunction with the presence of PI4P (Levine and Munro, 2002).

1.1.1 Phosphoinositide 3,4,5-trisphosphate

The phosphoinositide species PIP_3 is vital for the transduction of extracellular signals at the plasma membrane (PM) and leads to upregulation of cellular processes that mediate cell growth and proliferation. Research of PIP_3 was initiated in the late 1980's and early 1990's, with the discovery of PIP_3 and the kinase that produced it. Knowledge of inositol phosphates was limited until 1988, when phosphoinositide 3-phosphate species were discovered (Stephens et al., 1989; Traynor-Kaplan et al., 1989, 1988; Whitman et al., 1988). A PI kinase was also discovered around the same time that led to phosphorylation at the 3' hydroxyl of the inositol head group of PI and associated with the oncoprotein polyoma middle T antigen (Whitman et al., 1988). The activity of this PI kinase was also found to mediate upregulation of PI-3-phosphates [PIP_3 and $PI(3,4)P_2$] upon growth factor stimulation (Auger et al., 1989). Since then, the role of PIP_3 and the enzymes that regulate PIP_3 levels have been studied extensively to identify PIP_3 as a second messenger molecule important for transduction of signalling pathways. PIP_3 levels are negligible in the cell but upon agonist stimulation of membrane receptors (i.e. growth factors) PIP_3 levels rise dramatically before returning to the low basal levels (Stephens et al., 1993, 1991).

Regulation of precise levels of PIP_3 is mediated through the enzymes that alter the phosphorylation state of the inositol headgroup. PIP_3 is produced by the phosphorylation of the inositol headgroup of $PI(4,5)P_2$ at the 3' hydroxyl. This action is executed by the class I phosphoinositide 3-kinases (PI3Ks) in response to growth factors and other agonists

that bind PM receptors such as receptor tyrosine kinases (RTKs) and their adaptors, and G-protein coupled receptors (GPCRs) (Fig. 2). The destruction of PIP_3 is mediated by phosphoinositide phosphatases. PTEN is the canonical PIP_3 phosphatase that dephosphorylates the 3' position of the inositol head group, producing $PI(4,5,)P_2$ at the PM (Cantley and Neel, 1999; Maehama and Dixon, 1998; Stambolic et al., 1998). More recently however, PTEN has been shown to also directly hydrolyse $PI(3,4)P_2$ (Goulden et al., 2018; Malek et al., 2017). The phosphatase SHIP1/2 acts to dephosphorylate PIP_3 at the 5' position to produce $PI(3,4)P_2$ (Damen et al., 1996). The generation of PIP_3 by class IA PI3Ks leads to recruitment of signalling proteins containing PIP_3 binding domains whereas the action of phosphatases acts to inhibit these signalling pathways.

Many signalling proteins are activated by PIP_3, including AGC family Ser/Thr kinases (i.e. Akt), TEK family tyrosine kinases (i.e. Btk), and modulators of Ras superfamily GTPases, specifically Guanine nucleotide exchange factors (GEFs, i.e. GRP1), and GTPase activating proteins. The binding of PIP_3 by these proteins is mediated by their specialised phosphoinositide binding domains, with PH domains being the most common PIP_3 binders (Hammond and Balla, 2015). As mentioned in the previous section, PH domains can have high affinity and selectivity for lipid species. The PH domains of Akt, Btk, and GRP1 all bind PIP_3 with sub-micromolar affinity (Manna et al., 2007). One of the most well studied PIP_3 effectors is Akt, which plays key roles in regulating growth and metabolism (Manning and Toker, 2017). Activation of Akt, also known as Protein Kinase B (PKB), was initially identified as a protein that was activated downstream of activated membrane receptors including PDGF and the Insulin receptor (Alessi et al., 1996; Franke et al., 1995; Kohn et al., 1995). Akt activation downstream of class I PI3Ks was later attributed to a combined effort between the binding of PIP_3 by Akt and another protein, PDK1, which phosphorylates Akt to activate it (Alessi et al., 1997; James et al., 1996; Stokoe et al., 1997). Further to this, inhibition of class I PI3Ks also abolishes Akt signalling downstream (Burgering and Coffer, 1995; Franke, 1997). Akt activation was then tied to mTOR, a master regulator of growth and proliferation, through its interaction with the tuberous sclerosis complex (TSC) (Inoki et al., 2002; Manning et al., 2002). Thus, PIP_3 is important for localisation of proteins to the PM and their activation.

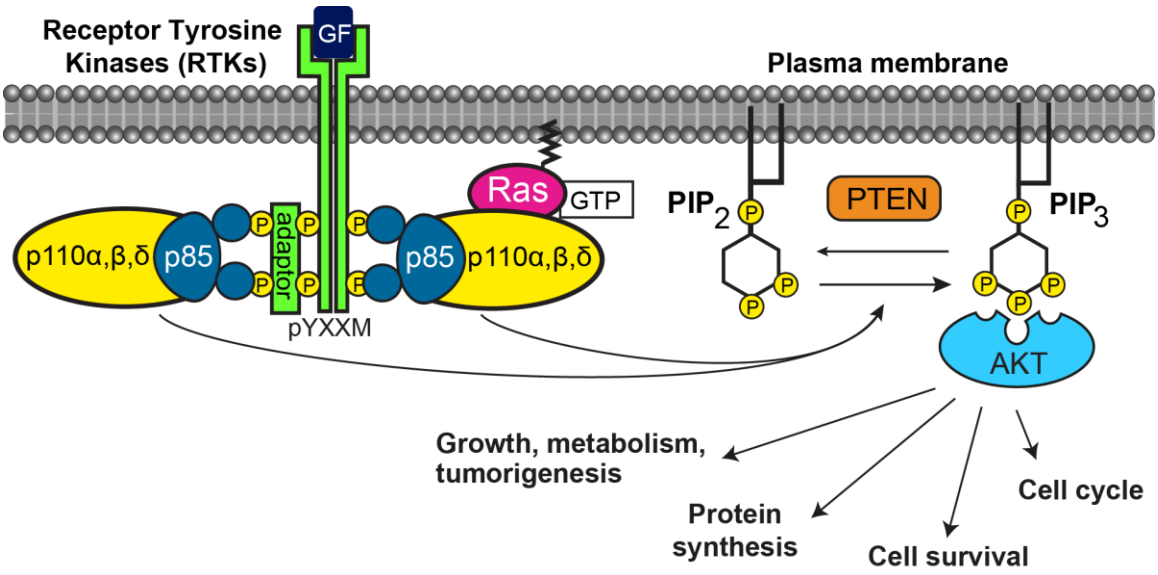

Figure 2: PIP3 regulation at the plasma membrane.
Growth factors bind to and activate membrane receptors (i.e. RTKs) that traverse the PM. Activated RTKs dimerise and auto-phosphorylate their C-terminal tails or phosphorylate adaptor proteins at pYXXM motifs. Inhibitory interfaces are broken by binding of the p85-like subunits of the p110/p85 complex to pYXXM motifs of RTKs and their adaptors. Binding of p110/p85 to RTKs also acts to recruit the complex to the PM to phosphorylate PI(4,5,)P_2 at the 3'position to produce PIP_3. Destruction of PIP_3 occurs via phosphatases, such as PTEN, which act to dephosphorylate PIP_3. Increased PIP_3 acts as a docking module, recruiting downstream proteins that propagate signals to mediate cellular processes involved in cell growth, metabolism, and survival. GF = Growth factor.

Regulation of PIP_3 levels and the downstream signalling processes mediated through PIP_3 binding proteins are involved in cell growth and proliferation. PI3K mediated production of PIP_3 has in general been shown to sustain cell proliferation and survival (Foukas et al., 2010, 2006). Increases in PI3K mediated PIP_3 levels were directly identified in response to insulin stimulation (Ruderman et al., 1990). Direct modulation of PIP_3 levels by insulin stimulation was further shown with PI3K association with the Insulin Receptor Substrate-1 (IRS-1) (Backer et al., 1992; Shoelson et al., 1992). Mice lacking genes for Insulin Receptor Substrate-1 (IRS-1) or insulin growth factor receptor (IGFR-1) exhibit severe growth deficiencies and were no longer sensitive to insulin (Liu et al., 1993; Tamemoto et al., 1994). PIP_3 levels are also important for the growth, survival, and development of immune cells. Specifically, control of tonic and agonist induced PIP_3 levels

mediate progression of B cell and T cell development at different stages (Okkenhaug, 2013; Okkenhaug et al., 2002). PIP_3 has also been shown to play a critical role in the activation of neutrophils (Kulkarni et al., 2011).

Due to the role of PIP_3 in the growth and proliferation of many cell types, levels of this second messenger must be tightly controlled. Aberrant PIP_3 levels lead to human diseases including cancers, diabetes, developmental disorders, and immunodeficiencies. These diseases can be mediated by either increased or decreased PIP_3 levels in specific tissues, as well as perturbation to downstream signalling proteins. Constitutively high PIP_3 levels have been identified as a signature of cancer, overgrowth syndromes, and immunodeficiency. Low levels of PIP_3 or rather, an inability of PIP_3 levels to increase upon agonist stimulation, can also lead to immunodeficiency, diabetes and developmental disorders. Mutations in PIP_3 regulating enzymes (PI3K, PTEN, etc.) are frequently found in these human diseases. Additionally, proteins upstream and downstream of PIP_3 production are also implicated in similar disease states. For example, mutations in the PH domain of Brutons tyrosine kinase (BTK) that impair its ability to bind PIP_3 lead to abrogated development of B-cells in a disease called X-linked agammaglobulinemia (Ohta et al., 1994; Vihinen et al., 1995). Inactivation of the PIP_3 binding protein AKT2 was also shown lead to severe insulin resistance and diabetes (George et al., 2004). Conversely, activation of downstream proteins and upregulation of the pathway also leads to disease. The E17K mutation in the PH domain of AKT-1 drives increased membrane localisation, leading to an activated pathway and occurrence in breast, colorectal, and ovarian cancers (Carpten et al., 2007). Understanding how mutations in members of the PI3K/AKT/mTOR pathways mediate disease is imperative to the design of novel therapeutics.

1.2 Phosphoinositide 3-Kinase Family

The phosphoinositide 3-kinase family of enzymes are responsible for production of phosphoinositide 3-phosphate species [PI3P, $PI(3,4)P_2$, $PI(3,5)P_2$ and $PI(3,4,5)P_3$] and are composed of three different classes – I, II, and III. All classes of PI3K share a similar core set of domains. A C2 domain, a helical domain, and a bi-lobal kinase domain that is referred to as the N- and C-lobes. The kinase domain of all classes of PI3K, and the type

III phosphoinositide 4-kinase (PI4K) enzymes, is highly conserved (Brown and Auger, 2011).

The classes of PI3Ks are defined by their differences in regulation and the products they make. The class III PI3K mediates production of PI3P and forms large complexes with different regulatory subunits while the class II PI3Ks have been shown to produce PI3P, $PI(3,4)P_2$ but is a single protein regulated by autoinhibitory mechanisms (Burke, 2018; Marat et al., 2017; Rostislavleva et al., 2015; H. Wang et al., 2018). The class I PI3Ks all act on phosphoinositide 4,5-bisphosphate [$PI(4,5)P_2$ or PIP_2] to produce phosphoinositide 3,4,5-trisphosphate [$PI(3,4,5)P_3$ or PIP_3] but can be separated further into 2 sub-groups: Class IA and class IB. The class IA enzymes are defined by their status as an obligate heterodimer composed of the catalytic subunit p110 and the p85-like regulatory subunits. Class IB contains a single isoform, PI3Kγ, which can exist as the monomeric p110γ but can also form complexes with its regulatory subunits p84 or p101. The class I PI3Ks are essential mediators of signalling downstream of cell-surface receptors, and play essential roles in numerous cellular processes, including growth, metabolism, and differentiation (Burke and Williams, 2015). For the purpose of this thesis, only class IA PI3Ks will be discussed at length.

1.2.1 Regulation of class IA PI3Ks

Class IA PI3Ks exert their diverse cellular roles through multiple, complex regulatory mechanisms. Fundamental to this are numerous inter- and intra-protein interfaces formed in both subunits of the PI3K heterodimer. The class IA PI3Ks are composed of three p110 catalytic subunits (p110α, p110β, p110δ), which form an obligate and constitutive heterodimeric complex (Geering et al., 2007) with one of five p85-like regulatory subunits (p85α, p85β, p55α, p50α, p55γ). Each of the catalytic subunits bound to any of the p85-like subunits creates the respective PI3K isoform (PI3Kα, PI3Kβ, and PI3Kδ), and p110 catalytic subunits do not exist in the cell in the absence of a regulatory subunit. Class IA PI3Ks are activated downstream of receptor tyrosine kinases (RTKs) and other tyrosine phosphorylated receptors/adaptors, G-protein coupled receptors (GPCRs), and Ras superfamily GTPases.

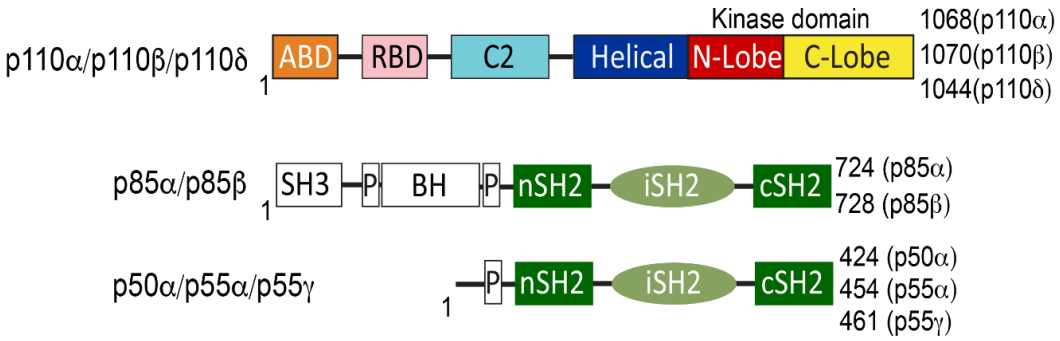

Figure 3: Domain architecture of the class IA PI3K subunits.
The catalytic subunit, p110, is present as three different isoforms: p110α, p110β, and p110δ. There are five regulatory p85-like subunits, p85α, p85β, p50α, p55α, and p55γ. All regulatory subunits contain a C- and N-terminal SH2 domain, connected through the inter SH2 (iSH2) domain. Both p85α and p85β are extended at the N-terminus, with an SH3 domain, a BH domain and two proline rich regions. The p50α, p55α, and p55γ subunits lack these N-terminal domains. p50α and p55α are splice variants of PIK3R1, the gene that encodes p85α.

Both the p110 catalytic subunit and p85-like regulatory subunit are large, dynamic multi-domain proteins (Fig. 3,4). X-ray crystallography has yielded structures of all class IA catalytic subunits alone or in complex with portions of p85-like subunits including p110α in complex with the nSH2 and iSH2 of p85α, p110β in complex with the iSH2 and cSH2 of p85β, and p110δ in complex with the iSH2 of p85α (Berndt et al., 2010; T P Heffron et al., 2016; Hon et al., 2012; Huang et al., 2008; Mandelker et al., 2009; Miled et al., 2007; Miller et al., 2014; Zhang et al., 2011). This structural data has paved the way to understanding the complex inter and intra-protein interactions of the p110 and p85-like subunits and, in combination with biochemical data has revealed the basic molecular architecture of the class IA PI3Ks.

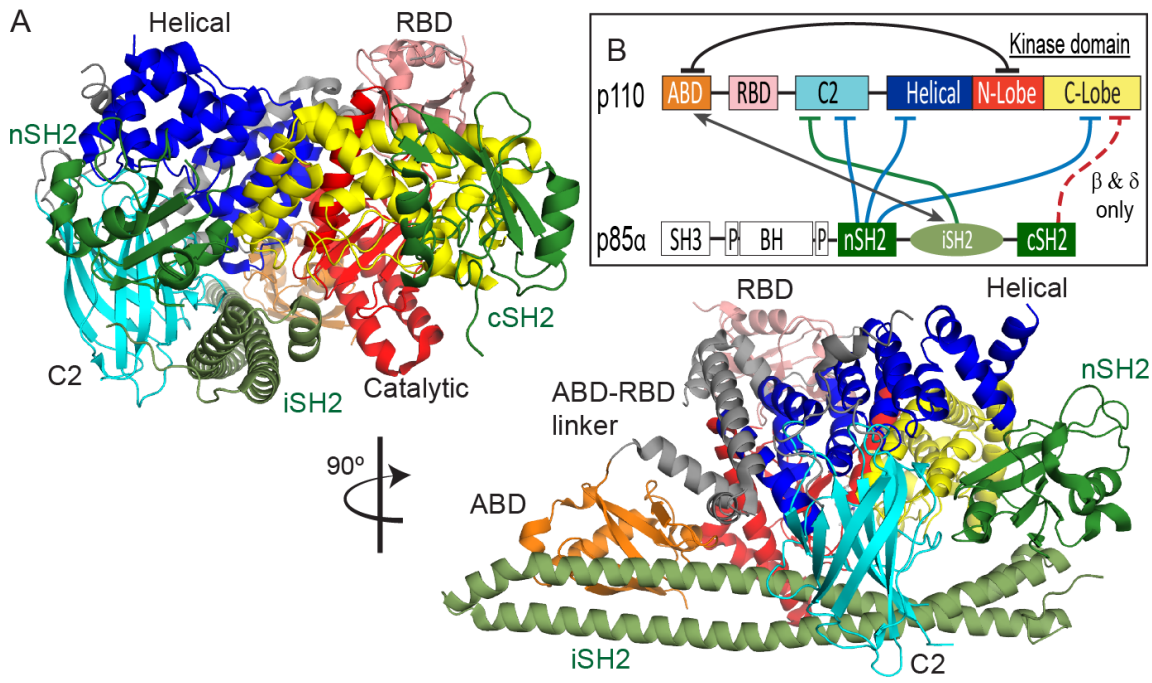

Figure 4: Class IA PI3Ks are large, dynamic machines with multiple domains that form an intricate network to mediate kinase activity.
(A) Structural model of PI3K based on PI3Kδ (p110δ/p85; PDB: 5DXU, 3HHM, 2Y3A) highlighting the different domains and their orientation from two angles. The domains are colour-coded to the domain architecture representation in (B) Wiring diagram showing the specific domain interfaces between p110 subunits and p85-like regulatory subunits mapped onto the domain architecture representation of each subunit. The grey double ended arrow represents the stabilising binding interface between the ABD (p110) and the iSH2 (p85). The flat ended arrows represent inhibitory interfaces between p110 and p85. The dotted flat ended arrow represents the cSH2-kinase interface that occurs only in the p110α and p110δ isoforms.

p110 is composed of an adaptor binding domain (ABD), which interacts with p85, a Ras binding domain (RBD), which mediates interaction with Ras superfamily GTPases, a C2 domain, a helical domain, and a bi-lobed kinase domain, composed of an N-lobe and a C-lobe connected through a flexible hinge. All class IA regulatory subunits contain two Src homology 2 domains (referred to as nSH2 and cSH2 to denote N-terminal and C-terminal) connected by a coiled-coil domain known as the inter SH2 (iSH2). The nSH2, iSH2, and in some isoforms the cSH2 (p110β and p110δ), form the primary inhibitory interfaces with the catalytic subunit to mediate inhibition of the kinase. Both p85α and

p85β subunits also contain a Src Homology 3 domain (SH3) and a bar cluster region homology domain (BH). The main interface holding the PI3K heterodimer together is the tight interaction of the ABD of p110 with the iSH2 domain of p85 (Dhand et al., 1994; Miled et al., 2007). Comparison of class IA PI3Ks with protein kinases reveals multiple similarities. Src family kinases also contain accessory domains that mediate inhibition of a bilobal kinase domain with an active site cleft (Jura et al., 2011). The Src family kinase Hck mediates inhibition of its kinase activity through its SH2/SH3 domains binding of the kinase domain, and inhibition is relieved through SH2 binding of phosphorylated receptors. In contrast, PI3K inhibition is mediated primarily through its SH2 domains as well as multiple inter protein interfaces of its extensive accessory domains. A comparison of class IA PI3K domain organization compared with an SH2 containing Hck protein kinase of the Src family of kinases reveals the large size and complexity of the p110/p85 complex relative to other signaling kinases (Fig. 5D,E).

Phosphorylation of lipid substrate is mediated through the kinase domain of the p110 subunit in class I PI3Ks. The active site is located in a cleft between the N-lobe and C-lobe, where ATP binds (Fig. 5B). The kinase domain is also host to the catalytic machinery required for catalysing the phosphotransfer between ATP and lipid substrate. Key features of the kinase domain of PI3Ks include the regulatory arch, the activation loop, and the catalytic loop (Fig. 5C). Binding of lipid substrate is mediated through the activation loop, which coordinates lipid substrate towards the catalytic center adjacent to the ATP binding site (Miller et al., 2014). The activation loop also confers specificity of the lipid substrate; Exchanging the loop sequence of class IA PI3Ks with those from the class II or class III PI3Ks altered the lipid substrate specificity (Bondeva et al., 1998; Pirola et al., 2001). The catalytic loop mediates phosphotransfer between ATP and the lipid substrate. The dynamic catalytic and activation loops are thought to undergo conformational changes to accommodate substrate and catalyse phosphotransfer, in a similar mechanism to protein kinases where conformational changes occur in the catalytic site to coordinate ATP for the phosphotransfer to protein targets (Williams et al., 2009). These different conformations are thought to indicate active or inactive states. The structures of class I PI3Ks are all thought to be putative inactive forms. However, the catalytic loop of VPS34 differs from previous PI3K structures; The highly conserved DRH

motif of the loop is pointing toward the catalytic center, which could indicate the active conformation of the catalytic loop (Miller et al., 2010; Walker et al., 1999). Encompassing both the activation loop and the catalytic loop is the regulatory arch, a structure composed of the two to three terminal alpha helices: kα10, kα11, and in some PI3Ks (VPS34, p110γ, p110β) the kα12 (Berndt et al., 2010; Huang et al., 2007; Miller et al., 2010; Zhang et al., 2011). This structure is conformationally dynamic, where the kα12 helix alternates between an open and closed conformation. In the closed conformation, the kα12 helix impinges on the activation and catalytic loops to prevent substrate access. In the p110β and p110δ isoforms, the cSH2 domain of the p85α subunits binds to the regulatory arch to lock the kinase in an inactive state (Burke et al., 2011; Zhang et al., 2011). The kα12 helix of VPS34 also binds membrane, and upon binding of phosphorylated receptors the regulatory arch of class IA PI3Ks undergoes conformational changes, potentially opening up the arch to allow access to the lipid substrate (Burke et al., 2011; Miller et al., 2010).

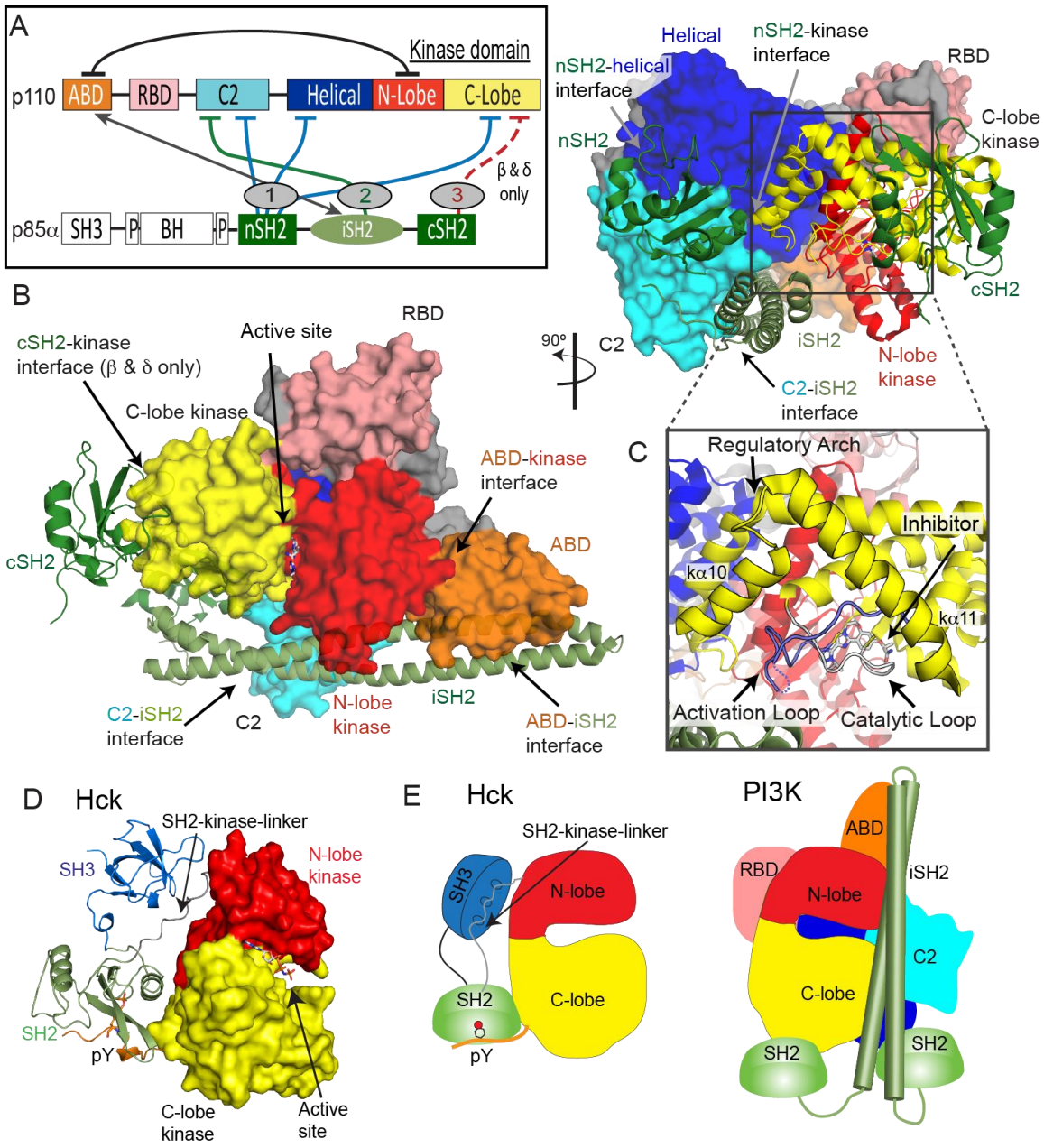

Figure 5: Class IA PI3K regulation is mediated by numerous inter- and intra-protein interfaces.

(A) Wiring diagram domain architecture representation showing the specific domain interfaces between p110 subunits and p85-like regulatory subunits. The grey double ended arrow represents the stabilising binding interface between the ABD (p110) and the iSH2 (p85). The flat ended arrows represent inhibitory interfaces between p110 and p85. The dotted flat ended arrow represents the cSH2-kinase interface that occurs only in the p110α and p110δ isoforms. (B) Structural model of PI3Kδ (p110δ/p85; PDB: 5DXU, 3HHM, 2Y3A) highlighting the key inhibitory interfaces of p110/p85-like subunits. (C) A zoomed in visualisation of the active site. Highlighted are the regulatory arch, the ATP binding site,

the activation loop and the catalytic loop. The ATP binding site is indicated here by an ATP competitive inhibitor marked ‘Inhibitor’. The catalytic loop is shown in white with a black outline, the activation loop is shown as purple-blue also outlined in black and missing residues extended by a dotted line. The regulatory arch is outlined in black and labelled kα10 and kα11 to denote two helices of the arch that exist in all class IA PI3K structures. (D) A structure of inhibited Src family protein kinase Hck, an example of another SH2-regulated kinase [PDB: 1AD5 (Sicheri et al., 1997)]. (E) Cartoon representations of class IA PI3Ks and Src family protein kinase Hck. In both protein kinases and class IA PI3Ks, a bi-lobal kinase domain is functionally regulated through SH2 domains. These cartoons also represent the enhanced complexity of class IA PI3K regulation through its many accessory domains. Adapted from Dornan and Burke, 2018.

The class IA p85-like regulatory subunits have three key roles: they stabilise the p110 catalytic subunit, they inhibit p110 catalytic activity, and they allow for the activation of activity downstream of proteins containing phosphorylated YXXM motifs through engagement of p85 SH2 domains (Escobedo et al., 1991; Geering et al., 2007; Vadas et al., 2011; Yu et al., 1998b). These roles are mediated through multiple interactions with the p110 subunits (Fig. 5A). While class IA catalytic subunits require a regulatory subunit for stability, the p85 subunits have been postulated to exist alone, and can mediate cellular functions free of p110 (Cheung et al., 2015, 2011). Biochemical/biophysical studies have informed the molecular mechanism of how regulatory subunits bind and inhibit the different p110 catalytic subunits (Burke et al., 2012, 2011; Burke and Williams, 2013; Huang et al., 2007; Mandelker et al., 2009; Miled et al., 2007; Vadas et al., 2017, 2011; Vadas and Burke, 2015; Yu et al., 1998b, 1998b; Zhang et al., 2011). A number of inter and intra-subunit interactions mediate inhibition of each of the class IA catalytic subunits (Annotated on the domain schematic in Fig. 5B). In all class IA PI3Ks the ABD domain forms an intra-subunit inhibitory contact with the N-lobe of the kinase domain (Huang et al., 2007). The ABD-RBD linker packs against the ABD and interacts with the kinase domain. The C2 domain of p110 forms an inhibitory contact with the iSH2 domain of p85 regulatory subunits. Intriguingly, different p110 subunits have diverse capabilities to be inhibited by this interaction, with p110β being less inhibited by the C2-iSH2 interaction (Dbouk et al., 2012), compared to p110α and p110δ. The iSH2 coiled-coil is composed primarily of two helices, with a third smaller and mobile helix at the C-terminal end.

Structural data has captured the third helix in multiple conformations however, the third helix appears to interact with the activation loop of the kinase domain (T P Heffron et al., 2016; Miller et al., 2014).

The N-terminal SH2 domain (nSH2) forms inhibitory interactions with the C2, helical, and C-lobe of all p110 catalytic subunits (Burke et al., 2011; Burke and Williams, 2013; Huang et al., 2007; Mandelker et al., 2009; Miled et al., 2007). The C-terminal SH2 domain, which interacts with the C-lobe of the kinase domain, only inhibits p110β (Zhang et al., 2011) and p110δ (Burke et al., 2011). This interaction cannot occur in p110α due to a loop extension that sterically prevents this inhibitory interaction. Intriguingly, the nSH2 and cSH2 domains have different inhibitory interfaces, with the nSH2 interacting with p110 through its pY binding site, and the cSH2-p110 interface not directly involving the pY binding site. Together, the cSH2 and nSH2 domains bind to specific sites on phosphorylated receptors with high affinity (Klippel et al., 1992; McGlade et al., 1992; Panayotou et al., 1993). Mutation of tyrosines 740 and 751 in the kinase insert region of the platelet derived growth factor β (PDGFR-β) abrogates PI3K binding (Kashishian et al., 1992). Upon interaction with phosphorylated tyrosine motifs in phosphorylated receptors and their adaptors, the nSH2 and cSH2 interfaces with p110 are disrupted. Both the nSH2 and cSH2 of the p85-like subunits are highly specific to pYXXM motifs. The phosphorylated tyrosine and the methionine bind to the SH2 domains in a “plug” type fashion, where the phosphorylated tyrosine binds to an arginine in a deep pocket of the SH2 and the methionine binds to tyrosine in a loop (Breeze et al., 1996; Nolte et al., 1996). The similar specificity indicates a potential evolutionary mechanism where by having two “readers” for signal transduction, the regulation of class IA PI3K activation can be tightly controlled. Different regulation of class IA PI3Ks by their regulatory subunits has important functional implications for how they can be activated by different activating stimuli.

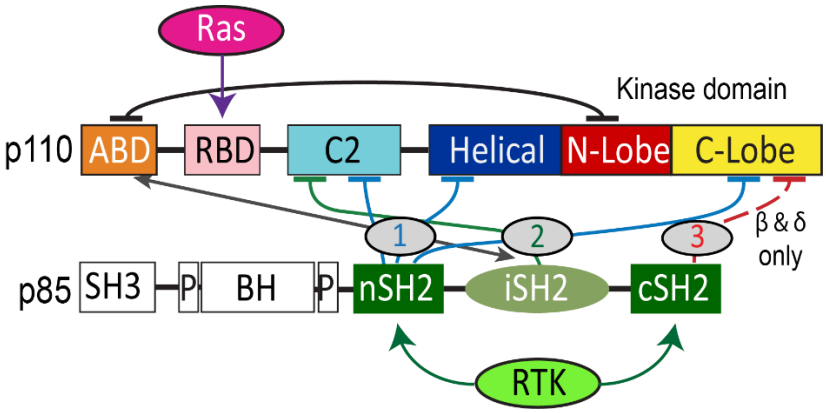

Figure 6: Class IA PI3Ks are activated downstream of membrane receptors. Domain architecture of both subunits, demonstrating the high affinity, stabilising interaction between the ABD and iSH2 through a pointed arrow and inhibitory interfaces mediated through p85-like subunits shown as flat ended arrows. The numbers represent the inhibitory interfaces mediated by their specific domain, (1) nSH2, (2) iSH2, or in the case of p110β and p110δ, (3) cSH2. Small GTPases, indicated as Ras (Pink), mediate PI3K activation through interaction with the RBD. RTKs and their adaptors harbouring phosphorylated YXXM motifs (Green) activate class IA PI3Ks by binding nSH2 and cSH2 to break inhibitory interfaces and recruit PI3K to the membrane.

Mutations in both catalytic and regulatory subunits frequently activate lipid kinase activity through modification/disruption of inhibitory interfaces between the two subunits. Fundamental to understanding how mutations in different catalytic and regulatory subunits modify PI3K signalling in different cells/tissues is understanding how unique class IA p110 catalytic isoforms are regulated by their p85 regulatory subunits, and how they are activated downstream of different activating stimuli.

1.2.2 Signalling inputs of class IA PI3Ks

The ability of PI3K isoforms to mediate signalling in different tissues is a balance between differential expression of class IA PI3K isoforms and their unique ability to be activated by GPCRs, Ras superfamily GTPases, and phosphorylated receptors/adaptors (Fig. 6). PI3Ks can also be activated by more than one signalling input at a time, adding another layer of regulation to precisely control PIP_3 production. The ability of different isoforms to be activated downstream of different upstream stimuli plays a key role in

determining the capability for activating somatic point-mutations to mediate human disease.

Receptor tyrosine kinases (RTKs) are transmembrane receptors at the plasma membrane that receive and transduce extracellular signals mediated through ligand binding (i.e. growth factors). Upon simulation by external cues at the extracellular N-terminus, RTKs dimerize and are auto-phosphorylated by the cytoplasmic C-terminal tyrosine kinase. These phosphorylated tyrosyl motifs (i.e. pYXXM, pYEEI)act to recruit downstream proteins to mediate signalling cascades. Some of these downstream proteins are adaptors, binding to the RTK and being phosphorylated at similar motifs, which can similarly recruit phosphotyrosine motif binding proteins in signal cascades. A classic example of an RTK adaptor is IRS-1, which binds to the Insulin receptor downstream of insulin binding. Recruitment of proteins to the pYXXM motifs occurs through SH2 domains. All class IA isoforms can be activated by proteins containing phosphorylated YXXM motifs, as this leads to SH2 mediated recruitment of regulatory subunits, and disruption of SH2 inhibitory contacts with the p110 catalytic subunits (Burke et al., 2011; Burke and Williams, 2013; Miled et al., 2007; Yu et al., 1998b). Some of the phosphorylated receptors and adaptors that bind class IA PI3Ks include the PDGFR and other members of the PDGF family of receptors, epidermal growth factor receptor (EGFR), and IRS-1 (Backer et al., 1992; Hu et al., 1992; Kaplan et al., 1987; Kazlauskas and Cooper, 1990; McGlade et al., 1992). The SH2 domains of class IA PI3Ks also exhibit differences in binding affinity and specificity. The cSH2 domain mediates the high affinity interaction between p85 and phosphorylated receptors (Klippel et al., 1992). Additionally, the nSH2 binds pYXXM sites with distinctly different affinities. Both SH2 domains bind the pY751 site of PDGFR-β with similarly high affinity, however the nSH2 affinity for pY740 is 100-fold lower (Panayotou et al., 1993). This potentially indicates a mechanism that specifically orients the class IA PI3K complexes with regards to the membrane.

p110α is more sensitive to activation downstream of phosphopeptides derived from Platelet-derived growth factor receptor (PDGFR) than either p110β or p110δ in vitro (Burke and Williams, 2013), and this is likely due to the absence the cSH2 inhibitory interface, which makes the cSH2 more accessible to interact with pYXXM motifs. In vivo

evidence in support of free SH2 domains being more available to pYXXM motifs is that the oncogenic E545K mutant of p110α, which disrupts the nSH2 helical interface (described further in section 1.3), is more readily recruited to phosphorylated Insulin receptor substrate (IRS) proteins (Yang et al., 2011).

Class IA PI3Ks are activated downstream of the Ras superfamily of GTPases through interactions with the RBD domain present in p110 catalytic subunits (Pacold et al., 2000; Rodriguez-Viciana et al., 2004). The Ras superfamily is large and diverse, composed of five main families (Ras, Rho, Rab, Ran, and Arf) (Cherfils and Zeghouf, 2013). The PI3K isoforms are differentially activated downstream of Ras superfamily members (Fritsch et al., 2013; Rodriguez-Viciana et al., 1994), with p110α and p110δ being activated downstream of Ras family GTPases, and p110β being activated downstream of Rho family GTPases. Ras activates PI3K through enhanced membrane interaction, with Ras activation being strongly synergistic with activation downstream of phosphorylated receptors (Buckles et al., 2017; Siempelkamp et al., 2017). Mutant p110α deficient in its ability to be activated by Ras leads to decreased oncogenic transformation, tumour maintenance, and angiogenesis downstream of mutant Ras (Castellano et al., 2013; Gupta et al., 2007; Murillo et al., 2014).

Class IA PI3Ks can synergize direct and indirect inputs downstream of specific upstream stimuli. p110β is unique in being activated downstream of phosphorylated receptors/adaptors, GPCRs, and Rho family GTPases (Dbouk et al., 2012). The ability of p110β to integrate signals from RTKs and GPCRs is critical in its signalling role in myeloid cells (Houslay et al., 2016). p110α is sensitive to activation downstream of insulin receptors due to it being both directly and indirectly activated through RTK mediated activation of Ras (i.e. GRB2 binds and is activated by an activated RTK, which in turn binds a Ras GEF SOS).

1.2.3 Physiological Roles of class IA PI3Ks

The class IA PI3K enzymes mediate many physiological roles. While there is a degree of redundancy in the roles of the class IA PI3Ks, the different isoforms display variation in their expression profiles, signalling inputs, and inter-protein regulatory

mechanisms. The p110α and p110β catalytic subunits are ubiquitously expressed, while the p110δ and the class IB isoform p110γ subunits share a more restricted immune cell specific expression profile (Chantry et al., 1997; Kok et al., 2009; Vanhaesebroeck et al., 1997). Knock-in genetic models and isoform-selective inhibitors have revealed the essential roles of specific PI3K isoforms, and these isoform specific roles are described below.

The p110α isoform is vital for growth, metabolism, and proliferation. Loss of expression or activity of the catalytic subunit p110α leads to embryonic lethality, characterised by proliferative defect and developmental delays in the embryo (Bi et al., 1999; Foukas et al., 2006). Mice heterozygous for a kinase dead mutation in p110α showed significant decreases in somatic growth of skeletal muscle, which also occurred alongside increased adiposity, hyperinsulinemia and glucose intolerance (Foukas et al., 2006). Numerous studies have now outlined the critical role that the PI3Kα isoform plays in metabolic regulation, as PI3Kα is the primary isoform downstream of the insulin receptor (Foukas et al., 2006; Knight et al., 2006; Zhao et al., 2006). PI3Kα is also activated downstream of other growth factor receptors, where it is activated by epidermal growth factor receptor (EGFR) in human breast tissue and also shows redundancy with the PI3Kδ isoform for development of pre-B cells in the immune system (Juvin et al., 2013; Ramadani et al., 2010). The p110β subunit is also essential, and knockout of this isoform in mice also leads to embryonic lethality (Bi et al., 2002). P110β has also been implicated in immune cell development as well as platelet function, and spermatogenesis (Ciraolo et al., 2010; Jackson et al., 2005; Kulkarni et al., 2011). The PI3Kβ specific inhibitor TGX-221 was shown to block thrombus formation and platelet adhesion in mice (Jackson et al., 2005).

While all p110 isoforms can sustain cell growth and survival, the development of immune cells requires the p110δ isoform. As such, PI3Kδ is activated downstream of immune specific receptors such as the B Cell Receptor (BCR) or CD19, and PIP_3 production leads to recruitment of PH containing effectors such as AKT and BTK. Mice with a catalytically inactive p110δ exhibit impaired antigen receptor signalling in B- and T-cells, and levels of phosphorylated AKT are attenuated even in the presence of agonist stimulated B cell or T cell receptors (BCR and TCR) (Bilancio et al., 2006; Okkenhaug et

al., 2002; Ramadani et al., 2010). At the organismal level, these mice exhibited impaired immune responses and mild inflammatory bowel disease. In the example of B cell signalling, PI3Kδ is redundant with the PI3Kα isoform in the development of pre-B cells, however only PI3Kδ is necessary for the development of B-cells at their later stages (Foukas et al., 2010; Ramadani et al., 2010). Knockout of PI3Kδ leads to a blockade of B-cells in their production of natural antibodies and development of marginal zone B cells, processes which are mediated through BCR signalling (Ramadani et al., 2010). The kinase dead mice exhibited a complete reduction in marginal zone B cells (Okkenhaug et al., 2002). In this regard, PI3Kα is not capable of BCR-mediated responses, and is only producing the low, basal levels of PIP_3. High levels of PIP_3 lead to an inhibition of FOXO transcription factors via phosphorylation by activated AKT (Brunet et al., 1999). Genes under FOXO control include *aid* and *bcl6*, which are key for generation of class switched B cells to produce high affinity antibodies in response to antigen binding of the BCR (Okkenhaug, 2013). Constitutive activation of PI3K signalling maintains FOXO inhibition and abrogates development. Thus, PI3K signalling must be tightly controlled to produce precise levels of PIP_3 at appropriate times during B cell development. PI3Kδ is also important for T cell development, where normal signalling leads to differentiation of T cells into different T helper cell types (Okkenhaug et al., 2006).

Due to this fundamental role in a plethora of vital functions, the misregulation of PI3K signalling occurs in a variety of human diseases, including cancer, immunodeficiency, and diabetes (Fruman et al., 2017). Disease can be caused by overactive and inactive PI3K signalling, underlying the importance of maintaining regulated levels of PI3K activity, and thus the production of PIP_3.

1.3 Class IA PI3Ks in cancer

The catalytic isoform p110α is one of the most mutated genes in cancer. Somatic point mutation frequency in cancer in both PIK3CA (Samuels et al., 2004) and PIK3R1 (Cheung et al., 2011; Urick et al., 2011) are indicated in Fig. 7A-B. Intriguingly, de novo germline and postzygotic, somatic mosaic mutations in similar locations in PIK3CA and PIK3R2 (p85β) also lead to overgrowth and developmental disorder syndromes (Lindhurst

et al., 2012; Mirzaa et al., 2015; Nakamura et al., 2014; Orloff et al., 2013; Rivière et al., 2012; Terrone et al., 2016), revealing that the same mutant can lead to cancer and/or developmental disorders (Table 1). There are two hotspot regions in PIK3CA located at the nSH2-helical interface (E542K, E545K) and the C-terminus of the kinase domain (H1047R) involved in membrane binding (Fig. 7A-B). However, in addition there are numerous rare mutations distributed throughout the primary sequence, primarily localised at the ABD-kinase interface, ABD-RBD linker, C2-iSH2 interface, and the regulatory arch of the kinase domain which is situated over the active site (Fig 7A, D). Rare mutations activate lipid kinase activity, induce oncogenic transformation (Burke et al., 2012; Gymnopoulos et al., 2007; Zhao and Vogt, 2008) and are found in endometrial cancers (Rudd et al., 2011).

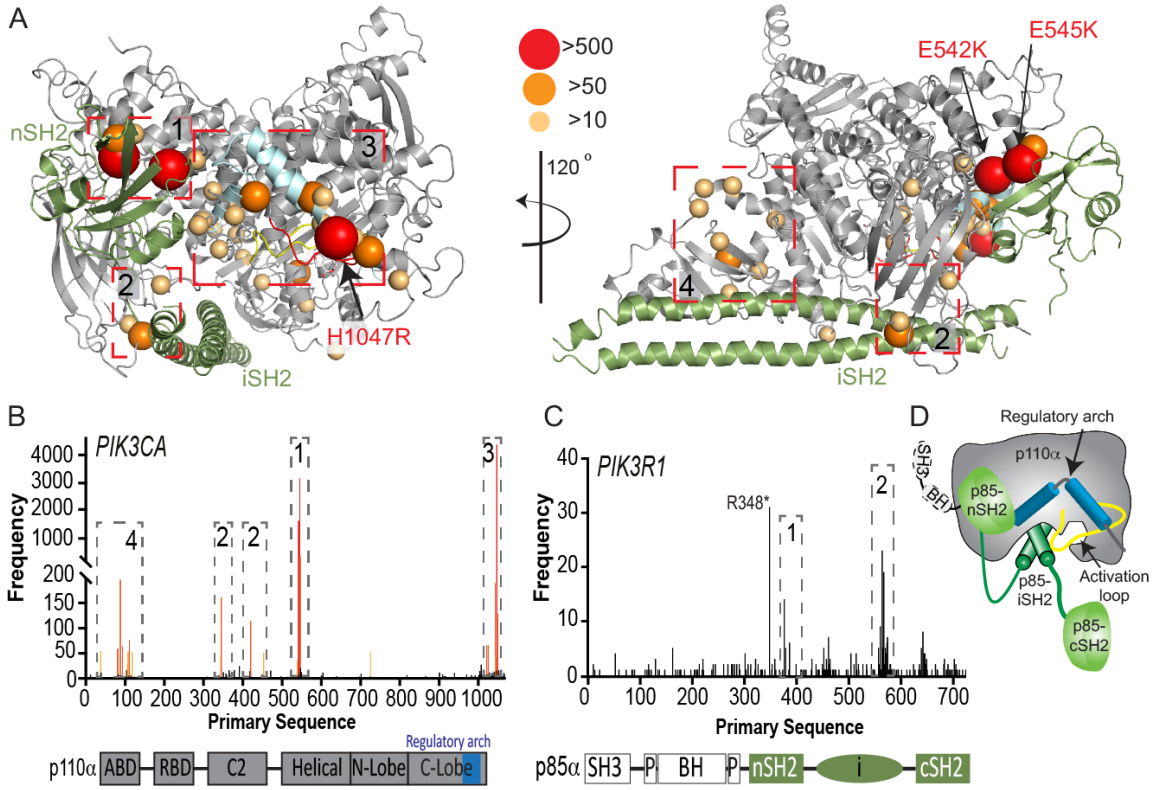

Figure 7: Activating mutations in PIK3CA and PIK3R1 are oncogenic.
(A) Structural model of PI3Kα (p110α/p85α) highlighting the location of activating mutations as spheres. Sphere size and colour correspond to the frequency of mutations. Frequency graphs representing the number of times each residue of (B) PIK3CA or (C) PIK3R1 is found mutated in solid tumours as reported in the COSMIC database (Forbes et al., 2016). The numbered boxes (1-4) correspond to mutation hotspots at regulatory interfaces. (D) Cartoon representation of PI3Kα (p110α/p85α). The regulatory arch is shown here in blue, and the activation loop is shown in yellow. Adapted from Dornan and Burke, 2018.

Mutants located at the ABD-kinase, C2-iSH2, and nSH2-helical interfaces activate lipid kinase activity through disruption of these inhibitory contacts. Intriguingly there appears to be allosteric long range coupling between these sites, as disruption of the C2-iSH2 interface also leads to disruption of the ABD-kinase interface (Burke et al., 2012). Mutations within the regulatory arch (a region composed of the two most C-terminal helices, kα10 and kα11, residues 1017-1049) appear to work through a separate mechanism, where conformational changes induced by these mutations drive increased membrane recruitment (Burke et al., 2012; Hon et al., 2012). The regulatory arch lies

directly over the active site of the enzyme (Fig. 7A). Different mutations induce oncogenic transformation through different mechanisms, with the H1047R mutant requiring p85 mediated recruitment to RTKs, and no longer requiring Ras for transformation, while the E545K mutation still requires input from Ras, and no longer requires p85 mediated RTK activation (Zhao and Vogt, 2008). This is consistent with the putative mechanism of Ras activation, where Ras drives membrane recruitment, and H1047R evades this requirement due to enhanced membrane binding (Buckles et al., 2017; Siempelkamp et al., 2017).

Somatic cancer associated point mutations in PIK3R1 are similarly localized at regulatory interfaces (Fig. 7A, C), with the most frequent mutation occurring at the C2-iSH2 interface (N564K/D). These mutants primarily activate PI3K signalling through p110α activation (Jaiswal et al., 2009; Jimenez et al., 1998; Urick et al., 2011). Loss of p85α is also a driver of cancer as it acts as a tumour suppressor, and oncogenic transformation due to loss of p85α is also driven by p110α (Thorpe et al., 2017). Several deletions/truncations identified in PIK3R1 also can mediate oncogenic transformation through different mechanisms. Truncations at the C-terminus of the iSH2 domain can still interact with p110 subunits, and disrupt inhibitory contacts (Jimenez et al., 1998), leading to increased PI3K activity. Intriguingly oncogenic truncations also occur N-terminal to the iSH2 domain, and they are unable to bind p110 subunits. These truncations are proposed to function through modification of free p85 interactions with binding partners (Cheung et al., 2015, 2014, 2011), including the antagonist of PI3K signalling, the phosphatase PTEN.

1.4 Class IA PI3Ks in developmental disorders

Mutations in PIK3R1 leading to decreased PI3K signalling are also found in patients with developmental disorders, with autosomal dominant or de novo mutations in the cSH2 (R649W, K653*, and Y657*; more mutations listed in Table 1) leading to insulin resistance, and dramatically decreased PI3K signalling (Bárcena et al., 2014; Chudasama et al., 2013; Dyment et al., 2013; Huang-Doran et al., 2016; Klatka et al., 2017; Schroeder et al., 2014; Thauvin-Robinet et al., 2013). This condition is defined as SHORT syndrome (**S**hort stature, **h**yperextensibility of joints and/or inguinal hernia, **o**cular depression, **R**ieger anomaly, and **t**eething delay), and is caused by the inability of the cSH2 domain to interact

with phosphorylated RTKs, as mutation of R649 disrupts the FLVR motif critical for SH2 binding to phosphorylated pYXXM motifs. While not mediating inhibitory interfaces through p110α, the cSH2 drives the high affinity interaction between class IA PI3Ks and pYXXM motifs and this leads to decreased class IA PI3K activation (Klippel et al., 1992).

1.5 Class IA PI3Ks in primary immunodeficiencies

Activating, autosomal dominant and de novo mutations in the genes encoding the PI3Kδ subunits have been discovered in patients with primary immunodeficiencies, and this condition is called activating PI3K delta syndrome (APDS). Mutations were identified via whole-exome sequencing in both PIK3CD (p110δ) and PIK3R1 (p85α) where activating mutations in PIK3CD are classified as APDS1 and mutations in PIK3R1 are identified as APDS2 (Angulo et al., 2013; Deau et al., 2014). Patients with APDS present with diverse clinical manifestations but are characterised by common features. Common clinical features of APDS include recurrent infections of the respiratory tract and sinus, increased susceptibility to persistent or recurrent viral infection, specifically with members of the herpes virus family (i.e Epstein barr virus), as well as increased occurrence of benign lymphoproliferation and increased risk of B cell lymphoma (Lucas et al., 2016). Patients with APDS2 can also present with symptoms of growth retardation that are typical of SHORT syndrome.

Mutations in PIK3CD were originally identified in patients exhibiting B-cell immunodeficiency (Jou et al., 2006). The first APDS1 mutation characterised was the E1021K mutation located in the C-lobe of the kinase domain, and within 6 Å of the kinase-cSH2 interface (Angulo et al., 2013). This mutation, similar to the corresponding p110α mutation H1047R, has been the most frequently identified APDS mutation. Prior to, and over the course of this study, further mutations have been discovered and identified in PID patients at the C2-iSH2 interface (N334K, R405C, C416R), nSH2-helical interface (Y524N, E525K, E525A), and at the C-terminus of the kinase domain (R929C, E1025G) (Fig. 8, Table 1) (Coulter et al., 2017; Crank et al., 2014; Dulau-Florea et al., 2017; Elgizouli et al., 2016; Hartman et al., 2015; Heurtier et al., 2017; Liu et al., 2016; Lucas et al., 2013; Luo et al., 2018; Rae et al., 2017; Saettini et al., 2017; Teranishi et al., 2017;

Tsujita et al., 2016; Y. Wang et al., 2018; Wentink et al., 2017). A recent mutation, P658L, is located in the helical domain within 6 Å of the C2 and the iSH2 but not close to the helical-nSH2 interface (Lougaris et al., 2019).

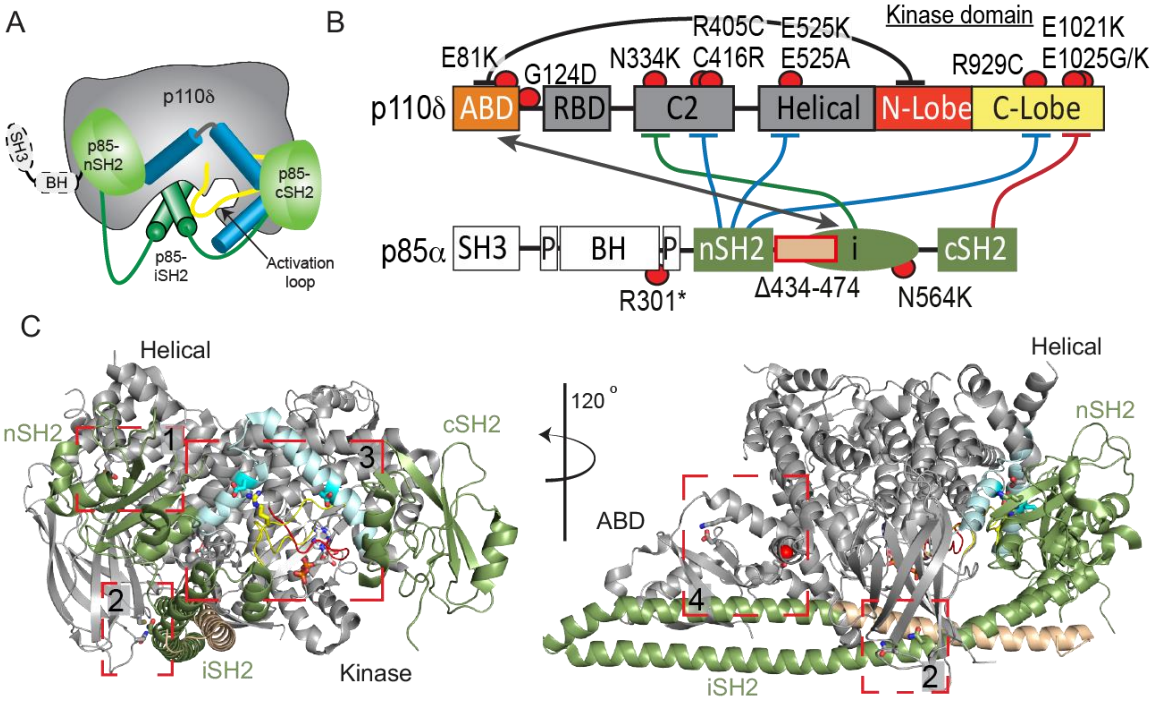

Figure 8: Activating mutations in PIK3CD and PIK3R1 lead to the primary immunodeficiency, APDS.

(A) Cartoon representation of p110δ/p85α. The regulatory arch is shown here in blue, and the activation loop is shown in yellow. (B) Wiring and mutation schematic of p110δ/p85α. Highlighted here are the regulatory interfaces between p110δ/p85α with APDS and related immunodeficiency mutations mapped onto the domain architecture. The double ended arrow between the ABD and iSH2 represents the stabilising interface of the p110δ/p85α heterodimer. The flat ended arrows represent the inhibitory interfaces between p110δ/p85α. A full list of APDS1/2 mutations can be found in Table 1. (C) Structural model of p110δ/p85α highlighting the location of activating mutations. The numbered boxes (1-4) correspond to mutation hotspots at regulatory interfaces. Colour coded to match the cartoon representation and the wiring diagram. Adapted from Dornan and Burke, 2018.

APDS1 mutations in PIK3CD are found in similar locations to oncogenic mutations in p110α, throughout the primary sequence primarily at hot spot regions of key regulatory interfaces between p110 and p85. While the corresponding mutations in p110α

have been previously characterised (Burke et al., 2012), the exact mechanisms mediating the activation of p110δ have yet to be defined. Further questions remain as to how these mutations might differ compared to those in PIK3CA due to the previously defined differences in regulation between PI3Kα and PI3Kδ. For example, the E1021K mutation might affect the kinase-cSH2 interface observed in PI3Kδ but not in PI3Kα.

Mutations in PIK3R1, that are classified as APDS2, have also been identified in a number of immunodeficiency patients, with the most frequent mutation resulting in a splice variant that removes exon 11; The result is a deletion in p85α of the region spanning residues 434-475, which is located at the N-terminus of the iSH2 domain (Deau et al., 2014; Hauck et al., 2017; Kuhlen et al., 2016; Lucas et al., 2014; Petrovski et al., 2016). This mutant may decrease protein stability of p110 subunits, and there have been reports of these patients having symptoms consistent with both SHORT syndrome and APDS (Bravo García-Morato et al., 2017; Petrovski et al., 2016). Another activating point mutation has been identified in the iSH2 domain of PIK3R1 at the C2-iSH2 interface (N564K), causing APDS2 symptoms (Wentink et al., 2017). This mutant is also found in solid tumors, and it appears in certain situations it can drive p110α mediated oncogenesis or drive p110δ mediated immunodeficiency.

Loss of function mutations in both PIK3CD and PIK3R1 also occur in immune disorders, with patients identified with autosomal recessive nonsense mutations in PIK3R1 (W298*, R301*) leading to Agammaglobulinemia, and severe defects in B-cell development (Conley et al., 2012; Tang et al., 2018). Another study found a complex mutation in PIK3CD (V552Sfs*26) that results in the truncation of p110δ within the helical domain and rendering the complex non-functional due to the loss of the catalytic kinase domain (Sogkas et al., 2018). Patients harbouring this mutation presented with similar clinical features (B-cell developmental defects, agammaglobulinemia) as well as another less common characteristic of inflammatory bowel disease. Another LOF mutation was identified in PIK3CD (Q721*), which also leads to a truncation that removes the kinase domain. These patients exhibited common APDS1 clinical manifestations along with those not associated with APDS due to the dual loss of another protein.

1.6 Therapeutic Interventions of Class IA PI3K Disease

Since the identification of p110α/p85α as oncoproteins and due to the involvement of all p110 isoforms in a wide range of human disease, PI3Ks have been key targets for drug design. The first PI3K inhibitors include Wortmannin, a covalent inhibitor derived from multiple fungal species, and LY294002, the first synthesized PI3K inhibitor (Powis et al., 1994; Vlahos et al., 1994; Wymann et al., 1996). Since then, many therapeutic avenues surrounding PI3K pathway activation have been investigated and include the identification of pan-PI3K inhibitors, p110 isoform specific inhibitors, activating mutation specific inhibitors, and inhibitors that target other members of the PI3K/AKT/mTOR signalling pathway. Despite multiple avenues and a push to develop novel inhibitors of PI3Ks, very few PI3K inhibitors have been successfully approved by the FDA (Janku et al., 2018).

The major issues affecting progress of PI3K inhibitor development for therapeutic interventions include lack of efficacy and severe side effects due to on- and off-target effects. The p110α isoform is expressed ubiquitously and mediates insulin signalling in cells. Pan-PI3K and p110α selective inhibitors cause severe side effects associated with abrogated insulin signaling. Additionally, it was recently shown that insulin levels can recover post p110α inhibition (insulin feedback) and re-activate the PI3K/AKT/mTOR signalling axis in tumours, despite p110α inhibition (Hopkins et al., 2018). By controlling insulin feedback through a ketogenic diet that decreases serum insulin levels, p110α inhibition lead to better side-effects profile and efficacy. Future clinical trials of compounds that target p110α may benefit from dietary intervention in patients, as this could be the key factor for improved therapeutic efficacy.

Engineering of PI3K isoform specific inhibitors is also expected to reduce off-target effects and toxicity. There are currently multiple compounds in various phase clinical trials (phases I-III) for all isoforms of class I PI3Ks however, the first PI3K inhibitor to be FDA approved was the potent p110δ specific inhibitor Idelalisib for chronic lymphocytic leukaemia (Furman et al., 2014; Herman et al., 2010). Despite these promising results for idelalisib, further studies have reported high risk of adverse effects associated with an

abrogation of the immune system including hepatotoxicity, lung infection, sepsis, and pneumonitis among others (Barr et al., 2016; Lampson et al., 2016). Clinical trials are underway for novel p110δ specific inhibitors due to the role of p110δ in respiratory infections and APDS.

Prior to identification of activating mutations in p110δ/p85α as a cause of primary immunodeficiencies, APDS patients received treatment courses that targeted their phenotypes. APDS patients commonly exhibit antibody deficiency, lymphopenia and recurrent infections. To treat these symptoms, patients were, and still are, treated with prophylactic antibiotic therapy, steroids, immunoglobulin replacement therapy (IRT), or a combination thereof (Coulter and Cant, 2018; Rae et al., 2017). This treatment course has been reported to be beneficial to many patients with regards to respiratory tract infections but fails to elicit improvement in herpes virus infections and lymphoproliferation or lymphoma (Coulter and Cant, 2018). Haematopoietic stem cell transplantation (HSCT) is another therapeutic option for patients with severe disease progression that do not respond to other treatments. Patients with severe APDS1 or APDS2 have responded well to HSCT treatment, with many undergoing successful chimerism and few complications. HSCT does have associated risks, such as poor chimerism leading to a return to previous therapies or death (Coulter et al., 2017; Coulter and Cant, 2018).

After confirmation of APDS1/2 through PIK3CD/PIK3R1 sanger sequencing, many patients have been started on the allosteric mTOR inhibitor Rapamycin (Sirolimus) (Coulter and Cant, 2018; Lucas et al., 2016, 2013; Rae et al., 2016). This intervention has shown good results in reducing symptoms of lymphoproliferation and has also been combined with IRT to target the wide range of symptoms exhibited in APDS (Rae et al., 2016). Idelalisib, the PI3Kδ specific inhibitor, is unlikely to be of interest as an APDS therapeutic due to its significant adverse effects profile mentioned previously. Other compounds that specifically target PI3Kδ are currently under investigation as a therapeutic intervention for APDS patients, with a focus on inhaled delivery of the compound (Coulter and Cant, 2018). Initial biochemical characterisation and clinical trials of Leniolisib (CDZ173, trial ID: NCT02859727) showed dose-dependent inhibition of PI3Kδ both *in vitro* and in patient cells (Rao et al., 2017). Importantly, circulating B-cell populations were

normalised and lymphoproliferation was reduced; these therapeutic benefits did not coincide with significant adverse effects. This trial has been extended to a longer-term, placebo controlled and randomized study (trial ID: NCT02435173). Another inhaler-based compound currently in clinical trials is Nemiralisib (GSK2269557, trial ID: NCT02593539). Nemiralisib has previously been tested for persistent, uncontrolled asthma (trial ID: NCT02567708) and in healthy subjects (trial IDs: NCT02972905, NCT02691325) to test the safety and tolerability of the compound in humans (Ino et al., 2019; Khindri et al., 2018; Wilson et al., 2018). Neither of the three clinical trials revealed any adverse effects in healthy subjects or patients with asthma indicating a promising safety profile for treatment of patients with APDS. Even though p110δ inhibitors have shown promise as therapeutics, careful consideration of unexpected complications is critical, as long-term inhibition of p110δ signalling can lead to B cell genomic instability through an Activation-induced cytidine deaminase (AID) dependent mechanism (Compagno et al., 2017).

1.7 Research objectives

The identification of activating mutations/deletions in class IA PI3K subunits leading to numerous disease states has highlighted their intricate isoform specific regulation. Deletions in the p85 regulatory subunit have divergent/contrasting effects on its ability to regulate different class IA p110 catalytic subunits, where a deletion in the N-terminal region of the coiled-coil iSH2 of p85 leads to p110δ driven immunodeficiency and C-terminal iSH2 deletions can lead to a putative p110α driven cancer formation. C-terminal deletions downstream of the iSH2 or perturbations to the cSH2 specifically can lead to SHORT syndrome. The mechanistic basis of how these deletions drive isoform specific phenotypes is undefined. APDS1 mutations in the p110δ catalytic subunit occur throughout the primary sequence; while these mutations could be driving disease through similar mechanisms as the corresponding oncogenic p110α mutations, differences in regulation between the two isoforms could yield novel insights into how p110δ is regulated. Insights gained from answering these questions could lead to novel therapeutic strategies for class IA PI3K driven disease.

The aims of this dissertation were to gain novel insight into the molecular mechanisms mediating class IA PI3K regulation by studying diseases driven by PI3K activating mutations. To this end, the following questions were addressed:

1. What are the molecular mechanisms of PIK3CD mutations, and how are they mediating disease? Are the mechanisms of PIK3CD mutations similar to oncogenic PIK3CA mutations or are they specific to the PI3Kδ isoform?

2. What are the specific mechanisms mediating PIK3R1 deletions driving different disease outcomes (APDS, cancer)?

To answer these questions, I have used a sophisticated combination of biochemistry and hydrogen-deuterium exchange mass spectrometry (HDX-MS) to probe the function and allosteric conformational changes in WT and clinical mutants of class IA PI3Ks. Class IA PI3Ks are peripheral membrane proteins that undergo conformational changes to exert their biological function. Characterising these dynamic changes is difficult using only static structural information, thus HDX-MS provides a unique opportunity to study regulatory mechanisms of class IA PI3Ks that are mediated through conformational movement during natural activation. The data presented in this thesis have elucidated novel mechanisms of class IA PI3K isoform regulation and further our overall knowledge of PI3K biology and the natural activation cycle.

Chapter 2:
Materials, Methods, and an Overview of Hydrogen-deuterium Exchange Mass Spectrometry (HDX-MS) for the Study of Lipid Signaling Enzymes

Adapted from:

Vadas, O., Jenkins, M.L., **Dornan, G.L.**, & Burke, J.E. (2017). Chapter Seven - Using Hydrogen–Deuterium Exchange Mass Spectrometry to Examine Protein–Membrane Interactions. Methods Enzymol. M.H. Gelb, ed. (Academic Press), pp. 143–172.

Dornan, G.L., Siempelkamp, B.D., Jenkins, M.L., Vadas, O., Lucas, C.L., & Burke, J.E. (2017). Conformational disruption of PI3Kδ regulation by immunodeficiency mutations in PIK3CD and PIK3R1. *Proc Natl Acad Sci*. 114: 1982–1987.

Contributions:

OV, MLJ, and JEB wrote manuscript for Methods Enzymol. For PNAS, **GLD** generated the expression constructs. **GLD** and BDS generated the virus, expressed, and purified the protein. **GLD** generated lipid vesicles. **GLD** performed HDX-MS experiments. **GLD** and JEB designed research. OV and CLL contributed new reagents/analytic tools. **GLD**, BDS, MLJ, and JEB analysed data. **GLD**, BDS, CLL and JEB wrote the paper.

2.1 Introduction

Hydrogen deuterium exchange mass spectrometry (HDX-MS) measures the exchange rate of amide hydrogens in solution, providing insight into protein structure and dynamics. Amide hydrogens are excellent probes for protein dynamics due to their involvement in hydrogen bonds in secondary structure elements (α helices and β sheets). The exchange rates of hydrogens in proteins are determined by multiple factors discussed further below, however, the only hydrogens exchanging with water under physiological conditions are the amide hydrogens and the hydrogens at polar/charged amino acids and the N and C-termini (Fig. 9). Sidegroup and termini hydrogens can be excluded from measurements as they exchange extremely rapidly independent of protein structure. The amide hydrogens exchange at rates that vary from seconds to days depending on dynamics of secondary structure. Proteins are dynamic molecules and protein regulation is driven by conformational changes. The ability to measure dynamic changes allow one to answer questions on protein conformation; this information when taken in combination with static structures, can be used to define key mechanisms of protein function.

The fundamental basis of hydrogen exchange in proteins has been studied since the 1950's, where hydrogen exchange of proteins was originally measured using density gradients or liquid scintillation counting of the radioactive isotope tritium. Hydrogen deuterium exchange coupled with mass spectrometry was not established until the early 1990's (Englander, 2006). As such, the hydrogen exchange mechanism is well defined in proteins and the use of MS to analyse the exchange rate has undergone rapid development. Below, I will describe practical methodology of HDX-MS and briefly discuss examples of the applications of the method to probe different aspects of protein structure and function. To summarise the method, amide hydrogens undergo exchange reactions which are both acid-base catalysed, making the exchange reaction pH sensitive with a global minimum of pH~2.5 (Molday et al., 1972). The kinetics of deuterium incorporation can be dramatically decreased by rapidly reducing the pH to the minimum at 2.5, which allows for locking exchange into place following incubation at physiological pH. Following this step, proteins are proteolytically digested and analysed by LC/MS to quantify deuterium incorporation within distinct peptides. This information itself can be useful in determining the overall

level of structure within a protein where regions of order would include alpha helices or beta sheets and regions that show high level of disorder such as disordered loops. Subsequently this information can be compared to data derived from the same protein in a different state to identify the changes that a protein undergoes during different conditions (i.e. enzyme binding its substrate).

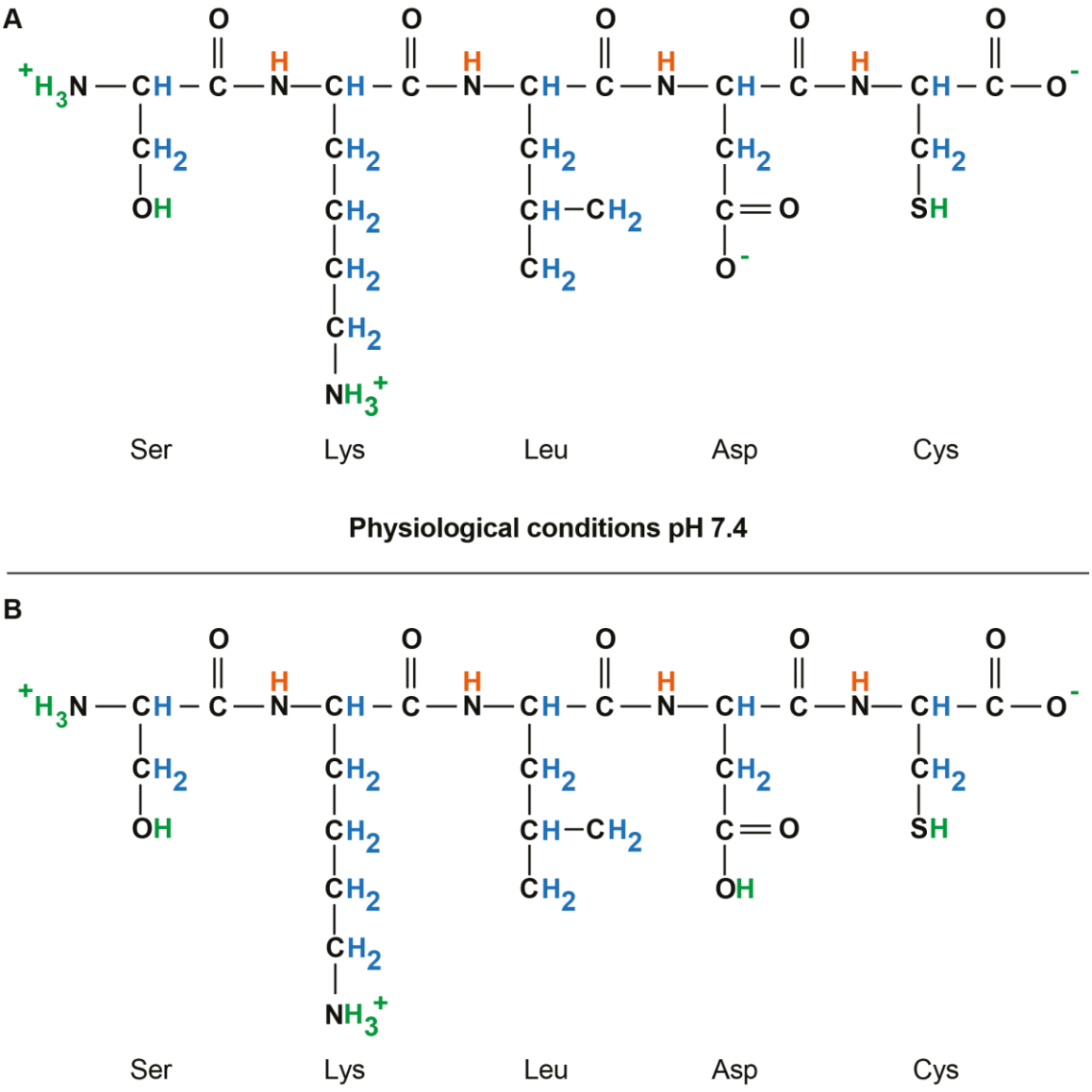

Figure 9: Hydrogens in protein.

There are three types of hydrogens in proteins. Amide hydrogens (orange) are integral in forming secondary structure elements through hydrogen bonding; Amide hydrogen deuterium exchange rates are measurable on a practical scale, occurring between seconds and weeks. Hydrogens in the side chains and at the N- and C-terminal amine and carboxylic acid exchange too rapidly to be measured (green). Carbon bonded hydrogens (blue) exchange with deuterium too slowly to be measured. The protonation state of amino acid C- and N-terminal groups are affected by the buffer pH ($COOH/COO^-$ or NH_2/NH_3^+). The protonation state of side chains of amino acids can also change, depending on the amino acid. A) An example peptide under physiological conditions (pH 7.4) or B) at the hydrogen deuterium exchange minimum (pH 2.5).

2.2 Methodology

Hydrogen Deuterium Exchange

Hydrogen-deuterium exchange (HDX) was originally utilized by Linderstrøm-Lang in the early 1950's and the kinetics of HDX in the context of proteins has been expertly reviewed previously (Engen, 2009; Englander, 2006; Vadas and Burke, 2015), so I will limit this discussion to relevant factors that affect exchange rates. To briefly summarize, the exchange rate of amide hydrogen with deuterium is affected by multiple parameters including pH, temperature, protein conformation (involvement in hydrogen bonding), primary sequence, and solvent accessibility (Bai et al., 1994, 1993; Connelly et al., 1993; Skinner et al., 2012). By controlling the pH, temperature and primary sequence in experiments, the measured exchange rate of hydrogens can be attributed primarily to the secondary structure and solvent accessibility of the protein. The consensus in the field is that the secondary structure or protein conformation dictates the exchange rate of hydrogen with deuterium more significantly than solvent exposure (Skinner et al., 2012). Thus, HDX data can inform on the presence and stability of secondary structure in proteins.

As the hydrogen deuterium exchange is both acid-base catalysed, these reactions are highly sensitive to perturbations in pH. The charge state of peptides is affected by different pH levels. The amino termini of amino acids have pKa values greater than 8.5 while the pKa values of the carboxy termini of amino acids are less than 2.4 (with the exception of tryptophan at ~2.8). Some of the amino acid side chains also possess pKa values (Cys, His, Asp, Glu, Tyr, Lys, Arg), meaning the charge states of these side chains are also determined by the pH of the buffer. The pKa values are important as they indicate the state of a molecule at specific pH values. The Henderson-Hasselbalch equation defines the relationship between pH and pKa, where pH is equivalent to pKa + log ([conjugate base]/[acid]). When the acid and conjugate base are at equivalence, pH is equal to pKa. When pH is lower than pKa, there is an abundance of protons and that species becomes protonated whereas when pH is higher than pKa, a species will become deprotonated. For amino acids at physiological pH of approximately 7.4, the carboxy terminus becomes deprotonated and holds a negative charge as the pH is higher than the pKa (Fig. 9A). The

amino terminus is positively charged as the pKa is greater than the pH. When the pH is higher than the pKa, the proton is donated whereas when the pH is lower than the pKa, the species becomes protonated (Fig. 9A). The deuterium exchange chemistry relies on these principles as well, where the amide group possesses strong acid and base pKa values (Englander, 2006). These values influence indicate why the deuterium exchange reaction is acid and base catalysed. The reaction has multiple steps, where the amide is deprotonated, followed by protonation of the carbonyl oxygen, and finally protonation of the nitrogen, which is the rate limiting step. Changes in pH will affect the rates of each step, as this will alter the level of OH^- and H_3O^+ that drive base and acid catalysed rates through the acceptance or donation of protons. The acid and base catalysed rates are also influenced by the different amino acid side chains (Englander et al., 1972; Molday et al., 1972). As some side chains are strongly affected by pH, this in turn will also affect their ability to influence acid and base catalysed rates. Thus, changes to pH can affect exchange rates through multiple aspects which will lead to differences in exchange rates. The pH must be strongly considered when planning HDX experiments and pH must be tightly controlled between samples in experiments as varying rates will ultimately affect the total deuterium incorporation for HDX-MS experiments.

Measurement of the deuterium incorporation at different time points allows for a more comprehensive understanding of protein structure and dynamics. The HDX experiments presented in this thesis involve the exposure of proteins to a deuterium buffer over time, where multiple samples are subjected to deuterium exchange for different amounts of time (Fig. 10A). Time point selection depends on the goal of the project. Short time points (i.e. 3 seconds) can provide information regarding regions of high disorder or flexibility, such as exposed loops that are not part of a hydrogen bonding network. Regions of highly stable secondary structure (involvement in hydrogen bonding or protection from solvent) can be identified with longer periods of deuterium exchange (i.e. 300-3000 seconds) (Vadas and Burke, 2015). The HDX reactions are then stopped through addition of a quench buffer to the sample at the specified time point and through immediate snap freezing in liquid nitrogen for long term storage (~2 weeks) until samples can be processed (Fig. 10B). The quench buffer reduces the pH to 2.5 and the temperature to 0°C, conditions

that reduce hydrogen-deuterium exchange rates to a minimum (Molday et al., 1972; Walters et al., 2012). All processing of samples after this point must be maintained at a pH of 2.5 and a temperature of 0°C to minimize back exchange that can occur in UPLC buffers.

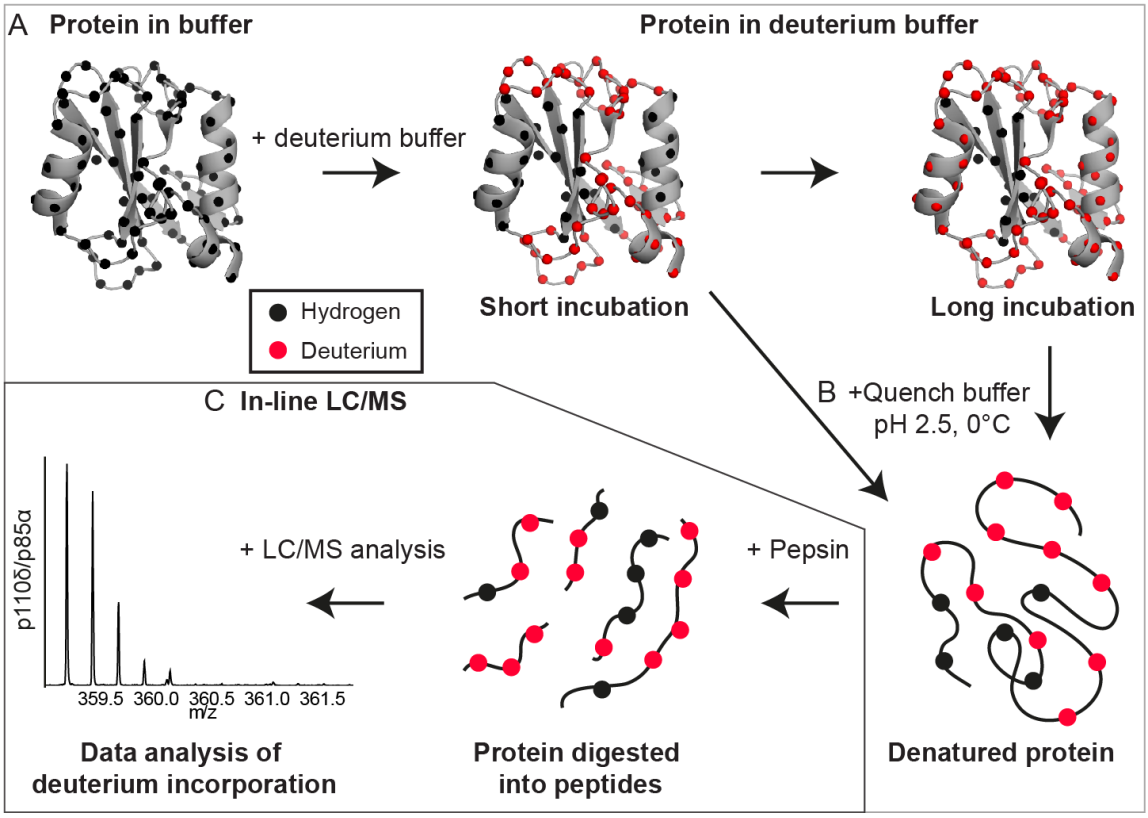

Figure 10: Overview of the methodology of HDX-MS.
(A) Proteins in aqueous buffer are incubated in a deuterium buffer for multiple lengths of time (i.e. one set of samples at 3 seconds, another set of the same samples at 300 seconds). (B) Deuterium exchange reactions are quenched by addition of quench buffer which drops the pH to 2.5 and the temperature to 0°C. This step also denatures the protein sample. (C) Protein samples are then injected onto an Ultra Performance Liquid Chromatography (UPLC) system with in-line pepsin columns that digest the denatured protein samples into peptides. Peptides are separated by reverse phase liquid chromatography before being injected onto the mass spectrometer for mass measurement.

Protein Digestion, Peptide Identification, and Deuterium Quantification

Digestion of proteins into distinct peptides of varying lengths allows for spatial localisation of deuterium incorporation, which can then be attributed to specific regions of a protein for biological analysis. Following digestion, peptides are then separated by

reverse phase chromatography and injected onto the MS for mass measurement (Fig. 10C) (Zhang and Smith, 1993). As pH must be maintained at 2.5 to reduce back exchange of deuterium to a minimum, an acid functional protease must be used for efficient digestion of proteins. This is achieved through tandem in-line pepsin columns; specifically, these columns contain pepsin immobilised on ethyl-bridge hybrid (BEH) particles. Additionally, running these columns under high pressure conditions (>10,000 psi) leads to enhanced protein digestion (Ahn et al., 2012; Jones et al., 2010). Peptides are then separated through a reverse-phase C18 column before injection onto the MS for mass measurement. Once the peptides are injected onto the MS, they are ionised using an electrospray ionisation source and fragmented by collision induced dissociation (CID) into ion pairs. Through MS/MS, peptide maps of the non-deuterated protein(s) are generated which allows tracking of deuterated peptides in downstream analysis to the protein primary sequence.

Found below are the peptide maps for class IA PI3K p110δ/p85α (Fig. 11 & 12). Deuterium incorporation information is lost at the two amides adjacent to the cleavage site, this can be overcome through generation of overlapping peptides to improve spatial resolution of deuterium incorporation (Kan et al., 2013; Walters et al., 2012).

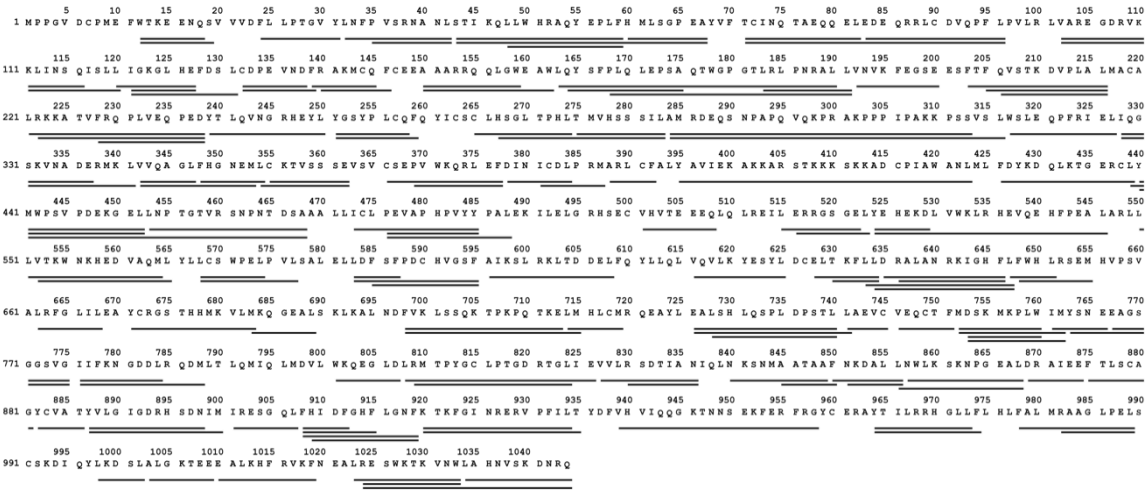

Figure 11: Peptide coverage map for the p110δ protein.
Identified and analyzed pepsin-digested peptides are shown under the primary sequence of p110δ as black bars. A peptide digestion protocol was optimized for WT full-length p110α/p85α heterodimer and allowed for the identification of 227 peptides spanning 93.8% of p110α.

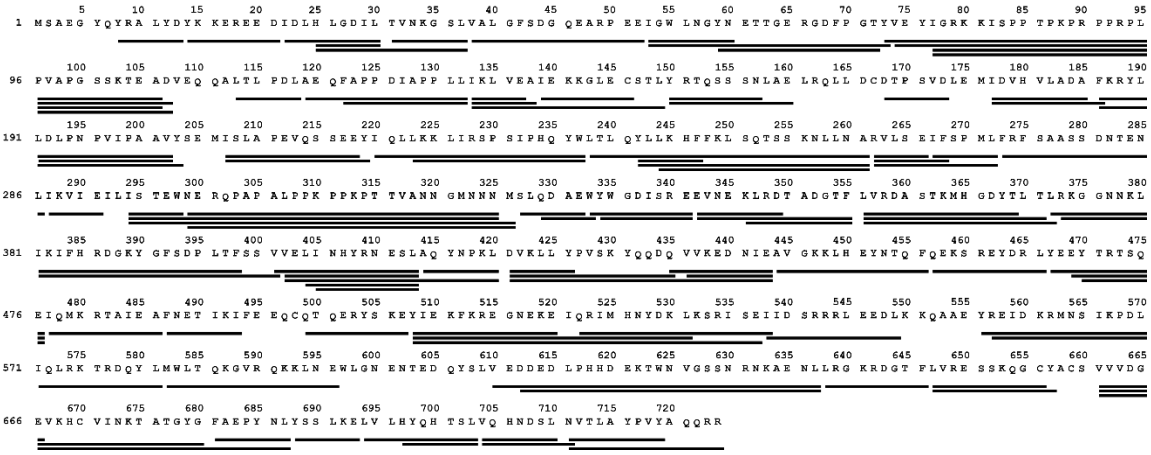

Figure 12: Peptide coverage map for the p85α protein.
Identified and analyzed pepsin-digested peptides are shown under the primary sequence of p85α as black bars. A peptide digestion protocol was optimized for WT full-length p110α/p85α heterodimer and allowed for the identification of 133 peptides spanning 96% of p85α.

The total ion count (TIC) is generated through analysis of all major ions detected from the fragmented peptides over the total time it takes to inject all peptides (Fig. 13A). Specific time points throughout the TIC curve represent the various peptide spectra (Fig. 13B). Each spectrum represents a single peptide, and the spectrum for each peptide is how the deuterium incorporation can be tracked (Fig. 13C). In the example presented, the left spectrum for the specific peptide represents a non-deuterated control with the right spectra showing two time-points of deuterium exchange for two protein conditions (WT [top] vs. Mutant [bottom]). As deuterium is heavier than hydrogen, increasing levels of deuterium incorporation will cause spectra to shift towards the right. This allows the quantification of deuterium incorporation at specific peptides.

HDX-MS generates large volumes of data which scales with the size of the protein(s) being analysed. Methods of deuterium quantification have been extensively developed over the past 15-20 years to produce solutions to automation of data analysis through computational means. There are now multiple HDX-MS data analysis packages on the market, which have recently been reviewed elsewhere (Gallagher and Hudgens, 2016). The HDX-MS data in this thesis was exclusively analysed using the HD-Examiner software, which allows for the automatic calculation of the level of deuterium incorporation

of each peptide and the output shown below (Fig. 13C). Relative deuterium incorporation levels can be determined through this software, and presented as deuterium incorporation over time (Fig. 13D). Deuterium incorporation levels can be compared between two states (i.e. WT protein vs mutant protein) and the increases/decreases in deuterium incorporation can be mapped onto structural models and cartoon representations for visualisation of the data (Fig. 13E).

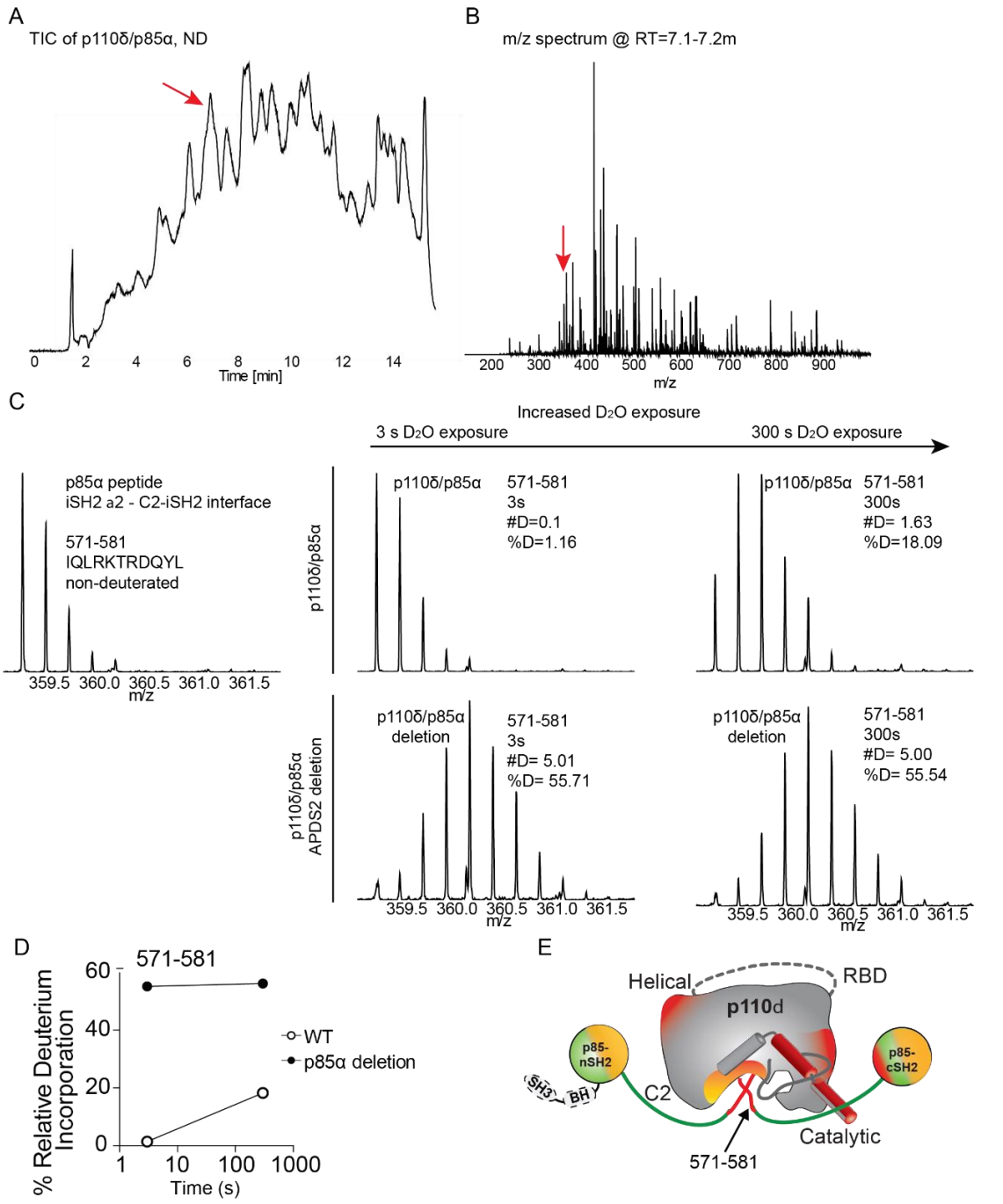

Figure 13: Peptide identification and deuterium quantification.

(A) Representative UPLC total ion count (TIC) trace of a p110δ/p85α peptic digest. (B) MS spectra for the time window selected in the TIC in A. (C) Raw data for the peptide 571-581 in p85α showing the shift in mass centroid upon deuterium incorporation after 0 (nondeuterated, ND), 3 and 300 s exposure to D2O buffer. The difference in HDX in this peptide is highlighted for the WT and p85 APDS2 deletion constructs. (D) HDX incorporation plots for this peptide in the WT and p85 APDS2 deletion constructs. (E) Cartoon model of PI3Kδ indicating the region with increased deuterium incorporation.

2.3 Applications of HDX-MS

Recent advances in HDX-MS have led to increased accessibility to study protein conformation and function, which in turn has led to broader applications of the method. HDX-MS application has expanded to studies of protein-ligand interactions, protein-protein interactions, and as a complementary method (i.e. identifying regions of disorder to guide X-ray crystallographic strategies). This method has been especially useful in the study of large, complex macromolecular machines that associate with membranes such as PI3Ks. Structures of these enzymes exist; however, these static structures do not fully explain the endogenous/physiological mechanisms of activation. Thus, HDX-MS represents a particularly useful method to probe enzyme function in solution and in more physiologically representative environments.

Structural dynamics and mechanisms of regulation of all classes of PI3Ks (I, II, III) have been probed using HDX-MS to identify conformational changes, PI3K interactions with binding partners and membranes, and inhibitor binding of PI3Ks. The ability of HDX-MS to provide information on the structure and conformation of proteins in solution has greatly expanded knowledge of the function of PI3Ks. The class I enzymes undergo allosteric conformational changes in their natural activation downstream of membrane receptor phosphorylation and these changes in conformation can be determined by HDX-MS. The natural activation mechanisms downstream of membrane receptors have previously been probed for all class I enzymes using HDX-MS (Burke et al., 2012, 2011; Burke and Williams, 2013; Dbouk et al., 2012; Siempelkamp et al., 2017; Vadas et al., 2013; Walser et al., 2013). HDX-MS was also used to show differential regulatory mechanisms of p110δ compared with p110α as mediated through p85α and that activating oncogenic mutations in p110α and p85α led to conformational changes that mimic natural activation (Burke et al., 2012, 2011). Mechanisms of class I PI3K activation downstream of other membrane receptors have also been investigated, showing HDX-MS ability to identify both the protein-protein interactions as well as changes in protein conformation induced upon binding of receptors to PI3K (Dbouk et al., 2012; Siempelkamp et al., 2017; Vadas et al., 2013; Walser et al., 2013). Finally, HDX-MS has been used to identify

membrane binding and membrane mediated activation of class I PI3Ks (Burke et al., 2012, 2011; Dbouk et al., 2012).

In addition to the class I PI3Ks, HDX-MS has also been used to probe mechanisms of class II and class III regulation. HDX-MS enabled identification of a novel autoregulation mechanism of the class II PI3KC2α. The C-terminal PX-C2 domains unique to class II PI3Ks were shown to make intramolecular contacts with both the kinase domain and the RBD (H. Wang et al., 2018). The complex dynamics, and membrane binding regions of the class III PI3K VPS34 were also revealed using HDX-MS (Baskaran et al., 2014; Ohashi et al., 2016; Rostislavleva et al., 2015). Further elucidation of the class II and class III PI3K mechanisms of regulation, mediated through interacting protein partners or membrane binding, will likely benefit from further studies using HDX-MS due to the complicated nature of these proteins and protein complexes.

As all PI3Ks are implicated in a wide variety of human disease, identification of novel small molecule therapeutics is desirable. HDX-MS to screen and guide design of compounds is increasingly attractive, either on its own or as a complimentary method in conjunction with X-ray crystallography or NMR. The use of HDX-MS in drug discovery has been recently reviewed in depth (Masson et al., 2017a). One of the major challenges of characterising novel inhibitor mechanisms of action is the acquisition of high-resolution data of the compound bound to the target protein. Large proteins and protein complexes can be difficult to work with due to the protein quantity requirements and the ability of the protein to form crystals that will yield high-resolution structural data. HDX-MS can overcome these difficulties, as protein-ligand binding is characterised in solution and relatively low quantities are required. Recent characterisation of a panel of PI3K inhibitors bound to p110α has shown the power of this method in screening inhibitors against large complex proteins. Data was acquired at single amino-acid resolution and was able to show binding of even low affinity inhibitors, allowing comparison of inhibitor binding effects on conformation (Masson et al., 2017b).

Molecular mechanisms that mediate class IA PI3K regulation during natural activation is difficult to study using more traditional methods such as X-ray crystallography

which captures static structural information, in part due to the dynamic nature of the enzymes and due to their interactions with membrane substrates. The ability to probe conformational dynamics of these large complexes in the presence of membrane substrates has made HDX-MS the ideal technique to study the complex regulatory mechanisms of class IA PI3Ks in their natural activation cycle and upon pathogenic mutation.

2.4 Materials and Methods

Materials

Original plasmids of the wild-type p110α, p110δ and p85α were a kind gift from the Williams laboratory at the Laboratory of Molecular Biology (Cambridge, UK) and the Vadas laboratory at the University of Geneva (Geneva, Switzerland).

Cloning

All point mutations were produced using site-directed mutagenesis, where the WT plasmid is PCR amplified using primers that overlap and contain the mutation of interest. All deletion constructs, including the p85α (Δ434-475) APSD2 construct and the C-terminal truncation constructs, were generated using a PCR based cloning method that follows the same flowpath as site-directed mutagenesis. The construct was amplified by PCR using two primers that flank the deletion site and contain an overlap. PCR reactions were performed on the wild-type p110 or p85α (primers listed in the appendix) and incubated with Dpn1 at 37C for 1 hour to overnight (Q5 High-Fidelity 2X MasterMix, New England Biosciences #M0492L; Dpn1, New England Biosciences #R0176S). The PCR product was then purified and transformed into competent *E. coli* cells according to manufacturers protocols (QiaQuick PCR Purification Kit, Qiagen #28104; XL10-Gold Ultracompetent Cells #200315). Single colonies were isolated, and plasmids were purified according to manufacturer protocols (QIAprep Spin Miniprep Kit, Qiagen #27106). Plasmid identity and mutation status was confirmed by Sanger sequencing (Eurofins Genomics).

Baculovirus Generation

Plasmids harbouring p110α, p110δ, wild-type p85α, and deletion were transformed into DH10MultiBac cells (MultiBac, Geneva Biotech, Switzerland) containing the MultiBac baculovirus viral genome (bacmid) and a helper plasmid expressing transposase to transpose the expression cassette harbouring the gene of interest into the baculovirus genome. Bacmids with successful incorporation of the expression cassette were identified by blue-white screening and were purified from a single white colony using a standard isopropanol-ethanol extraction method. Briefly, colonies were grown overnight (~16 hours) in 2xYT (BioBasic #SD7019). Cells were pelleted by centrifugation and the pellet was resuspended in P1 Buffer (50 mM Tris-cl, pH 8.0, 10 mM EDTA, 100 ug/mL RNase A), chemically lysed by the addition of Buffer P2 (1% sodium dodecyl sulfate (SDS) (W/V), 200 mM NaOH), and the lysis reaction was neutralized by addition of Buffer N3 (3.0 M potassium acetate, pH 5.5). Following centrifugation at 21130 rcf (Eppendorf Centrifuge 5424 R), the supernatant was separated and mixed with isopropanol to precipitate the DNA out of solution. Further centrifugation pelleted the Bacmid DNA, which was then washed with 70% Ethanol three times. The Bacmid DNA pellet was then dried for 1 minute and resuspended in Buffer EB (10 mM Tris-Cl, pH 8.5; All buffers from QIAprep Spin Miniprep Kit, Qiagen #27104).

Purified bacmid was then transfected into *Spodoptera frugiperda* (Sf9) cells between 0.3-0.5×10^6 cells/mL. Two mL of Sf9 cells between 0.3-0.5×10^6 cells/mL were aliquoted into the wells of a 6-well plate and allowed to attach, creating a monolayer of cells at ~70-80% confluency. Transfection reactions were prepared by the addition of 2-10 μg of bacmid DNA to 100 μL 1xPBS and 12 μL PEI at 1 mg/mL (Polyethyleneimine "Max" (MW 40.000), Polysciences #24765, USA) to 100 μL 1X PBS. The bacmid-PBS and the PEI-PBS were mixed together, and the reaction occurred for 20-30 minutes before the mixture was added drop-by-drop to a Sf9 containing well. This transfection proceeded between 5-7 days, before the supernatant was harvested as a P1 viral stock.

Viral stocks were amplified by adding P1 viral stocks to suspension Sf9 cells between 1-2x10^6 cells/mL at a 1/100 volume ratio. This amplification produces a P2 stage viral stock that can be used in final protein expression. The amplification proceeded for 4-5 days before harvesting, with cell shakings at 120 RPM in a 27°C shaker (New

Brunswick). Harvesting of P2 viral stocks was carried out by centrifuging cell suspensions in 50 mL Falcon tubes at 2281 RCF (Beckman GS-15).

Protein Expression

To express PI3K complexes, an optimised ratio of p110δ:p85α baculovirus was used to co-infect Sf9 cells between 1-2×10^6 cells/mL. Co-infections were harvested between 42-72 hours, washed with ice-cold 1X PBS, snap-frozen in LN2, and stored at -80°C.

Purification of p110/p85α WT and APDS1 or Oncogenic Mutants

All PI3K variants were purified in an identical method by lysing cells and performing nickel affinity, streptavidin affinity, and size exclusion purifications. All steps in protein purification were carried out on ice, or in a 4°C cold room.

Frozen Sf9 pellets were re-suspended in lysis buffer (20 mM Tris pH 8.0, 100 mM NaCl, 10 mM imidazole pH 8.0, 5% glycerol (v/v), 2 mM bME, protease inhibitor (Protease Inhibitor Cocktail Set III, Sigma)) and sonicated on ice for 1 minute 30 seconds (15s on, 15s off, level 4.0, Misonix sonicator 3000). Triton X-100 was added to the lysate at a concentration of 0.2% and centrifuged at 20,000 g for 45 minutes (Beckman Coulter Avanti J-25I, JA 25.50 rotor). The supernatant was then loaded onto a 5 mL HisTrap™ FF crude column (GE Healthcare #11000458) that had been equilibrated in NiNTA A buffer (20 mM Tris pH 8.0, 100 mM NaCl, 20 mM imidazole pH 8.0, 5% (v/v) glycerol, 2 mM bME). The column was washed with 20 mL of high salt NiNTA A buffer (20 mM Tris pH 8.0, 1 M NaCl, 20 mM imidazole pH 8.0, 5% (v/v) glycerol, 2 mM βME), 15 mL of NiNTA A buffer, 20 mL of 6% NiNTA B buffer (20 mM Tris pH 8.0, 100 mM NaCl, 500 mM imidazole pH 8.0, 5% (v/v) glycerol, 2 mM βME) before being eluted with 100% NiNTA B. The elution was loaded onto 2x tandem 1 mL StrepTrap™ HP columns (GE Healthcare #29048653) equilibrated in Hep A buffer (20 mM Tris pH 8.0, 100 mM NaCl, 5% (v/v) glycerol, 2 mM bME). The columns were washed with 2 mL of Hep A buffer before addition of a tobacco etch virus protease containing a stabilizing lipoyl domain. Tobacco etch virus cleavage proceeded overnight (~ 12–16 h) before elution of cleaved protein in

1–2 mL of Gel Filtration Buffer (20 mM HEPES pH 7.5, 150 mM NaCl, 0.5 mM tris(2-carboxyethyl)phosphine (TCEP)). Fractions were pooled and concentrated in a 50,000 MWCO Amicon concentrator (Millipore) to between 300-1000 µL. Concentrated protein was injected onto a Superdex™ 200 10/300 GL Increase size-exclusion column (GE Healthcare #28990944) equilibrated in Gel Filtration Buffer. Proteins were concentrated to a concentration between 0.5-4 mg/mL. Protein was aliquoted, snap-frozen in liquid nitrogen, and stored at -80 °C.

Purification of p110/p85α WT and APDS2 Mutants (p85-Δ434-475)

Complexes of p110 catalytic subunits with APDS2 mutants p85α (Δ434-475) were highly unstable and expressed at a much lower level than WT or APDS1 mutants. The only way to generate pure protein (>90% by SDS page analysis) was through the use of a N-terminal streptavidin tag. Protein was unstable to concentration, and for this reason all purifications and analyses were carried out within 10 hours. Both PI3K wild-type (p110/p85α) and PI3K APDS2 mutants (p110/p85α Δ434-475) containing a N-terminal streptavidin (strep) tag (Strep-tag® II) in the p110 subunit were expressed and lysed as previously described. All steps were performed at 4°C or on ice. The supernatant was loaded onto a 1 mL StrepTrap™ HP column (GE Healthcare) equilibrated in Hep A-Deletion buffer (20 mM Tris pH 8.0 RT, 100 mM NaCl, 10% (v/v) glycerol, 2 mM βME). The StrepTrap™ HP column was washed with 3 mL of Hep B-Deletion buffer (20 mM Tris pH 8.0 RT, 1 M NaCl, 10% (v/v) glycerol, 2 mM βME) followed by 3 mL of HEP A-Deletion buffer. To cleave the strep-tag, 1 mL of a TEV protease solution (~0.08 mg/mL) was loaded onto the column and incubated for 3 hours. Protein was eluted using 2 mL of Hep A-Deletion buffer. The entire StrepTrap™ HP elution was loaded onto a 1 mL HiTrap™ Q HP column (GE healthcare) equilibrated in Hep A-Deletion buffer. The HiTrap™ Q HP column was washed with 3 mL of Hep A-Deletion buffer to remove the TEV protease. PI3Ks were eluted using 2 mL of HEP Elution Buffer (20 mM Tris pH 8.0 RT, 350 mM NaCl, 10% (v/v) glycerol, 2 mM βME) into 100 µL fractions. The concentration of PI3K in each fraction was determined via NanoDrop (Thermo Scientific) and corrected using band intensities following Coomassie staining on SDS-PAGE. The fractions with the highest concentrations were pooled and used for subsequent experiments.

Lipid Vesicle Preparation

The lipid vesicles used include a negatively charged lipid vesicle and a plasma membrane mimic vesicle. We generated negatively charged lipid vesicles (5% C8:PIP_2, 95% brain PS), which are the optimal substrate for class IA PI3Ks. Vesicles were prepared by evaporating the organic solvent of the PS under a stream of N2 gas. The lipid film was desiccated under vacuum for 60 minutes. The PS was resuspended in lipid buffer (20 mM HEPES pH 7.5 (RT), 100 mM KCl, 0.5 mM EDTA) containing C8:PIP_2 to a final lipid concentration of 1 mg/mL followed by sonication for 10 minutes. Plasma membrane mimic vesicles (5% brain phosphatidylinositol 4,5- bisphosphate (PIP2), 30% brain phosphatidylserine (PS), 50% brain phosphatidylethanolamine (PE), 15% brain phosphatidylcholine (PC)), were generated to provide a biologically relevant substrate for class IA PI3Ks. Vesicles were prepared by thoroughly mixing all lipid species in dissolved in organic solvent together, before evaporating the organic solvent under a stream of N2 gas to create a lipid film. The lipid film was desiccated under vacuum for 60 minutes. The lipid film was resuspended in lipid buffer (20 mM HEPES pH 7.5 (RT), 100 mM KCl, 0.5 mM EDTA) to a final lipid concentration of 1 mg/mL followed by sonication for 10 minutes.

The vesicle solutions were subjected to three freeze-thaw cycles by snap freezing in LN2 and warming the solution quickly in a warm water bath. Vesicles were extruded 11 times through a 100 nm filter using an Avanti mini-extruder (Avanti). Vesicles were aliquoted into 50 μL aliquots, snap-frozen in LN2, and stored at -80°C.

PDGFR phosphopeptide (pY)

All peptides were custom ordered from New England Peptide (NEP). Three peptides in total were ordered. The initial peptide, referred to as “PDGFR pY” spans residues 735-767 of the platelet derived growth factor receptor (PDGFR) and is phosphorylated at residues 740 (pY740) and 751 (pY751). The other two peptides were prepared with the same residues, differing in their phosphorylation. “Peptide 1” is phosphorylated only at pY740 and “Peptide 2” is phosphorylated only at pY751.

Lipid Kinase Activity Assays

Lipid kinase assays monitoring hydrolysis of ATP were carried out using the Transcreener ADP^2 Fluorescence Intensity (FI) assay (Bellbrook labs). Lipid vesicles were used at a final concentration of 0.45 mg/ml, with ATP present at 100 μM. Protein solutions containing either PDGFR pY (final concentration in assay 1 μM) or blank solution in 2X PI3K kinase buffer (100 mM HEPES pH 7.5, 200 mM NaCl, 6 mM MgCl2, 2 mM EDTA, 0.06% CHAPS, 2 mM TCEP) were allowed to equilibrate for 10 minutes at 23°C. Kinase reactions were started by addition of 2 μL of protein solution to 2 μL of 2X substrate solution (0.9 mg/mL lipid vesicles, 200 μM ATP) in a 384-well black microplate (Corning). The reaction was allowed to proceed at 23°C for 60 minutes before the addition of 2X Stop and Detect buffer (1X Stop and Detect Buffer, 8 nM ADP Alexa594 Tracer, 93.7 μg/mL ADP2 Antibody-IRDye QC-1). Antibody, tracer, and ADP were equilibrated for 60 minutes. Fluorescence intensity was measured using a Spectramax M5 plate reader with λexcitation = 590 nm and λemission = 620 nm (20 nm bandwidth; Molecular Devices). Specific activity was calculated using an ATP/ADP standard curve according to the Transcreener ADP FI protocol. Fold activation was determined by normalising mutant specific activity values to the specific activity of the wild-type PI3K complex.

IC50 Measurement

The potent PI3K inhibitor Idelalisib (SelleckChem) was used for IC50 measurements. Dilutions were generated from a 1 mM master stock of Idelalisib in 100% DMSO. Inhibitor was diluted to 100 μM in DMSO, and subsequent dilutions were all carried out in 1% final DMSO. Inhibitor dilution curves were carried out in triplicate and then mixed with substrate solution. All other lipid kinase assay steps were carried out according to the protocol described above. Values were imported into Prism (GraphPad Software, La Jolla, CA) for graphing and calculations of IC50 values.

Hydrogen Deuterium Exchange Sample Preparation

HDX experiments were conducted in 50 μL reactions with a final concentration of 120 nM for APDS1 mutants and WT PI3Kδ. Three conditions were tested: PI3K alone,

and PI3K in the presence of phosphopeptide (5 μM pY) with and without lipid vesicles (5% PIP2, 30% PS, 50% PE, 15% PC present at 100 μg/mL). Deuterium exchange was initiated by the addition of 40 μL deuterated buffer (10 mM HEPES pH 7.5, 100 mM NaCl, 98% (v/v) D2O). Exchange was carried out for three time points (3 s, 30 s, and 300 s at 23°C) and terminated by the addition of 20 μL ice-cold quench buffer (2 M guanidine-HCl, 3% formic acid). For APDS2 experiments, 70 μL reactions with a final concentration of 60 nM were used. Deuterium exchange was initiated by the addition of 50 μL deuterated buffer and exchange was carried out for two time points (3s, 300s at 23°C). The reaction was terminated by the addition of 25 μL quench buffer. All experiments were carried out in triplicate. Samples were immediately frozen in liquid nitrogen and stored at -80°C.

Protein samples were rapidly thawed and injected onto a UPLC system at 2°C. The protein was run over two immobilized pepsin columns (Applied Biosystems; porosyme, 2-3131-00) at 10°C and 2°C at 200 μL/min for 3 minutes, and peptides were collected onto a VanGuard precolumn trap (Waters). The trap was subsequently eluted in line with an Acquity 1.7 μm particle, 100 × 1 mm2 C18 UPLC column (Waters), using a gradient of 5-36% B (buffer A 0.1% formic acid, buffer B 100% acetonitrile) over 16 minutes. Mass spectrometry experiments were performed on an Impact II TOF (Bruker) acquiring over a mass range from 350 to 1500 m/z using an electrospray ionization source operated at a temperature of 200°C and a spray voltage of 4.5 kV. Peptides were identified using data-dependent acquisition methods following tandem MS/MS experiments (0.5 s precursor scan from 150-2000 m/z; twelve 0.25 s fragment scans from 150-2000 m/z). MS/MS datasets were analyzed using PEAKS7 (PEAKS), and a false discovery rate was set at 1% using a database of purified proteins and known contaminants.

Hydrogen Deuterium Exchange Data Analysis

HD-Examiner Software (Sierra Analytics) was used to automatically calculate the level of deuterium incorporation into each peptide. All peptides were manually inspected for correct charge state and presence of overlapping peptides. Deuteration levels were calculated using the centroid of the experimental isotope clusters. Results for these proteins

are presented as relative levels of deuterium incorporation and the only control for back exchange was the level of deuterium present in the buffer.

Analysis from Dornan et al., PNAS, 2017 and Takeda et al., J Clin Aller Immunol, 2017

The level of deuterium present in the buffer was 78%-PI3K and 70%-Deletion. The real level of deuteration will be ∼25–35% higher than shown, based on tests performed with fully deuterated standard peptides. The average error of all time points and conditions for each HDX project was less than 0.3 Da (Dornan et al., 2017) and the average error of all time points and conditions for HDX project of N-terminal mutations was less than 0.2 Da (Takeda et al., 2017). Therefore, changes in deuterium level in any peptide at any time point greater than both 7% and 0.7 Da between conditions with an unpaired t-test value of $p<0.05$ was considered significant. The full deuterium incorporation for all experiments is shown in the following: N-terminal APDS1 mutations in Fig. A1.1 (Takeda et al., 2017), APDS1 and APDS2 mutations in Fig. A1.2, A1.4 and A1.5 (Dornan et al., 2017). Differences between conditions are shown for APDS1 and APDS2 mutations in Fig. A1.3, A1.4, and A1.5 (Dornan et al., 2017).

Analysis from Dornan et al., in preparation

The level of deuterium present in the buffer was 76.8% for all experiments. The real level of deuteration will be ∼25–35% higher than shown, based on tests performed with fully deuterated standard peptides. . Changes in any peptide at any time point greater than specified cut-offs (both 7% and 0.4 Da between conditions for the Q572* mutant versus wild-type and both 4% and 0.4 Da between conditions for the PDGFR pY dose experiment) and with an unpaired t-test value of $p<0.05$ was considered significant.

The oncogenic Q572* mutation as well as the C-terminal p85α pathogenic and engineered mutations in Fig. A1.6 and A1.8 respectively. Differences between conditions are shown for the oncogenic Q572* mutation as well as the C-terminal p85α pathogenic and engineered mutations in Fig. A1.7 and A1.9.

Mapping of HDX-MS data on structural models

All changes in deuterium incorporation that met the thresholds (see above for specific conditions per experiment) were mapped onto structural models. All mapping was performed using the PyMOL software (The PyMOL Molecular Graphics System, Version 2.0 Schrödinger, LLC). All structural models contained in figures throughout this thesis use the following structural models unless otherwise noted and cited.

PI3Kδ

The structural model for PI3Kδ was prepared using the following PDB files: 5DXU, 2Y3A, and 3HHM (Timothy P. Heffron et al., 2016; Mandelker et al., 2009; Zhang et al., 2011). The PDB file 5DXU provided the p110δ catalytic subunit in complex with the p85α iSH2. 2Y3A provided the p85β cSH2. The PDB file 3HHM provided the p85α nSH2. The structural model was prepared by aligning all three PDB structures at the iSH2 of p85s and removing all but desired components.

PI3Kα

The structural model for PI3Kα was prepared using the following PDB files: 4OVU, 2Y3A, and 3HHM (Mandelker et al., 2009; Miller et al., 2014; Zhang et al., 2011). 4OVU provided the p110α catalytic subunit in complex with the p85α iSH2. 2Y3A provided the p85β cSH2. 3HHM provided the p85α nSH2. The structural model was prepared by aligning all three PDB structures at the iSH2 of p85s and removing all but desired components.

Chapter 3:
Identifying the molecular mechanisms of PI3K regulation mediated by the catalytic subunit p110δ via the investigation of immunodeficiency mutations in the gene PIK3CD

Adapted from:

Dornan, G.L., Siempelkamp, B.D., Jenkins, M.L., Vadas, O., Lucas, C.L., & Burke, J.E. (2017). Conformational disruption of PI3Kδ regulation by immunodeficiency mutations in PIK3CD and PIK3R1. *Proc Natl Acad Sci*. 114: 1982–1987.

Takeda, A.J., Zhang, Y., **Dornan, G.L.**, Siempelkamp, B.D., Jenkins, M.L., Matthews, H.F., McElwee, J.J., Bi, W., Seeborg, F.O., Su, H.C., Burke, J.E., & Lucas, C.L. (2017). Novel PIK3CD mutations affecting N-terminal residues of p110δ cause activated PI3Kδ syndrome (APDS) in humans. J Allergy Clin Immunol. 140: 1152-1156.

Contributions:

GLD generated the expression constructs. **GLD** and BDS generated the virus, expressed, and purified the protein. **GLD** generated lipid vesicles. **GLD** performed kinase activity assays. **GLD** and JEB performed IC50 measurements. **GLD** performed HDX-MS experiments. **GLD** and JEB designed research. OV and CLL contributed new reagents/analytic tools. **GLD**, BDS, MLJ, and JEB analysed data. **GLD**, BDS, CLL and JEB wrote the paper.

3.1 Introduction

The tight regulation of PI3Kδ is vital for the proper development of immune cells (Okkenhaug et al., 2002; Ramadani et al., 2010). Perturbations leading to increased or decreased PI3Kδ activity lead to a lack of B- and T-cells in all developmental states. This in turn leads to significant clinical manifestations including persistent respiratory infections, chronic or persistent viral infections, and increased risk of B cell lymphoma (Lucas et al., 2016). Mutations in the genes that encode PI3Kδ (PIK3CD or PIK3R1) lead to the primary immunodeficiency APDS, of which there are two classes depending on the gene harbouring the mutation (APDS1 and APDS2 for PIK3CD and PIK3R1, respectively). APDS1 mutations have thus far been found throughout the primary sequence of p110δ with the majority of cases occurring at the regulatory interfaces between p110δ and its regulatory subunit p85α (Fig. 14).

To understand how these mutations might be mediating the observed activation in patients, the complex regulation of PI3Ks must be considered. The most frequent APDS1 mutation, E1021K, is located in the α11 helix of the regulatory arch (Angulo et al., 2013; Jou et al., 2006; Lucas et al., 2016). The regulatory arch encompasses the catalytic and activation loops, forms important interfaces with the nSH2 and cSH2 domains of the p85-like regulatory subunits, and is a conformationally dynamic structure that also mediates membrane binding (Vadas et al., 2011). Additionally, the site of mutation is within 6Å of the kinase-cSH2 interface that occurs in PI3Kδ and PI3Kβ (Burke et al., 2011; Zhang et al., 2011). The second most common APDS1 mutation is E525K, which is situated in the helical domain at the helical-nSH2 interface (Huang et al., 2008; Miled et al., 2007). Another common APDS1 mutation, N334K, occurs in the C2 domain near the C2-iSH2 interface. APDS1 mutations have thus far corresponded to activating oncogenic mutations in PIK3CA, the p110α isoform that is ubiquitously expressed (Jaiswal et al., 2009; Samuels et al., 2004). These similarities could be driven through the same factor, that mutations in class IA PI3Ks lead to disruption of key inhibitory interfaces or lead to conformational changes that mimic the natural activation of PI3Ks.

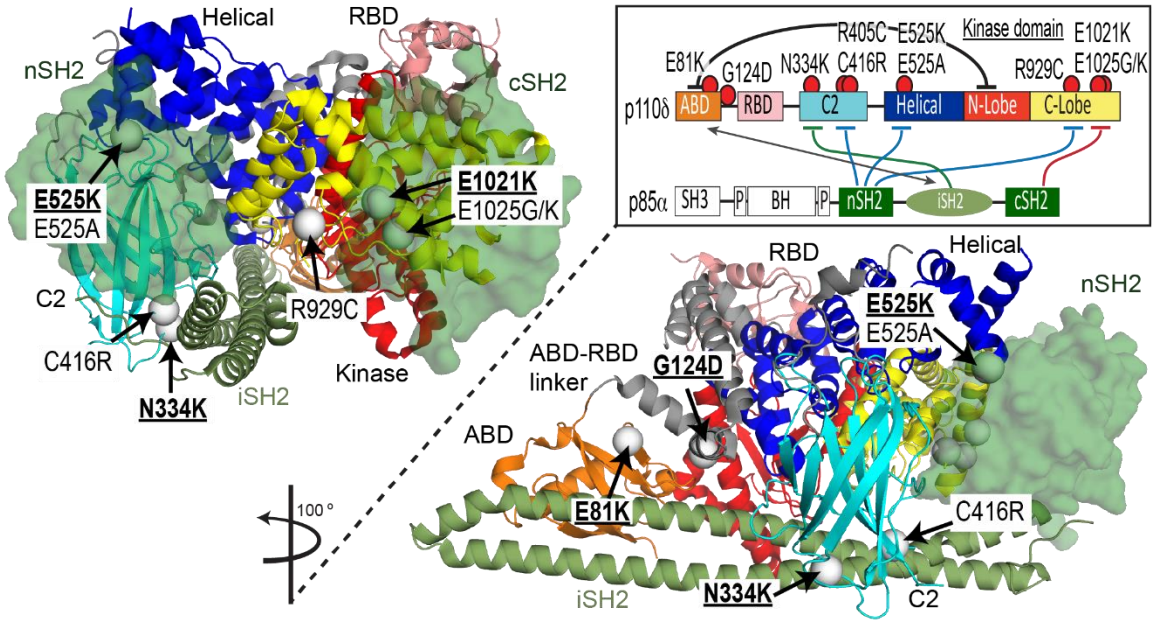

Figure 14: APDS1 mutations occur throughout the primary sequence of the catalytic subunit p110δ.

The location of all APDS1 mutations in p110δ reported to date are mapped on a model of the PI3Kδ (p110δ/p85α) complex (PI3Kδ structural model prepared as reported in Chapter 2: Methods). The nSH2 and cSH2 are shown in transparent surface representation, with APDS1 mutations shown as white spheres. A domain schematic of p110δ/p85α is included with inhibitory interfaces highlighted and all identified APSD1 mutations shown as red spheres. Mutations that are underlined on the structural model indicate those studied in this chapter.

Investigations into the molecular mechanisms of regulation in class IA PI3Ks and other large, dynamic enzymes have previously led to an expanded understanding of the complex regulatory network of the two subunits p110 and p85. The oncogenic isoform p110α and binding partner p85α are two of the most mutated genes in cancer (Jaiswal et al., 2009; Lawrence et al., 2014; Samuels et al., 2004). A panel of these activating mutations was probed using HDX-MS to reveal conformational changes in PI3Kα mutants mimic the natural activation mechanisms (Burke et al., 2012), however, no study has been completed on activating mutations in p110δ. As p110α and p110δ exhibit isoform specific regulatory mechanisms, activating mutations in p110δ could be studied to further understand PI3Kδ specific inhibition and activation.

We set out to identify the molecular mechanisms mediating the activation phenotype of APDS1 mutations in PIK3CD, and to further understand the molecular basis of PI3Kδ regulation. In this study, we use HDX-MS and biochemical assays to probe a panel of APDS1 mutations throughout the primary sequence of p110δ. These include the most common APDS1 mutations: E1021K in the kinase domain, E525K in the helical domain at the helical-nSH2 interface, and N334K in the C2 domain (Fig. 14). Our collaborators from the Lucas lab at Yale also provided us with two APDS1 patient mutations that had not been previously described in the literature. These were at G124D in the ABD-RBD linker region and E81K in the ABD (Fig. 14). Here I have shown that all mutations are activating basally, as well as in the presence of an activating PDGFR pY, and that these mutations mimic the activating mechanisms of corresponding oncogenic mutations found in PIK3CA (p110α). Finally, we show that all PI3Kδ mutants are inhibited by the FDA approved potent and selective p110δ inhibitor Idelalisib. From the biochemical and biophysical analyses of these mutants, we were able to generate a panel of engineered mutations, which revealed novel insight into the regulatory mechanisms by which PI3Ks are regulated. Overall these data on mutations of the p110δ subunit of class IA PI3Ks revealed novel therapeutic strategies for primary immunodeficiency patients with APDS1, as well as approaches to identify novel mutations in primary immunodeficiency mutations.

3.2 Results

Lipid kinase activity of APDS1 mutations

To identify how clinical APDS1 mutations alter the function of the PI3K enzyme and how this leads to an activated PI3K pathway, we characterised the lipid kinase activity of APDS1 mutants. Mutant and WT proteins were prepared as described in Chapter 2: Material and Methods. In brief, WT and mutant p110/p85 heterodimers were produced through baculovirus mediated protein expression and purified using standard affinity and chromatography purification techniques. All proteins were produced in the same manner, with a single chromatographic peak eluting at roughly the same time from the size exclusion chromatography column indicating that mutants do not disrupt the overall fold of the WT heterodimer. The studied APDS1 mutations include three previously described

mutations as well as two mutations that had not previously been attributed to APDS1 (Fig. 14). The previously described mutations occur in the C2 domain (N334K), the helical domain (E525K), and the kinase domain (E1021K) (Lucas et al., 2016). The N334K and E525K mutations occur in known regulatory interfaces, where N334K is at the C2-iSH2 interface and E535K is at the helical-nSH2 interface. E1021K is located at the catalytically important C-terminus of the kinase domain near the lipid-binding region and the kinase-cSH2 inhibitory interface with p85α. The patient mutations that had been newly identified in APDS1 were located in the N-terminal region of the p110δ subunit within the ABD (E81K) and the ABD-RBD linker (G124D). Carrie Lucas' lab at Yale identified these mutations and characterised the T-cells of the patients to reveal that these cells had an activated PI3K pathway (Takeda et al., 2017). Both mutations occur near the ABD-kinase interface, providing a potential mechanism for activation as these mutations could lead to conformational changes that disrupt this interface. Additionally, these mutations correspond to oncogenic mutations found in PIK3CA, the p110α subunit (Chalhoub and Baker, 2009; Samuels et al., 2004).

Lipid kinase activity of WT and APDS1 mutants was measured in the absence (basal) or presence (+pY) of a stimulating RTK phosphopeptide derived from the platelet derived growth factor receptor (PDGFR) and in the presence of a negatively charged membrane substrate which is the optimal substrate for class IA PI3Ks (95% PS, 5% PIP2). The specific activity was then normalised against WT basal activity to yield a fold-increase in activity compared to WT basal.

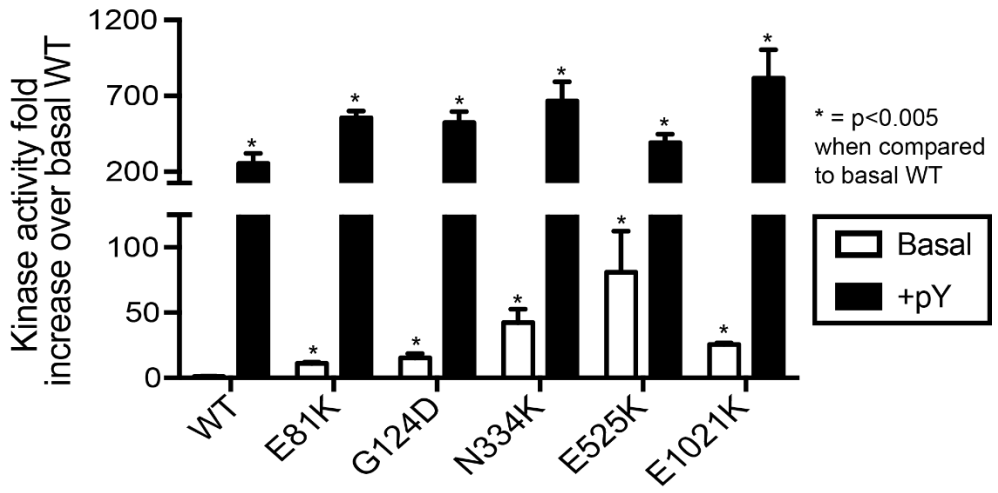

Figure 15: APDS1 p110δ mutants lead to increased basal and PDGFR pY-activated lipid kinase activity compared with WT.
Fold activation of APDS1 mutations in p110δ in the presence (+pY) or absence (basal) of a stimulating RTK-derived phosphopeptide. Assays measured the production of ADP in the presence of 0.1–100 nM of enzyme, 100 μM ATP, and 5% PIP2/95% PS vesicles. Kinase assays were performed in triplicate (error shown as SD; n = 3). The differences between the mutant PI3K activity and the WT were assessed using standard student's T-test. All differences with a $p<0.05$ were considered significant. All conditions with a * were compared to basal WT. Mutant PI3K +pY condition was also compared to WT +pY and all comparisons had $p<0.05$ values. Adapted from Dornan et al., 2017 and Takeda et al., 2017.

The basal lipid kinase activity (−pY) of all APDS1 mutants results in a significant activation ($p<0.05$) compared with WT, with E525K showing the highest level of activation (~60-fold), followed by N334K (~40-fold). E1021K and G124D were activated to ~20-fold compared to WT, while E81K showed the lowest level of activation at ~10-fold (Fig. 15). The activation of basal lipid kinase activity by p110δ mutants is very similar to the activation of p110α by oncogenic mutations in similar positions (Burke et al., 2012) with the exception of E1021K, which is not as potently activated as the H1047R mutation in p110α. The E525K mutant likely disrupts the inhibitory interface between the nSH2 and the p110δ helical domains, mimicking activation downstream of PDGFR pY stimulation, so it would be expected that this mutation would cause the largest increase in activity. The equivalent position in p110α, E545K, leads to full activation, and no further stimulation is achieved by the addition of PDGFR pY. The lack of full activation in p110δ with E525K is consistent with the additional inhibitory cSH2–kinase domain interface present in p110δ

that is perhaps unaffected by this mutation, as suggested by our results (Burke et al., 2011; Burke and Williams, 2013).

Both the APDS1 mutants and WT PI3Kδ were activated by PDGFR pY, with all APDS1 mutants being hyperactivated compared with WT (Fig. 15). The highest level of hyperactivation was shown by E1021K at ~3-fold. The C2 mutant N334K and the N-terminal mutants E81K and G124D were hyperactivated by ~2-fold, while E525K was the least hyperactivated at ~1.5-fold. The overall trend in activation of RTK-stimulated activity of PI3K by APDS1 mutants closely matches the results for oncogenic mutations in p110α; however, a much lower activation fold was displayed by E1021K in p110δ compared with the similar H1047R mutation in p110α (Burke et al., 2012). Additionally, E525K still showed hyperactivation in the presence of the PDGFR pY whereas the corresponding oncogenic mutant in p110α, E545K, showed no further activation. This could correspond with the cSH2-kinase domain interface still remaining intact and indicating possible differences in natural activation mechanisms.

HDX-MS of WT p110δ/p85α in the presence of PDGFR pY and/or Membranes

To understand how activating mutations mediate their effects, we must first understand the natural activation mechanisms of PI3Ks. In the absence of growth factors, class IA PI3Ks remain inhibited and cytosolic. Upon growth factor stimulation of membrane receptors, class IA PI3Ks are activated. The natural activation of class IA PI3Ks has two stages: (1) binding of SH2 domains to an RTK and (2) binding of the complex to the lipid substrate (Fig. 16). Using HDX-MS, we aimed to identify the conformational dynamics that define the stages of natural activation in PI3Kδ (p110δ/p85α). We measured the deuterium exchange rate of the WT p110δ/p85α across three different time points (3s, 30s, 300s) between three different states: basal (representing the cytosolic, inhibited state), PDGFR pY bound, and membrane bound (Fig. 16). These states were measured with addition and incubation for ~2 min of blank solutions in the basal state, a membrane blank solution and 5 μM PDGFR pY in the RTK activated state, and membrane vesicles that mimic the PM composition (5% PIP2, 30% PS, 50% PE, 15% PC present at 100 μg/mL) in addition to 5 μM PDFGFR pY in the membrane bound state.

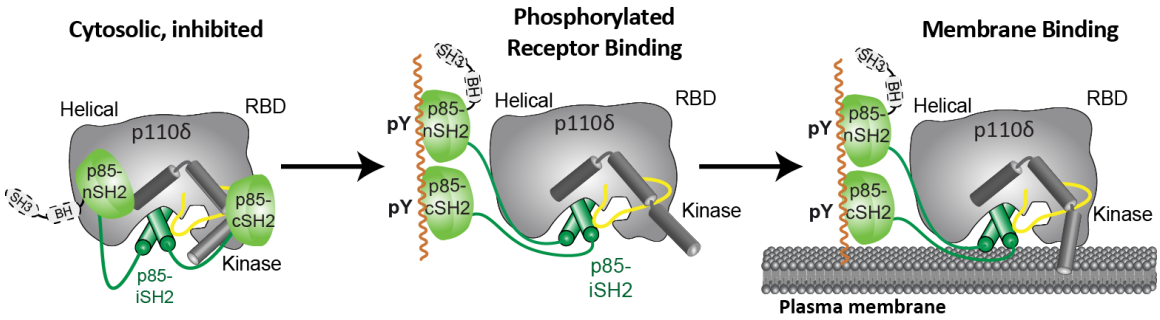

Figure 16: The natural activation mechanism of PI3Kδ.
A cartoon representation of PI3Kδ in the three major stages of natural activation. (Left) In the cytosolic inhibited state, the SH2 domains of the regulatory subunit p85α bind to the catalytic subunit preventing lipid kinase activity. Both SH2 domains are bound to the catalytic isoform p110δ. (Middle) In the presence of phosphorylated RTKs and their adaptors, the SH2 domains of p85α bind to pYXXM motifs and break the inhibitory interactions with the catalytic subunit. (Right) After SH2 mediated recruitment to pYXXM motifs of receptors, class IA PI3Ks bind to its lipid substrate PIP_3 at thePM.

Dynamic changes in WT p110δ/p85α upon PDGFR pY activation

Addition of PDGFR pY led to observed changes in deuterium exchange at the expected SH2 interfaces and at regions distant to PDGFR pY binding, similar to previous HDX-MS studies of PI3Kδ and PI3Kα (Burke et al., 2012, 2011) (Fig.4A,C,D). Both the nSH2 and the cSH2 exhibited decreases in deuterium exchange at regions that surround the previously defined PDGFR pY-nSH2 interface (Nolte et al., 1996). Structures showing nSH2-helical and cSH2-kinase interfaces reveal a differential SH2 interface, where the nSH2 FLVR (PDGFR pY binding motif) is pointed inward towards the catalytic subunit and the cSH2 FLVR is pointed outward (Huang et al., 2007; Zhang et al., 2011). The cSH2 contacts the kinase at a region separate from PDGFR pY binding (681-687), and this region shows increased exchange upon addition of PDGFR pY as this interface is broken and those residues are no longer protected from exchange through hydrogen bonding. This increase in exchange was not detected in p85α when in complex with p110α, consistent with a lack of cSH2-catalytic interface (Burke et al., 2011). Throughout the rest of the regulatory subunit were large increases in exchange observed throughout the iSH2 coiled-coil. These increases were primarily distant to the iSH2-ABD interface and situated at the coiled-coil interface (444-456), the iSH2-C2 interface (467-476, 556-570), the nSH2-iSH2

interface (571-581), and where the iSH2 interfaces with the activation loop of the kinase domain (582-596).

The helical domain (524-529) and kinase domain (1023-1044) also exhibit these increases in exchange due to a breaking of their SH2 interfaces. As the cSH2-kinase interface is broken upon PDGFR pY binding, the catalytic arch in the kinase domain is no longer "clamped" in to a closed, inhibited conformation (Vadas et al., 2011). The regulatory arch exhibited increases in exchange (1023-1044), likely indicating an opening up of the helices. The regulatory arch is also critical for kinase activity, and deletion of this region abolishes kinase activity in p110δ and in the class III PI3K VPS34 (Burke et al., 2011; Miller et al., 2010). The activation loop mediates lipid substrate binding and increases in deuterium exchange (920-935) were observed in region distal to the DFG motif. Increases in exchange at the helical-nSH2 interface were previously observed in both p110δ and p110α, however increases in the activation loop and the regulatory arch were only seen in p110δ/p85α (Burke et al., 2012, 2011). All data described here are consistent with previous findings showing that the PDGFR pY acts to break inhibitory interfaces.

Dynamic changes in WT p110δ/p85α upon binding membranes

In the presence of both the PDGFR pY and a vesicle membrane that mimics PM composition, further changes in deuterium incorporation are observed in both catalytic and regulatory subunits (Fig. 17A-D). Two regions of the kinase domain undergo decreased deuterium incorporation (850-856, 1023-1044). Region 850-856 has previously been proposed to participate in membrane binding, and this decrease in exchange would support that as participation in bonding networks leads to a decrease in deuterium exchange rates (Burke et al., 2011; Huang et al., 2007). The C-terminal region (1023-1044) is at the catalytic arch, where upon binding the lipid substrate the C-terminal region tucks inward (Vadas et al., 2011). Additionally, minor decreases in exchange were observed in the activation loop (920-935). Interestingly, there were no large decreases in exchange observed at regions covering the DGF motif in the activation loop as was reported previously for membrane binding of PI3Kδ (Burke et al., 2011). Decreases in exchange at

this region did not meet our significance threshold, potentially due to differences in experimental setup and equipment. Finally, further decreases in exchange were observed in the nSH2 domain (414-420), indicating a potential nSH2-membrane binding interface.

At the ABD and the ABD-RBD linker regions (71-96, 120-127) we observed increases in exchange, consistent with previous reports(Burke et al., 2012, 2011) in both p110δ/p85α and p110α/p85α (Fig. 17B-D). Increases in exchange of the ABD-RBD linker region were not observed in PI3Kδ previously, although this appears to be due to a lack of peptide coverage at this region (Burke et al., 2011). Further increases in exchange were also observed in the iSH2-C2 region (467-476, 556-570), indicating that membrane binding further promotes disruption of inhibitory interfaces.

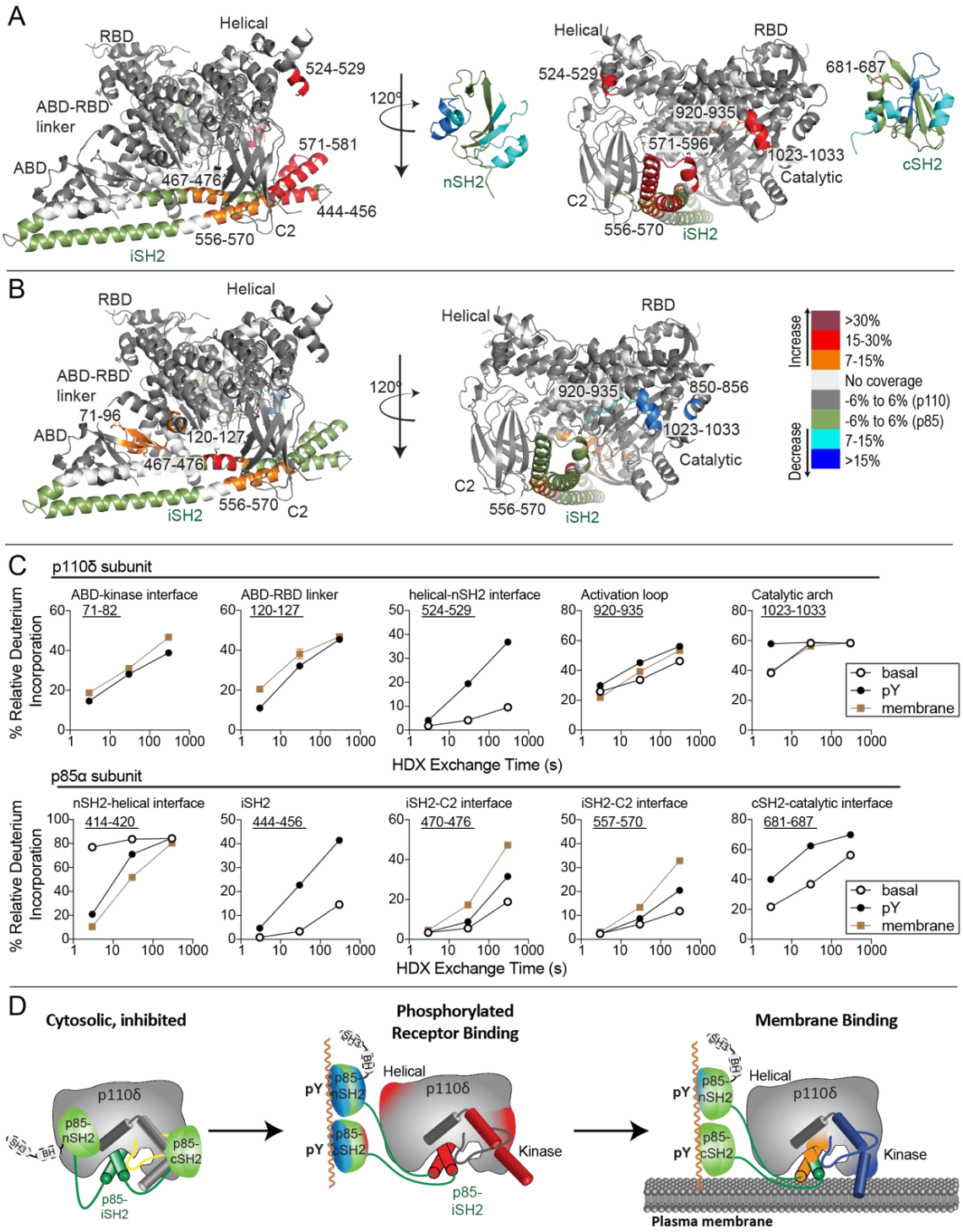

Figure 17: Dynamic changes that occur in WT PI3Kδ during the natural activation mechanism.

(A) Peptides in p110δ and the iSH2 of p85α that showed differences in HDX both greater than 0.7 Da and 7% with an unpaired T-Test value of $p<0.05$ between the basal and pY-activated WT or (B) between the pY-activated WT with and without membranes, are highlighted on both the structure of p110δ /iSH2-p85α (PDB: 5DXU) and on a schematic

as in Fig. 16. Upon pY binding to the nSH2 and cSH2 of p85α, there were increases in exchange seen in the helical domain interface with the nSH2, the kinase domain interface with the cSH2, as well as the S9 activation loop. Upon membrane binding, the catalytic domain showed increases in exchange in the ABD domain at the interface with the kinase domain, the ABD-RBD linker, as well as regions of both the C2 and iSH2 domains at the C2/iSH2 interface. Decreases in exchange were observed in the putative membrane-binding surface in the activation loop and kα11 helix of the kinase domain. (C) Time course of deuterium incorporation for a selection of peptides in both p110δ and p85α that showed differences in HDX either upon pY or membrane addition (or both). (D) Cartoon schematic highlighting changes in deuterium exchange that occur in the different stages of PI3Kδ natural activation. Adapted from Dornan et al., 2017.

HDX-MS of the APDS1 mutants

To understand the molecular basis for how APDS1 mutations in the catalytic subunit of p110δ modify the dynamic regulation of p110δ/p85α to mediate activation, we carried out HDX-MS experiments. For four mutants including E81K, G124D, E525K, and E1021K, we used HDX-MS to compare the basal states of the WT to the mutants. HDX-MS of G124D, E525K and E1021K mutants compared to WT were carried out in three states: basal, PDGFR pY-activated, and PDGFR pY-activated bound to membranes. The full set of peptides and their corresponding deuterium incorporation data for both p110δ and p85α under all conditions and time points is shown in Appendix A.1, Figs. A1.1 (N-terminal mutants in the basal state only) and A1.2 (all APDS1 mutants except E81K, in all conditions), with differences between states for highlighted peptides shown in Appendix A.1, Fig A1.3 (Shown for all APDS1 mutants except E81K and under all conditions). The differences in exchange between WT PI3Kδ and APDS1 mutants showed that APDS1 mutants mimic and enhance conformational dynamics seen in the activation of the WT enzyme (Fig. 18-20, 9-10, 11-12), a mechanism that is similar to the activation of p110α by oncogenic mutations (Burke et al., 2012).

HDX-MS of the E81K mutant in the ABD

To identify conformational changes that would describe the basal activation observed in E81K lipid kinase activity, HDX-MS was used to compare the WT and E81K mutant (Fig. 18A). An increase in exchange was observed in the ABD-RBD linker region

of p110δ (residues 102-120). Increased flexibility in the ABD-RBD linker region is associated with the natural activation state of WT PI3Kδ upon membrane binding. This small change and the lack of changes in deuterium exchange in the nSH2-helical, the C2-iSH2, and the cSH2-kinase likely explain the minor activation seen in the E81K mutant. These changes are also similar to the changes previously observed between the WT and oncogenic G106V mutant in p110α, which is also located in the ABD. This mutant lead to an increase in exchange in the p110α subunit at residues 100-119 (Burke et al., 2012). Although the E81K mutant was only assayed through HDX-MS in the basal context, the lack of disruption between the SH2 interfaces also likely accounts for the ability of the mutants to be activated upon PDGFR pY stimulation.

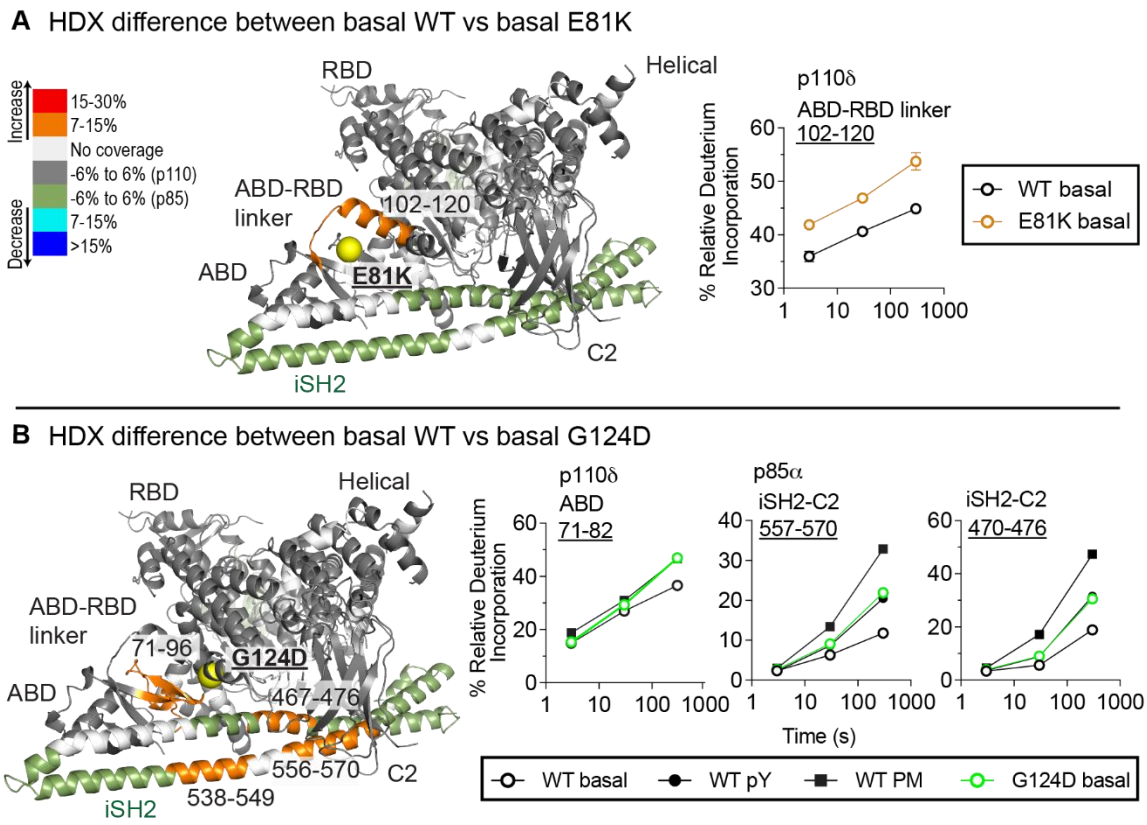

Figure 18: HDX-MS of the basal state of N-terminal APDS1 mutants compared to the basal state of WT PI3Kδ.

(A) HDX-MS of the E81K mutation in the ABD. HDX differences of δ-E81K compared with WT p110δ of greater than 0.7 Da and 7% deuterium incorporation and with an unpaired T-Test value of $p<0.05$ mapped onto the structural model of p110δ. Time course of deuterium incorporation for a representative peptide in p110δ with differences in HDX in the APDS1 N-terminal mutant p110δ-E81K (error shown as SD; n = 3). (B) HDX-MS of the G124D mutation in the ABD-RBD linker. HDX differences of N-terminal PIK3CD patient mutation p110δ-G124D mutant compared with WT p110δ of greater than 0.7 Da and 7% deuterium incorporation and with an unpaired T-Test value of $p<0.05$ mapped onto the structural model of PI3Kδ. Time course of deuterium incorporation for representative peptides in both p110δ and p85α with differences in HDX in the N-terminal p110δ-G124D mutant (error shown as SD; n = 3). Adapted from Takeda et al., 2017.

HDX-MS of the G124D mutant in the ABD-RBD linker

The G124D mutation occurs near the ABD-kinase inhibitory interface (Fig. 14), and this residue potentially leads to a steric clash with T76 in the ABD which could disrupt the ABD-kinase interface. To determine the mechanisms mediating G124D activation, the

basal state of the G124D mutant was also studied using HDX-MS and compared to WT p110δ/p85α (Fig. 18B). This mutation led to increases in deuterium exchange in both the catalytic and regulatory subunits. The increase in deuterium exchange in p110δ was within the ABD (residues 71-96). The changes observed in the regulatory subunit p85α occurred in the iSH2 domain (residues 467-476, 538-549, & 556-570). The 556-570 residues correspond to the iSH2-C2 interface and 467-476 is the coiled-coil pair interface of 556-570. Increases in exchange at these regions are observed in the natural activation mechanism for WT p110δ/p85α. These increases in deuterium exchange occur both in the PDGFR pY stimulated state and the membrane bound state, with the iSH2-C2 interface peptides exhibiting increases in both states. However, the changes observed in the natural activation are larger than the basal mutant and other key interfaces in the G124D mutant, including the nSH2-helical and the cSH2-kinase, exhibit no changes in deuterium incorporation indicating that they are likely still intact. Combined, this would explain the relatively minor activation seen in the lipid kinase activity of G124D in the basal state and how G124D mutant is still capable of PDGFR pY stimulation.

HDX-MS of the G124D mutant in the presence of stimulating PDGFR pY

HDX-MS was also conducted on the G124D mutant in the PDGFR pY stimulated state and the membrane bound state (Fig. 19A-B). Overall, the changes observed were similar to that of the WT p110δ/p85α upon PDGFR pY stimulation and membrane binding. PDGFR pY leads to decreases in exchange observed at both the nSH2 and cSH2 domains where PDGFR pY peptides have been shown to bind (Nolte et al., 1996) and increases in exchange were observed throughout the iSH2, at the helical-nSH2 interface (p110δ: 524-529), and in the regulatory arch of the kinase domain (p110δ: 1023-1044). The G124D mutant exhibited unique increases in deuterium exchange in the p110δ subunit upon PDGFR pY binding. One of these increases was observed at the C2-iSH2 interface (328-337). Further increases were observed in a region of the kinase domain that undergoes decreased exchange upon membrane binding (850-856) as well as a helix within binding distance of this region (830-836). These regions are within 6 Å of the regulatory arch and the catalytic loop, a region of the kinase domain that undergoes conformational changes upon PDGFR pY binding as the kinase domain switches to an open conformation (Vadas

et al., 2011). Further increases in deuterium exchange were also observed in the catalytic loop (908-919), and increases in deuterium exchange of the activation loop (920-935) and the regulatory arch (1023-1033) were extended compared to the WT enzyme. These changes together represent conformational allosteric changes in the WT enzyme that are enhanced in the mutant.

HDX-MS of the G124D mutant in the presence of stimulating PDGFR pY and membrane

Upon membrane binding, the G124D mutant showed overall similar trends of exchange when compared to the WT PI3Kδ (Fig. 19A, C). Interestingly, changes in deuterium incorporation in regions of p110δ associated with membrane binding were larger and more extensive in the G124D mutant compared with WT (840-856, 908-935, 978-989, 998-1002, 1023-1033). The only changes in deuterium incorporation observed in the membrane bound state of G124D were in the nSH2 domain (414-420). In the G124D mutant, the p85α subunit lacked the increases in deuterium exchange observed throughout the iSH2 in the WT enzyme. As these regions underwent increases in deuterium incorporation in the basal state, and the increases upon PDGFR pY binding were larger than that of the WT, it is possible that these regions have already undergone the full extent of conformational changes.

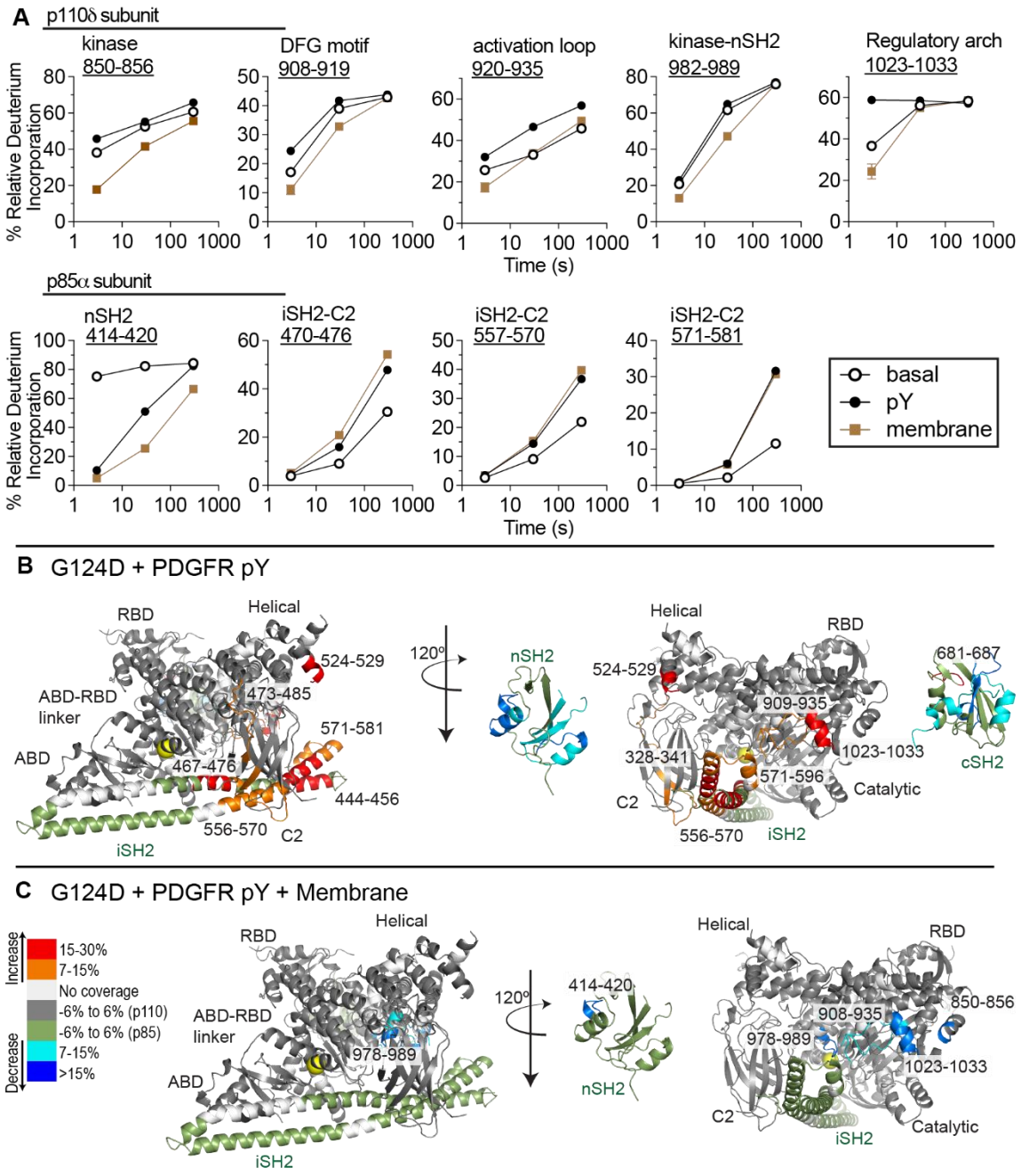

Figure 19: HDX-MS of the G124D mutation in the ABD-RBD linker upon PDGFR pY stimulation and membrane binding.

(A) Time course of deuterium incorporation for a selection of peptides in both p110δ and p85α with differences in HDX in the APDS1 N-terminal mutant G124D (error shown as SD; n = 3). (B) HDX differences greater than 0.7 Da and 7% deuterium incorporation and with an unpaired T-Test value of $p<0.05$ in G124D bound to 5 uM PDGFR pY compared to G124D basal state. (C) HDX differences greater than 0.7 Da and 7% deuterium incorporation and with an unpaired T-Test value of $p<0.05$ in G124D bound to 5 uM

PDGFR pY and PM mimic vesicles (5% PIP2, 30% PS, 50% PE, 15% PC present at 100 µg/mL) compared to G124D bound only to 5 uM PDGFR pY. Adapted from Takeda et al., 2017.

Engineered mutations of the ABD and ABD-RBD linker region

To fully understand the structural mechanism of the N-terminal mutants mediating the conformational disturbances of p110δ/p85α, we used existing structural data to predict mutations that might mimic or rescue the disruption caused by APDS1 mutations in the ABD and ABD-RBD linker (Fig. 20A). The K111 residue within hydrogen bonding distance of E81 could lead to a charge/charge repulsion upon mutation of glutamic acid to lysine. Mutation of the glycine at residue 124 to the bulkier aspartic acid appears to confer a potential steric clash with the threonine at residue 76. Both these instances might disrupt the positioning of the ABD-RBD linker with relation to the ABD domain, which forms a highly stable interaction with the iSH2 (Yu et al., 1998b). Residue K111 is also a site for existing activating oncogenic mutations identified in the COSMIC database (K111E, K111N, K111, & K111Q) and K111E was previously shown to activate WT p110α/p85α activity (Burke et al., 2012; Forbes et al., 2016). To test this hypothesis, we conducted an extended mutagenesis screen of kinase activity to determine whether we could "rescue" WT activity (Fig. 20B). The oncogenic mutations K111E, K111Q, and T76G were produced alongside double mutants E81K-K111E and T76G-G124D. If we were correct that these residues are disrupted, then the double mutants should relieve the charge/charge repulsion or steric clash and lead to a reduction to WT or near WT kinase activity levels.

All single mutants lead to activation over WT p110δ/p85α activity, however to a lesser extent than the APDS1 mutations (<5 fold activation). This aligns with data showing activation of the K111E mutation in p110α (Burke et al., 2012). K111Q is a previously defined oncogenic mutation in p110α, and many mutations in p110α are activating (Zehir et al., 2017). Thus, it would be predicted to also lead to an activation of kinase activity in the p110δ isoform. T76 has not been previously identified as oncogenic in any p110 isoforms nor as an APDS1 mutation. The E81K-K111E double mutant showed the same activity as the E81K single mutation, with no significant differences. The T76G-G124D

double was also unable to relieve the activation observed in either the single mutants. These results indicate that either we were incorrect in our predictions. Additionally, this shows evidence that the ABD-RBD linker region is exquisitely sensitive to precise conformations, and that only a small subset of conformations exist that preserve the inhibited state of PI3Ks.

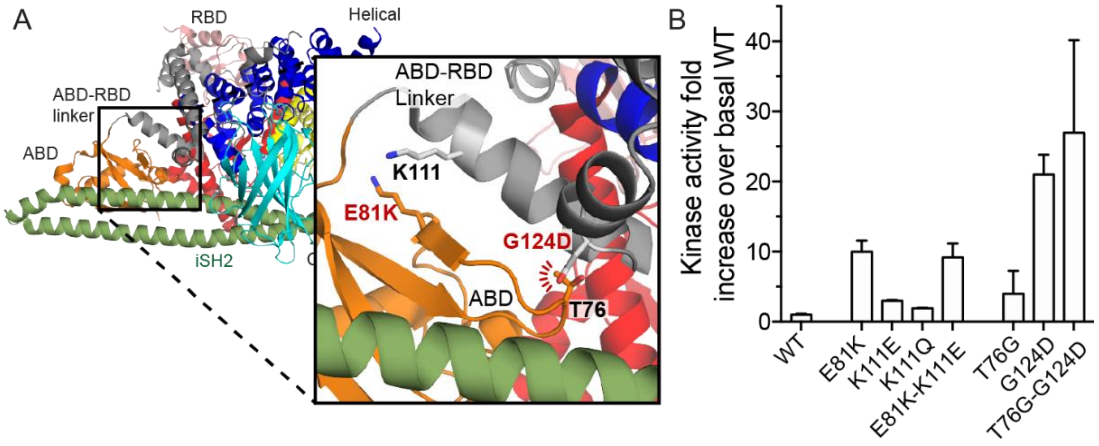

Figure 20: Structural analysis of N-terminal APDS1 mutations.
(A) The Structural environment of the N-terminal APDS1 mutations E81K and G124D. Zoomed-in view of mutant residues, where E81K likely leads to a charge/charge repulsion of the K111 residue and with a putative steric clash between G124D and T76 in red. PI3Kδ structural model prepared as reported in Chapter 2: Methods. (B) Kinase activity of single and double mutants. Fold activation of APDS1 mutations and putative binding residue mutants in p110δ under basal, unstimulated condition. Assays measured the production of ADP in the presence of 0.1–100 nM of enzyme, 100 μM ATP, and 5% PIP2/95% PS vesicles. Kinase assays were performed in triplicate (error shown as SD; n = 3). Unpaired T-Test comparisons between WT and mutants were performed and yielded $p<0.01$ for all differences. This statistical measure was also applied to compare the single mutants to the double mutant, yielding $p<0.01$. Adapted from Takeda et al., 2017.

HDX-MS of the E525K mutant in the helical domain

HDX-MS comparing the basal state of WT and E525K showed increases in exchange at both sides of the helical-nSH2 interface (p110δ:524-529; p85α:372-380; Fig. 21). A further increase was also seen in 444-456 of p85α. These data, combined with activity data showing a large basal hyperactivation over WT p110δ/p85α, indicate that the nSH2-helical interface is likely broken. These increases are similar to the changes seen in

PDGFR pY-binding HDX-MS experiments for both WT PI3Kδ and WT PI3Kα (Burke et al., 2012). No changes were seen at the cSH2-kinase interface, indicating that the interface is still intact as expected from the lipid kinase activity measurements where the E525K mutant was still capable of PDGFR pY stimulation.

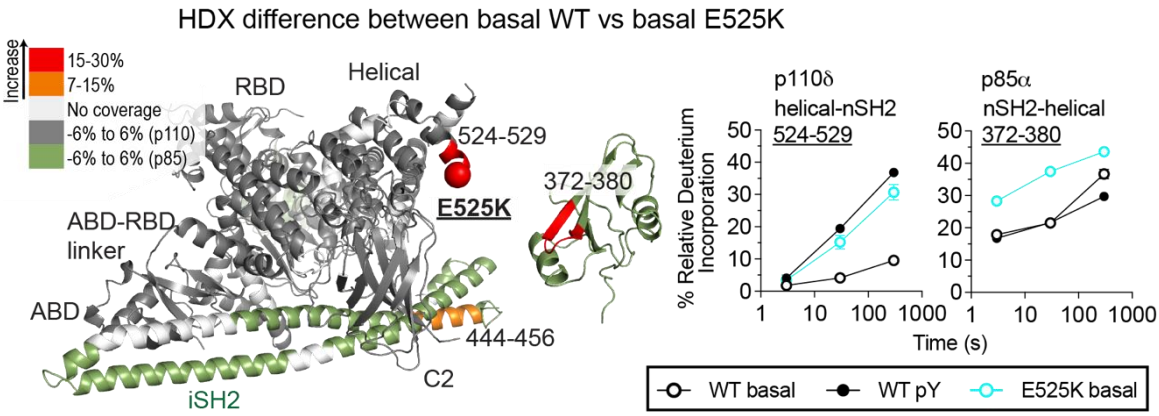

Figure 21: HDX-MS of the basal state of helical APDS1 mutant compared to the basal state of WT PI3Kδ.

HDX differences between the p110δ-E525K mutant compared with WT p110δ of greater than 0.7 Da and 7% deuterium incorporation and with an unpaired T-Test value of $p<0.05$ mapped onto the structural model of p110δ/p85α. Time course of deuterium incorporation for representative peptides in both p110δ and p85α with differences in HDX in the p110δ-E525K mutant (error shown as SD; n = 3). Adapted from Dornan et al., 2017.

HDX-MS of the E525K mutant in the presence of stimulating PDGFR pY

The deuterium incorporation of E525K upon PDGFR pY binding was compared to the basal state to identify whether the mutation was leading to further conformational changes (Fig 22A, B). Upon PDGFR pY stimulation, E525K exhibited overall similar changes in deuterium incorporation as WT. Of note, the p110δ helical region encompassing the mutation did not undergo further increases in deuterium exchange indicating that the mutation likely fully disrupts helical-nSH2 interface. Decreases in exchange in the nSH2 that are associated with the PDGFR pY binding interface were also larger in the E525K mutant compared to WT (p85α: 333-341, 372-380, & 402-420). 372-380 does not undergo any changes in deuterium exchange in WT, as this region goes from nSH2-helical interface to nSH2-PDGFR pY interface. The other regions are further exposed in E525K due to the

disruption of the nSH2-helical interface which explains the larger decreases upon PDGFR pY binding.

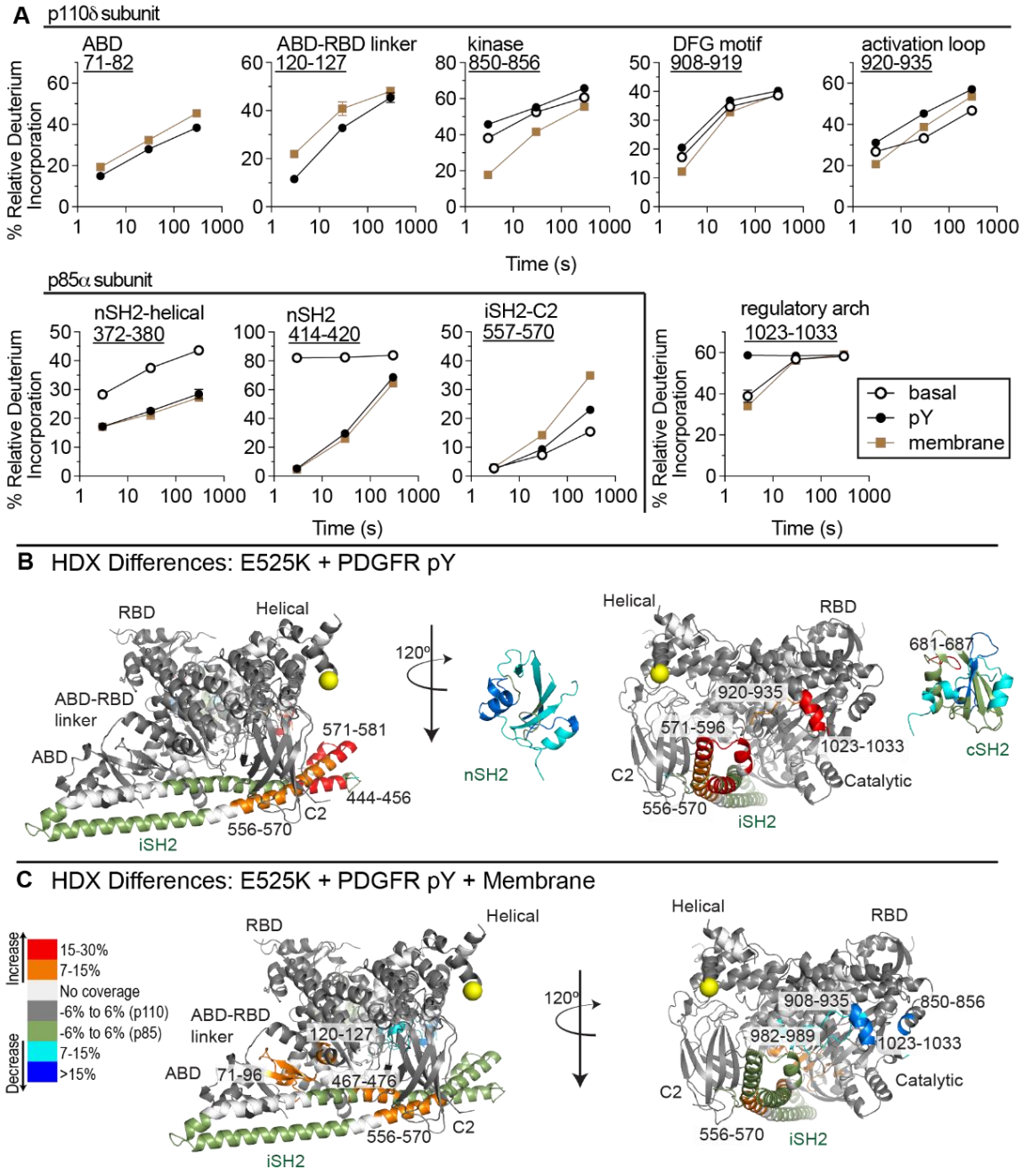

Figure 22: HDX-MS of the E525K mutation in the helical domain upon PDGFR pY stimulation and membrane binding.

(A) Time course of deuterium incorporation for a selection of peptides in both p110δ and p85α with differences in HDX in the APDS1 helical domain mutant E525K (error shown as SD; n = 3). (B) HDX differences greater than 0.7 Da and 7% deuterium incorporation

and with an unpaired T-Test value of $p<0.05$ in E525K bound to 5 uM PDGFR pY compared to E525K basal state. (C) HDX differences greater than 0.7 Da and 7% deuterium incorporation and with an unpaired T-Test value of $p<0.05$ in E525K bound to 5 uM PDGFR pY and PM mimic vesicles (5% PIP2, 30% PS, 50% PE, 15% PC present at 100 µg/mL) compared to E525K bound only to 5 uM PDGFR pY. Adapted from Dornan et al., 2017.

HDX-MS of the E525K mutant in the presence of stimulating PDGFR pY and membrane

The effect of membrane binding on the conformation of the E525K mutant upon membrane binding was determined by comparing deuterium incorporation of E525K bound to PDGFR pY and membrane substrate to incorporation of the pY only state (Fig. 22A, C). Increases in deuterium exchange seen in both the p85α and p110δ of E525K were similar to those seen in the WT PI3Kδ. As with the G124D mutation upon membrane binding, larger and more extensive decreases in exchange were seen throughout the kinase domain of the p110δ subunit of E525K compared to WT (840-856, 908-935, 1023-1044). These decreases in deuterium exchange indicate that regions of the kinase domain are binding more tightly to the membrane substrate and that this could be driving the hyperactivation observed in the PDGFR pY stimulated lipid kinase activity of E525K.

Mutational analysis of the helical-nSH2 interface

E525 on p110δ in the helical region binds with K379 in the nSH2 of p85α to form the nSH2-helical inhibitory interface (Fig. 23A). Mutation of the glutamic acid at residue 525 to a lysine switches the charge state of the reside from negative to positive. This would lead to a charge/charge repulsion of K379, and this potentially disturbs the nSH2-helical interface enough to completely break it. To test this hypothesis, we produced the oncogenic K379E mutation in p85α identified in COSMIC as well as a p110δ-E525K/p85α-K379 double mutant complex (Forbes et al., 2016). A rescue of the WT p110δ/p85α activity would indicate that K379 was the primary residue at the interface disrupted by the APDS1 E525K mutation.

Both single mutations led to hyperactivation over WT p110δ/p85α activity (Fig. 23B). This was expected, based on the kinase activity previously determined (Fig. 15) and as both of these mutations were previously shown to cause hyperactivation in the context

of p110α (Burke et al., 2012). The double mutation appeared to rescue WT p110δ/p85α activity when compared to both the single mutants. This rescue effect indicates that one of the primary residues disrupted by E525K is K379. As the activity was not fully rescued, there are likely further residues that are perturbed by E525K or by K379E although to a lesser extent. Another APDS1 patient was identified with a glutamic acid at 525 mutated to an alanine. This mutation could be mediating activation through another mechanism, where the glutamic acid-lysine salt bridge is required for a strong inhibitory interface and an alanine would reduce or abolish this interface.

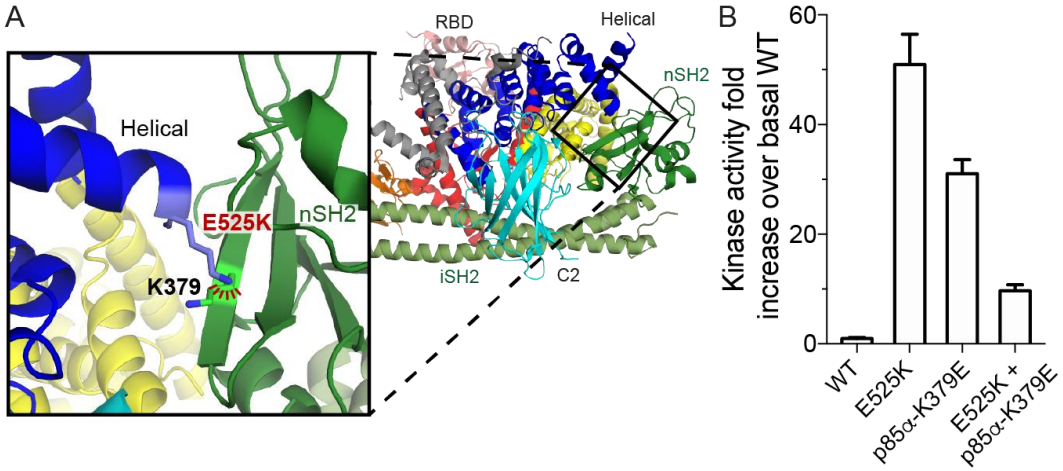

Figure 23: Structural analysis the helical APDS1 mutation.
(A) The Structural environment of the E525K helical mutant. Zoomed-in view of the E525K mutation which is located at the nSH2-helical domain interface, with a predicted charge/charge repulsion between K525 and K379 shown in red. PI3Kδ structural model prepared as reported in Chapter 2: Methods. (B) Kinase activity of single and double mutants. Fold activation of APDS1 mutations and putative binding residue mutants in p110δ under basal, unstimulated condition. Assays measured the production of ADP in the presence of 0.1–100 nM of enzyme, 100 μM ATP, and 5% PIP2/95% PS vesicles. Kinase assays were performed in triplicate (error shown as SD; n = 3). Unpaired T-Test comparisons between WT and mutants were performed and yielded $p<0.01$ for all differences. This statistical measure was also applied to compare the single mutants to the double mutant, yielding $p<0.01$. Adapted from Dornan et al., 2017.

HDX-MS of the E1021K mutant in the kinase domain

The E1021K mutant showed increases in exchange in the C-terminus of the kinase domain (residues 998-1002 & 1010-1019; Fig. 24). These residues reside in the Kα10 and Kα11 helices that are part of the regulatory arch, a structure in the C-lobe of the kinase that locks in the catalytic and activation loops to inhibit catalytic activity. Increases in deuterium exchange in this structure might explain the activated basal activity of E1021K, as increased flexibility might decrease the inhibition of the regulatory arch. An unanswered question for E1021K was whether this mutation also led to disruption of the cSH2–kinase interface, as this mutation is located within 6 Å of the cSH2; however, there were no differences in exchange within the cSH2 between WT and PI3Kδ-E1021K, suggesting that this interface is preserved.

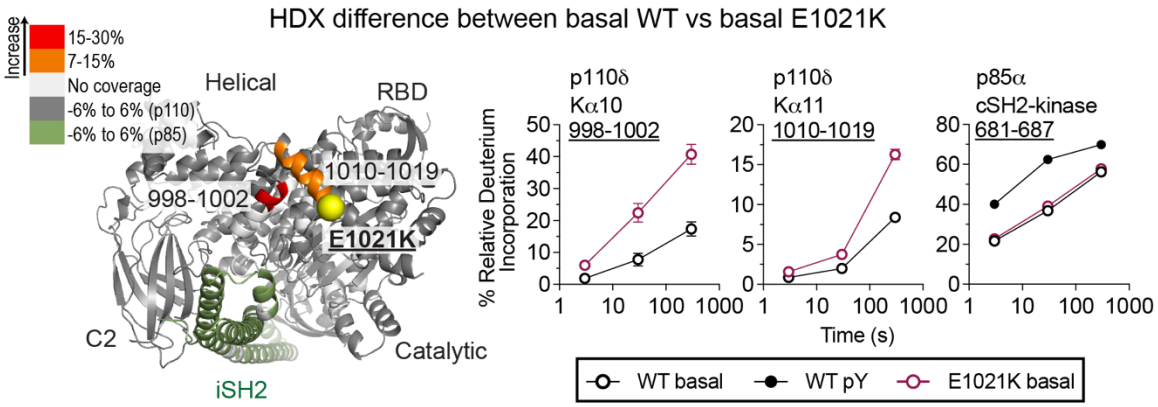

Figure 24: HDX-MS of the basal state of the kinase APDS1 mutant compared to the basal state of WT PI3Kδ

HDX-MS of the p110δ-E1021K mutation in the regulatory arch of the kinase domain. HDX differences between the p110δ-E1021K mutant compared with WT p110δ of greater than 0.7 Da and 7% deuterium incorporation and with an unpaired T-Test value of $p<0.05$ mapped onto the structural model of p110δ/p85α. Time course of deuterium incorporation for representative peptides in both p110δ and p85α with differences in HDX in the p110δ-E1021K mutant (error shown as SD; n = 3). Adapted from Dornan et al., 2017.

HDX-MS of the E1021K mutant in the presence of stimulating PDGFR pY and membrane

The E1021K mutant showed similar trends in the changes in deuterium exchange as the other APDS1 mutants in both the p110δ and p85α subunit in both states, PDGFR pY bound and membrane bound (Fig. 17, 19, 22, 25A-C). E1021K showed the largest decreases in deuterium exchange in the presence of membrane vesicles, indicating that this mutation is driving tighter membrane binding and consistent with previous studies (Fig. 25A, C). E1021K was shown through FRET membrane binding assays to increase binding of the membrane and the similarly located mutation in p110α, H1047R, also exhibits this effect (Angulo et al., 2013; Burke et al., 2012).

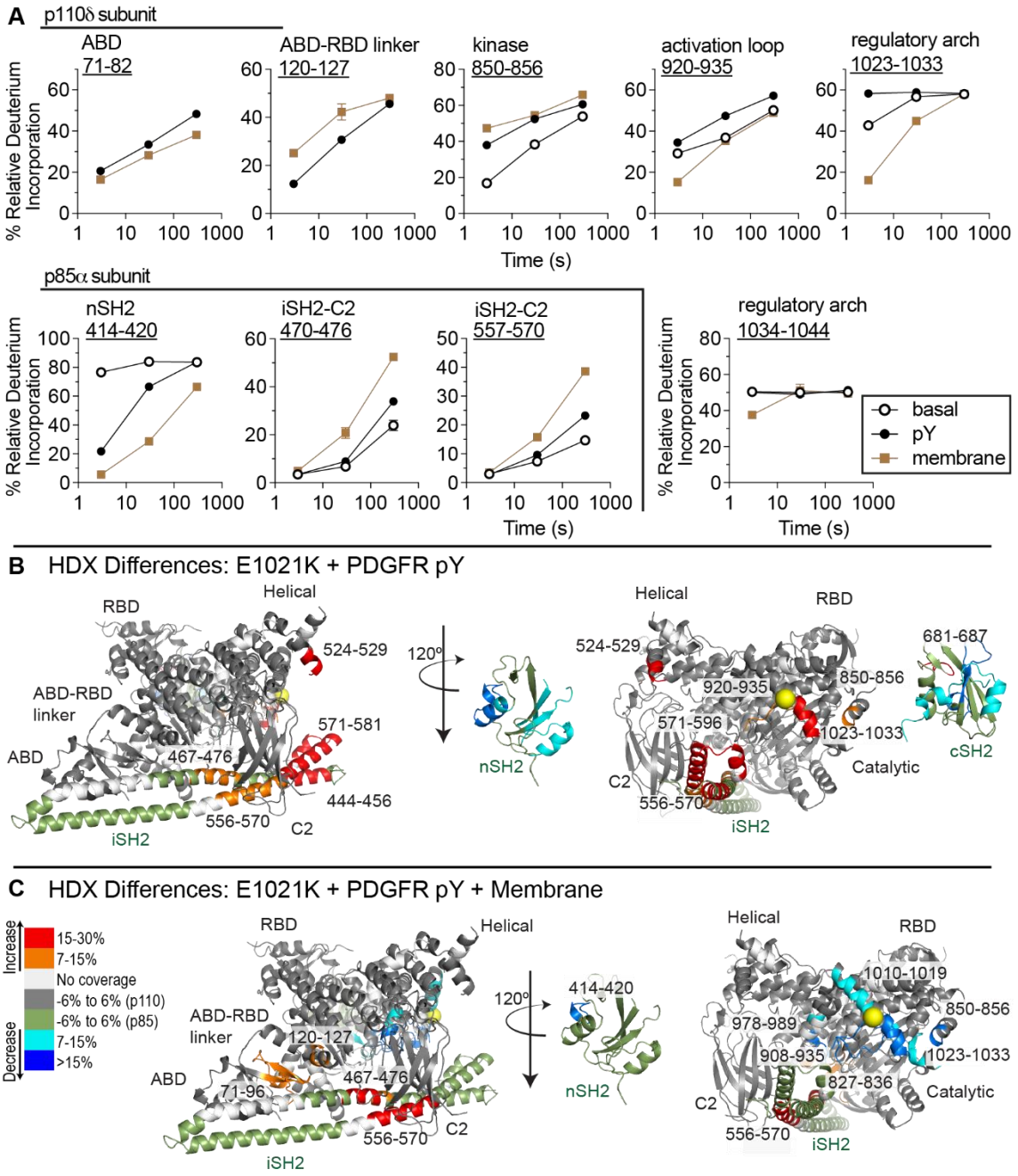

Figure 25: HDX-MS of the E1021K mutation in the helical domain upon PDGFR pY stimulation and membrane binding.

(A) Time course of deuterium incorporation for a selection of peptides in both p110δ and p85α with differences in HDX in the APDS1 helical domain mutant E1021K (error shown as SD; n = 3). (B) HDX differences greater than 0.7 Da and 7% deuterium incorporation and with an unpaired T-Test value of $p<0.05$ in E1021K bound to 5 uM PDGFR pY compared to E1021K basal state. (C) HDX differences greater than 0.7 Da and 7% deuterium incorporation and with an unpaired T-Test value of $p<0.05$ in E1021K bound to 5 uM PDGFR pY and PM mimic vesicles (5% PIP2, 30% PS, 50% PE, 15% PC present at

100 µg/mL) compared to E1021K bound only to 5 uM PDGFR pY. Adapted from Dornan et al., 2017.

Mutational analysis of the regulatory arch

The glutamic acid at residue 1021 is near the histidine at 689 (~6 Å; Fig. 26A). As there were no differences in exchange observed at the cSH2, disruption of this interface appeared to be an unlikely activating mechanism. Over the course of this study, an APDS1 patient with the glutamic acid of 1025 mutated to lysine was also identified (Dulau-Florea et al., 2017). We were interested in the extent of basal activation of WT p110δ/p85α of this mutant as well as whether the double mutant would lead to an additive effect which could be due to different mechanisms of activation. The single mutations at both E1025K and E1021K were activating as expected. The double mutation (E1021K, E1025K) led to a slight increase in activation of E1021K, although it is difficult to tell how much of an additive effect the second mutation imposes. As E1025 is in closer proximity to the cSH2 interface it could be leading to disruption. Mutations in the regulatory arch likely have similar effects to E1021K, in that they are not disrupting SH2 interfaces but leading to conformational changes in the arch that mimic an activated state. It is possible that both mechanisms are occurring in the double mutant, but further inquiry with HDX-MS would be required to determine if this mutant is capable of a similar PDGFR pY disruption as WT p110δ/p85α. Kinase activity to test PDGFR pY would unlikely lead to an answer, as the E1021K mutant is hyperactivating in the stimulated condition over WT p110δ/p85α due to its increased affinity for membrane.

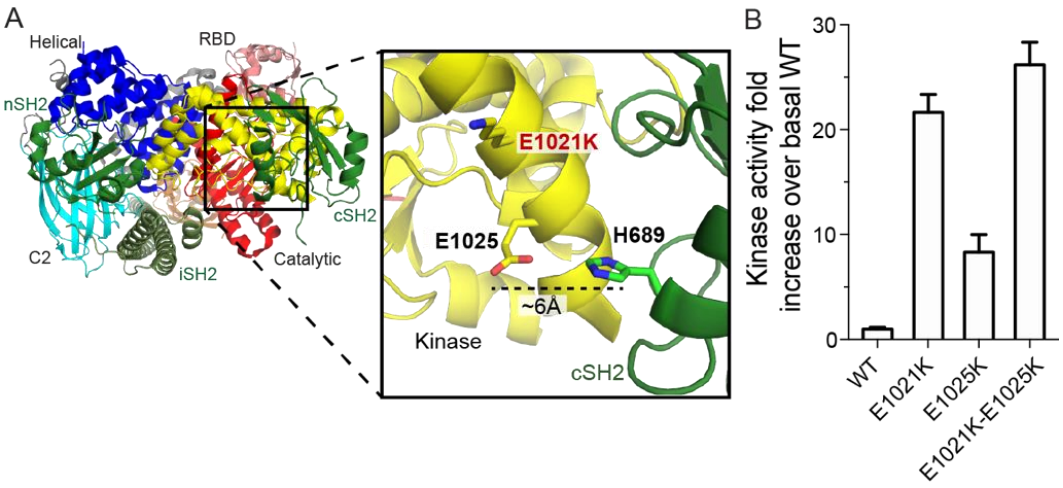

Figure 26: Structural analysis the APDS1 mutation in the regulatory arch of the kinase domain.

(A) The Structural environment of the E1021K kinase domain mutant. The E1021K mutation is located in the C-terminus of the kinase domain, near the cSH2 interface in the kinase domain. Zoomed-in view of the E1021K mutation which is located in the regulatory arch, where it is in close proximity to the H689 residue of p85α. The APDS1 mutations E1025K and E1025G are located closer to H689 of the cSH2, potentially disrupting the cSH2-kinase interface. PI3Kδ structural model prepared as reported in Chapter 2: Methods. (B) Kinase activity of single and double mutants. Fold activation of APDS1 mutations and putative binding residue mutants in p110δ under basal, unstimulated condition. Assays measured the production of ADP in the presence of 0.1–100 nM of enzyme, 100 μM ATP, and 5% PIP2/95% PS vesicles. Kinase assays were performed in triplicate (error shown as SD; n = 3). Unpaired T-Test comparisons between WT and mutants were performed and yielded $p<0.01$ for all differences. This statistical measure was also applied to compare the single mutants to the double mutant, yielding $p<0.01$. Adapted from Dornan et al., 2017.

APDS1 mutations in PI3Kδ are potently inhibited by the PI3Kδ specific inhibitor Idelalisib

To determine if conformational differences identified in APDS1 mutants of PI3Kδ would lead to differential inhibition by ATP competitive kinase inhibitors, we carried out lipid kinase assays in the presence or the absence of the clinically approved PI3Kδ inhibitor idelalisib (Somoza et al., 2015). All APDS1 mutants in p110δ exhibited ~4 fold higher IC50s compared to WT but were all capable of full inhibition (Fig. 27), indicating that all might be targetable by idelalisib and similar small molecule inhibitors.

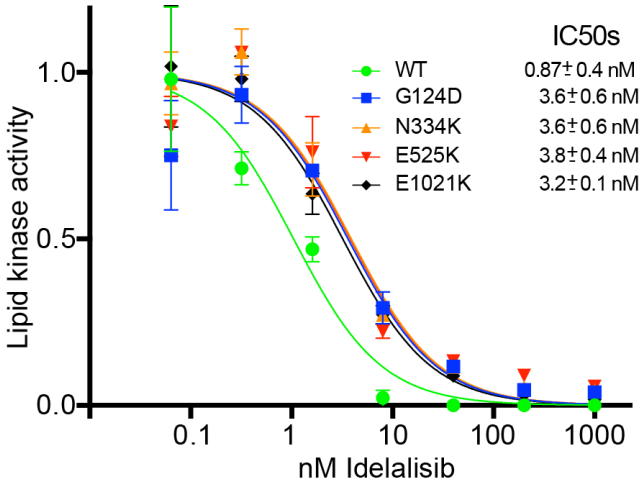

Figure 27: Inhibition of WT and APDS1 mutants by the potent PI3Kδ inhibitor Idelalisib.
Lipid kinase activity was normalised to kinase activity in the absence of inhibitors. IC_{50} values were generated from triplicate independent inhibitor dilutions, and error is shown as SD. Adapted from Dornan et al., 2017.

3.3 Discussion

APDS1 mutations occur in the PIK3CD gene, which encodes the p110δ catalytic isoform that is part of the PI3Kδ heterodimer complex. To summarise, all APDS1 mutants were hyperactivated compared to WT PI3Kδ in both the basal state and the PDGFR pY activated state. Previous studies have linked APDS1 mutations to the phenotype by showing an activated PI3K/AKT pathway in patient lymphocytes. The E1021K mutation was previously the most characterised, showing hyperactivation of the enzyme and increased membrane binding through lipid kinase and lipid FRET assays (Angulo et al., 2013). This study also showed for the first time that an APDS1 mutant can be inhibited by idelalisib to a similar level of WT. What has been lacking in the field is a more comprehensive study of the mechanisms of APDS1 mutant activation of PI3Kδ. Understanding how these mutations mediate the activation phenotype which leads to severe immunodeficiencies is key to further understanding PI3Kδ physiological role and for the development of novel therapeutics.

All APDS1 mutations led to hyperactivation. Our data complements previous data on E1021K, as deuterium exchange experiments on this mutant in the presence of PDGFR pY and membrane show an increased membrane binding (Angulo et al., 2013). No

extended studies had been completed on the other APDS1 mutants probed, however the mutant that is analogous to E525K in p110α, E545K, has been well characterised through the same methods. One of the key differences between the mutation in p110α is that the enzyme was not capable of further activation by PDGFR pY. E545 in p110α binds to K379 in p85α, and the same charge reversal mutation in this residue, K379E, was also unable to be stimulated by PDGFR pY (Burke et al., 2012; Miled et al., 2007). The HDX-MS data further showed that this interface had been broken, and this is the only interface broken by PDGFR pY. In p110δ however, E525K was still able to be further activated by PDGFR pY. HDX-MS showed full disruption of the nSH2-helical interface however in p110δ the cSH2 binds to the kinase domain to lock the regulatory arch into a "closed" confirmation (Vadas et al., 2011). The lack of any changes seen between the WT and mutant enzymes in the cSH2-kinase interface explains how PI3Kδ is still capable of activation by RTKs.

Increases in membrane binding have been previously emphasised as a mechanism of class IA PI3Ks (Angulo et al., 2013; Burke et al., 2012; Hon et al., 2012; Mandelker et al., 2009). Indeed, all APDS1 mutants probed via HDX-MS in the context of membrane binding showed larger changes in deuterium incorporation in regions associated with membrane binding. This mechanism is not unique to activating mutations, as HRas binding of PI3Kα was also shown to drive increased membrane binding as a mechanism of activation (Buckles et al., 2017; Siempelkamp et al., 2017). GPCR activation of PI3Kβ and the class IB PI3Kγ, have also shown an importance in membrane binding for activation of PI3Ks through GPCR signalling. These studies revealed conformational changes in the region of PI3Ks that is unique to the Gβγ subunit of GPCRs (Dbouk et al., 2012; Vadas et al., 2013). Our data coincides with existing studies and emphasises the importance of membrane binding in the natural activation of PI3Ks and in activating mutations.

To further understand how APDS1 mutations led to disturbance of p110δ/p85α, we engineered mutations based on structural data that could potentially rescue or lead to further activation of p110δ activity. The double mutants containing both APDS1 mutation and an engineered mutation (E81K-K111E, G124D-T76G, E525K-p85α-K379E) would be expected to lead to a rescue effect, returning to WT p110δ/p85α activity levels. For example, E525K-p85α-K379E should relieve electrostatic repulsion and reinstate the salt

bridge that exists between E525 and K379 (p85α) however, the WT activity level is not fully rescued indicating that the conformation of the double mutant PI3K is different from WT. The double mutants in the N-terminus of p110δ showed no rescue effect. This indicates that inhibition of class IA PI3Ks is exquisitely sensitive to a specific set of conformations, and even minor differences in conformation can lead to activation of class IA PI3Ks.

In this chapter I used biochemical and HDX-MS experiments to investigate how APDS1 mutations lead to the activation of PI3Kδ and thus, the disease. By understanding the molecular mechanisms that mediate this phenotype I was also able to provide novel insight towards isoform regulatory mechanisms of p110δ. This data is the first investigation into the conformational dynamics of mutations in the p110δ subunit and have shown that overall, these mutations exert their activation phenotype through mechanisms that mimic the natural activation of PI3Kδ. Further to this, we have shown that the p110δ specific inhibitor Idelalisib can inhibit all APDS1 mutants to a similar level, making p110δ specific inhibitors a desirable therapeutic option.

Chapter 4:

Oncogenic and immunodeficiency mutations in PIK3R1 reveal novel insights into the molecular mechanisms of PI3K regulation mediated by p85α

Adapted from:

Dornan, G.L., Siempelkamp, B.D., Jenkins, M.L., Vadas, O., Lucas, C.L., & Burke, J.E. (2017). Conformational disruption of PI3Kδ regulation by immunodeficiency mutations in PIK3CD and PIK3R1. *Proc Natl Acad Sci*. 114: 1982–1987.

Dornan, G.L., Stariha, J.T.B., Rathinaswamy, M.K., Powell, C.J., Boulanger, M.J., Burke, J.E. Defining the p85α mechanisms that mediate the inhibition and activation of PI3K. *In preparation.*

Contributions:

GLD generated the expression constructs. **GLD** and BDS generated the virus. BDS produced and purified the protein. **GLD** generated lipid vesicles. **GLD** performed kinase activity assays. **GLD** and JEB performed IC50 measurements. **GLD**, MLJ and JEB performed HDX-MS experiments. CJP performed ITC experiments. **GLD** and JEB designed research. OV and CLL contributed new reagents/analytic tools. **GLD**, BDS, MLJ, JTBS, CJP, MJB and JEB analysed data. **GLD**, BDS, CLL and JEB wrote the paper in PNAS. **GLD** and JEB wrote the paper in preparation.

4.1 Introduction

Pathogenic mutations in the gene that encodes p85α, PIK3R1, lead to a plethora of diseases including cancer, developmental syndromes, and immunodeficiencies (Dornan and Burke, 2018; Fruman et al., 2017). The p85-like regulatory subunits are required for all class IA catalytic p110 isoforms for both stability of the PI3K complex, and activation downstream of phosphorylated receptors despite apparent isoform specific regulatory mechanisms (Escobedo et al., 1991; Yu et al., 1998b). These roles are mediated through the nSH2, iSH2, and cSH2 domains that all p85-like subunits possess. Binding of pYXXM motifs of phosphorylated receptors is mediated by the nSH2 and cSH2 domains that are connected by the iSH2 is a coiled-coil that stabilises p110 subunits through binding of the ABD (Klippel et al., 1992; Miled et al., 2007; Yu et al., 1998b, 1998a). The p85-like subunits mediate inhibition of p110 catalytic isoforms through their interfaces: nSH2-helical, iSH2-C2, and in the p110β and p110δ isoforms the cSH2-kinase interface. Disruption of these interfaces can cause activation of class IA PI3K isoforms, and can lead to disease.

Mutations in PIK3R1 appear to drive disease through p110 isoform specific mechanisms and these pathogenic mutations in the regulatory p85-like subunits cluster in three regions: the N-terminal region of iSH2 α1 helix, the C-terminal region of the iSH2 α2 and α3 helices, and within the cSH2 (Fig. 28A-B,D). Activating PI3K Delta Syndrome type 2 (APDS2) is a primary immunodeficiency caused by activating mutations in PIK3R1. The most common APDS2 patient mutations in PIK3R1 lead to a splice site mutation that excludes Exon 11, resulting in a deletion within the N-terminus of the iSH2 coiled-coil domain (Δ434-475; Fig. 28, 29) (Bravo García-Morato et al., 2017; Deau et al., 2014; Hauck et al., 2017; Kuhlen et al., 2016; Lucas et al., 2014; Petrovski et al., 2016; Sugiyama et al., 2017; Wentink et al., 2017). Patients with APDS2 have increased PIP_3 levels, defects in both B and T cell functions, recurrent respiratory infections, and increased susceptibility to herpes viruses, all of which are a phenocopy of APDS1 patients who have mutations in the PIK3CD which encodes the p110δ subunit (Angulo et al., 2013; Jou et al., 2006; Lucas et al., 2016, 2013). The clinical phenocopy of APDS1 patients with mutations in p110δ by APDS2 patients with mutations in p85α is surprising, as p85α associates with all of the

class IA catalytic isoforms (Tsolakos et al., 2018). Therefore, it is expected that this mutant would also cause activation of p110α, leading to oncogenic transformation or overgrowth syndromes. Mutations at the C-terminal region of the iSH2 exhibit oncogenic, p110α driven phenotypes and not p110δ APDS2 phenotypes. These mutations in PIK3R1 can lead to deletions/truncation of p85-like subunits starting within the α2 helix or the α3 helix and can also lead to loss of the cSH2 (Forbes et al., 2016; Giannakis et al., 2016; Jimenez et al., 1998; Shekar et al., 2005). The Q572* mutation has previously been shown to constitutively activate p110α in vitro, due to disruption of the C2-iSH2 inhibitory interface and an nSH2-iSH2 packing interface that is important for orienting the nSH2 (Shekar et al., 2005; Wu et al., 2009). The molecular basis of how these mutations lead to p110α selective phenotypes is unknown. Finally, there are point mutations in, and truncations of, the cSH2 that lead to developmental disorders (SHORT syndrome) characterised by impaired PI3K signalling as opposed to overactive signalling commonly seen in class IA PI3K driven diseases (Bárcena et al., 2014; Chudasama et al., 2013; Dyment et al., 2013; Huang-Doran et al., 2016; Klatka et al., 2017; Schroeder et al., 2014; Thauvin-Robinet et al., 2013). The most frequent mutation in SHORT syndrome occurs at the cSH2 FLVR motif, which is important for binding pYXXM motifs of phosphorylated receptors and the activation of class IA PI3Ks downstream of these receptors. Due to the obligate nature of p85-like regulatory subunits in the class IA PI3K complexes, it would be predicted that mutations in p85α affect all isoforms. Perplexingly, some PIK3R1 mutations show isoform specific phenotypes.

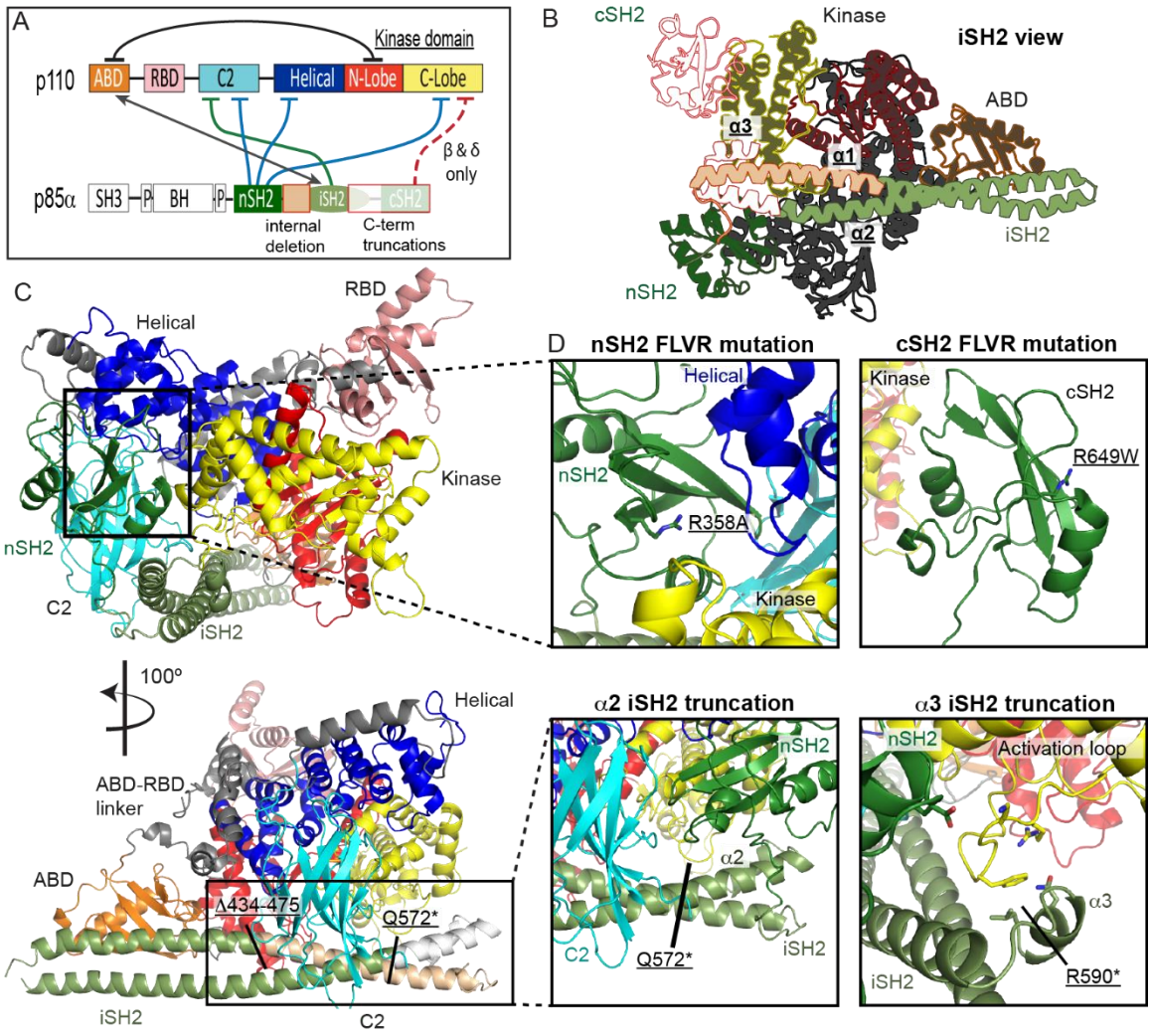

Figure 28: Pathogenic and engineered PIK3R1 mutations in the iSH2 and cSH2.
(A) Wiring diagram indicating two regions of mutations that lead to deletions/truncations in the iSH2 domain. The most common APDS2 mutation leads to a splice site variant yielding a truncation of ~42 amino acids within the N-terminal region of the iSH2 (Shown in beige). Oncogenic mutations lead to truncation of p85α at the C-terminus at I571 and N600 (Q572* and E601*; Shown in white). (B) An alternate view to emphasize the iSH2 domain architecture. The three helices of the iSH2 labelled: α1, α2, α3. The regions of the iSH2 with patient mutations are colour coded as in section (A) with the N-terminal in-frame deletion in wheat and the C-terminal truncations shown in white. (C) The mutations in PIK3R1 shown on a structural model of PI3Kα (Prepared as in chapter 2: Methods). The most common SHORT mutation R649W leads to perturbation of PDGFR pY binding at the cSH2 domain (Top Right panel). Other mutations included are not pathogenic mutations, although pathogenic mutations frequently occur in these regions. These include R358A and R590*. These mutations were designed specifically to probe the unique structural features of the iSH2 and how they mediate inhibition of different p110 isoforms.

By investigating these mutations, we aim to characterise isoform specific regulatory mechanisms driven by p85α and understand the mechanistic basis of disease mutations in PIK3R1. Particularly, we want to understand the role of the iSH2 in mediating inhibition and activation of p110. How are the N-terminus or the C-terminus of the iSH2 coiled-coil contributing to regulation of p110 subunits by p85α? Does the α3 helix of the iSH2 also exert effects on the overall regulation of p110? To understand the molecular mechanisms that mediate isoform specific regulation in the regulatory subunit p85, we examined both the conformational dynamics and lipid kinase activity of APDS2, oncogenic, and SHORT syndrome mutations using hydrogen-deuterium exchange mass spectrometry (HDX-MS) and biochemical assays. This chapter will first discuss the APDS2 findings, followed by our study of oncogenic iSH2 mutants, and finally the mutants which disrupt the nSH2 and cSH2 FLVR motifs.

The APDS2 p85α splice variant was examined in complex with both p110α and p110δ, and unexpectedly we find that this variant of p85α leads to a selective activation of PI3Kδ with only a minimal effect on PI3Kα activity basally. HDX-MS revealed that the p85α APDS2 splice variant disrupted all inhibitory interactions between p85α and p110δ, while only a partial disruption of p85α-mediated inhibitory interactions was observed in p110α. We also find that the WT and APDS2 mutant are similarly inhibited by the potent p110δ inhibitor idelalisib (Gopal et al., 2014; Herman et al., 2010). To further investigate whether mutations that result in isoform specific phenotypes are mediated by isoform specific regulation by p85α, we then investigated oncogenic mutations that lead to C-terminal truncations of p85α in complex with p110α and p110δ. We find that truncation of p85α at residue 571 leads to full activation of both isoforms and that PI3Kα constructs lacking the cSH2 are unable to be activated by stimulating PDGFR phosphopeptide. Our results provide novel molecular insights into the conformational mechanisms by which p110δ and p110α are activated in human disease, and reveal how mutations in PIK3R1 (p85α) can specifically phenocopy gain-of-function mutations in PIK3CD (p110δ) and PIK3CA (p110α) to drive isoform specific activation.

4.2 Results

Generation of PIK3R1 Constructs

To answer key questions pertaining to PI3K regulation using biochemical and structural methods, I first recombinantly produced all proteins required following methods described in Chapter 2 (Fig. 29). Mutant and WT proteins were prepared as described in Chapter 2: Material and Methods. In brief, WT and mutant p110/p85 heterodimers were produced through baculovirus mediated protein expression and purified using standard affinity and chromatography purification techniques. All proteins were produced in the same manner (with the exception of APDS2 proteins, also described in depth in Chapter 2: Materials and Methods), with a single chromatographic peak eluting at roughly the same time from the size exclusion chromatography column indicating that mutants do not disrupt the overall fold of the WT heterodimer. This included the WT PI3Kδ (p110δ/p85α) and PI3Kα (p110α/p85α) as well as PI3Ks harbouring mutations in the p85α subunit. For studies on the APDS2 N-terminal iSH2 deletion, both PI3Kδ and PI3Kα were produced in the context of the p85α mutation, Δ434–475. The APDS2 deletion removes the first 42 residues of α1 helix in the iSH2 coiled-coil. In WT PI3K complexes, this region interacts with helices α2 and α3 in the iSH2 coiled-coil and makes contacts with the C2 and kinase domains of the catalytic subunit. The iSH2-ABD interface is an extremely high affinity interaction and so this inner-iSH2 deletion would likely not disrupt the positioning of the iSH2. Rather, the decrease might be expected to misposition the nSH2, disrupting the nSH2-helical interface. To further understand isoform specific regulation mediated by p85α and to investigate how the C-terminal region of the iSH2 mediates regulation, we also prepared oncogenic mutation that occur in this region (Q572*, R590*, E601*). R590* itself is not a patient mutation, however many complex and truncating mutations exist in this region and we wanted to specifically probe the role of the α3 helix in regulation of p110 subunits. Oncogenic mutants were also produced in the context of both PI3Kδ and PI3Kα, and lead to the truncation of the C-terminus of iSH2 at 571, 589, and 600 respectively. The Q572* mutation truncates p85α at the C-terminal portion of the iSH2 near the iSH2 coiled-coil pair interface as well as the iSH2-C2 interface. Finally, we prepared two point mutations in the pYXXM binding motif (FLVR) of the nSH2 and cSH2

domains: R358A and R649W. The R649W mutation is also the most common SHORT mutation, and leads to impaired PI3K signalling.

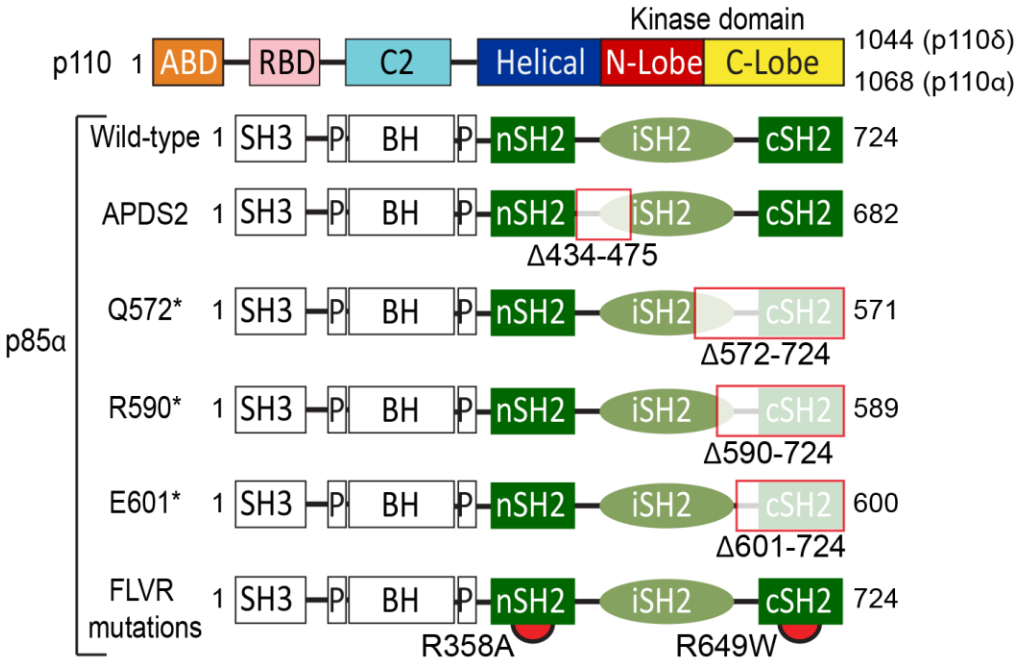

Figure 29: Schematic of PI3K (p110/p85α) constructs used in this chapter.
Both p110δ and p110α were used in conjunction with the various p85α constructs. WT p85α in complex with either p110 formed the WT PI3K complexes. All other p85α constructs represent disease mutants which form mutant PI3K complexes with either of the p110s. White or beige boxes with red outline indicate the region that is absent in mutants. Red circles indicate the location of single residue mutations.

Lipid kinase activity of APDS2 splice variants.

To understand how clinical mutations in the regulatory subunits (p85α) alter the function of PI3Kδ, we characterized the lipid kinase activity of APDS2 mutants. Lipid kinase experiments on WT and APDS2 PI3K complexes were carried out on phosphatidylserine vesicles containing 5% PIP2 in both the presence and the absence of a PDGFR phosphopeptide (PDGFR pY) to mimic activation by RTKs.

Intriguingly, the APDS2 splice variant showed a very large isoform-specific difference in basal lipid kinase activity. The APDS2 p85α splice variant with p110δ showed an ~400-fold increase in activity over the WT p110δ/p85α complex (Fig. 30-Left). However, the APDS2 p85α splice variant with p110α was minimally activated

(approximately twofold) compared with WT p110α/p85α (Fig. 30-Right). The PI3Kδ complex with the APDS2 p85α splice variant appeared to be close to fully active in the absence of stimulation (−pY) and showed only limited activation upon pY stimulation (approximately twofold). In contrast, the PI3Kα complex with the APDS2 p85α splice variant was further activated in the presence of pY, with an ∼10-fold increase in lipid kinase activity upon pY stimulation. This indicates that the SH2 inhibitory interfaces from p85α are almost fully disrupted in PI3Kδ, whereas the nSH2–helical inhibitory interface is likely partially conserved in the PI3Kα APDS2 complex. The PI3Kα APDS2 p85α complex was more active than WT PI3Kα in the presence of pY.

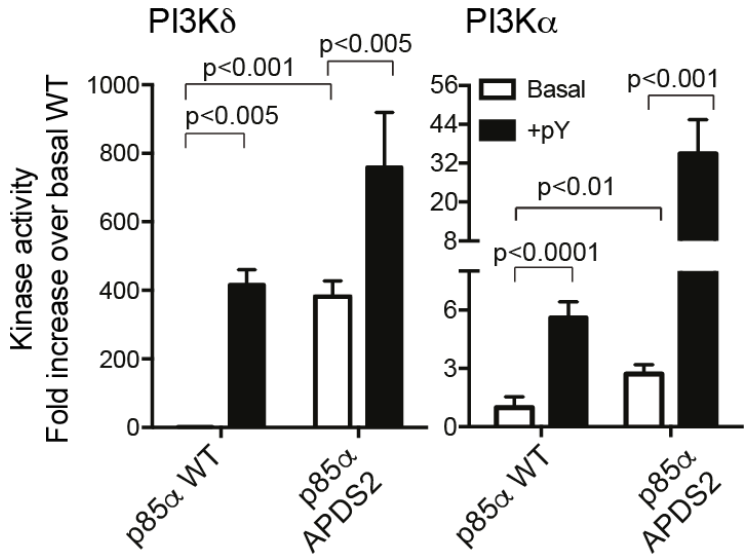

Figure 30: APDS2 deletion of the N-terminal region of the iSH2 leads to increased basal and pY-activated lipid kinase activity compared with WT.

Lipid kinase assays of WT PI3Kδ or PI3Kα with WT p85α or the APDS2 p85α splice variant [p85α (Δ434–475)] in the presence (+pY) or absence (basal) of a stimulating PDGFR-derived phosphopeptide (1 μM). Specific activity was normalized to respective WT (p110δ/p85α or p110α/ p85α). Left: Fold activation of APDS2 mutation in the context of PI3Kδ. Right: Fold activation of APDS2 mutation in the context of PI3Kα. Assays measured the production of ADP in the presence of 0.1–100 nM of enzyme, 100 μM ATP, and 5% PIP2/95% PS vesicles. Kinase assays were performed in triplicate (error shown as SD; n = 3). Unpaired T-Test was performed between conditions and the p-values are indicated in the graph. Adapted from Dornan et al., 2017.

HDX-MS Reveals That APDS2 Mutations in PIK3R1 Lead to Disruption of Inhibitory Interfaces in PI3Kδ.

To investigate the molecular mechanisms by which APDS2 mutations in PIK3R1 led to considerable activation of PI3Kδ, we used HDX-MS to compare dynamics of WT p110δ/p85α and WT p110δ/Δ434–475 p85α. The full set of all peptides analyzed for both p110δ and p85α is shown in Appendix A.1, Fig. 42. A number of regions in both p110δ and p85α of the APDS2 mutant PI3Kδ showed significant changes (defined as greater than 7% and 0.7 Da change in deuterium incorporation at any time point) compared with WT (Fig. 31). Within p85, peptides spanning the nSH2–helical interface and cSH2–kinase interface had large increases in exchange, suggesting that the APDS2 p85α deletion disrupts both the nSH2 and the cSH2 inhibitory inputs. Apart from the iSH2 portion that contacts the ABD and remained unaffected, all of the iSH2 showed considerable increases in exchange (>50%) and were fully deuterated at 3 s of exposure with D2O, indicating a lack of secondary structure. This includes the inhibitory contacts between the iSH2 and C2 domains.

Several regions in the p110δ catalytic subunit showed increases in HDX in the APDS2 mutant compared with the WT (Fig. 31), including many regions with similar increases in HDX upon either pY binding or membrane binding in the WT. This included the ABD-RBD linker and the ABD domain at the interface with helix α1 of the iSH2, as well as the interface with the kinase domain (Appendix A.1, Fig. 42). Every inhibitory interface with the p85α subunit showed increases in HDX, including the C2–iSH2, helical–nSH2, and kinase–cSH2 interfaces. A network of connected secondary structure elements in every domain of the catalytic subunit had increased HDX, suggesting a possible destabilization of the catalytic subunit. Together, the HDX results for p110δ bound to the APDS2 splice variant of p85α implied that the removal of the first helix α1 of the iSH2 leads to a disruption of all inhibitory interfaces on the kinase domain of p110δ.

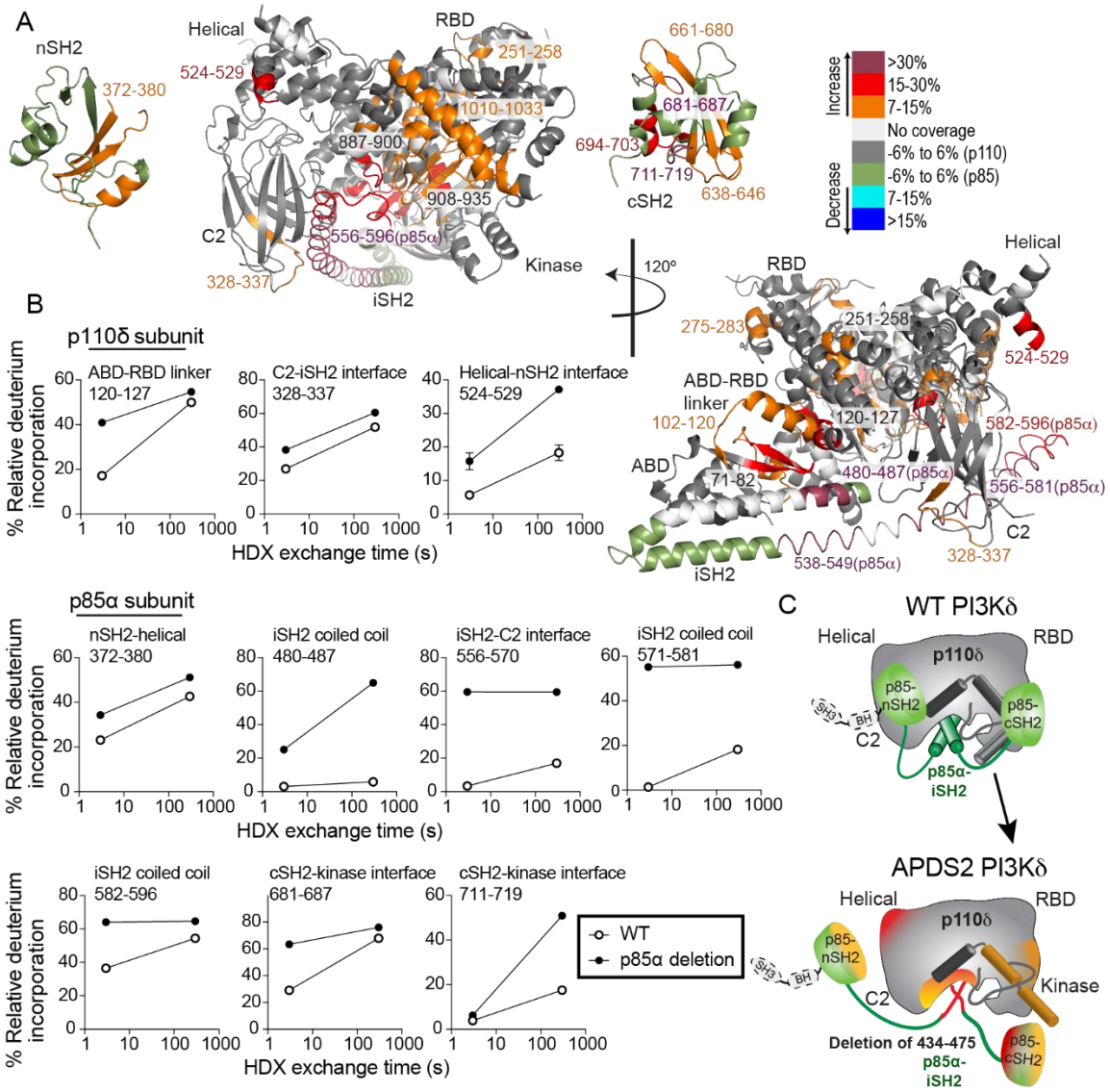

Figure 31: HDX-MS reveals that APDS2 mutation in p85α leads to disruption of inhibitory interactions in PI3Kδ.

(A) Peptides in p110δ and p85α that showed differences in HDX both greater than 0.7 Da and 7% in the APDS2 p85α mutation compared with the WT are highlighted on the structural model from Fig. 28A according to the legend. nSH2 and cSH2 are shown disconnected from the catalytic subunit as the HDX data suggest that these interfaces are disrupted. (B) Time course of deuterium incorporation for a selection of peptides in both p110δ and p85α with differences in HDX in the APDS2 p85α mutant (error shown as SD; n = 3). (C) Schematic model of WT PI3Kδ and conformational changes that occur in the complex with the APDS2 splice variant of p85. Adapted from Dornan et al., 2017.

HDX-MS Reveals That APDS2 Mutations in PIK3R1 Lead to Partial Disruption of Inhibitory Interfaces in PI3Kα.

To understand how the APDS2 splice variant of p85α led to only a partial activation of PI3Kα compared with PI3Kδ, we carried out HDX-MS experiments on the complex of WT p110α/p85α and a complex containing p110α with the p85α APDS2 splice variant (Fig. 32). The full set of all peptides analyzed for both p110α and p85α is shown in Appendix A.1 Fig. 43. Compared with WT p85α, association with the p85α APDS2 splice variant caused large increases in HDX in the p110α catalytic subunit in the ABD-RBD linker, and the p85α inhibitory C2–iSH2, C2–nSH2, and helical–nSH2 interfaces, similar to regions that showed increases in exchange either upon pY or membrane binding in the WT (Fig. 32) (Burke et al., 2012). Within peptides spanning p85α there were numerous regions that showed increases in HDX. The iSH2 coiled-coil outside of the ABD interface showed very large increases in HDX, similar to the APDS2 PI3Kδ complex, suggesting that in both complexes the p85α splice variant leads to large portions of the iSH2 becoming disordered. Intriguingly, regions of the nSH2 in contact with the catalytic subunit showed increases in exchange, suggesting that part of the interface is disrupted. However, these changes were less pronounced than those seen in the APDS2 PI3Kδ complex. This is best highlighted by a region in the nSH2 that directly contacts the kinase domain (residues 356–371) that showed a larger increase in exchange in the APDS2 PI3Kδ complex compared with the APDS2 PI3Kα complex (Fig. 32C).

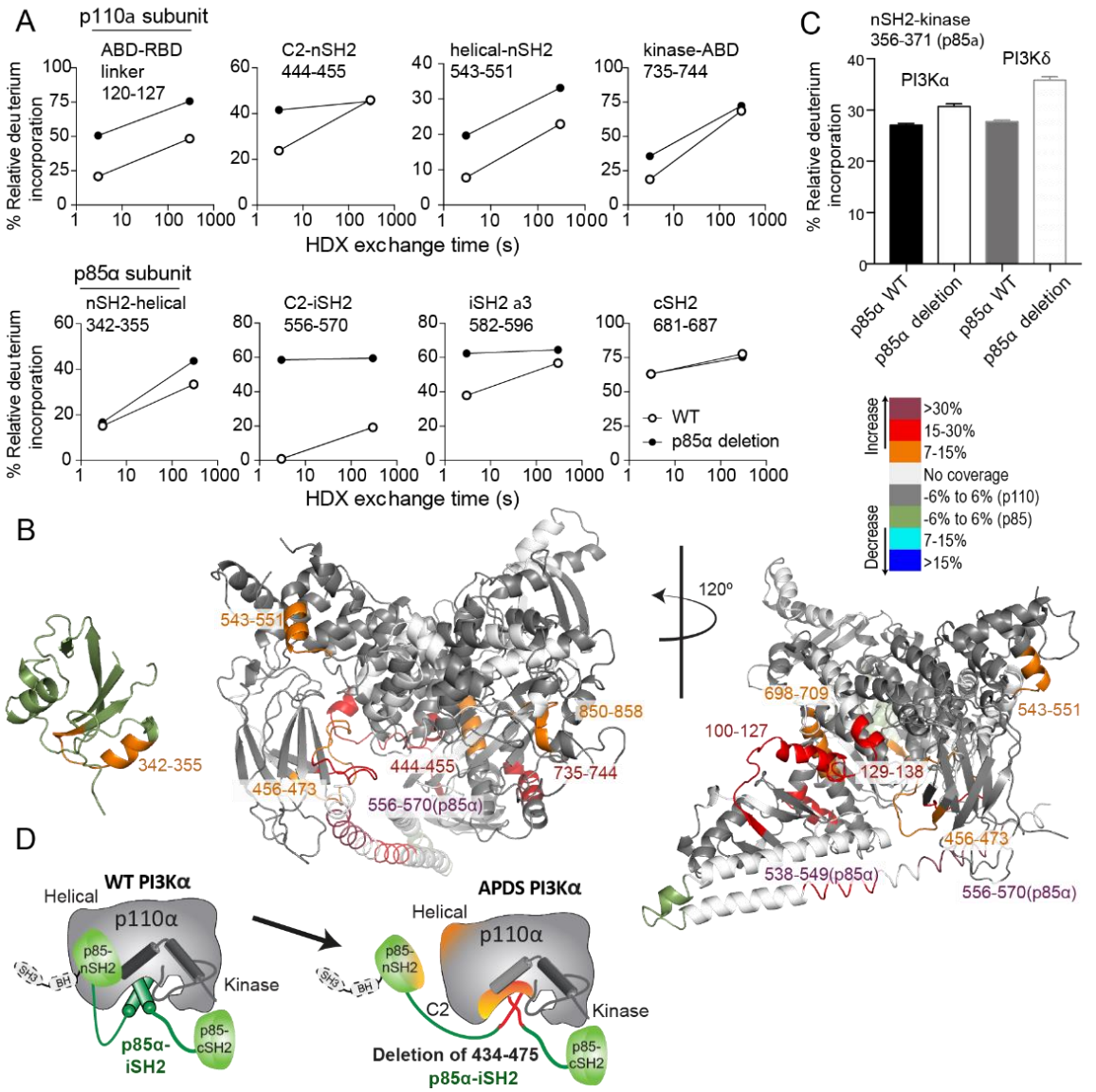

Figure 32: HDX-MS reveals that APDS2 mutation in p85α leads to partial disruption of inhibitory interactions in PI3Kα.

(A) Peptides in p110α and p85α that showed differences in HDX both greater than 0.7 Da and 7% in the APDS2 p85α mutation compared with the WT are highlighted on the structure of p110α bound to the nSH2 and iSH2 of p85α [PDB: 3HHM (38)]. The nSH2 domain is shown disconnected from the catalytic subunit, as the HDX data suggest that this interface is partially disrupted. (B) Time course of deuterium incorporation for a selection of peptides in both p110α and p85α with HDX differences in the APDS2 PIK3R1 mutant. (C) HDX exchange levels for the APDS2 complex of PI3Kα and PI3Kδ compared with WT for a peptide in the nSH2 of p85α located at the nSH2–kinase interface at the 300-s time point. Error bars in all graphs represent SD (n = 3). (D) Schematic model of WT PI3Kα and conformational changes that occur in the complex with the APDS2 splice variant of p85α. Adapted from Dornan et al., 2017.

The APDS2 mutant is potently inhibited by the FDA approved PI3Kδ-specific inhibitor Idelalisib

To determine if conformational differences identified in the APDS2 mutant of PI3Kδ would lead to differential inhibition by ATP competitive kinase inhibitors, we carried out lipid kinase assays in the presence or the absence of the clinically approved PI3Kδ inhibitor idelalisib (Somoza et al., 2015). The APDS2 mutant in the p85α regulatory subunit exhibited a very similar IC50 value compared with the WT (Fig. 33), indicating that this mutant protein might be targeted by idelalisib.

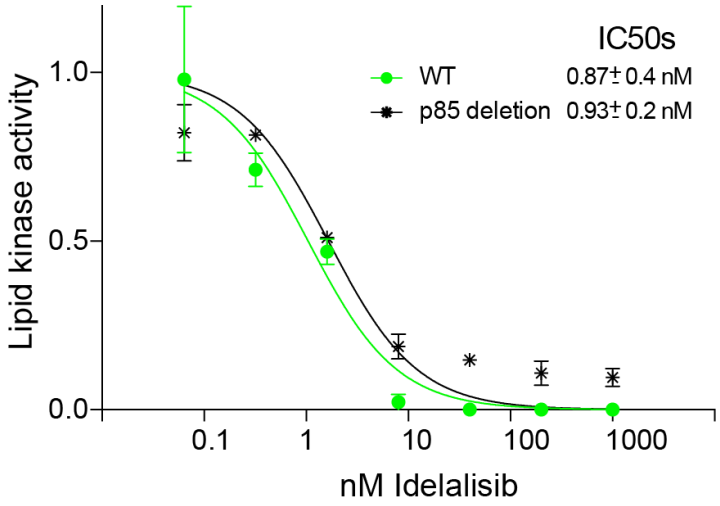

Figure 33: Inhibition of WT and APDS2 mutant PI3Kδ by the potent PI3Kδ inhibitor idelalisib.
Lipid kinase activity was normalised to kinase activity in the absence of inhibitors. IC_{50} values were generated from triplicate independent inhibitor dilutions, and error is shown as SD. Adapted from Dornan et al., 2017.

C-terminal truncations of p85α lead to decreased sensitivity to PDGFR pY stimulation

As the APDS2 mutation led to a surprising isoform-specific activation mechanism, we were interested in whether other mutations of PIK3R1 that appear to drive isoform specific phenotypes might also provide novel insight into isoform specific regulatory elements. Additionally, the APDS2 deletion occurs within the N-terminus of the iSH2 and we wanted to investigate the regulatory mechanisms of other structural features of the iSH2 coiled-coil. To this end, we identified two oncogenic mutations (Q572* and

E601*) from the COSMIC database that produce truncations of p85α iSH2 domain within the C-terminal α2 helix and just after the α3 helix of the iSH2 (Forbes et al., 2016); Fig. 28D-E, 29). To further probe the regulatory roles mediated by the iSH2 helices, we also engineered a third iSH2 mutation (R590*) that truncates p85α immediately before the α3 helix of the iSH2. Although this specific mutation has not been identified as an oncogenic patient mutation, many mutations occur in that region of the iSH2 indicating that it is sensitive to perturbation.

The cSH2 forms an inhibitory contact in PI3Kδ but not in PI3Kα, however the cSH2 drives the high affinity binding of pYXXM of PDGFR and both sites appear to be required for full activation as mutation of either cSH2 or nSH2 pYXXM binding sites leads to a 50% reduction in binding and activation downstream of IRS-1 (Klippel et al., 1992; Panayotou et al., 1993; Rordorf-Nikolic et al., 1995). To further differentiate the role of the cSH2 in both isoforms, we used p85α-E601* which truncates p85α immediately after the α3 helix of the iSH2, effectively removing the cSH2. The α3 helix of the iSH2 packs against the activation loop of the kinase domain and part of the coiled-coil of the iSH2 in both isoforms (Timothy P. Heffron et al., 2016; Miller et al., 2014). We wondered whether the α3 helix interfaces might be contributing to inhibition of class IA PI3Ks. Finally, we asked whether the oncogenic mutation that leads to the 571 truncation of p85α (Q572*) was activating due to the disruption of the C2-iSH2 contact as previously seen in PI3Kα, and whether this effect was also observed in PI3Kδ (Wu et al., 2009). This portion of the iSH2 also makes contacts with the nSH2, and potentially contributes to proper positioning of the nSH2 (Huang et al., 2007; Shekar et al., 2005).

To investigate the effect these truncations exerted on the function of class IA PI3Ks and whether there were isoform specific regulatory mechanisms, we measured the kinase activity of the C-terminal truncations in the context of both PI3Kα and PI3Kδ. Kinase activity of the enzymes was measured on a plasma membrane mimic vesicle in the absence (basal activity) or presence of 1 uM PDGFR bis-phosphorylated pY peptide (referred to afterwords as PDGFR pY) representing residues 735-767 with the pY740 and pY751 phosphorylation sites.

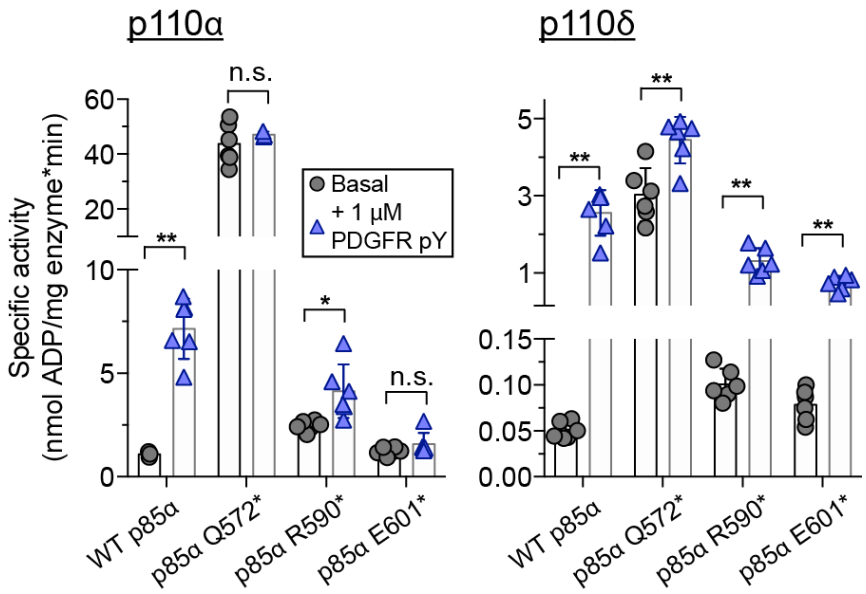

Figure 34: Lipid kinase activity of the WT and C-terminal truncations of p110α/p85α and p110δ/p85α.

Lipid kinase activity was measured in the presence (+pY) or absence (Basal) of a stimulating PDGFR derived phosphopeptide (1 uM). Assays measured the production of ADP in the presence of 0.1–1100 nM of enzyme, 100 μM ATP, and PM mimic vesicles containing 5% PIP2. Kinase assays were performed in triplicate (error shown as SD; n = 3). Unpaired T-Tests were performed and results are as follows: n.s. = non significant, $p>0.05$, * = $p<0.05$, ** = $p<0.01$.

Compared to the respective WT enzyme (PI3Kα or PI3Kδ), all truncations showed decreased stimulation by 1 uM PDGFR pY (Fig. 34). The largest truncation (p85α-Q572*) leads to hyperactivation of both isoforms basally, where in PI3Kδ the activation was at the level of an PDGFR stimulated state in the wildtype, similar to the effect of the APDS2 deletion mutant. The p85α-Q572* truncation mutant in PI3Kα was between 5-6 fold higher activity compared to the PDGFR pY stimulated state of wildtype. This is consistent with previous studies that showed the p85α-Q572* mutation led to a constitutively active PI3Kα (Shekar et al., 2005; Wu et al., 2009). In complex with p110δ, p85α-Q572* was still mildly activated by an PDGFR pY, whereas p85α-Q572* was unable to be activated by PDGFR pY in complex with p110α. The previous literature identified the 581-593 region of the iSH2 as an important nSH2 interface and predicted that the loss of this region due to the truncation at 571 would lead to disruption of the nSH2-iSH2 interface to mediate constitutive activity (Shekar et al., 2005). If this prediction is correct, then perhaps the PI3Kα and PI3Kδ isoforms differ at this interface. Existing structures of p110δ in complex

with the p85α subunit contain only the iSH2 (Castanedo et al., 2017; Erra et al., 2018; Timothy P. Heffron et al., 2016; Qin et al., 2017). The p85α-R590* and p85α-E601* truncations (α3 helix and cSH2 truncations) showed little to no hyperactivation at the basal state and reduced stimulation by PDGFR pY. Interestingly, PI3Kα lacking the cSH2 (p85α-E601*) was unable to be stimulated by 1 uM PDGFR pY despite this isoform lacking the cSH2-kinase interface. This result was unexpected, as the PI3Kα isoform is highly sensitive to PDGFR pY stimulation, requiring ~10 nM for full activation, and the cSH2 forms no interface with the kinase in this isoform (Burke and Williams, 2013). As the cSH2 forms no interface with the kinase in this isoform, a loss of the cSH2 might be expected to have low consequence towards the activation by pYXXM containing receptors.

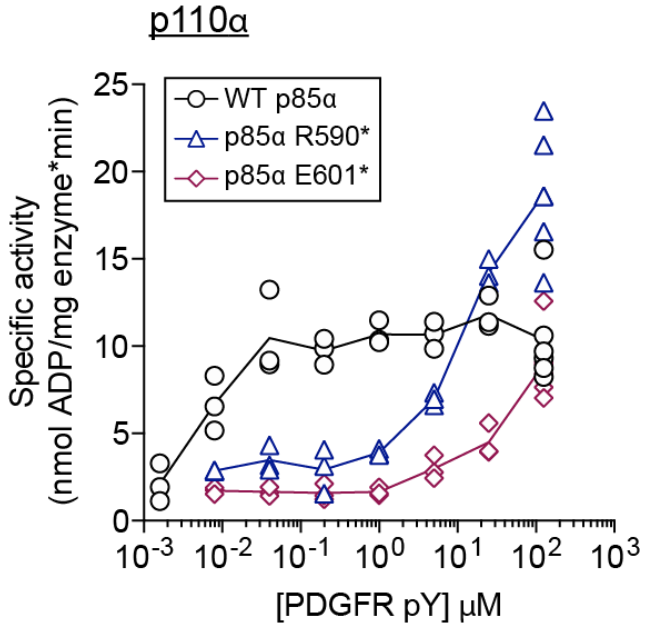

Figure 35: Dose response of bis-phosphorylated PDGFR phosphopeptide (PDGFR pY) concentration of the WT and the C-terminal truncations p85α-R590* and p85α-E601* in complex with p110α.

Lipid kinase activity was measured at seven to eight different concentrations of PDGFR pY (0.0016 nM – 125 uM). Assays measured the production of ADP in the presence of 0.1–100 nM of enzyme, 100 μM ATP, and PM mimic vesicles containing 5% PIP2. Kinase assays were performed in triplicate (error shown as SD; n = 3).

To determine whether the ability of PI3Kα to be activated by PDGFR pY was completely abolished, we performed a PDGFR pY titration for two of the PI3Kα constructs (Fig. 35). The WT PI3Kα was fully activated at ~30 nM PDGFR pY, similar to previously published values for WT mentioned above, whereas the C-terminal truncations were activated by PDGFR pY at much higher concentrations. The p85α-R590* truncation lacking the α3 helix of the iSH2 onward required a larger concentration of PDGFR pY for full activation. The p85α-E601* truncation lacking the cSH2 was able to be activated to the same extent as WT but required 125 uM of PDGFR pY. These data indicate that the cSH2 is required for efficient activation of PI3Kα despite the cSH2 not forming inhibitory interfaces with the catalytic subunit as in other isoforms, and that loss of the cSH2 leads to decreased sensitivity to activation by PDGFR pY.

C-terminal truncation of p85α in the iSH2 coiled-coil leads to disruption of key inhibitory interfaces

To investigate the molecular mechanisms that lead to the hyperactivation of the p85α-Q572* truncation mutant when in complex with p110α, we used HDX-MS to probe for conformational changes between the WT and the p85α-Q572* truncation in the basal state as the Q572* truncation was already fully activated without PDGFR pY stimulation. The full set of all peptides analyzed for both p110α and p85α is shown in Appendix A.1 Fig. 44. Differences between the WT and mutant protein in the basal state are shown in Appendix A.1, Fig. 45.

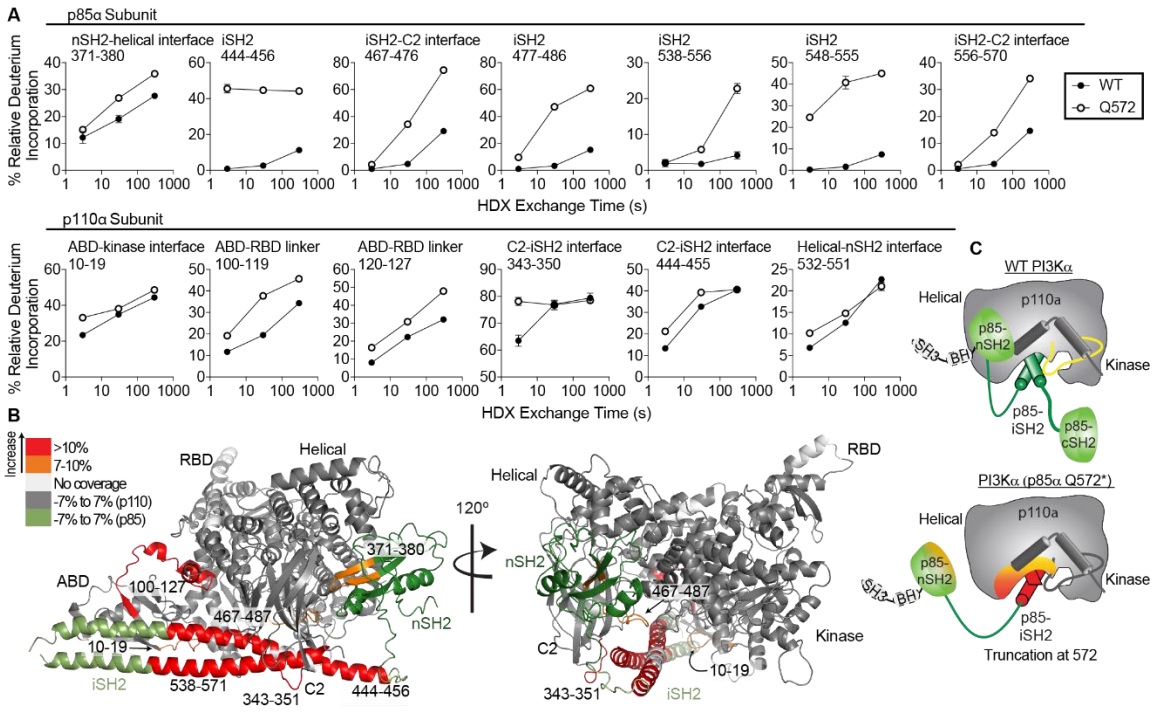

Figure 36: Hydrogen deuterium eXchange reveals disruption of key inhibitory interfaces in the Q572* C-terminal truncation mutant in complex with p110α.
(A) Time course of deuterium incorporation for a selection of peptides in both p85α and p110α with HDX differences in the Q572* mutant. (B) Peptides in p85α and p110α that showed differences in HDX that were greater than both 0.4 Da and 7% in the Q572* C-terminal truncation mutant compared with the WT are mapped on the structure of p110α bound to both the nSH2 and iSH2 of p85α [PDB: 2OVU (Miller et al., 2014)]. (C) Schematic model of WT PI3Kα (p85α/p110α) and the conformational changes that occur in the complex with the p85α Q572* variant exhibiting C-terminal truncation.

HDX experiments examining the difference between WT PI3Kα and the C-terminal p85α-Q572* PI3Kα truncation revealed increases at key inhibitory interfaces between the regulatory and the catalytic subunit (Fig. 36). There were large increases in exchange in the p85α-Q572* truncation at all regions of the iSH2 not in contact with the ABD domain. This confirms the previous report that the p85α-Q572* mutation in complex with p110α leads to disruption of the iSH2-C2 interface and explains why other mutations in the iSH2 are not additive in their activation effects as the inhibitory contacts through the iSH2 are likely fully disrupted (Wu et al., 2009). Large increases in exchange were also observed in the ABD-RBD linker region, the ABD-kinase interface, and the nSH2-helical interface. Surprisingly, the peptide spanning the helical-nSH2 interface on p110α did not

reach significance. This contrasts with the APDS2 PIK3R1 deletion results in the context of PI3Kα (Fig. 30 & 32). The kinase activity assays showed that PI3Kα was only mildly activated in the basal state but was still able to be activated in the presence of a stimulating PDGFR pY. In the current study, the p85α-Q572* truncation shows hyperactivation in the basal state, so we might expect to see similar increases in deuterium exchange at this interface. However, the only observed increases in exchange in the APSD2 mutant in the nSH2 were distant from the nSH2-helical interface. These increases indicate that the inhibitory interfaces between the subunits of the heterodimer are likely disrupted, accounting for the hyperactivation of the mutant construct compared to WT. As the nSH2-helical contact is the key PI3Kα inhibitory interface, disruption of this contact potentially explains the inability of this mutant to be further stimulated by PDGFR pY.

Both SH2 domains are required for full and efficient PI3K activation

The key inhibitory interface of PI3Kα is the nSH2 interface with the helical domain of p110α (Burke et al., 2012, 2011). PI3Kβ and PI3Kδ are also regulated by the cSH2 interface with the C-lobe of the kinase domain (Burke et al., 2012; Burke and Williams, 2013; Zhang et al., 2011). Despite the lack of cSH2 interface in PI3Kα, evidence supports a role for the cSH2 in regulation. PDGFRβ contains two pYXXM sites that PI3K binds, pY740 and pY751 (Kashishian et al., 1992). The cSH2 has been shown to be sufficient for maximal binding in the context of free p85, with similar affinities for both PDGFR pY sites to full p85, whereas the nSH2 has a much lower affinity for one of the pYXXM motifs of PDGFRβ (Klippel et al., 1992; Panayotou et al., 1993). Existing models to describe the regulatory mechanisms of the SH2 domains of p85α in the PI3K heterodimer show evidence for either two-site or one-site binding (Rordorf-Nikolic et al., 1995; Yu et al., 1998b). To further investigate the role of the cSH2 domain in the context of PI3Kα, we compared WT PI3Kα to PI3Kα constructs with abrogated nSH2 or cSH2 FLVR sites, which is key for binding RTK pYXXM motifs. We singly mutated the FLVR motifs in the SH2 domains to create two constructs with a non-functional nSH2 (R358A) or a non-functional cSH2 (R649W), which is also the most common SHORT mutation (Fig. 28D, 29). We then measured kinase activity under differing PDGFR pY conditions, using either a bis-phosphorylated pY peptide or peptides phosphorylated at either the

pY740 or pY751 (Fig. 37A). The first condition compares basal activity and PDGFR stimulated activity of 1 uM PDGFR pY that is bis-phosphorylated, followed by a dose response of the bis-phosphorylated PDGFR pY.

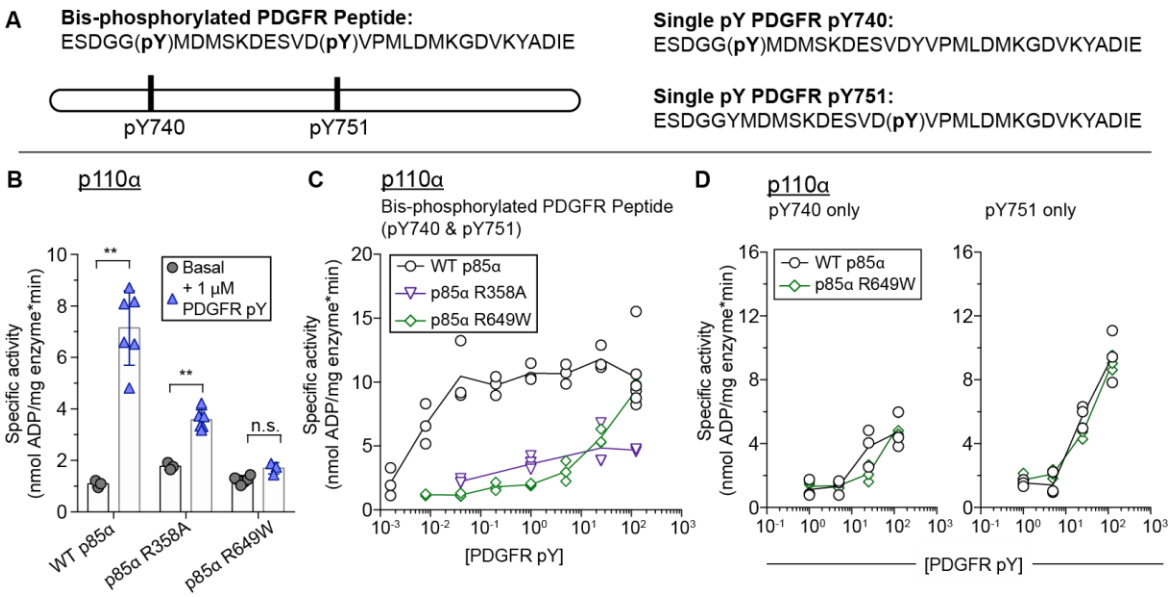

Figure 37: SHORT mutation of key phosphopeptide binding residue leads to decreased phosphopeptide sensitivity.

(A) Sequences of the PDGFR pY variants. Phosphorylation of tyrosines represented as (pY). (B) Lipid kinase activity of the WT and the SH2 FLVR mutations R358A and R649W in the absence (Basal) or presence (+1 uM pY) of PDGFR bis-phosphorylated pY. Assays measured the production of ADP in the presence of 0.1–100 nM of enzyme, 100 μM ATP, and PM mimic vesicles containing 5% PIP2. Kinase assays were performed in triplicate (error shown as SD; n = 3). Unpaired T-Tests were performed and results are as follows: n.s. = non significant, $p>0.05$, * = $p<0.05$, ** = $p<0.01$. (C) Dose response of bis-phosphorylated PDGFR pY concentrations of WT and the SH2 FLVR mutations R358A and R649W. Lipid kinase activity was measured at four to eight different concentrations of PDGFR pY (0.0016 nM – 125 uM). Assays measured the production of ADP in the presence of 0.1–100 nM of enzyme, 100 μM ATP, and PM mimic vesicles containing 5% PIP2. Kinase assays were performed in triplicate (error shown as SD; n = 3). (D) Dose response of single phosphorylated PDGFR pY peptides (pY peptide 1 corresponds to pY740 and pY peptide 2 corresponds to pY751 of PDGF kinase-insert region) concentration of the wild-type and the SH2 FLVR mutation R649W. Lipid kinase activity was measured at four different concentrations of PDGFR pY (1 nM – 125 uM). Assays measured the production of ADP in the presence of 0.1–100 nM of enzyme, 100 μM ATP, and PM mimic vesicles containing 5% PIP2. Kinase assays were performed in triplicate (error shown as SD; n = 3).

The SHORT mutation R649W, which decreases the affinity for PDGFR pY binding in the cSH2 domain, mimicked the results of the E601* mutant (Fig. 34), where the basal activity was the same as basal WT activity and the mutant was unable to be stimulated by 1 uM PDGFR pY (Fig. 37B). The nSH2 FLVR motif mutant was able to be stimulated by PDGFR pY, however this was minimal compared to WT (Fig. 37B). To test whether higher concentrations of PDGFR pY would lead to full activation of the mutants, we conducted a similar dose response activity experiment as previously described (Fig. 35). A PDGFR pY dose response revealed that the SHORT mutation in the cSH2 further mimicked the activity of E601*, where full activation was achieved at a high concentration of PDGFR pY (Fig. 37C). This shows that the nSH2-helical interface is still broken, however the cSH2 binding of pYXXM is required for sensitivity to PDGFR pY. The nSH2 FLVR mutant revealed activation at lower concentrations of PDGFR pY, however even at high concentrations the nSH2 FLVR mutant was not capable of reaching full activation (Fig. 37C). This is likely due to the inability of PDGFR pY to break the nSH2-helical interface in the nSH2-FLVR mutant R358A.

Using the single monophosphorylated PDGFR pY peptides, we performed similar titrations on the WT p85α and the R649W SHORT mutant p85α in the context of the PI3Kα heterodimer (Fig. 37D). When incubated with PDGFR pY740, both the WT and mutant PI3Kα exhibited a similar trend to that of the PI3Kα R358A mutant lacking the nSH2 FLVR binding site. At 125 uM of the single peptide, both PI3Kα constructs never reached full activation indicating that binding of this site alone was not able to break the nSH2-helical interface. For the R649W mutant, where only the nSH2 in theory can now bind pYXXM motifs, this is expected as the nSH2 has a much lower affinity for this specific site (Panayotou et al., 1993). For WT, it would be expected that the cSH2 would bind pY740 due to the high affinity of the cSH2 for this site (Panayotou et al., 1993). This is likely what is happening, as binding of the cSH2 alone would not be expected to break nSH2-helical interface. In the context of the PDGFR pY751, both the WT and the mutant PI3Kα reached full activation at high concentrations of PDGFR pY similar to the trend seen in the E601* and R649W mutants in the context of the bis-phosphorylated PDGFR pY. Both the nSH2 and the cSH2 can bind the pY751 site with high affinity. The ability of the R649W mutant to mimic a bis-phosphorylated peptide response indicates that pY751

is likely the site which the nSH2 binds. The WT result which also mimics an nSH2 driven binding/activation event indicates that despite availability of both SH2 domains, the pY751 is being bound by nSH2 over cSH2. These results taken together indicate that there could be a preferential binding orientation of the PI3Kα heterodimer with the kinase-insert region of PDGFR pY.

Absence of the cSH2 leads to decreases in conformational changes associated with full class IA PI3K activation

To investigate how the C-terminal truncations were mediating the observed PDGFR pY activity differences, we used HDX-MS on WT, R590*, E601* and R649W p85α mutants in the context of the PI3Kα heterodimer. PI3Kα constructs were incubated with 0 uM, 1 uM, or 20 uM PDGFR pY and exchange reactions proceeded for three different time points (3, 30, 300s). The full set of all peptides analyzed for both p110α and p85α is shown in Appendix A.1 Fig. 46. Differences between states are shown for both p110α and p85α of WT and mutant proteins in Appendix A.1 Fig. 47.

The WT p85α PI3Kα heterodimer exhibited changes in deuterium incorporation previously observed when comparing basal to PDGFR pY activated states (Fig. 38A; (Burke et al., 2012)). Increases in deuterium exchange were observed in key interface regions including the helical-nSH2 interface of p110α (532-551), and the C2-iSH2 interface (343-350 and 444-473). Other regions of increase included the ABD-RBD linker of p110α (100-119), and the regions of the p85-iSH2 nearest to the SH2 domains and including the α3 helix (444-456 and 582-596). Both nSH2 and the cSH2 showed large decreases in exchange consistent with PDGFR pY binding. The WT p85α PI3Kα changes were all observed between 0 uM PDGFR pY and 1 uM PDGFR pY, with only mild differences in exchange between the 1 uM PDGFR pY and the 20 uM PDGFR pY (Fig. 38B).

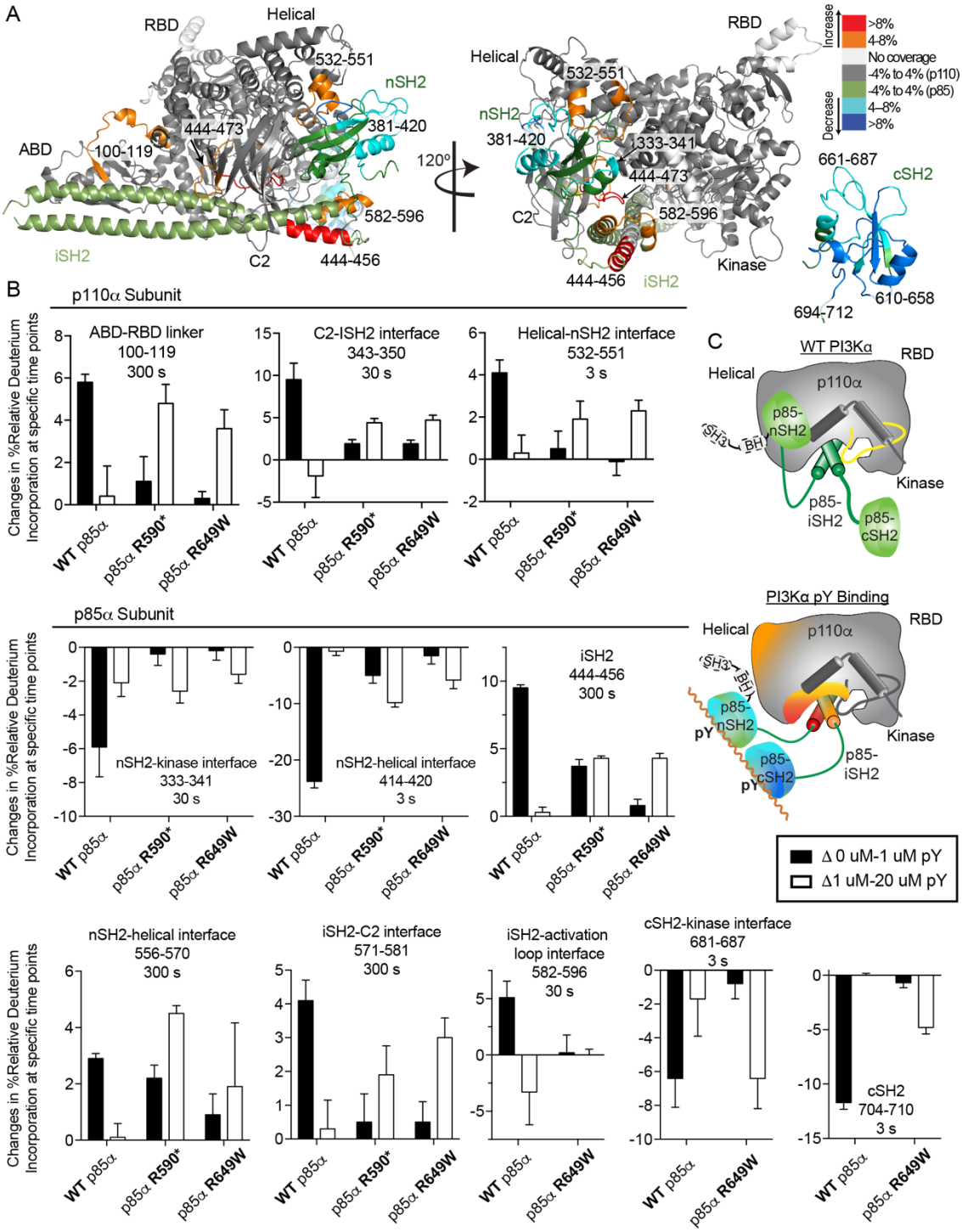

Figure 38: Hydrogen deuterium eXchange reveals decreased sensitivity of C-terminal variants compared to wild-type p110α/p85α.

(A) Peptides in p85α and p110α that showed differences in HDX that were greater than both 0.4 Da and 4% in the wild-type PI3Kα in the absence or presence of PDGFR pY (1 uM or 20 uM) peptide are mapped on the structure of p110α bound to both the nSH2 and iSH2 of p85α (Prepared as described in Chapter 2: Methods). (B) The changes in % relative

deuterium incorporation of PI3K variants in the presence of different PDGFR pY peptide concentration (0 uM, 1 uM, or 20 uM) represented as changes observed upon binding low level PDGFR pY peptide concentration (deuterium incorporation of specified peptide at 0 uM pY subtracted from deuterium incorporation of specified peptide at 1 uM pY binding) and upon binding to a larger concentration of PDGFR pY peptide (deuterium incorporation of specified peptide at 1 uM pY subtracted from deuterium incorporation of specified peptide at 20 uM pY binding). Graphs represent peptides in both p85α and p110α of wild-type and C-terminal variants PI3Kα at specific time points. (C) Schematic model of WT PI3Kα (p85α/p110α) and the conformational changes that occur in the complex upon binding to 1 uM PDGFR pY peptide.

Both the R590* and R649W p85α mutant PI3Kα exhibited similar changes in deuterium incorporation as WT, however, these changes were smaller and only observed between 1 uM PDGFR pY and 20 uM PDGFR pY (Fig. 38B). This indicates that the C-terminal truncations are being activated by the same mechanisms as WT but are less sensitive to the PDGFR pY. One exception is in the case of the p85-R590* mutant, which also exhibits large increases in deuterium incorporation near the truncation site in the iSH2 coiled-coil (556-570). These changes are seen in both concentrations of PDGFR pY. The truncations of the α3 helix could be destabilizing this region of the iSH2, and driving the mild activation seen both basally and upon addition of PDGFR pY at 1 uM (Fig. 34). If the α3 helix had no regulatory role, we would expect to see a similar kinase activity to the p85-E601* mutant. Interestingly, the cSH2 domain of the p85-R649W mutant still exhibits decreases in deuterium incorporation in the same regions associated with PDGFR pY binding (681-687 and 704-710). These changes occurred only in the presence of 20 uM PDGFR pY, and were smaller decreases than in WT. It is possible that the peptide can still associate with the SH2 domain, although at a lower affinity and that this high affinity interaction is imperative to efficient activation of PI3Kα. The p85-E601* mutant PI3Kα did not exhibit any significant changes in deuterium incorporation even at 20 uM PDGFR pY.

4.3 Discussion

The results presented here demonstrate the complexity of isoform specific regulatory mechanisms in class IA PI3Ks, and underscore the importance of studying disease linked mutations in the regulatory subunit p85α to bridge important knowledge gaps in regulatory mechanisms of class IA PI3Ks. In this chapter, I set out to investigate how disease linked mutations led to perplexingly specific phenotypes, despite the necessary role of the p85α in complex with all class IA p110 isoform. Mutations in PIK3R1, which encodes the regulatory subunit p85α, have been identified in solid tumours, the primary immunodeficiency APDS2, and in the developmental disorder SHORT syndrome. PIK3CA, encoding p110α, is one of the most mutated gene in cancers and activating mutations in p110α disrupt inhibitory interfaces of the p110α/p85α complex (Burke et al., 2012; Huang et al., 2007; Samuels et al., 2004). Similarly, activating mutations in PIK3CD, which were presented in the previous chapter, mimic the activation mechanisms of corresponding PIK3CA mutations and drive the primary immunodeficiency APDS1 (Dornan et al., 2017; Takeda et al., 2017). Some phenotypes of PIK3R1 mutations appear to be driven by specific catalytic isoforms. The mutation in the N-terminus of the iSH2 α1 helix is the most frequently identified APDS2 mutation whereas oncogenic mutations of PIK3R1 that cluster around the C-terminal region of the iSH2 in the α2 and α3 helices. By investigating the molecular mechanisms that mediate activation of the observed disease mutations, I was able to uncover novel aspects of isoform specific regulation (APDS2 mutation) and mechanisms of regulation mediated by different structural components of the iSH2.

The APDS2 mutation that results in a loss of exon 11 and a deletion of residues 434-475 at the N-terminus of the iSH2 α1 helix showed a differential activation of p110δ compared to p110α. In the context of p110δ, the APDS2 mutation caused full, hyperactivation of the enzyme in the absence of RTK stimulation whereas p110α was only minimally affected and still required RTK stimulation for hyperactivation. HDX-MS of both mutant proteins in the basal context revealed that this difference was due to full disruption of PI3Kδ compared to PI3Kα, where the nSH2 showed minimal disruption. The nSH2 binds more tightly to the p110α isoform, and is more sensitive to PDGFR pY

stimulation (Burke and Williams, 2013). This difference in nSH2 binding of the catalytic subunit likely allows the nSH2-helical interface to remain intact in p110α/p85α. It was previously thought that the deletion of the N-terminal region of the iSH2 would lead to full disruption of the nSH2-helical interface in all isoforms, as a deletion in this region would lead to a shortening of the iSH2 helix connected to the nSH2 (Lucas et al., 2014). However, the HDX-MS results revealed that the regions of the iSH2 not in contact with the ABD were completely disordered. Unravelling of the helical structure in this region likely allows enough length for the nSH2 to bind the helical interface in p110α and still mediate inhibition.

PIK3R1 mutations in the C-terminal region of the p85α iSH2 revealed similar trends when in complex with either p110α or p110δ. One of the main functional differences identified was the ability of p85α-E601* in complex with p110δ to be activated by 1 uM PDGFR pY while p110α required much higher concentrations. This led to investigations of the cSH2 FLVR mutant which abrogates the cSH2 ability to bind phosphorylated YXXM motifs of RTKs and their adaptors. Both the p85α-E601* in complex with p110α and the cSH2 FLVR mutant rely solely on the nSH2 ability to bind pYXXM motifs. Their dose response to stimulating PDGFR pY was the same. The nSH2 FLVR mutant showed opposite activation, where it was still sensitive to PDGFR pY but was never able to achieve full activation. Studies on the nSH2 and cSH2 of p85α have previously shown that the cSH2 drives a high affinity interaction with PDGFR, and that both SH2 domains are necessary for full activation of class IA PI3Ks (Klippel et al., 1992; Rordorf-Nikolic et al., 1995). There is also evidence that the motif environment of the peptide is important for high affinity binding and PI3K binds with higher affinity to a bis-phosphorylated RTK (Kashishian et al., 1992). The pY740 monophosphorylated peptide lead to partial activation of both cSH2 mutant and WT p110α, similar to the mutant where only the cSH2 can bind pYXXM (R358A). However, the pY751 monophosphorylated peptide in WT and the cSH2 FLVR mutant showed the same results as the cSH2 mutant in the context of the bis-phosphorylated PDGFR pY indicating that when both SH2 domains are capable of binding with high affinity, the nSH2 likely binds pY751. In the presence of bis-phosphorylated peptide, mutants lacking a competent cSH2 domain showed decreased changes in deuterium exchange associated with binding of PDGFR pY.

This study set out to investigate human diseases that appeared to be driven through p110 isoform specific mechanisms. The APDS2 mutation that leads to a deletion of part of the N-terminus of the iSH2 did show isoform specific regulatory mechanisms of class IA p110s. However, this was not the case for oncogenic mutations in the C-terminus of the iSH2, and both p110α and p110δ isoforms were similarly activated. Although mutations in this region have only been identified in solid tumour samples, their frequency is very rare and is not indicative that disease is driven through an isoform specific mechanism. It was unknown whether the APDS2 mutations would be inhibited from the p110δ specific inhibitor idelalisib. We were able to show that the most frequent APDS2 mutation was inhibited by idelalisib, leading to p110δ inhibitors as strong candidates for therapeutic intervention in these patients. This study shows the power of HDX-MS combined with biochemical tools in probing conformations of protein complexes that are difficult to study through other structural techniques.

Chapter 5:
Discussion and Future Directions

5.1 Summary of research objectives

Class IA PI3Ks are vital for the propagation of extracellular signals through their production of PIP_3, leading to cell growth, metabolism, and proliferation. The class IA enzymes are obligate heterodimers composed of a catalytic subunit (p110) and a regulatory subunit (p85-like) that mediates the inhibition of and the activation of enzymatic activity downstream of phosphorylated receptors at the PM. The complex regulatory network of interfaces that occurs within and between the two proteins, along with other regulation mechanisms such as cellular subset expression and a variety of upstream and downstream signalling partners makes the study of class IA PI3K biology challenging. The class IA PI3Ks have been extensively studied starting in the early 1990's, with approximately 3000 new publications on these enzymes now released every year. Despite this abundance of knowledge, questions remain regarding the regulation of these complex enzymes.

During the course of this thesis, I have set out to answer key questions regarding the regulatory mechanisms that mediate class IA PI3K activity in the context of both its inhibition and its activation downstream of phosphorylated receptors (RTKs and adaptors). To this end, I have used a sophisticated suite of biochemical tools combined with HDX-MS to probe allosteric conformational mechanisms of class IA PI3K regulation. Prior elucidation of PI3K regulatory mechanisms through determination of allosteric conformational changes has paved the way for the methodological flow-path used in this thesis (Burke et al., 2012, 2011; Vadas et al., 2011).

The primary objective of this dissertation has been to identify the mechanisms that mediate the natural activation cycle of class IA PI3Ks and to characterise how activating disease mutations lead to perturbations to the normal class IA PI3K function. In chapter 4 I addressed how mutations in PIK3CD that result in single residue mutations in the p110δ isoform of the catalytic subunit mediate activation over the WT enzyme. In chapter 5 I

investigated the consequences of mutations in PIK3R1 that result in truncations of the regulatory subunit p85α, and how different mutations could exhibit isoform specific activation. In this chapter, I will discuss the implications of the results from chapter 4 and chapter 5 and the questions that remain. Finally, I will discuss the therapeutic potential with relation to the results displayed in this thesis, followed by future directions to further probe the complex class IA PI3K regulatory network.

5.2 Mutations of class IA PI3Ks

The class IA PI3Ks are integral in mediating growth, proliferation, survival and development in cells. The inter and intra protein interactions of class IA PI3Ks and their ability to be activated downstream of a wide array of membrane receptors combine to make a complex regulatory network. PIP_3 levels must be precisely controlled in this network to mediate the correct cellular role in response to extracellular signals. Perturbations to the natural function of PI3Ks leads to a wide variety of human diseases, including diabetes, cancers, developmental disorders, and immunodeficiency.

The majority of mutations identified as causative in PI3K driven disease states have been activating mutations, leading to increased PIP_3 levels and thus, increased downstream signalling due to the role of PIP_3 in localising and activating proteins containing PIP_3 specific binding domains. The most well studied activating mutations have been those that drive oncogenesis, with a focus on mutations in PIK3CA, the gene that encodes p110α. PIK3CA is one of the most mutated genes in many cancers and prevalence of these activating, oncogenic mutations is considerably higher than in other subunits (Millis et al., 2016; Samuels et al., 2004). Somatic mutations in PIK3CD can lead to cancers of the blood, however, germline mutations in PIK3CD can result in activation of p110δ which lead to primary immunodeficiency. Low or absent PIP_3 levels can also be pathogenic. Mutations in PIK3R1, encoding the regulatory subunit p85α (and in some cases, p55α, p50α) have been identified in patients with the developmental disorder SHORT syndrome. These mutations lead to an inability of PI3K to be properly activated downstream of agonist stimulated membrane receptors. There have also been patients recently identified with PIK3CD mutations that lead to abolished p110δ driven PI3K signalling. These mutations

lead to a premature stop site before the kinase domain, or deletion of key residues in the ATP binding cleft (Cohen et al., 2018; Sogkas et al., 2018).

Interestingly, pathogenic mutations appear to occur in specific subsets of PI3K subunits. For example, activating mutations in PIK3CB, or p110β, are distinctly lacking. Both p110α and p110β are expressed ubiquitously and are necessary for cell growth and proliferation (Bi et al., 2002, 1999; Foukas et al., 2010). Activating mutations often lead to disruption of inhibitory interfaces to drive increased activity or conformational changes that mimic natural activation mechanisms of PI3Ks, so it is mysterious as to why activating mutations are not more frequently found in PIK3CB.

The regulatory subunits also exhibit isoform differences, where mutations in PIK3R1 can be oncogenic (somatic) or can lead to primary immunodeficiency (germline). Somatic mutations in PIK3R2 can lead to overgrowth and developmental disorders, with far fewer oncogenic mutations identified in PIK3R2 or PIK3R3 (Forbes et al., 2016).

Molecular mechanisms of activating mutations in PIK3CD mediating conformational disruption of p110δ/p85α

Since the discovery of activating germline mutations in PIK3CD, nine residues with eleven total mutations have been identified (Angulo et al., 2013; Jou et al., 2006). These mutations occur throughout the primary sequence of p110δ and include E81K, G124D, N334K, R405C, C416R, E525A/E, R929C, E1021K, and E1025G/K (Crank et al., 2014; Dulau-Florea et al., 2017; Edwards et al., 2019; Lucas et al., 2013; Rae et al., 2017; Takeda et al., 2017; Tsujita et al., 2016; Wentink et al., 2017). The p110α isoform is frequently mutated in cancer, and mutations are distributed throughout the primary sequence (Samuels et al., 2004). The APDS1 mutations identified in p110δ are located in similar locations to oncogenic mutations that have been identified in p110α (Rudd et al., 2011). One of the major questions is whether mutations in p110δ lead to activation of lipid kinase activity by a mechanism similar to oncogenic mutations in p110α. HDX-MS experiments on WT PI3Kδ showed that there are four conformational differences upon pY activation and membrane binding: (*i*) disruption of the nSH2 and cSH2 inhibitory contacts, (*ii*) disruption of the C2–iSH2 interface, (*iii*) reorientation of the ABD relative to the rest of the catalytic

subunit, and (*iv*) interaction of the kinase domain with membranes. All of the tested p110δ mutations mimicked or enhanced one of these conformational differences.

The E81K and G124D mutants both led to a reorientation of the ABD relative to the rest of the catalytic subunit. Additionally, G124D also showed disruption of the C2-iSH2 interface. The E525K mutant led to disruption of the nSH2–helical interface, similar to the level seen upon WT binding to phosphopeptide. The E1021K mutant led to conformational changes within the kinase domain in regions that interact with the membrane surface, with similar effects to those seen in the H1047R p110α mutant. The location of the cSH2–kinase interface near the E1021K mutation had alluded to a mechanism of activation through disruption of the cSH2 interface that increases membrane affinity (Angulo et al., 2013); however, no conformational differences in the cSH2 were observed, implying that this inhibitory interface is maintained. The likely mechanism for activation of E1021K is increased membrane recruitment, similar to H1047R in p110α. Indeed, HDX-MS of all mutants tested in the presence of PM mimic membrane showed enhanced membrane binding and the E1021K mutant showed the largest changes in these regions.

As APDS1 mutations in p110δ and oncogenic mutations in p110α both stimulate PI3K activity by similar mechanisms, we could expect mutations in p110δ that occur in analogous regions to oncogenic mutants in p110α will cause APDS. Similar to p110α H1047R mutation, E1021K of p110δ is the most common APDS1 mutation identified to date. Despite this, the overall frequency of E1021K is lower in relation to other activating mutation sites as opposed to H1047R which is the most frequent. What this indicates is that APDS1 mutations are more frequently found throughout the primary sequence. Patients exhibiting an undefined primary immunodeficiency should therefore have their entire PIK3CD coding region screened for mutations, as opposed to SNP genotyping, to ensure APDS can be diagnosed efficiently.

Molecular mechanisms of how mutations in PIK3R1 lead to isoform specific activation of class IA PI3Ks

The p85-like regulatory subunits are necessary for the stability of the class IA PI3K heterodimers; They mediate the inhibition and activation of PI3K complexes downstream of phosphorylated receptors harbouring the pYXXM motif that is bound by the SH2 domains that all p85-like subunits have. Mutations in the regulatory subunits lead to perplexing phenotypes reminiscent of isoform specific cellular roles and that mimic activating mutations that occur in specific catalytic p110 isoforms. This led to the idea that perhaps there exist isoform specific regulatory mechanisms mediated through the p85-like subunits through their interactions with different class IA catalytic isoforms. The most common APDS2 mutation leads to an internal deletion at the N-terminus of the iSH2 (Deau et al., 2014; Lucas et al., 2014). Oncogenic mutations that are putatively p110α driven exist that lead to deletions of p110α at the C-terminus. These mutations, which exhibit isoform specific phenotypes, were an opportunity to study isoform specific regulatory mechanisms and further define the role of the iSH2 in mediating regulation of p110 subunits.

Our biochemical and structural studies show that the APDS2 mutant of p85α leads to a substantial basal activation of PI3Kδ at a level close to the fully activated state when bound to phosphopeptide mimicking RTK stimulation. The APDS2 complex of PI3Kα was only weakly basally activated and was hyperactivated by RTK pY. HDX-MS results showed a disruption of the C2–iSH2 and reorientation of the ABD in the PI3Kα APDS2 complex, and this provides a possible mechanism for RTK pY hyperactivation compared with WT. The APDS2 PI3Kδ complex was only weakly hyperactivated by RTK pY, possibly suggesting that the ABD and C2–iSH2 interfaces are already broken in the absence of RTK pY. The HDX-MS results revealed that in the APDS2 PI3Kδ complex all inhibitory interfaces between the nSH2, iSH2, and cSH2 of p85α were; however, in PI3Kα the inhibitory interface with the nSH2 is only partially disrupted. Previous HDX-MS comparisons between PI3Kα and PI3Kδ showed that the nSH2 is more tightly bound to p110α compared with p110δ (Burke and Williams, 2013). Both the HDX-MS and kinase assays indicate that an intact coiled-coil is required to maintain the nSH2 and cSH2 interactions in PI3Kδ, whereas the tighter interaction between nSH2 and p110α is able to

maintain a partial level of inhibition in the absence of the full iSH2 coiled-coil. This difference in activation level in the APDS2 complex of PI3Kδ compared with PI3Kα provides a possible molecular mechanism for how APDS2 mutations in *PIK3R1* phenocopy the APDS1 mutations in *PIK3CD*. The basal partial activation in p110α/Δ434–475 p85α may still be relevant as an oncogene due to its discovery as being somatically mutated in endometrial carcinomas (Urick et al., 2011). The hyperactivation of the APDS2 complex of PI3Kα by pY compared with WT further underscores this potential relevance; however, further study will be required to examine the expression and stability of the APDS2 PI3Kα complex to understand the difference between oncogenicity in germline and somatic mutations.

The oncogenic and engineered C-terminal mutants result in truncation of the iSH2 at distinct structural points. Biochemical data showed that disruption of the coiled-coil within the α2 helix led to full activation of the Q572* mutation in both p110α and p110δ complexes. HDX-MS of p110α/p85α-Q572* showed disruption of most of the inhibitory interfaces, mimicking all four of the major conformational changes identified in the PI3K natural activation cycle as stated above. Interestingly, the other deletion mutants led to a desensitization of the p110/p85 complexes to the stimulating PDGFR pY. The mutants were able to reach full activation, however they required a higher concentration to do so. The SHORT mutation of the FLVR domain (R649W) that binds the pYXXM motifs of PDGFR and other phosphorylated membrane receptors/proteins is known to result in decreased PI3K pathway signalling (Chudasama et al., 2013; Dyment et al., 2013). Our results show that R649W leads to the same observed activity, where desensitisation to PDGFR pY occurs. The impairment of PI3K signalling upon agonist stimulation specifically due to the loss of pYXXM binding by the cSH2 is mildly perplexing in the case of p110α, as in this isoform the cSH2 does not make contacts with the catalytic subunit (Burke et al., 2012). However, the cSH2 drives high affinity binding of pYXXM motifs over the nSH2 and the nSH2 binds more tightly in p110α (Burke and Williams, 2013; Klippel et al., 1992). Taken together, these data further identify the role of the cSH2-pYXXM binding as a type of template, acting to localise PI3K to activated receptors and to the membrane. HDX-MS of the cSH2 FLVR mutant showed reduced changes associated

with PDGFR pY binding and activation compared to WT, even at a high concentration. The E601* cSH2 truncation showed a complete lack of changes associated with pYXXM binding, even in the nSH2. This indicates that without the cSH2 domain, access to the nSH2 might be limited as the nSH2 can still bind one of the PDGFR pYXXM motifs (pY740) with high affinity (Panayotou et al., 1993).

5.3 Therapeutic Potential of Class IA PI3Ks

The role of class IA PI3Ks in a variety of devastating human diseases make them prime targets for drug design. Indeed, many attempts have been made to develop compounds that target class IA PI3Ks, and the focus has been shifted towards the promise of isoform specific inhibitors to reduce the intense side effects that have come to be associated with PI3K inhibitors.

Many of the APDS1 and APDS2 mutants in p110δ/p85α led to conformational changes in the active site of the enzyme. APDS1/2 treatment strategies have previously used Rapamycin, an mTOR inhibitor, to target the overactive PI3K/AKT/mTOR signalling pathway and recent studies have been initiated on the use of oral and inhaled p110δ specific inhibitors (Khindri et al., 2018; Rao et al., 2017). Reports of the severe side effects caused by idelalisib make it a less desirable therapeutic however more recent p110δ specific inhibitor have shown more promising safety profiles with no reports of severe side effects (Ino et al., 2019; Rao et al., 2017; Wilson et al., 2018). Identification of conformation specific inhibitors that target mutant proteins like those of BRAF kinase mutant V600E (Flaherty et al., 2010; Tsai et al., 2008) is unlikely for APDS as it is relatively rare and mutations appear more disperse than in oncogenic p110α mutations where H1047R occurs at much higher frequency over any other mutation. It was previously unknown whether p110δ inhibitors could target APDS2 mutations. We showed that the potent and specific p110δ inhibitor Idelalisib was as effective at targeting all APDS1 and APDS2 mutants with similar IC_{50} values as the WT enzyme for the APDS2 mutant and ~4 Fold higher IC50s for APDS1 mutants. The differences in IC_{50} values could be due to conformational changes in the active site that were too small to meet our significance threshold in the HDX-MS experiments but still effectively modify how Idelalisib binds. Regardless, these data are

promising for development of further p110δ specific inhibitors. These data pave the way to more effectively address therapeutic options for all APDS patients, and could lead to novel therapeutic options for patients with APDS2.

5.4 Future Explorations

Class IA PI3Ks are heterodimers composed of the p110 catalytic isoforms in complex with the p85-like regulatory subunits. The work in this thesis has elucidated novel mechanisms of class IA PI3K regulation in the context of p110δ and p110α catalytic isoforms in complex with the regulatory subunit p85α. The existence of five total p85-like regulatory subunits and three p110 catalytic isoforms leads to the possibility of seventeen different heterodimer complex combinations. Each catalytic isoform is also activated downstream of different activating stimuli, including phosphorylated receptors (RTKs) and their adaptors, small GTPases, and heterotrimeric GPCRs. Characterising class IA PI3K subunit interactions and how upstream proteins interact with class IA PI3Ks to activate their activity will lead to a more comprehensive understanding of the complex nature of class IA PI3K regulation and could pave the way for better understanding class IA PI3K driven disease.

Recent work has shown preferential binding of catalytic isoforms with p85-like subunits. The p110δ isoform preferentially binds to p85α, whereas p110α and p110β showed no preference for either p85α or p85β (Tsolakos et al., 2018). This could explain the absence of p85β mutations in APDS patients, where mutations in this subunit might not affect p110δ activation in the cell due to a dominance of p110δ/p85α heterodimers. To fully understand these differences in observed heterodimer formation, the conformational differences associated with p110/p85 complex formation between different isoforms will need to be characterised. The dose of PI3K, both in levels and in output of PIP_3, also appears to play a role in cellular consequences. Investigations of the most frequent oncogenic p110α activating mutation H1047R ability to lead to cellular transformation revealed that heterozygosity of the mutation alone was not enough to lead to transformation and that further mutations in p110α mutations or other members of the pathway was necessary (Madsen et al., 2019). This is particularly interesting as patients with APDS1/2

exhibit a high degree of variability in the severity of the disease, regardless of the mutation location (Lucas et al., 2016). The existence of patients with activating or loss of function mutations in p110δ also highlights the necessity of finely tuned levels of activity (Cohen et al., 2018; Lucas et al., 2016; Sogkas et al., 2018; Tangye et al., 2019). Thus, understanding how class IA PI3K levels are precisely tuned is clearly important.

Another level of complexity to class IA PI3K regulatory mechanisms is the existence of free p85-like subunits. In low stimulation or unstimulated cellular conditions, there was an enrichment of p85 monomers at PDGFRs (Tsolakos et al., 2018). Free p85 has also been postulated to down regulate insulin signalling through sequestration of IRS-1 and ablation of p85α leads to hypoglycemia and increased sensitivity to insulin (Luo et al., 2005; Thorpe et al., 2017). Stoichiometry of free p85 to p110/p85 heterodimers have also been shown to differ depending on cell type, with some cell types showing a 2:1 ratio of free p85 to heterodimer (Cheung et al., 2011; Geering et al., 2007) and homodimers of p85 potentially regulate PTEN activity (Cheung et al., 2015; LoPiccolo et al., 2015). Understanding of how free p85-like subunits form homodimers, or interactions with membrane receptors, and how these functions can mediate class IA PI3K regulation will also further clarify the complex regulation of class IA PI3K signalling.

5.5 Conclusion

The class IA PI3Ks mediate many cellular processes involved in cell growth and proliferation, and perturbation of class IA PI3K regulation can lead to devastating human diseases. Understanding the natural regulation of these enzymes thus has huge implications in basic cell biology and the identification of novel therapeutics. This thesis has defined the molecular mechanisms of activating mutations in PIK3CD and PIK3R1. which has led to the identification of novel isoform specific regulatory mechanisms of class IA PI3Ks. This information is imperative to creating a fully comprehensive understanding of class IA PI3K biology, and in the design of novel therapeutic strategies to treat patients with cancer, APDS, diabetes, or overgrowth syndromes.

Bibliography

Ahn J, Jung MC, Wyndham K, Yu YQ, Engen JR. 2012. Pepsin Immobilized on High-Strength Hybrid Particles for Continuous Flow Online Digestion at 10 000 psi. *Analytical Chemistry* **84**:7256–7262. doi:10.1021/ac301749h

Alessi DR, Andjelkovic M, Caudwell B, Cron P, Morrice N, Cohen P, Hemmings BA. 1996. Mechanism of activation of protein kinase B by insulin and IGF-1. *EMBO J* **15**:6541–6551.

Alessi DR, James SR, Downes CP, Holmes AB, Gaffney PRJ, Reese CB, Cohen P. 1997. Characterization of a 3-phosphoinositide-dependent protein kinase which phosphorylates and activates protein kinase Bα. *Current Biology* **7**:261–269. doi:10.1016/S0960-9822(06)00122-9

Angulo I, Vadas O, Garçon F, Banham-Hall E, Plagnol V, Leahy TR, Baxendale H, Coulter T, Curtis J, Wu C, Blake-Palmer K, Perisic O, Smyth D, Maes M, Fiddler C, Juss J, Cilliers D, Markelj G, Chandra A, Farmer G, Kielkowska A, Clark J, Kracker S, Debré M, Picard C, Pellier I, Jabado N, Morris JA, Barcenas-Morales G, Fischer A, Stephens L, Hawkins P, Barrett JC, Abinun M, Clatworthy M, Durandy A, Doffinger R, Chilvers ER, Cant AJ, Kumararatne D, Okkenhaug K, Williams RL, Condliffe A, Nejentsev S. 2013. Phosphoinositide 3-kinase δ gene mutation predisposes to respiratory infection and airway damage. *Science* **342**:866–871. doi:10.1126/science.1243292

Auger KR, Serunian LA, Soltoff SP, Libby P, Cantley LC. 1989. PDGF-dependent tyrosine phosphorylation stimulates production of novel polyphosphoinositides in intact cells. *Cell* **57**:167–175. doi:10.1016/0092-8674(89)90182-7

Backer JM, Myers MG, Shoelson SE, Chin DJ, Sun XJ, Miralpeix M, Hu P, Margolis B, Skolnik EY, Schlessinger J. 1992. Phosphatidylinositol 3'-kinase is activated by association with IRS-1 during insulin stimulation. *EMBO J* **11**:3469–3479.

Bai Y, Milne JS, Mayne L, Englander SW. 1994. Protein stability parameters measured by hydrogen exchange. *Proteins: Structure, Function, and Genetics* **20**:4–14. doi:10.1002/prot.340200103

Bai Y, Milne JS, Mayne L, Englander SW. 1993. Primary Structure Effects on Peptide Group Hydrogen Exchange. *Proteins* **17**:75–86. doi:10.1002/prot.340170110

Bárcena C, Quesada V, Sandre-Giovannoli AD, Puente DA, Fernández-Toral J, Sigaudy S, Baban A, Lévy N, Velasco G, López-Otín C. 2014. Exome sequencing identifies a novel mutation in PIK3R1 as the cause of SHORT syndrome. *BMC Medical Genetics* **15**:51. doi:10.1186/1471-2350-15-51

Barr PM, Saylors GB, Spurgeon SE, Cheson BD, Greenwald DR, O'Brien SM, Liem AKD, Mclntyre RE, Joshi A, Abella-Dominicis E, Hawkins MJ, Reddy A, Paolo JD, Lee H, He J, Hu J, Dreiling LK, Friedberg JW. 2016. Phase 2 study of idelalisib and entospletinib: pneumonitis limits combination therapy in relapsed refractory CLL and NHL. *Blood* **127**:2411–2415. doi:10.1182/blood-2015-12-683516

Baskaran S, Carlson L-A, Stjepanovic G, Young LN, Kim DJ, Grob P, Stanley RE, Nogales E, Hurley JH. 2014. Architecture and dynamics of the autophagic phosphatidylinositol 3-kinase complex. *eLife* **3**:1497. doi:10.7554/eLife.05115

Berndt A, Miller S, Williams O, Le DD, Houseman BT, Pacold JI, Gorrec F, Hon W-C, Liu Y, Rommel C, Gaillard P, Rückle T, Schwarz MK, Shokat KM, Shaw JP, Williams RL. 2010. The p110δ structure: mechanisms for selectivity and potency of new PI(3)K inhibitors. *Nature Chemical Biology* **6**:117–124. doi:10.1038/nchembio.293

Bi L, Okabe I, Bernard DJ, Nussbaum RL. 2002. Early embryonic lethality in mice deficient in the p110β catalytic subunit of PI 3-kinase. *Mammalian Genome* **13**:169–172. doi:10.1007/BF02684023

Bi L, Okabe I, Bernard DJ, Wynshaw-Boris A, Nussbaum RL. 1999. Proliferative defect and embryonic lethality in mice homozygous for a deletion in the p110alpha subunit of phosphoinositide 3-kinase. *J Biol Chem* **274**:10963–10968.

Bilancio A, Okkenhaug K, Camps M, Emery JL. 2006. Key role of the p110δ isoform of PI3K in B-cell antigen and IL-4 receptor signaling: comparative analysis of genetic and pharmacologic interference with interference with p110δ function in B cells. *Blood*.

Bondeva T, Pirola L, Bulgarelli-Leva G, Rubio I, Wetzker R, Wymann MP. 1998. Bifurcation of Lipid and Protein Kinase Signals of PI3Kγ to the Protein Kinases PKB and MAPK. *Science* **282**:293–296. doi:10.1126/science.282.5387.293

Bravo García-Morato M, García-Miñaúr S, Molina Garicano J, Santos Simarro F, Del Pino Molina L, López-Granados E, Ferreira Cerdán A, Rodríguez Pena R. 2017. Mutations in PIK3R1 can lead to APDS2, SHORT syndrome or a combination of the two. *Clinical Immunology* **179**:77–80. doi:10.1016/j.clim.2017.03.004

Breeze AL, Kara BV, Barratt DG, Anderson M, Smith JC, Luke RW, Best JR, Cartlidge SA. 1996. Structure of a specific peptide complex of the carboxy-terminal SH2 domain from the p85 alpha subunit of phosphatidylinositol 3-kinase. *EMBO J* **15**:3579–3589.

Brown JR, Auger KR. 2011. Phylogenomics of phosphoinositide lipid kinases: perspectives on the evolution of second messenger signaling and drug discovery. *BMC Evolutionary Biology 2011 11:1* **11**:4. doi:10.1186/1471-2148-11-4

Brunet A, Bonni A, Zigmond MJ, Lin MZ, Juo P, Hu LS, Anderson MJ, Arden KC, Blenis J, Greenberg ME. 1999. Akt Promotes Cell Survival by Phosphorylating and Inhibiting a Forkhead Transcription Factor. *Cell* **96**:857–868. doi:10.1016/S0092-8674(00)80595-4

Buckles TC, Ziemba BP, Masson GR, Williams RL, Falke JJ. 2017. Single-Molecule Study Reveals How Receptor and Ras Synergistically Activate PI3Kα and PIP3 Signaling. *Biophysical Journal* **113**:2396–2405. doi:10.1016/j.bpj.2017.09.018

Burgering BMT, Coffer PJ. 1995. Protein kinase B (c-Akt) in phosphatidylinositol-3-OH kinase signal transduction. *Nature* **376**:599. doi:10.1038/376599a0

Burke JE. 2018. Structural Basis for Regulation of Phosphoinositide Kinases and Their Involvement in Human Disease. *Molecular Cell* **71**:653–673. doi:10.1016/j.molcel.2018.08.005

Burke JE, Perisic O, Masson GR, Vadas O, Williams RL. 2012. Oncogenic mutations mimic and enhance dynamic events in the natural activation of phosphoinositide 3-kinase p110α (PIK3CA). *Proc Natl Acad Sci USA* **109**:15259–15264. doi:10.1073/pnas.1205508109

Burke JE, Vadas O, Berndt A, Finegan T, Perisic O. 2011. Dynamics of the phosphoinositide 3-kinase p110δ interaction with p85α and membranes reveals aspects of regulation distinct from p110α. *Structure* **19**:1127–1137. doi:10.1016/j.str.2011.06.003

Burke JE, Williams RL. 2015. Synergy in activating class I PI3Ks. *Trends in Biochemical Sciences*. doi:10.1016/j.tibs.2014.12.003

Burke JE, Williams RL. 2013. Dynamic steps in receptor tyrosine kinase mediated activation of class IA phosphoinositide 3-kinases (PI3K) captured by H/D exchange (HDX-MS). *Adv Biol Regul* **53**:97–110. doi:10.1016/j.jbior.2012.09.005

Cantley LC, Neel BG. 1999. New insights into tumor suppression: PTEN suppresses tumor formation by restraining the phosphoinositide 3-kinase/AKT pathway. *PNAS* **96**:4240–4245. doi:10.1073/pnas.96.8.4240

Carpten JD, Faber AL, Horn C, Donoho GP, Briggs SL, Robbins CM, Hostetter G, Boguslawski S, Moses TY, Savage S, Uhlik M, Lin A, Du J, Qian Y-W, Zeckner DJ, Tucker-Kellogg G, Touchman J, Patel K, Mousses S, Bittner M, Schevitz R, Lai M-HT, Blanchard KL, Thomas JE. 2007. A transforming mutation in the pleckstrin homology domain of AKT1 in cancer. *Nature* **448**:439–444. doi:10.1038/nature05933

Castanedo GM, Blaquiere N, Beresini M, Bravo B, Brightbill H, Chen J, Cui H-F, Eigenbrot C, Everett C, Feng J, Godemann R, Gogol E, Hymowitz S, Johnson A, Kayagaki N, Kohli PB, Knüppel K, Kraemer J, Krüger S, Loke P, McEwan P, Montalbetti C, Roberts DA, Smith M, Steinbacher S, Sujatha-Bhaskar S,

Takahashi R, Wang X, Wu LC, Zhang Y, Staben ST. 2017. Structure-Based Design of Tricyclic NF-κB Inducing Kinase (NIK) Inhibitors That Have High Selectivity over Phosphoinositide-3-kinase (PI3K). *J Med Chem* **60**:627–640. doi:10.1021/acs.jmedchem.6b01363

Castellano E, Sheridan C, Thin MZ, Nye E, Spencer-Dene B, Diefenbacher ME, Moore C, Kumar MS, Murillo MM, Grönroos E, Lassailly F, Stamp G, Downward J. 2013. Requirement for Interaction of PI3-Kinase p110α with RAS in Lung Tumor Maintenance. *Cancer Cell* **24**:617–630. doi:10.1016/j.ccr.2013.09.012

Chalhoub N, Baker SJ. 2009. PTEN and the PI3-kinase pathway in cancer. *Annu Rev Pathol* **4**:127–150. doi:10.1146/annurev.pathol.4.110807.092311

Chantry D, Vojtek A, Kashishian A, Holtzman DA, Wood C, Gray PW, Cooper JA, Hoekstra MF. 1997. p110δ, a Novel Phosphatidylinositol 3-Kinase Catalytic Subunit That Associates with p85 and Is Expressed Predominantly in Leukocytes. *J Biol Chem* **272**:19236–19241. doi:10.1074/jbc.272.31.19236

Cherfils J, Zeghouf M. 2013. Regulation of Small GTPases by GEFs, GAPs, and GDIs. *Physiological Reviews* **93**:269–309. doi:10.1152/physrev.00003.2012

Cheung LW, Walkiewicz KW, Besong TM, Guo H, Hawke DH, Arold ST, Mills GB. 2015. Regulation of the PI3K pathway through a p85α monomer–homodimer equilibrium. *eLife* **4**:e06866. doi:10.7554/eLife.06866

Cheung LWT, Hennessy BT, Li J, Yu S, Myers AP, Djordjevic B, Lu Y, Stemke-Hale K, Dyer MD, Zhang F, Ju Z, Cantley LC, Scherer SE, Liang H, Lu KH, Broaddus RR, Mills GB. 2011. High frequency of PIK3R1 and PIK3R2 mutations in endometrial cancer elucidates a novel mechanism for regulation of PTEN protein stability. *Cancer Discovery* **1**:170–185. doi:10.1158/2159-8290.CD-11-0039

Cheung LWT, Yu S, Zhang D, Li J, Ng PKS, Panupinthu N, Mitra S, Ju Z, Yu Q, Liang H, Hawke DH, Lu Y, Broaddus RR, Mills GB. 2014. Naturally Occurring Neomorphic PIK3R1 Mutations Activate the MAPK Pathway, Dictating Therapeutic Response to MAPK Pathway Inhibitors. *Cancer Cell* **26**:479–494. doi:10.1016/j.ccell.2014.08.017

Chudasama KK, Winnay J, Johansson S, Claudi T, König R, Haldorsen I, Johansson B, Woo JR, Aarskog D, Sagen JV, Kahn CR, Molven A, Njølstad PR. 2013. SHORT Syndrome with Partial Lipodystrophy Due to Impaired Phosphatidylinositol 3 Kinase Signaling. *The American Journal of Human Genetics* **93**:150–157. doi:10.1016/j.ajhg.2013.05.023

Ciraolo E, Morello F, Hobbs RM, Wolf F, Marone R, Iezzi M, Lu X, Mengozzi G, Altruda F, Sorba G, Guan K, Pandolfi PP, Wymann MP, Hirsch E. 2010. Essential Role of the p110β Subunit of Phosphoinositide 3-OH Kinase in Male Fertility. *MBoC* **21**:704–711. doi:10.1091/mbc.e09-08-0744

Cohen SB, Bainter W, Johnson JL, Lin T-Y, Wong JCY, Wallace J, Jones J, Mir F, Qamar F, Cantley LC, Geha RS, Chou J. 2018. Human primary immunodeficiency caused by expression of a kinase-dead p110δ mutant. *Journal of Allergy and Clinical Immunology*. doi:10.1016/j.jaci.2018.10.005

Compagno M, Wang Q, Pighi C, Cheong T-C, Meng F-L, Poggio T, Yeap L-S, Karaca E, Blasco RB, Langellotto F, Ambrogio C, Voena C, Wiestner A, Kasar SN, Brown JR, Sun J, Wu CJ, Gostissa M, Alt FW, Chiarle R. 2017. Phosphatidylinositol 3-kinase δ blockade increases genomic instability in B cells. *Nature* **542**:489–493. doi:10.1038/nature21406

Conley ME, Dobbs AK, Quintana AM, Bosompem A, Wang Y-D, Coustan-Smith E, Smith AM, Perez EE, Murray PJ. 2012. Agammaglobulinemia and absent B lineage cells in a patient lacking the p85α subunit of PI3K. *J Exp Med* **209**:463–470. doi:10.1084/jem.20112533

Connelly GP, Bai Y, Jeng MF, Englander SW. 1993. Isotope effects in peptide group hydrogen exchange. *Proteins* **17**:87–92. doi:10.1002/prot.340170111

Coulter TI, Cant AJ. 2018. The Treatment of Activated PI3Kδ Syndrome. *Front Immunol* **9**. doi:10.3389/fimmu.2018.02043

Coulter TI, Chandra A, Bacon CM, Babar J, Curtis J, Screaton N, Goodlad JR, Farmer G, Steele CL, Leahy TR, Doffinger R, Baxendale H, Bernatoniene J, Edgar JDM, Longhurst HJ, Ehl S, Speckmann C, Grimbacher B, Sediva A, Milota T, Faust SN, Williams AP, Hayman G, Kucuk ZY, Hague R, French P, Brooker R, Forsyth P, Herriot R, Cancrini C, Palma P, Ariganello P, Conlon N, Feighery C, Gavin PJ, Jones A, Imai K, Ibrahim MAA, Markelj G, Abinun M, Rieux-Laucat F, Latour S, Pellier I, Fischer A, Touzot F, Casanova J-L, Durandy A, Burns SO, Savic S, Kumararatne DS, Moshous D, Kracker S, Vanhaesebroeck B, Okkenhaug K, Picard C, Nejentsev S, Condliffe AM, Cant AJ. 2017. Clinical spectrum and features of activated phosphoinositide 3-kinase δ syndrome: A large patient cohort study. *J Allergy Clin Immunol* **139**:597-606.e4. doi:10.1016/j.jaci.2016.06.021

Crank MC, Grossman JK, Moir S, Pittaluga S, Buckner CM, Kardava L, Agharahimi A, Meuwissen H, Stoddard J, Niemela J, Kuehn H, Rosenzweig SD. 2014. Mutations in PIK3CD can cause hyper IgM syndrome (HIGM) associated with increased cancer susceptibility. *J Clin Immunol* **34**:272–276. doi:10.1007/s10875-014-0012-9

Damen JE, Liu L, Rosten P, Humphries RK, Jefferson AB, Majerus PW, Krystal G. 1996. The 145-kDa protein induced to associate with Shc by multiple cytokines is an inositol tetraphosphate and phosphatidylinositol 3,4,5-triphosphate 5-phosphatase. *PNAS* **93**:1689–1693. doi:10.1073/pnas.93.4.1689

Dbouk HA, Vadas O, Shymanets A, Burke JE, Salamon RS, Khalil BD, Barrett MO, Waldo GL, Surve C, Hsueh C, Perisic O, Harteneck C, Shepherd PR, Harden TK,

Smrcka AV, Taussig R, Bresnick AR, Nürnberg B, Williams RL, Backer JM. 2012. G Protein–Coupled Receptor–Mediated Activation of p110β by Gβγ Is Required for Cellular Transformation and Invasiveness. *Sci Signal* **5**:ra89. doi:10.1126/scisignal.2003264

Deau M-C, Heurtier L, Frange P, Suarez F, Bole-Feysot C, Nitschke P, Cavazzana M, Picard C, Durandy A, Fischer A, Kracker S. 2014. A human immunodeficiency caused by mutations in the PIK3R1 gene. *J Clin Invest* **124**:3923–3928. doi:10.1172/JCI75746

Dhand R, Hara K, Hiles I, Bax B, Gout I, Panayotou G, Fry MJ, Yonezawa K, Kasuga M, Waterfield MD. 1994. PI 3-kinase: structural and functional analysis of intersubunit interactions. *EMBO J* **13**:511–521.

Dornan GL, Burke JE. 2018. Molecular Mechanisms of Human Disease Mediated by Oncogenic and Primary Immunodeficiency Mutations in Class IA Phosphoinositide 3-Kinases. *Front Immunol* **9**. doi:10.3389/fimmu.2018.00575

Dornan GL, Siempelkamp BD, Jenkins ML, Vadas O, Lucas CL, Burke JE. 2017. Conformational disruption of PI3Kδ regulation by immunodeficiency mutations in PIK3CD and PIK3R1. *PNAS* **114**:1982–1987. doi:10.1073/pnas.1617244114

Dulau-Florea AE, Braylan RC, Schafernak KT, Williams KW, Daub J, Goyal RK, Puck JM, Rao VK, Pittaluga S, Holland SM, Uzel G, Calvo KR. 2017. Abnormal B-Cell Maturation in the Bone Marrow of Patients with Germline Mutations in PIK3CD. *J Allergy Clin Immunol* **139**:1032-1035.e6. doi:10.1016/j.jaci.2016.08.028

Dyment DA, Smith AC, Alcantara D, Schwartzentruber JA, Basel-Vanagaite L, Curry CJ, Temple IK, Reardon W, Mansour S, Haq MR, Gilbert R, Lehmann OJ, Vanstone MR, Beaulieu CL, FORGE Canada Consortium, Majewski J, Bulman DE, O'Driscoll M, Boycott KM, Innes AM. 2013. Mutations in PIK3R1 cause SHORT syndrome. *Am J Hum Genet* **93**:158–166. doi:10.1016/j.ajhg.2013.06.005

Edwards ESJ, Bier J, Cole TS, Wong M, Hsu P, Berglund LJ, Boztug K, Lau A, Gostick E, Price DA, O'Sullivan M, Meyts I, Choo S, Gray P, Holland SM, Deenick EK, Uzel G, Tangye SG. 2019. Activating PIK3CD mutations impair human cytotoxic lymphocyte differentiation and function and EBV immunity. *Journal of Allergy and Clinical Immunology* **143**:276-291.e6. doi:10.1016/j.jaci.2018.04.030

Elgizouli M, Lowe DM, Speckmann C, Schubert D, Hülsdünker J, Eskandarian Z, Dudek A, Schmitt-Graeff A, Wanders J, Jørgensen SF, Fevang B, Salzer U, Nieters A, Burns S, Grimbacher B. 2016. Activating PI3Kδ mutations in a cohort of 669 patients with primary immunodeficiency. *Clin Exp Immunol* **183**:221–229. doi:10.1111/cei.12706

Engen JR. 2009. Analysis of Protein Conformation and Dynamics by Hydrogen/Deuterium Exchange MS. *Anal Chem* **81**:7870–7875. doi:10.1021/ac901154s

Englander SW. 2006. Hydrogen Exchange and Mass Spectrometry: A Historical Perspective. *J Am Soc Mass Spectrom* **17**:1481–1489. doi:10.1016/j.jasms.2006.06.006

Englander SW, Downer NW, Teitelbaum H. 1972. Hydrogen Exchange. *Annual Review of Biochemistry* **41**:903–924. doi:10.1146/annurev.bi.41.070172.004351

Erra M, Taltavull J, Bernal FJ, Caturla JF, Carrascal M, Pagès L, Mir M, Espinosa S, Gràcia J, Domínguez M, Sabaté M, Paris S, Maldonado M, Hernández B, Bravo M, Calama E, Miralpeix M, Lehner MD, Calbet M. 2018. Discovery of a Novel Inhaled PI3Kδ Inhibitor for the Treatment of Respiratory Diseases. *Journal of Medicinal Chemistry* **61**:9551–9567. doi:10.1021/acs.jmedchem.8b00873

Escobedo JA, Navankasattusas S, Kavanaugh WM, Milfay D, Fried VA, Williams LT. 1991. cDNA cloning of a Novel 85 kd protein that has SH2 domains and regulates binding of PI3-kinase to the PDGF β-receptor. *Cell* **65**:75–82. doi:10.1016/0092-8674(91)90409-R

Ferguson KM, Kavran JM, Sankaran VG, Fournier E, Isakoff SJ, Skolnik EY, Lemmon MA. 2000. Structural basis for discrimination of 3-phosphoinositides by pleckstrin homology domains. *Mol Cell* **6**:373–384. doi:10.1038/35036032

Flaherty KT, Puzanov I, Kim KB, Ribas A, McArthur GA, Sosman JA, O'Dwyer PJ, Lee RJ, Grippo JF, Nolop K, Chapman PB. 2010. Inhibition of Mutated, Activated BRAF in Metastatic Melanoma. *New England Journal of Medicine* **363**:809–819. doi:10.1056/NEJMoa1002011

Forbes SA, Beare D, Bindal N, Bamford S, Ward S, Cole CG, Jia M, Kok C, Boutselakis H, De T, Sondka Z, Ponting L, Stefancsik R, Harsha B, Tate J, Dawson E, Thompson S, Jubb H, Campbell PJ. 2016. COSMIC: High-Resolution Cancer Genetics Using the Catalogue of Somatic Mutations in Cancer. *Curr Protoc Hum Genet* **91**:10.11.1-10.11.37. doi:10.1002/cphg.21

Foukas LC, Berenjeno IM, Gray A, Khwaja A, Vanhaesebroeck B. 2010. Activity of any class IA PI3K isoform can sustain cell proliferation and survival. *Proceedings of the National Academy of Sciences* **107**:11381–11386. doi:10.1073/pnas.0906461107

Foukas LC, Claret M, Pearce W, Okkenhaug K, Meek S, Peskett E, Sancho S, Smith AJH, Withers DJ, Vanhaesebroeck B. 2006. Critical role for the p110α phosphoinositide-3-OH kinase in growth and metabolic regulation. *Nature* **441**:366–370. doi:10.1038/nature04694

Franke TF. 1997. Direct Regulation of the Akt Proto-Oncogene Product by Phosphatidylinositol-3,4-bisphosphate. *Science* **275**:665–668. doi:10.1126/science.275.5300.665

Franke TF, Yang S-I, Chan TO, Datta K, Kazlauskas A, Morrison DK, Kaplan DR, Tsichlis PN. 1995. The protein kinase encoded by the Akt proto-oncogene is a target of the PDGF-activated phosphatidylinositol 3-kinase. *Cell* **81**:727–736. doi:10.1016/0092-8674(95)90534-0

Fritsch R, de Krijger I, Fritsch K, George R, Reason B, Kumar MS, Diefenbacher M, Stamp G, Downward J. 2013. RAS and RHO families of GTPases directly regulate distinct phosphoinositide 3-kinase isoforms. *Cell* **153**:1050–1063. doi:10.1016/j.cell.2013.04.031

Fruman DA, Chiu H, Hopkins BD, Bagrodia S, Cantley LC, Abraham RT. 2017. The PI3K Pathway in Human Disease. *Cell* **170**:605–635. doi:10.1016/j.cell.2017.07.029

Furman RR, Sharman JP, Coutre SE, Cheson BD, Pagel JM, Hillmen P, Barrientos JC, Zelenetz AD, Kipps TJ, Flinn I, Ghia P, Eradat H, Ervin T, Lamanna N, Coiffier B, Pettitt AR, Ma S, Stilgenbauer S, Cramer P, Aiello M, Johnson DM, Miller LL, Li D, Jahn TM, Dansey RD, Hallek M, O'Brien SM. 2014. Idelalisib and Rituximab in Relapsed Chronic Lymphocytic Leukemia. *New England Journal of Medicine* **370**:997–1007. doi:10.1056/NEJMoa1315226

Gallagher ES, Hudgens JW. 2016. Mapping Protein–Ligand Interactions with Proteolytic Fragmentation, Hydrogen/Deuterium Exchange-Mass SpectrometryMethods in Enzymology. Elsevier. pp. 357–404. doi:10.1016/bs.mie.2015.08.010

Geering B, Cutillas PR, Nock G, Gharbi SI, Vanhaesebroeck B. 2007. Class IA phosphoinositide 3-kinases are obligate p85-p110 heterodimers. *PNAS* **104**:7809–7814. doi:10.1073/pnas.0700373104

George S, Rochford JJ, Wolfrum C, Gray SL, Schinner S, Wilson JC, Soos MA, Murgatroyd PR, Williams RM, Acerini CL, Dunger DB, Barford D, Umpleby AM, Wareham NJ, Davies HA, Schafer AJ, Stoffel M, O'Rahilly S, Barroso I. 2004. A Family with Severe Insulin Resistance and Diabetes Due to a Mutation in AKT2. *Science* **304**:1325–1328. doi:10.1126/science.1096706

Giannakis M, Mu XJ, Shukla SA, Qian ZR, Cohen O, Nishihara R, Bahl S, Cao Y, Amin-Mansour A, Yamauchi M, Sukawa Y, Stewart C, Rosenberg M, Mima K, Inamura K, Nosho K, Nowak JA, Lawrence MS, Giovannucci EL, Chan AT, Ng K, Meyerhardt JA, Van Allen EM, Getz G, Gabriel SB, Lander ES, Wu CJ, Fuchs CS, Ogino S, Garraway LA. 2016. Genomic Correlates of Immune-Cell Infiltrates in Colorectal Carcinoma. *Cell Rep* **15**:857–865. doi:10.1016/j.celrep.2016.03.075

Gopal AK, Kahl BS, de Vos S, Wagner-Johnston ND, Schuster SJ, Jurczak WJ, Flinn IW, Flowers CR, Martin P, Viardot A, Blum KA, Goy AH, Davies AJ, Zinzani

PL, Dreyling M, Johnson D, Miller LL, Holes L, Li D, Dansey RD, Godfrey WR, Salles GA. 2014. PI3Kδ inhibition by idelalisib in patients with relapsed indolent lymphoma. *N Engl J Med* **370**:1008–1018. doi:10.1056/NEJMoa1314583

Goulden BD, Pacheco J, Dull A, Zewe JP, Deiters A, Hammond GRV. 2018. A high-avidity biosensor reveals plasma membrane PI(3,4)P $_2$ is predominantly a class I PI3K signaling product. *The Journal of Cell Biology* jcb.201809026. doi:10.1083/jcb.201809026

Gupta S, Ramjaun AR, Haiko P, Wang Y, Warne PH, Nicke B, Nye E, Stamp G, Alitalo K, Downward J. 2007. Binding of Ras to Phosphoinositide 3-Kinase p110α Is Required for Ras- Driven Tumorigenesis in Mice. *Cell* **129**:957–968. doi:10.1016/j.cell.2007.03.051

Gymnopoulos M, Elsliger M-A, Vogt PK. 2007. Rare cancer-specific mutations in PIK3CA show gain of function. *Proceedings of the National Academy of Sciences* **104**:5569–5574. doi:10.1073/pnas.0701005104

Hammond GRV, Balla T. 2015. Polyphosphoinositide binding domains: Key to inositol lipid biology. *Biochimica et Biophysica Acta (BBA) - Molecular and Cell Biology of Lipids*, Phosphoinositides **1851**:746–758. doi:10.1016/j.bbalip.2015.02.013

Hartman HN, Niemela J, Hintermeyer MK, Garofalo M, Stoddard J, Verbsky JW, Rosenzweig SD, Routes JM. 2015. Gain of Function Mutations of PIK3CD as a Cause of Primary Sclerosing Cholangitis. *Journal of Clinical Immunology* **35**:11–14. doi:10.1007/s10875-014-0109-1

Hauck F, Magg T, Krolo A, Bilic I, Hirschmugl T, Laass M, Rösen-Wolff A, Luksch H, Boztug K, Roesler J. 2017. Variant PIK3R1 Hypermorphic Mutation and Clinical Phenotypes in a Family with Short Statures, Mild Immunodeficiency and Lymphoma. *Klinische Pädiatrie* **229**:113–117. doi:10.1055/s-0043-104218

Heffron T P, Heald RA, Ndubaku C. 2016. The Rational Design of Selective Benzoxazepin Inhibitors of the α-Isoform of Phosphoinositide 3-Kinase Culminating in the Identification of (S)-2-((2-(1-Isopropyl-1 H- …. *Journal of medicinal …*.

Heffron Timothy P., Heald RA, Ndubaku C, Wei B, Augistin M, Do S, Edgar K, Eigenbrot C, Friedman L, Gancia E, Jackson PS, Jones G, Kolesnikov A, Lee LB, Lesnick JD, Lewis C, McLean N, Mörtl M, Nonomiya J, Pang J, Price S, Prior WW, Salphati L, Sideris S, Staben ST, Steinbacher S, Tsui V, Wallin J, Sampath D, Olivero AG. 2016. The Rational Design of Selective Benzoxazepin Inhibitors of the α-Isoform of Phosphoinositide 3-Kinase Culminating in the Identification of (S)-2-((2-(1-Isopropyl-1H-1,2,4-triazol-5-yl)-5,6-dihydrobenzo[f]imidazo[1,2-d][1,4]oxazepin-9-yl)oxy)propanamide (GDC-0326). *J Med Chem* **59**:985–1002. doi:10.1021/acs.jmedchem.5b01483

Herman SEM, Gordon AL, Wagner AJ, Heerema NA, Zhao W, Flynn JM, Jones J, Andritsos L, Puri KD, Lannutti BJ, Giese NA, Zhang X, Wei L, Byrd JC, Johnson AJ. 2010. Phosphatidylinositol 3-kinase-δ inhibitor CAL-101 shows promising preclinical activity in chronic lymphocytic leukemia by antagonizing intrinsic and extrinsic cellular survival signals. *Blood* **116**:2078–2088. doi:10.1182/blood-2010-02-271171

Heurtier L, Lamrini H, Chentout L, Deau M-C, Bouafia A, Rosain J, Plaza J-M, Parisot M, Dumont B, Turpin D, Merlin E, Moshous D, Aladjidi N, Neven B, Picard C, Cavazzana M, Fischer A, Durandy A, Stephan J-L, Kracker S. 2017. Mutations in the adaptor-binding domain and associated linker region of p110δ cause Activated PI3K-δ Syndrome 1 (APDS1). *Haematologica* haematol.2017.167601-13. doi:10.3324/haematol.2017.167601

Hon W-C, Berndt A, Williams RL. 2012. Regulation of lipid binding underlies the activation mechanism of class IA PI3-kinases. *Oncogene* **31**:3655–3666. doi:10.1038/onc.2011.532

Hopkins BD, Pauli C, Xing D, Wang DG, Li X, Wu D, Amadiume SC, Goncalves MD, Hodakoski C, Lundquist MR, Bareja R, Ma Y, Harris EM, Sboner A, Beltran H, Rubin MA, Mukherjee S, Cantley LC. 2018. Suppression of insulin feedback enhances the efficacy of PI3K inhibitors. *Nature*. doi:10.1038/s41586-018-0343-4

Houslay DM, Anderson KE, Chessa T, Kulkarni S, Fritsch R, Downward J, Backer JM, Stephens LR, Hawkins PT. 2016. Coincident signals from GPCRs and receptor tyrosine kinases are uniquely transduced by PI3Kβ in myeloid cells. *Sci Signal* **9**:ra82. doi:10.1126/scisignal.aae0453

Hu P, Margolis B, Skolnik EY, Lammers R, Ullrich A, Schlessinger J. 1992. Interaction of phosphatidylinositol 3-kinase-associated p85 with epidermal growth factor and platelet-derived growth factor receptors. *Molecular and Cellular Biology* **12**:981–990. doi:10.1128/MCB.12.3.981

Huang C-H, Mandelker D, Gabelli SB, Amzel LM. 2008. Insights into the oncogenic effects of PIK3CA mutations from the structure of p100α/p85α. *Cell Cycle* **7**:1151–1156. doi:10.4161/cc.7.9.5817

Huang C-H, Mandelker D, Schmidt-Kittler O, Samuels Y, Velculescu VE, Kinzler KW, Vogelstein B, Gabelli SB, Amzel LM. 2007. The structure of a human p110alpha/p85alpha complex elucidates the effects of oncogenic PI3Kalpha mutations. *Science* **318**:1744–1748. doi:10.1126/science.1150799

Huang-Doran I, Tomlinson P, Payne F, Gast A. 2016. Insulin resistance uncoupled from dyslipidemia due to C-terminal PIK3R1 mutations. *JCI insight* **1**. doi:10.1172/jci.insight.88766

Ino H, Wilson R, Terao T, Ogura H, Igarashi H, Cahn A, Numachi Y. 2019. Evaluation of the Safety, Tolerability, and Pharmacokinetics of GSK2269557 (Nemiralisib)

Administered Via Dry Powder Inhaler to Healthy Japanese Subjects. *Clinical Pharmacology in Drug Development* **8**:78–86. doi:10.1002/cpdd.614

Inoki K, Li Y, Zhu T, Wu J, Guan K-L. 2002. TSC2 is phosphorylated and inhibited by Akt and suppresses mTOR signalling. *Nature Cell Biology* **4**:648–657. doi:10.1038/ncb839

Jackson SP, Schoenwaelder SM, Goncalves I, Nesbitt WS, Yap CL, Wright CE, Kenche V, Anderson KE, Dopheide SM, Yuan Y, Sturgeon SA, Prabaharan H, Thompson PE, Smith GD, Shepherd PR, Daniele N, Kulkarni S, Abbott B, Saylik D, Jones C, Lu L, Giuliano S, Hughan SC, Angus JA, Robertson AD, Salem HH. 2005. PI 3-kinase p110β: a new target for antithrombotic therapy. *Nature Medicine* **11**:507–514. doi:10.1038/nm1232

Jaiswal BS, Janakiraman V, Kljavin NM, Chaudhuri S. 2009. Somatic mutations in p85α promote tumorigenesis through class IA PI3K activation. *Cancer Cell*.

James SR, Downes CP, Gigg R, Grove SJA, Holmes AB, Alessi DR. 1996. Specific binding of the Akt-1 protein kinase to phosphatidylinositol 3,4,5-trisphosphate without subsequent activation. *Biochemical Journal* **315**:709–713. doi:10.1042/bj3150709

Janku F, Yap TA, Meric-Bernstam F. 2018. Targeting the PI3K pathway in cancer: are we making headway? *Nature Reviews Clinical Oncology* **15**:273–291. doi:10.1038/nrclinonc.2018.28

Jimenez C, Jones DR, Rodríguez-Viciana P, Gonzalez-García A, Leonardo E, Wennström S, Kobbe C von, Toran JL, R-Borlado L, Calvo V, Copin SG, Albar JP, Gaspar ML, Diez E, Marcos MAR, Downward J, Martinez-A C, Mérida I, Carrera AC. 1998. Identification and characterization of a new oncogene derived from the regulatory subunit of phosphoinositide 3-kinase. *The EMBO Journal* **17**:743–753. doi:10.1093/emboj/17.3.743

Jones LM, Zhang H, Vidavsky I, Gross ML. 2010. An On-Line, High-Pressure Digestion System for Protein Characterization by Hydrogen/Deuterium Exchange and Mass Spectrometry. *Anal Chem* **82**:1171–1174. doi:10.1021/ac902477u

Jou S-T, Chien Y-H, Yang Y-H, Wang T-C, Shyur S-D, Chou C-C, Chang M-L, Lin D-T, Lin K-H, Chiang B-L. 2006. Identification of variations in the human phosphoinositide 3-kinase p110δ gene in children with primary B-cell immunodeficiency of unknown aetiology. *International Journal of Immunogenetics* **33**:361–369. doi:10.1111/j.1744-313X.2006.00627.x

Jura N, Zhang X, Endres NF, Seeliger MA, Schindler T, Kuriyan J. 2011. Catalytic Control in the EGF Receptor and Its Connection to General Kinase Regulatory Mechanisms. *Molecular Cell* **42**:9–22. doi:10.1016/j.molcel.2011.03.004

Juvin V, Malek M, Anderson KE, Dion C, Chessa T, Lecureuil C, Ferguson GJ, Cosulich S, Hawkins PT, Stephens LR. 2013. Signaling via Class IA Phosphoinositide 3-Kinases (PI3K) in Human, Breast-Derived Cell Lines. *PLOS ONE* **8**:e75045. doi:10.1371/journal.pone.0075045

Kan Z-Y, Walters BT, Mayne L, Englander SW. 2013. Protein hydrogen exchange at residue resolution by proteolytic fragmentation mass spectrometry analysis. *PNAS* **110**:16438–16443. doi:10.1073/pnas.1315532110

Kaplan DR, Whitman M, Schaffhausen B, Pallas DC, White M, Cantley L, Roberts TM. 1987. Common elements in growth factor stimulation and oncogenic transformation: 85 kd phosphoprotein and phosphatidylinositol kinase activity. *Cell* **50**:1021–1029. doi:10.1016/0092-8674(87)90168-1

Kashishian A, Kazlauskas A, Cooper JA. 1992. Phosphorylation sites in the PDGF receptor with different specificities for binding GAP and PI3 kinase in vivo. *EMBO J* **11**:1373–1382.

Kazlauskas A, Cooper JA. 1990. Phosphorylation of the PDGF receptor beta subunit creates a tight binding site for phosphatidylinositol 3 kinase. *EMBO J* **9**:3279–3286.

Khindri S, Cahn A, Begg M, Montembault M, Leemereise C, Cui Y, Hogg A, Wajdner H, Yang S, Robertson J, Hamblin JN, Ludwig-Sengpiel A, Kornmann O, Hessel EM. 2018. A Multicentre, Randomized, Double-Blind, Placebo-Controlled, Crossover Study To Investigate the Efficacy, Safety, Tolerability, and Pharmacokinetics of Repeat Doses of Inhaled Nemiralisib in Adults with Persistent, Uncontrolled Asthma. *J Pharmacol Exp Ther* **367**:405–413. doi:10.1124/jpet.118.249516

Klatka M, Rysz I, Kozyra K, Polak A, Kołłątaj W. 2017. SHORT syndrome in a two-year-old girl – case report. *Italian Journal of Pediatrics* **43**:44. doi:10.1186/s13052-017-0362-z

Klippel A, Escobedo JA, Fantl WJ, Williams LT. 1992. The C-terminal SH2 domain of p85 accounts for the high affinity and specificity of the binding of phosphatidylinositol 3-kinase to phosphorylated platelet-derived growth factor beta receptor. *Molecular and Cellular Biology* **12**:1451–1459. doi:10.1128/MCB.12.4.1451

Knight ZA, Gonzalez B, Feldman ME, Zunder ER, Goldenberg DD, Williams O, Loewith R, Stokoe D, Balla A, Toth B, Balla T, Weiss WA, Williams RL, Shokat KM. 2006. A Pharmacological Map of the PI3-K Family Defines a Role for p110α in Insulin Signaling. *Cell* **125**:733–747. doi:10.1016/j.cell.2006.03.035

Kohn AD, Kovacina KS, Roth RA. 1995. Insulin stimulates the kinase activity of RAC-PK, a pleckstrin homology domain containing ser/thr kinase. *EMBO J* **14**:4288–4295.

Kok K, Geering B, Vanhaesebroeck B. 2009. Regulation of phosphoinositide 3-kinase expression in health and disease. *Trends in Biochemical Sciences* **34**:115–127. doi:10.1016/j.tibs.2009.01.003

Kuhlen M, Hönscheid A, Loizou L, Nabhani S, Fischer U, Stepensky P, Schaper J, Klapper W, Siepermann M, Schuster F, Meisel R, Borkhardt A. 2016. De novo PIK3R1 gain-of-function with recurrent sinopulmonary infections, long-lasting chronic CMV-lymphadenitis and microcephaly. *Clinical Immunology* **162**:27–30. doi:10.1016/j.clim.2015.10.008

Kulkarni S, Sitaru C, Jakus Z, Anderson KE, Damoulakis G, Davidson K, Hirose M, Juss J, Oxley D, Chessa TAM, Ramadani F, Guillou H, Segonds-Pichon A, Fritsch A, Jarvis GE, Okkenhaug K, Ludwig R, Zillikens D, Mocsai A, Vanhaesebroeck B, Stephens LR, Hawkins PT. 2011. PI3Kβ plays a critical role in neutrophil activation by immune complexes. *Sci Signal* **4**:ra23. doi:10.1126/scisignal.2001617

Lampson BL, Kasar SN, Matos TR, Morgan EA, Rassenti L, Davids MS, Fisher DC, Freedman AS, Jacobson CA, Armand P, Abramson JS, Arnason JE, Kipps TJ, Fein J, Fernandes S, Hanna J, Ritz J, Kim HT, Brown JR. 2016. Idelalisib given front-line for treatment of chronic lymphocytic leukemia causes frequent immune-mediated hepatotoxicity. *Blood* **128**:195–203. doi:10.1182/blood-2016-03-707133

Lawrence MS, Stojanov P, Mermel CH, Robinson JT, Garraway LA, Golub TR, Meyerson M, Gabriel SB, Lander ES, Getz G. 2014. Discovery and saturation analysis of cancer genes across 21 tumour types. *Nature* **505**:495–501. doi:10.1038/nature12912

Lemmon MA. 2008. Membrane recognition by phospholipid-binding domains. *Nature Reviews Molecular Cell Biology* **9**:99–111. doi:10.1038/nrm2328

Lemmon MA. 2007. Pleckstrin Homology (PH) domains and phosphoinositides. *Biochem Soc Symp* 81–93. doi:10.1042/BSS0740081

Levine TP, Munro S. 2002. Targeting of Golgi-Specific Pleckstrin Homology Domains Involves Both PtdIns 4-Kinase-Dependent and -Independent Components. *Current Biology* **12**:695–704. doi:10.1016/S0960-9822(02)00779-0

Lindhurst MJ, Parker VER, Payne F, Sapp JC, Rudge S, Harris J, Witkowski AM, Zhang Q, Groeneveld MP, Scott CE, Daly A, Huson SM, Tosi LL, Cunningham ML, Darling TN, Geer J, Gucev Z, Sutton VR, Tziotzios C, Dixon AK, Helliwell T, O'Rahilly S, Savage DB, Wakelam MJO, Barroso I, Biesecker LG, Semple RK. 2012. Mosaic overgrowth with fibroadipose hyperplasia is caused by somatic activating mutations in PIK3CA. *Nature Genetics* **44**:928–933. doi:10.1038/ng.2332

Liu H, Tang XL, Liu JR, Li HM, Zhao SY. 2016. [Clinical and genetic analysis for activated PI3K-δ syndrome by PIK3CD gene mutation]. *Zhonghua Er Ke Za Zhi* **54**:698–702. doi:10.3760/cma.j.issn.0578-1310.2016.09.013

Liu J-P, Baker J, Perkins AS, Robertson EJ, Efstratiadis A. 1993. Mice carrying null mutations of the genes encoding insulin-like growth factor I (Igf-1) and type 1 IGF receptor (Igf1r). *Cell* **75**:59–72. doi:10.1016/S0092-8674(05)80084-4

LoPiccolo J, Kim SJ, Shi Y, Wu B, Wu H, Chait BT, Singer RH, Sali A, Brenowitz M, Bresnick AR, Backer JM. 2015. Assembly and Molecular Architecture of the Phosphoinositide 3-Kinase p85α Homodimer. *J Biol Chem* **290**:30390–30405. doi:10.1074/jbc.M115.689604

Lougaris V, Baronio M, Moratto D, Tampella G, Gazzurelli L, Facchetti M, Martire B, Cardinale F, Lanzarotto F, Bondioni MP, Villanacci V, Grimbacher B, Plebani A. 2019. A novel monoallelic gain of function mutation in p110δ causing atypical activated phosphoinositide 3-kinase δ syndrome (APDS-1). *Clinical Immunology* **200**:31–34. doi:10.1016/j.clim.2019.01.003

Lucas CL, Chandra A, Nejentsev S, Condliffe AM, Okkenhaug K. 2016. PI3Kδ and primary immunodeficiencies. *Nat Rev Immunol*. doi:10.1038/nri.2016.93

Lucas CL, Kuehn HS, Zhao F, Niemela JE, Deenick EK, Palendira U, Avery DT, Moens L, Cannons JL, Biancalana M, Stoddard J, Ouyang W, Frucht DM, Rao VK, Atkinson TP, Agharahimi A, Hussey AA, Folio LR, Olivier KN, Fleisher TA, Pittaluga S, Holland SM, Cohen JI, Oliveira JB, Tangye SG, Schwartzberg PL, Lenardo MJ, Uzel G. 2013. Dominant-activating germline mutations in the gene encoding the PI(3)K catalytic subunit p110δ result in T cell senescence and human immunodeficiency. *Nat Immunol* **15**:88–97. doi:10.1038/ni.2771

Lucas CL, Zhang Y, Venida A, Wang Y, Hughes J, McElwee J, Butrick M, Matthews H, Price S, Biancalana M, Wang X, Richards M, Pozos T, Barlan I, Ozen A, Rao VK, Su HC, Lenardo MJ. 2014. Heterozygous splice mutation in PIK3R1 causes human immunodeficiency with lymphoproliferation due to dominant activation of PI3K. *J Exp Med* **211**:2537–2547. doi:10.1084/jem.20141759

Luo J, Field SJ, Lee JY, Engelman JA, Cantley LC. 2005. The p85 regulatory subunit of phosphoinositide 3-kinase down-regulates IRS-1 signaling via the formation of a sequestration complex. *The Journal of Cell Biology* **170**:455–464. doi:10.1083/jcb.200503088

Luo Y, Xia Y, Wang W, Li Z, Jin Y, Gong Y, He T, Li Q, Li C, Yang J. 2018. Identification of a novel de novo gain-of-function mutation of PIK3CD in a patient with activated phosphoinositide 3-kinase δ syndrome. *Clinical Immunology* **197**:60–67. doi:10.1016/j.clim.2018.08.007

Madsen RR, Knox RG, Pearce W, Lopez S, Mahler-Araujo B, McGranahan N, Vanhaesebroeck B, Semple RK. 2019. Oncogenic PIK3CA promotes cellular

stemness in an allele dose-dependent manner. *PNAS* 201821093. doi:10.1073/pnas.1821093116

Maehama T, Dixon JE. 1998. The Tumor Suppressor, PTEN/MMAC1, Dephosphorylates the Lipid Second Messenger, Phosphatidylinositol 3,4,5-Trisphosphate. *Journal of Biological Chemistry* **273**:13375–13378. doi:10.1074/jbc.273.22.13375

Malek M, Kielkowska A, Chessa T, Anderson KE, Barneda D, Pir P, Nakanishi H, Eguchi S, Koizumi A, Sasaki J, Juvin V, Kiselev VY, Niewczas I, Gray A, Valayer A, Spensberger D, Imbert M, Felisbino S, Habuchi T, Beinke S, Cosulich S, Le Novère N, Sasaki T, Clark J, Hawkins PT, Stephens LR. 2017. PTEN Regulates PI(3,4)P 2 Signaling Downstream of Class I PI3K. *Molecular Cell* **68**:566-580.e10. doi:10.1016/j.molcel.2017.09.024

Mandelker D, Gabelli SB, Schmidt-Kittler O, Zhu J, Cheong I, Huang C-H, Kinzler KW, Vogelstein B, Amzel LM. 2009. A frequent kinase domain mutation that changes the interaction between PI3Kalpha and the membrane. *Proc Natl Acad Sci USA* **106**:16996–17001. doi:10.1073/pnas.0908444106

Manna D, Albanese A, Park WS, Cho W. 2007. Mechanistic Basis of Differential Cellular Responses of Phosphatidylinositol 3,4-Bisphosphate- and Phosphatidylinositol 3,4,5-Trisphosphate-binding Pleckstrin Homology Domains. *J Biol Chem* **282**:32093–32105. doi:10.1074/jbc.M703517200

Manning BD, Tee AR, Logsdon MN, Blenis J, Cantley LC. 2002. Identification of the Tuberous Sclerosis Complex-2 Tumor Suppressor Gene Product Tuberin as a Target of the Phosphoinositide 3-Kinase/Akt Pathway. *Molecular Cell* **10**:151–162. doi:10.1016/S1097-2765(02)00568-3

Manning BD, Toker A. 2017. AKT/PKB Signaling: Navigating the Network. *Cell* **169**:381–405. doi:10.1016/j.cell.2017.04.001

Marat AL, Wallroth A, Lo W-T, Müller R, Norata GD, Falasca M, Schultz C, Haucke V. 2017. mTORC1 activity repression by late endosomal phosphatidylinositol 3,4-bisphosphate. *Science* **356**:968–972. doi:10.1126/science.aaf8310

Masson GR, Jenkins ML, Burke JE. 2017a. An overview of hydrogen deuterium exchange mass spectrometry (HDX-MS) in drug discovery. *Expert Opinion on Drug Discovery* **12**:981–994. doi:10.1080/17460441.2017.1363734

Masson GR, Maslen SL, Williams RL. 2017b. Analysis of phosphoinositide 3-kinase inhibitors by bottom-up electron-transfer dissociation hydrogen/deuterium exchange mass spectrometry. *Biochemical Journal* **474**:1867–1877. doi:10.1042/BCJ20170127

McGlade CJ, Ellis C, Reedijk M, Anderson D, Mbamalu G, Reith AD, Panayotou G, End P, Bernstein A, Kazlauskas A. 1992. SH2 domains of the p85 alpha subunit of

phosphatidylinositol 3-kinase regulate binding to growth factor receptors. *Molecular and Cellular Biology* **12**:991–997. doi:10.1128/MCB.12.3.991

Miled N, Yan Y, Hon WC, Perisic O, Zvelebil M. 2007. Mechanism of two classes of cancer mutations in the phosphoinositide 3-kinase catalytic subunit. *Science*.

Miller MS, Schmidt-Kittler O, Bolduc DM, Brower ET, Chaves-Moreira D, Allaire M, Kinzler KW, Jennings IG, Thompson PE, Cole PA, Amzel LM, Vogelstein B, Gabelli SB. 2014. Structural basis of nSH2 regulation and lipid binding in PI3Kα. *Oncotarget* **5**:5198–5208.

Miller S, Tavshanjian B, Oleksy A, Perisic O, Houseman BT, Shokat KM, Williams RL. 2010. Shaping development of autophagy inhibitors with the structure of the lipid kinase Vps34. *Science (New York, NY)* **327**:1638–1642. doi:10.1126/science.1184429

Millis SZ, Ikeda S, Reddy S, Gatalica Z, Kurzrock R. 2016. Landscape of Phosphatidylinositol-3-Kinase Pathway Alterations Across 19 784 Diverse Solid Tumors. *JAMA Oncol* **2**:1565–1573. doi:10.1001/jamaoncol.2016.0891

Mirzaa GM, Conti V, Timms AE, Smyser CD, Ahmed S, Carter M, Barnett S, Hufnagel RB, Goldstein A, Narumi-Kishimoto Y, Olds C, Collins S, Johnston K, Deleuze J-F, Nitschke P, Friend K, Harris C, Goetsch A, Martin B, Boyle EA, Parrini E, Mei D, Tattini L, Slavotinek A, Blair E, Barnett C, Shendure J, Chelly J, Dobyns WB, Guerrini R. 2015. Characterisation of mutations of the phosphoinositide-3-kinase regulatory subunit, PIK3R2, in perisylvian polymicrogyria: a next-generation sequencing study. *The Lancet Neurology* **14**:1182–1195. doi:10.1016/S1474-4422(15)00278-1

Molday RS, Englander SW, Kallen RG. 1972. Primary structure effects on peptide group hydrogen exchange. *Biochemistry* 9.

Murillo MM, Zelenay S, Nye E, Castellano E, Lassailly F, Stamp G, Downward J. 2014. RAS interaction with PI3K p110α is required for tumor-induced angiogenesis. *J Clin Invest* **124**:3601–3611. doi:10.1172/JCI74134

Nakamura K, Kato M, Tohyama J, Shiohama T, Hayasaka K, Nishiyama K, Kodera H, Nakashima M, Tsurusaki Y, Miyake N, Matsumoto N, Saitsu H. 2014. *AKT3* and *PIK3R2* mutations in two patients with megalencephaly-related syndromes: MCAP and MPPH: Letter to the Editor. *Clinical Genetics* **85**:396–398. doi:10.1111/cge.12188

Nolte RT, Eck MJ, Schlessinger J, Shoelson SE, Harrison SC. 1996. Crystal structure of the PI 3-kinase p85 amino-terminal SH2 domain and its phosphopeptide complexes. *Nat Struct Biol* **3**:364–374.

Ohashi Y, Soler N, García Ortegón M, Zhang L, Kirsten ML, Perisic O, Masson GR, Burke JE, Jakobi AJ, Apostolakis AA, Johnson CM, Ohashi M, Ktistakis NT,

Sachse C, Williams RL. 2016. Characterization of Atg38 and NRBF2, a fifth subunit of the autophagic Vps34/PIK3C3 complex. *Autophagy* **12**:2129–2144. doi:10.1080/15548627.2016.1226736

Ohta Y, Haire RN, Litman RT, Fu SM, Nelson RP, Kratz J, Kornfeld SJ, Morena M de la, Good RA, Litman GW. 1994. Genomic organization and structure of Bruton agammaglobulinemia tyrosine kinase: localization of mutations associated with varied clinical presentations and course in X chromosome-linked agammaglobulinemia. *PNAS* **91**:9062–9066. doi:10.1073/pnas.91.19.9062

Okkenhaug K. 2013. Signaling by the phosphoinositide 3-kinase family in immune cells. *Annu Rev Immunol* **31**:675–704. doi:10.1146/annurev-immunol-032712-095946

Okkenhaug K, Bilancio A, Farjot G, Priddle H, Sancho S, Peskett E, Pearce W, Meek SE, Salpekar A, Waterfield MD, Smith AJH, Vanhaesebroeck B. 2002. Impaired B and T cell antigen receptor signaling in p110delta PI 3-kinase mutant mice. *Science* **297**:1031–1034. doi:10.1126/science.1073560

Okkenhaug K, Patton DT, Bilancio A, Garçon F, Rowan WC, Vanhaesebroeck B. 2006. The p110δ Isoform of Phosphoinositide 3-Kinase Controls Clonal Expansion and Differentiation of Th Cells. *The Journal of Immunology* **177**:5122–5128. doi:10.4049/jimmunol.177.8.5122

Orloff MS, He X, Peterson C, Chen F, Chen J-L, Mester JL, Eng C. 2013. Germline PIK3CA and AKT1 Mutations in Cowden and Cowden-like Syndromes. *The American Journal of Human Genetics* **92**:76–80. doi:10.1016/j.ajhg.2012.10.021

Pacold ME, Suire S, Perisic O, Lara-Gonzalez S, Davis CT, Walker EH, Hawkins PT, Stephens L, Eccleston JF, Williams RL. 2000. Crystal Structure and Functional Analysis of Ras Binding to Its Effector Phosphoinositide 3-Kinase γ. *Cell* **103**:931–944. doi:10.1016/S0092-8674(00)00196-3

Panayotou G, Gish G, End P, Truong O, Gout I, Dhand R, Fry MJ, Hiles I, Pawson T, Waterfield MD. 1993. Interactions between SH2 domains and tyrosine-phosphorylated platelet-derived growth factor beta-receptor sequences: analysis of kinetic parameters by a novel biosensor-based approach. *Mol Cell Biol* **13**:3567–3576.

Petrovski S, Parrott RE, Roberts JL, Huang H, Yang J, Gorentla B, Mousallem T, Wang E, Armstrong M, McHale D, MacIver NJ, Goldstein DB, Zhong X-P, Buckley RH. 2016. Dominant Splice Site Mutations in PIK3R1 Cause Hyper IgM Syndrome, Lymphadenopathy and Short Stature. *J Clin Immunol* **36**:462–471. doi:10.1007/s10875-016-0281-6

Pirola L, Zvelebil MJ, Bulgarelli-Leva G, Van Obberghen E, Waterfield MD, Wymann MP. 2001. Activation loop sequences confer substrate specificity to phosphoinositide 3-kinase alpha (PI3Kalpha). Functions of lipid kinase-deficient

PI3Kalpha in signaling. *J Biol Chem* **276**:21544–21554. doi:10.1074/jbc.M011330200

Powis G, Bonjouklian R, Berggren MM, Gallegos A, Abraham R, Ashendel C, Zalkow L, Matter WF, Dodge J, Grindey G, Vlahos CJ. 1994. Wortmannin, a Potent and Selective Inhibitor of Phosphatidylinositol-3-kinase. *Cancer Res* **54**:2419–2423.

Qin L-Y, Ruan Z, Cherney RJ, Dhar TGM, Neels J, Weigelt CA, Sack JS, Srivastava AS, Cornelius LAM, Tino JA, Stefanski K, Gu X, Xie J, Susulic V, Yang X, Yarde-Chinn M, Skala S, Bosnius R, Goldstein C, Davies P, Ruepp S, Salter-Cid L, Bhide RS, Poss MA. 2017. Discovery of 7-(3-(piperazin-1-yl)phenyl)pyrrolo[2,1-f][1,2,4]triazin-4-amine derivatives as highly potent and selective PI3Kδ inhibitors. *Bioorganic & Medicinal Chemistry Letters* **27**:855–861. doi:10.1016/j.bmcl.2017.01.016

Rae W, Gao Y, Ward D, Mattocks CJ, Eren E, Williams AP. 2017. A novel germline gain-of-function variant in PIK3CD. *Clin Immunol* **181**:29–31. doi:10.1016/j.clim.2017.05.020

Rae W, Ramakrishnan KA, Gao Y, Ashton-Key M, Pengelly RJ, Patel SV, Ennis S, Williams AP, Faust SN. 2016. Precision treatment with sirolimus in a case of activated phosphoinositide 3-kinase δ syndrome. *Clinical Immunology* **171**:38–40. doi:10.1016/j.clim.2016.07.017

Ramadani F, Bolland DJ, Garcon F, Emery JL, Vanhaesebroeck B, Corcoran AE, Okkenhaug K. 2010. The PI3K Isoforms p110 and p110 Are Essential for Pre-B Cell Receptor Signaling and B Cell Development. *Sci Signal* **3**:ra60–ra60. doi:10.1126/scisignal.2001104

Rao VK, Webster S, Dalm VASH, Šedivá A, van Hagen PM, Holland S, Rosenzweig SD, Christ AD, Sloth B, Cabanski M, Joshi AD, de Buck S, Doucet J, Guerini D, Kalis C, Pylvaenaeinen I, Soldermann N, Kashyap A, Uzel G, Lenardo MJ, Patel DD, Lucas CL, Burkhart C. 2017. Effective "activated PI3Kδ syndrome"–targeted therapy with the PI3Kδ inhibitor leniolisib. *Blood* **130**:2307–2316. doi:10.1182/blood-2017-08-801191

Rivière J-B, Mirzaa GM, O'Roak BJ, Beddaoui M, Alcantara D, Conway RL, St-Onge J, Schwartzentruber JA, Gripp KW, Nikkel SM, Worthylake T, Sullivan CT, Ward TR, Butler HE, Kramer NA, Albrecht B, Armour CM, Armstrong L, Caluseriu O, Cytrynbaum C, Drolet BA, Innes AM, Lauzon JL, Lin AE, Mancini GMS, Meschino WS, Reggin JD, Saggar AK, Lerman-Sagie T, Uyanik G, Weksberg R, Zirn B, Beaulieu CL, Consortium FC, Majewski J, Bulman DE, O'Driscoll M, Shendure J, Graham JM, Jr, Boycott KM, Dobyns WB. 2012. De novo germline and postzygotic mutations in AKT3, PIK3R2 and PIK3CA cause a spectrum of related megalencephaly syndromes. *Nature genetics* **44**:934–940. doi:10.1038/ng.2331

Rodriguez-Viciana P, Sabatier C, McCormick F. 2004. Signaling specificity by Ras family GTPases is determined by the full spectrum of effectors they regulate. *Mol Cell Biol* **24**:4943–4954. doi:10.1128/MCB.24.11.4943-4954.2004

Rodriguez-Viciana P, Warne PH, Dhandt R, Vanhaesebroeckt B, Goutt I, Fry MJ, Waterfieldtt MD. 1994. Phosphatidylinositoi-3-0H kinase as a direct target of Ras. *Nature* **370**:6.

Rordorf-Nikolic T, Van Horn DJ, Chen D, White MF, Backer JM. 1995. Regulation of phosphatidylinositol 3'-kinase by tyrosyl phosphoproteins. Full activation requires occupancy of both SH2 domains in the 85-kDa regulatory subunit. *J Biol Chem* **270**:3662–3666.

Rostislavleva K, Soler N, Ohashi Y, Zhang L, Pardon E, Burke JE, Masson GR, Johnson C, Steyaert J, Ktistakis NT, Williams RL. 2015. Structure and flexibility of the endosomal Vps34 complex reveals the basis of its function on membranes. *Science* **350**:aac7365. doi:10.1126/science.aac7365

Rudd ML, Price JC, Fogoros S, Godwin AK, Sgroi DC, Merino MJ, Bell DW. 2011. A Unique Spectrum of Somatic PIK3CA (p110α) Mutations Within Primary Endometrial Carcinomas. *Clin Cancer Res* **17**:1331–1340. doi:10.1158/1078-0432.CCR-10-0540

Ruderman NB, Kapeller R, White MF, Cantley LC. 1990. Activation of phosphatidylinositol 3-kinase by insulin. *Proceedings of the National Academy of Sciences* **87**:1411–1415. doi:10.1073/pnas.87.4.1411

Saettini F, Pelagatti MA, Sala D, Moratto D, Giliani S, Badolato R, Biondi A. 2017. Early diagnosis of PI3Kδ syndrome in a 2 years old girl with recurrent otitis and enlarged spleen. *Immunology Letters* **190**:279–281. doi:10.1016/j.imlet.2017.08.021

Samuels Y, Wang Z, Bardelli A, Silliman N, Ptak J, Szabo S, Yan H, Gazdar A, Powell SM, Riggins GJ, Willson JKV, Markowitz S, Kinzler KW, Vogelstein B, Velculescu VE. 2004. High Frequency of Mutations of the PIK3CA Gene in Human Cancers. *Science* **304**:554–554. doi:10.1126/science.1096502

Schroeder C, Riess A, Bonin M, Bauer P, Riess O, Döbler-Neumann M, Wieser S, Moog U, Tzschach A. 2014. PIK3R1 mutations in SHORT syndrome. *Clinical Genetics* **86**:292–294. doi:10.1111/cge.12263

Shekar SC, Wu H, Fu Z, Yip S-C, Nagajyothi, Cahill SM, Girvin ME, Backer JM. 2005. Mechanism of constitutive phosphoinositide 3-kinase activation by oncogenic mutants of the p85 regulatory subunit. *J Biol Chem* **280**:27850–27855. doi:10.1074/jbc.M506005200

Shoelson SE, Chatterjee S, Chaudhuri M, White MF. 1992. YMXM motifs of IRS-1 define substrate specificity of the insulin receptor kinase. *Proceedings of the National Academy of Sciences* **89**:2027–2031. doi:10.1073/pnas.89.6.2027

Sicheri F, Moarefi I, Kuriyan J. 1997. Crystal structure of the Src family tyrosine kinase Hck. *Nature* **385**:602–609. doi:10.1038/385602a0

Siempelkamp BD, Rathinaswamy MK, Jenkins ML, Burke JE. 2017. Molecular mechanism of activation of class IA phosphoinositide 3-kinases (PI3Ks) by membrane-localized HRas. *J Biol Chem* **292**:jbc.M117.789263-12266. doi:10.1074/jbc.M117.789263

Skinner JJ, Lim WK, Bédard S, Black BE. 2012. Protein dynamics viewed by hydrogen exchange. *Protein …*.

Sogkas G, Fedchenko M, Dhingra A, Jablonka A, Schmidt RE, Atschekzei F. 2018. Primary immunodeficiency disorder caused by phosphoinositide 3–kinase δ deficiency. *Journal of Allergy and Clinical Immunology* **142**:1650-1653.e2. doi:10.1016/j.jaci.2018.06.039

Somoza JR, Koditek D, Villaseñor AG, Novikov N, Wong MH, Liclican A, Xing W, Lagpacan L, Wang R, Schultz BE, Papalia GA, Samuel D, Lad L, McGrath ME. 2015. Structural, biochemical, and biophysical characterization of idelalisib binding to phosphoinositide 3-kinase δ. *J Biol Chem* **290**:8439–8446. doi:10.1074/jbc.M114.634683

Stambolic V, Suzuki A, de la Pompa JL, Brothers GM, Mirtsos C, Sasaki T, Ruland J, Penninger JM, Siderovski DP, Mak TW. 1998. Negative Regulation of PKB/Akt-Dependent Cell Survival by the Tumor Suppressor PTEN. *Cell* **95**:29–39. doi:10.1016/S0092-8674(00)81780-8

Stephens L, Hawkins PT, Downes CP. 1989. Metabolic and structural evidence for the existence of a third species of polyphosphoinositide in cells: D-phosphatidyl-myo-inositol 3-phosphate. *Biochem J* **259**:267–276.

Stephens LR, Hughes KT, Irvine RF. 1991. Pathway of phosphatidylinositol(3,4,5)-trisphosphate synthesis in activated neutrophils. *Nature* **351**:33. doi:10.1038/351033a0

Stephens LR, Jackson TR, Hawkins PT. 1993. Agonist-stimulated synthesis of phosphatidylinositol(3,4,5)-trisphosphate: A new intracellular signalling system? *Biochimica et Biophysica Acta (BBA) - Molecular Cell Research* **1179**:27–75. doi:10.1016/0167-4889(93)90072-W

Stokoe D, Stephens LR, Copeland T, Gaffney PRJ, Reese CB, Painter GF, Holmes AB, McCormick F, Hawkins PT. 1997. Dual Role of Phosphatidylinositol-3,4,5-trisphosphate in the Activation of Protein Kinase B. *Science* **277**:567–570. doi:10.1126/science.277.5325.567

Sugiyama M, Iguchi A, Yamada M, Terashita Y, Ohshima J, Cho Y, Miyake N, Matsumoto N, Ueki M, Yamazaki Y, Takezaki S, Kobayashi I, Ariga T. 2017. Successful bone marrow transplantation in two sisters with activated phosphoinositide 3-kinase δ syndrome 2. *Bone Marrow Transplantation* **52**:1678–1680. doi:10.1038/bmt.2017.189

Takeda AJ, Zhang Y, Dornan GL, Siempelkamp BD, Jenkins ML, Matthews HF, McElwee JJ, Bi W, Seeborg FO, Su HC, Burke JE, Lucas CL. 2017. Novel PIK3CD mutations affecting N-terminal residues of p110δ cause activated PI3Kδ syndrome (APDS) in humans. *Journal of Allergy and Clinical Immunology* **140**:1152-1156.e10. doi:10.1016/j.jaci.2017.03.026

Tamemoto H, Kadowaki T, Tobe K, Yagi T, Sakura H, Hayakawa T, Terauchi Y, Ueki K, Kaburagi Y, Satoh S, Sekihara H, Yoshioka S, Horikoshi H, Furuta Y, Ikawa Y, Kasuga M, Yazaki Y, Aizawa S. 1994. Insulin resistance and growth retardation in mice lacking insulin receptor substrate-1. *Nature* **372**:182. doi:10.1038/372182a0

Tang P, Upton JEM, Barton-Forbes MA, Salvadori MI, Clynick MP, Price AK, Goobie SL. 2018. Autosomal Recessive Agammaglobulinemia Due to a Homozygous Mutation in PIK3R1. *J Clin Immunol* **38**:88–95. doi:10.1007/s10875-017-0462-y

Tangye SG, Bier J, Lau A, Nguyen T, Uzel G, Deenick EK. 2019. Immune Dysregulation and Disease Pathogenesis due to Activating Mutations in PIK3CD-the Goldilocks' Effect. *J Clin Immunol* **39**:148–158. doi:10.1007/s10875-019-00612-9

Teranishi H, Ishimura M, Koga Y, Eguchi K, Sonoda M, Kobayashi T, Shiraishi S, Nakashima K, Ikegami K, Aman M, Yamamoto H, Takada H, Ohga S. 2017. Activated phosphoinositide 3-kinase δ syndrome presenting with gut-associated T-cell lymphoproliferative disease. *Rinsho Ketsueki* **58**:20–25. doi:10.11406/rinketsu.58.20

Terrone G, Voisin N, Alfaiz AA, Cappuccio G, Vitiello G, Guex N, Amico AD rsquo, Barkovich AJ, Brunetti-Pierri N, Del Giudice E, Reymond A. 2016. De novo PIK3R2 variant causes polymicrogyria, corpus callosum hyperplasia and focal cortical dysplasia. *European Journal of Human Genetics* 1–4. doi:10.1038/ejhg.2016.7

Thauvin-Robinet C, Auclair M, Duplomb L, Caron-Debarle M, Avila M, St-Onge J, Le Merrer M, Le Luyer B, Héron D, Mathieu-Dramard M, Bitoun P, Petit J-M, Odent S, Amiel J, Picot D, Carmignac V, Thevenon J, Callier P, Laville M, Reznik Y, Fagour C, Nunes M-L, Capeau J, Lascols O, Huet F, Faivre L, Vigouroux C, Rivière J-B. 2013. PIK3R1 Mutations Cause Syndromic Insulin Resistance with Lipoatrophy. *The American Journal of Human Genetics* **93**:141–149. doi:10.1016/j.ajhg.2013.05.019

Thorpe LM, Spangle JM, Ohlson CE, Cheng H, Roberts TM, Cantley LC, Zhao JJ. 2017. PI3K-p110α mediates the oncogenic activity induced by loss of the novel tumor suppressor PI3K-p85α. *PNAS* **114**:7095–7100. doi:10.1073/pnas.1704706114

Traynor-Kaplan AE, Harris AL, Thompson BL, Taylor P, Sklar LA. 1988. An inositol tetrakisphosphate-containing phospholipid in activated neutrophils. *Nature* **334**:353–356. doi:10.1038/334353a0

Traynor-Kaplan AE, Thompson BL, Harris AL, Taylor P, Omann GM, Sklar LA. 1989. Transient increase in phosphatidylinositol 3,4-bisphosphate and phosphatidylinositol trisphosphate during activation of human neutrophils. *J Biol Chem* **264**:15668–15673.

Tsai J, Lee JT, Wang W, Zhang J, Cho H, Mamo S, Bremer R, Gillette S, Kong J, Haass NK, Sproesser K, Li L, Smalley KSM, Fong D, Zhu Y-L, Marimuthu A, Nguyen H, Lam B, Liu J, Cheung I, Rice J, Suzuki Y, Luu C, Settachatgul C, Shellooe R, Cantwell J, Kim S-H, Schlessinger J, Zhang KYJ, West BL, Powell B, Habets G, Zhang C, Ibrahim PN, Hirth P, Artis DR, Herlyn M, Bollag G. 2008. Discovery of a selective inhibitor of oncogenic B-Raf kinase with potent antimelanoma activity. *Proceedings of the National Academy of Sciences* **105**:3041–3046. doi:10.1073/pnas.0711741105

Tsolakos N, Durrant TN, Chessa T, Suire SM, Oxley D, Kulkarni S, Downward J, Perisic O, Williams RL, Stephens L, Hawkins PT. 2018. Quantitation of class IA PI3Ks in mice reveals p110-free-p85s and isoform-selective subunit associations and recruitment to receptors. *PNAS* 201803446. doi:10.1073/pnas.1803446115

Tsujita Y, Mitsui-Sekinaka K, Imai K, Yeh T-W, Mitsuiki N, Asano T, Ohnishi H, Kato Z, Sekinaka Y, Zaha K, Kato T, Okano T, Takashima T, Kobayashi K, Kimura M, Kunitsu T, Maruo Y, Kanegane H, Takagi M, Yoshida K, Okuno Y, Muramatsu H, Shiraishi Y, Chiba K, Tanaka H, Miyano S, Kojima S, Ogawa S, Ohara O, Okada S, Kobayashi M, Morio T, Nonoyama S. 2016. Phosphatase and tensin homolog (PTEN) mutation can cause activated phosphatidylinositol 3-kinase δ syndrome-like immunodeficiency. *J Allergy Clin Immunol* **138**:1672-1680.e10. doi:10.1016/j.jaci.2016.03.055

Urick ME, Rudd ML, Godwin AK, Sgroi D, Merino M, Bell DW. 2011. PIK3R1 (p85α) is somatically mutated at high frequency in primary endometrial cancer. *Cancer Res* **71**:4061–4067. doi:10.1158/0008-5472.CAN-11-0549

Vadas O, Burke JE. 2015. Probing the dynamic regulation of peripheral membrane proteins using hydrogen deuterium exchange-MS (HDX-MS). *Biochemical Society Transactions* **43**:773–786. doi:10.1042/BST20150065

Vadas O, Burke JE, Zhang X, Berndt A, Williams RL. 2011. Structural basis for activation and inhibition of class I phosphoinositide 3-kinases. *Sci Signal* **4**:re2. doi:10.1126/scisignal.2002165

Vadas O, Dbouk HA, Shymanets A, Perisic O, Burke JE, Abi Saab WF, Khalil BD, Harteneck C, Bresnick AR, Nürnberg B, Backer JM, Williams RL. 2013. Molecular determinants of PI3Kγ-mediated activation downstream of G-protein-coupled receptors (GPCRs). *Proc Natl Acad Sci USA* **110**:18862–18867. doi:10.1073/pnas.1304801110

Vadas O, Jenkins ML, Dornan GL, Burke JE. 2017. Using Hydrogen-Deuterium Exchange Mass Spectrometry to Examine Protein-Membrane Interactions. *Meth Enzymol* **583**:143–172. doi:10.1016/bs.mie.2016.09.008

Vanhaesebroeck B, Welham MJ, Kotani K, Stein R, Warne PH, Zvelebil MJ, Higashi K, Volinia S, Downward J, Waterfield MD. 1997. p110δ, a novel phosphoinositide 3-kinase in leukocytes. *PNAS* **94**:4330–4335. doi:10.1073/pnas.94.9.4330

Vihinen M, Zvelebil MJJM, Zhu Q, Brooimans RA, Ochs HD, Zegers BJM, Nilsson L, Waterfield MD, Smith CIE. 1995. Structural Basis for Pleckstrin Homology Domain Mutations in X-Linked Agammaglobulinemia. *Biochemistry* **34**:1475–1481. doi:10.1021/bi00005a002

Vlahos CJ, Matter WF, Hui KY, Brown RF. 1994. A specific inhibitor of phosphatidylinositol 3-kinase, 2-(4-morpholinyl)-8-phenyl-4H-1-benzopyran-4-one (LY294002). *J Biol Chem* **269**:5241–5248.

Walker EH, Perisic O, Ried C, Stephens L, Williams RL. 1999. Structural insights into phosphoinositide 3-kinase catalysis and signalling. *Nature* **402**:313–320. doi:10.1038/46319

Walser R, Burke JE, Gogvadze E, Bohnacker T, Zhang X, Hess D, Küenzi P, Leitges M, Hirsch E, Williams RL, Laffargue M, Wymann MP. 2013. PKCβ phosphorylates PI3Kγ to activate it and release it from GPCR control. *PLoS Biol* **11**:e1001587. doi:10.1371/journal.pbio.1001587

Walters BT, Ricciuti A, Mayne L, Englander SW. 2012. Minimizing Back Exchange in the Hydrogen Exchange-Mass Spectrometry Experiment. *Journal of The American Society for Mass Spectrometry* **23**:2132–2139. doi:10.1007/s13361-012-0476-x

Wang H, Lo W-T, Vujičić Žagar A, Gulluni F, Lehmann M, Scapozza L, Haucke V, Vadas O. 2018. Autoregulation of Class II Alpha PI3K Activity by Its Lipid-Binding PX-C2 Domain Module. *Molecular Cell* **71**:343-351.e4. doi:10.1016/j.molcel.2018.06.042

Wang Y, Wang W, Liu L, Hou J, Ying W, Hui X, Zhou Q, Liu D, Yao H, Sun J, Wang X. 2018. Report of a Chinese Cohort with Activated Phosphoinositide 3-Kinase δ Syndrome. *Journal of Clinical Immunology* **38**:854–863. doi:10.1007/s10875-018-0568-x

Wentink M, Dalm V, Lankester AC, van Schouwenburg PA, Schölvinck L, Kalina T, Zachova R, Sediva A, Lambeck A, Pico-Knijnenburg I, van Dongen JJM, Pac M, Bernatowska E, van Hagen M, Driessen G, van der Burg M. 2017. Genetic defects in PI3Kδ affect B-cell differentiation and maturation leading to hypogammaglobulineamia and recurrent infections. *Clin Immunol* **176**:77–86. doi:10.1016/j.clim.2017.01.004

Whitman M, Downes CP, Keeler M, Keller T, Cantley L. 1988. Type I phosphatidylinositol kinase makes a novel inositol phospholipid, phosphatidylinositol-3-phosphate. *Nature* **332**:644–646. doi:10.1038/332644a0

Williams R, Berndt A, Miller S, Hon W-C, Zhang X. 2009. Form and flexibility in phosphoinositide 3-kinases. *Biochemical Society Transactions* **37**:615–626. doi:10.1042/BST0370615

Wilson R, Jarvis E, Montembault M, Hamblin JN, Hessel EM, Cahn A. 2018. Safety, Tolerability, and Pharmacokinetics of Single and Repeat Doses of Nemiralisib Administered via the Ellipta Dry Powder Inhaler to Healthy Subjects. *Clinical Therapeutics* **40**:1410–1417. doi:10.1016/j.clinthera.2018.06.011

Wu H, Shekar SC, Flinn RJ, El-Sibai M, Jaiswal BS, Sen KI, Janakiraman V, Seshagiri S, Gerfen GJ, Girvin ME, Backer JM. 2009. Regulation of Class IA PI 3-kinases: C2 domain-iSH2 domain contacts inhibit p85/p110α and are disrupted in oncogenic p85 mutants. *PNAS* **106**:20258–20263. doi:10.1073/pnas.0902369106

Wymann MP, Bulgarelli-Leva G, Zvelebil MJ, Pirola L, Vanhaesebroeck B, Waterfield MD, Panayotou G. 1996. Wortmannin inactivates phosphoinositide 3-kinase by covalent modification of Lys-802, a residue involved in the phosphate transfer reaction. *Molecular and Cellular Biology* **16**:1722–1733. doi:10.1128/MCB.16.4.1722

Yang X, Turke AB, Qi J, Song Y, Rexer BN, Miller TW, Jänne PA, Arteaga CL, Cantley LC, Engelman JA, Asara JM. 2011. Using Tandem Mass Spectrometry in Targeted Mode to Identify Activators of Class IA PI3K in Cancer. *Cancer Res* **71**:5965–5975. doi:10.1158/0008-5472.CAN-11-0445

Yu J, Wjasow C, Backer JM. 1998a. Distinct roles for the N-terminal and C-terminal SH2 domains 6.

Yu J, Zhang Y, McIlroy J, Rordorf-Nikolic T, Orr GA, Backer JM. 1998b. Regulation of the p85/p110 phosphatidylinositol 3'-kinase: stabilization and inhibition of the p110alpha catalytic subunit by the p85 regulatory subunit. *Mol Cell Biol* **18**:1379–1387. doi:10.1128/MCB.18.3.1379

Zehir A, Benayed R, Shah RH, Syed A, Middha S, Kim HR, Srinivasan P, Gao J, Chakravarty D, Devlin SM, Hellmann MD, Barron DA, Schram AM, Hameed M, Dogan S, Ross DS, Hechtman JF, DeLair DF, Yao J, Mandelker DL, Cheng DT, Chandramohan R, Mohanty AS, Ptashkin RN, Jayakumaran G, Prasad M, Syed

MH, Rema AB, Liu ZY, Nafa K, Borsu L, Sadowska J, Casanova J, Bacares R, Kiecka IJ, Razumova A, Son JB, Stewart L, Baldi T, Mullaney KA, Al-Ahmadie H, Vakiani E, Abeshouse AA, Penson AV, Jonsson P, Camacho N, Chang MT, Won HH, Gross BE, Kundra R, Heins ZJ, Chen H-W, Phillips S, Zhang H, Wang J, Ochoa A, Wills J, Eubank M, Thomas SB, Gardos SM, Reales DN, Galle J, Durany R, Cambria R, Abida W, Cercek A, Feldman DR, Gounder MM, Hakimi AA, Harding JJ, Iyer G, Janjigian YY, Jordan EJ, Kelly CM, Lowery MA, Morris LGT, Omuro AM, Raj N, Razavi P, Shoushtari AN, Shukla N, Soumerai TE, Varghese AM, Yaeger R, Coleman J, Bochner B, Riely GJ, Saltz LB, Scher HI, Sabbatini PJ, Robson ME, Klimstra DS, Taylor BS, Baselga J, Schultz N, Hyman DM, Arcila ME, Solit DB, Ladanyi M, Berger MF. 2017. Mutational Landscape of Metastatic Cancer Revealed from Prospective Clinical Sequencing of 10,000 Patients. *Nat Med* **23**:703–713. doi:10.1038/nm.4333

Zhang X, Vadas O, Perisic O, Anderson KE, Clark J, Hawkins PT, Stephens LR, Williams RL. 2011. Structure of Lipid Kinase p110β/p85β Elucidates an Unusual SH2-Domain-Mediated Inhibitory Mechanism. *Mol Cell* **41**:567–578. doi:10.1016/j.molcel.2011.01.026

Zhang Z, Smith DL. 1993. Determination of amide hydrogen exchange by mass spectrometry: a new tool for protein structure elucidation. *Protein Sci* **2**:522–531.

Zhao JJ, Cheng H, Jia S, Wang L, Gjoerup OV, Mikami A, Roberts TM. 2006. The p110α isoform of PI3K is essential for proper growth factor signaling and oncogenic transformation. *PNAS* **103**:16296–16300. doi:10.1073/pnas.0607899103

Zhao L, Vogt PK. 2008. Helical domain and kinase domain mutations in p110 of phosphatidylinositol 3-kinase induce gain of function by different mechanisms. *Proceedings of the National Academy of Sciences* **105**:2652–2657. doi:10.1073/pnas.0712169105

Appendix A

This appendix contains additional figures and tables in support of the results discussed in the main body of this thesis.

A.1 Supplementary Figures

p110δ				WT Basal						E81K Basal						G124D Basal					
S	E	Z	RT	3	SD	30	SD	300	SD	3	SD	30	SD	300	SD	3	SD	30	SD	300	SD
12	18	2	4.1	65.0	0.9	66.6	0.6	66.9	0.4	66.6	0.7	66.3	0.9	66.9	0.9	66.6	0.8	66.9	1.4	66.6	0.6
12	19	2	4.1	64.9	0.9	66.1	0.3	66.3	1.3	67.4	0.6	65.8	0.2	67.6	0.7	66.4	0.8	66.8	0.9	66.6	0.6
24	31	2	12.4	3.4	0.3	13.7	0.3	22.6	0.3	3.3	0.1	14.1	0.1	26.0	0.6	4.2	0.2	16.6	0.1	24.6	0.1
32	42	2	9.5	23.6	0.2	32.9	0.5	34.0	0.2	24.6	0.9	32.4	0.4	34.0	0.7	22.8	0.6	32.5	0.5	33.7	0.1
35	42	2	5.2	34.3	1.1	47.3	0.8	48.8	0.6	35.9	1.2	46.9	1.2	50.3	0.8	33.9	0.6	47.7	0.3	49.4	0.1
43	59	4	11.6	5.4	0.2	11.3	0.1	19.9	0.3	5.5	0.4	11.4	0.2	19.8	0.4	5.1	0.1	12.0	0.1	21.7	0.3
43	67	4	12.1	15.3	0.3	24.8	0.3	32.1	0.3	15.7	0.7	24.6	0.1	31.9	0.4	15.0	0.1	24.7	0.5	32.8	0.3
48	59	3	11.8	8.7	0.4	17.8	0.3	28.9	0.3	8.7	0.5	17.9	0.3	28.2	0.5	8.3	0.2	18.7	0.3	30.5	0.3
60	67	2	6.2	38.5	0.7	54.0	0.6	63.0	0.6	40.2	1.1	54.8	0.6	63.6	0.6	39.4	0.5	54.2	0.5	63.1	0.4
71	82	1	8.1	17.6	0.6	28.6	0.2	39.5	0.5	##	##	##	##	##	##	16.7	0.4	30.8	0.4	51.0	1.1
71	82	2	8.1	17.7	0.6	27.9	0.5	38.7	0.2	##	##	##	##	##	##	16.7	0.3	30.2	0.5	49.8	0.3
71	96	3	12.5	22.2	0.5	36.7	0.1	49.8	0.3	25.0	0.6	37.3	0.4	53.3	0.7	20.5	0.1	38.1	0.4	57.6	0.3
83	96	3	11.1	9.9	0.2	23.7	0.2	40.0	0.5	##	##	##	##	##	##	9.6	0.3	25.8	0.6	45.4	0.9
102	116	4	6.1	54.2	0.5	59.5	0.4	59.6	1.2	58.2	0.6	58.7	0.1	59.9	0.9	55.6	1.0	60.0	0.5	59.4	0.7
102	120	3	10.3	36.0	1.0	40.6	0.4	44.9	0.3	41.9	0.8	46.9	0.8	53.7	1.6	37.4	1.2	42.1	0.7	48.9	0.7
120	127	3	5.6	12.5	1.0	29.5	0.8	45.4	1.9	16.6	1.0	37.3	1.9	47.2	0.3	12.8	0.3	27.6	0.7	41.4	0.9
121	127	2	4.2	12.6	0.8	31.3	0.2	47.9	1.0	17.2	1.3	41.2	0.8	48.5	0.9	13.8	0.1	29.7	0.8	41.5	0.3
121	131	3	9.6	14.0	0.3	27.5	0.5	30.1	0.3	16.6	0.6	28.4	0.4	29.7	0.2	11.2	0.4	26.3	0.3	29.4	0.7
132	138	1	4.8	7.1	1.0	15.7	0.9	40.8	1.6	7.6	1.2	18.3	0.7	44.3	1.0	6.1	0.8	17.8	0.2	43.4	1.6
132	139	1	9.3	4.8	0.3	11.4	0.2	30.6	0.8	5.4	0.6	13.2	0.3	31.6	1.0	4.5	0.7	13.1	0.7	31.2	0.4
139	145	2	7.3	4.4	0.1	17.7	0.2	38.4	0.7	4.9	0.3	18.5	1.1	40.4	0.5	4.1	0.1	19.3	0.4	41.3	0.4
150	162	3	11.1	18.4	0.4	37.2	0.2	56.7	0.2	18.0	0.5	38.1	0.5	56.7	0.4	17.1	0.2	38.2	0.5	56.9	0.2
163	190	3	12.9	47.7	0.0	58.7	0.1	65.3	0.1	47.3	0.5	57.8	0.3	64.4	0.3	46.9	0.5	57.8	0.4	64.8	0.1
168	191	3	12.2	55.2	0.3	65.4	0.2	70.3	0.1	54.5	0.6	64.2	0.7	69.1	0.3	54.0	0.7	64.5	0.4	69.6	0.2
183	191	3	9.3	53.5	0.8	73.1	0.5	80.8	0.4	52.7	0.3	73.2	0.5	79.8	0.6	52.2	0.7	74.1	0.6	79.1	1.0
192	200	1	6.9	29.7	0.5	38.3	0.4	45.2	0.9	29.8	0.4	38.2	0.8	46.5	1.0	29.4	0.3	38.5	0.9	46.3	0.5
203	216	3	12.4	16.8	0.4	30.7	0.1	34.3	0.4	16.5	0.7	30.4	0.2	34.1	0.9	15.6	0.2	30.6	0.2	34.0	0.2
205	216	2	11.1	11.7	0.6	28.2	0.1	32.2	0.3	11.4	0.8	28.1	0.6	32.4	0.9	10.0	0.3	28.1	0.7	32.8	0.4
206	216	2	9.4	15.0	0.6	34.0	0.2	39.1	0.2	14.6	0.8	33.6	0.2	39.3	0.7	13.3	0.2	33.9	0.4	39.2	0.3
221	238	4	7.0	48.6	0.4	57.0	0.1	62.5	0.5	49.1	0.6	56.8	0.7	62.6	0.5	47.9	0.5	57.4	0.2	62.3	0.3
222	238	4	6.8	52.6	0.3	60.7	0.6	66.0	0.4	52.6	0.7	60.0	0.5	65.8	0.5	51.6	0.2	61.1	0.1	65.7	0.2
239	250	3	9.0	4.6	0.1	5.0	0.1	7.3	0.2	5.1	0.3	5.0	0.2	7.4	0.4	4.5	0.1	5.0	0.1	7.3	0.0
251	258	1	9.5	11.1	0.3	12.0	0.5	12.3	0.1	11.7	0.3	11.3	0.6	12.0	0.8	11.9	1.6	11.5	0.4	11.8	0.4
251	259	2	12.8	5.8	0.1	6.0	0.1	6.3	0.2	6.0	0.5	5.5	0.3	6.2	0.6	5.5	0.3	5.6	0.3	5.9	0.0
265	274	3	7.8	13.5	0.3	17.4	0.2	22.7	0.3	14.1	0.4	17.2	0.5	23.0	0.5	13.8	0.2	17.6	0.1	22.7	0.1
267	283	4	9.2	4.1	0.1	4.9	0.1	7.3	0.4	4.5	0.2	4.8	0.2	7.7	0.7	4.1	0.1	4.9	0.0	7.4	0.2
284	313	5	4.8	65.7	0.7	67.6	0.2	69.2	0.4	66.6	0.7	67.2	0.7	69.2	0.4	66.3	0.6	67.7	0.4	68.9	0.3
284	316	5	6.1	60.8	0.6	62.3	0.4	63.3	0.5	61.3	0.5	61.8	0.5	63.1	0.3	61.2	0.7	62.3	0.5	62.8	0.3
317	327	2	13.8	10.2	0.1	15.7	0.1	21.9	0.1	10.0	0.3	15.2	0.3	22.0	0.3	9.8	0.1	15.7	0.2	21.9	0.1
328	337	2	4.1	18.0	0.8	35.7	0.4	44.8	0.6	18.8	1.2	36.7	0.7	45.7	0.4	17.7	0.4	38.5	0.2	45.2	0.1
328	341	4	6.8	14.0	0.0	22.8	0.2	29.8	0.4	14.4	0.4	23.2	0.4	30.6	0.7	13.7	0.2	24.4	0.1	29.6	0.6
342	353	2	9.7	8.2	0.2	13.6	0.2	16.6	0.4	8.1	0.7	13.1	0.2	16.3	0.2	7.8	0.2	13.3	0.0	16.5	0.3
355	362	2	3.4	30.6	0.8	46.0	0.5	49.4	0.3	30.1	1.5	46.2	0.8	49.7	0.4	29.0	0.3	46.6	0.5	48.9	0.6
366	377	3	11.2	15.5	0.2	23.1	0.1	34.9	0.3	15.1	0.4	22.9	0.1	35.0	0.1	14.8	0.3	23.4	0.3	36.8	0.2
378	384	2	12.5	1.0	0.3	1.2	0.0	3.1	0.2	1.1	0.4	1.2	0.2	3.1	0.2	1.1	0.1	1.1	0.0	3.2	0.2
395	423	5	8.4	12.3	0.2	15.1	0.3	16.1	0.3	12.7	0.2	14.5	0.7	16.0	0.5	11.8	0.3	14.9	0.3	15.8	0.3
426	439	4	9.1	16.9	0.1	25.1	0.5	31.3	0.5	16.8	0.4	24.5	0.5	31.7	0.5	15.9	0.3	24.8	0.3	31.6	0.2
439	452	2	12.4	33.4	0.1	36.2	0.2	40.4	0.4	32.9	0.3	35.4	0.3	39.6	0.7	32.6	0.3	34.7	0.4	39.5	0.3
440	452	2	11.6	38.6	0.1	41.8	0.2	46.8	0.2	40.4	0.4	44.6	0.4	50.7	2.9	37.9	0.5	40.1	0.4	46.3	0.1
440	468	3	10.9	31.4	0.3	42.2	0.1	52.1	0.6	31.1	0.6	41.9	0.4	51.6	0.7	29.8	0.4	40.6	0.3	51.4	0.2
453	468	2	5.5	41.3	0.8	57.3	0.2	70.7	0.1	41.3	1.0	57.9	0.3	71.3	0.3	39.4	0.3	56.8	0.2	70.5	0.7
473	485	2	10.9	26.3	0.4	36.8	1.4	51.9	0.7	25.8	1.5	35.1	0.5	51.8	1.3	25.1	1.2	36.6	0.4	53.9	1.3
476	485	2	8.5	23.3	0.7	35.3	0.1	56.9	0.8	22.9	0.8	34.9	0.2	57.3	0.9	21.7	0.2	35.3	0.4	57.7	0.2
476	488	2	10.5	29.1	0.6	41.4	0.1	58.7	0.2	28.7	0.6	41.1	0.1	58.7	0.4	27.9	0.2	41.1	0.3	58.8	0.1
501	508	2	4.3	36.0	0.8	46.7	1.0	65.2	0.3	34.8	0.7	47.7	1.2	66.1	0.4	34.2	0.3	48.4	0.4	65.7	0.4
515	522	2	4.2	53.7	1.5	54.8	0.4	54.6	1.0	54.7	0.8	53.5	1.5	55.3	0.9	55.0	0.7	54.8	0.8	54.2	0.2
516	523	2	4.1	53.7	1.5	54.5	0.3	54.6	1.0	54.9	0.6	53.7	1.7	55.5	0.7	55.2	0.5	54.9	0.8	54.5	0.4
524	546	5	11.4	2.5	0.1	5.3	0.1	7.7	0.3	2.5	0.3	5.2	0.0	7.7	0.5	2.2	0.1	5.0	0.2	7.7	0.2
550	564	4	8.4	1.1	0.1	4.0	0.1	5.6	0.1	1.2	0.1	3.7	0.1	5.7	0.3	1.0	0.1	4.0	0.0	5.5	0.1
568	574	2	13.2	11.1	0.4	27.1	0.3	45.7	1.1	10.0	0.9	26.2	0.8	45.5	1.1	9.9	0.5	26.6	0.1	46.5	0.5
568	577	2	14.2	22.4	1.1	40.9	1.3	56.9	0.3	21.3	1.0	40.2	0.8	57.1	1.3	20.3	0.3	41.1	0.8	57.4	1.1
583	587	1	13.0	17.3	0.3	34.3	0.8	51.1	0.3	16.5	1.0	33.6	1.1	50.3	0.5	16.1	0.8	36.2	0.3	51.3	0.3
583	595	2	13.2	8.3	0.1	18.5	0.2	33.5	0.4	8.3	0.5	17.2	0.5	32.7	0.4	7.4	0.2	17.0	0.3	31.5	0.1
585	595	2	12.3	5.0	0.2	12.2	0.2	27.5	0.3	5.0	0.6	11.1	0.8	26.9	0.4	4.1	0.1	10.0	0.1	25.1	0.0
596	608	2	8.4	8.0	0.0	13.0	0.5	19.4	0.2	8.4	0.4	13.0	0.1	19.5	0.9	8.1	0.5	12.9	0.3	19.2	0.6
616	625	2	11.0	15.3	0.4	23.8	0.1	32.3	0.1	14.7	0.6	23.6	0.2	32.4	0.4	14.6	0.3	24.1	0.2	33.4	0.2
628	634	2	11.3	2.9	0.7	2.5	0.2	2.4	0.7	3.1	0.2	2.6	0.4	3.4	0.6	3.0	0.6	2.6	0.4	2.8	0.7
630	634	2	10.4	0.8	1.3	0.2	0.7	1.0	0.5	0.2	0.4	-0.2	0.4	0.9	0.8	1.2	0.1	0.3	0.9	1.3	0.5
633	647	4	9.1	1.3	0.0	2.6	0.1	3.3	0.1	1.4	0.2	2.6	0.1	3.6	0.3	1.2	0.1	2.6	0.0	3.5	0.1
635	646	4	6.3	2.5	0.1	5.9	0.3	7.7	0.7	2.8	0.5	6.0	0.2	8.4	0.3	2.5	0.5	6.2	0.4	8.0	0.3
647	651	2	12.5	1.0	0.1	1.2	0.1	0.9	0.2	1.2	0.1	1.2	0.1	1.6	0.2	0.9	0.2	1.1	0.0	1.2	0.1
648	655	3	10.0	1.3	0.2	1.0	0.3	1.6	0.4	1.5	0.2	1.6	0.4	1.6	0.2	1.3	0.2	1.4	0.5	1.5	0.1
671	683	4	6.0	3.8	0.2	7.1	0.0	12.3	0.3	4.1	0.3	7.6	0.5	12.7	0.4	3.4	0.1	7.7	0.3	12.3	0.1
698	713	5	4.9	31.3	0.9	45.4	0.2	51.6	0.5	31.0	0.9	44.8	0.9	51.7	0.8	30.0	0.4	45.7	0.4	51.2	0.3
698	715	4	6.8	23.0	0.3	33.2	0.0	40.8	0.5	23.1	0.4	33.0	0.6	41.1	0.4	22.4	0.1	33.8	0.3	40.7	0.2
714	719	2	10.7	1.5	0.2	2.1	0.2	4.0	0.2	2.0	0.3	2.2	0.2	4.5	0.4	2.1	0.5	2.4	0.4	4.9	0.2
726	740	2	10.6	4.4	0.3	16.5	0.3	23.8	0.2	4.5	0.4	16.8	0.2	23.9	0.5	3.9	0.2	16.9	0.1	24.0	0.2
726	741	2	12.0	4.1	0.1	15.4	0.5	22.4	0.5	4.0	0.4	15.7	0.4	22.6	0.8	3.7	0.1	15.7	0.1	22.5	0.3
728	740	2	10.2	5.5	0.1	20.2	0.0	29.2	0.1	5.7	0.6	20.6	0.1	29.4	0.5	4.7	0.1	20.7	0.1	29.4	0.1
741	745	1	6.7	2.1	0.1	4.7	0.3	24.3	0.5	2.4	0.1	4.6	0.0	25.4	1.3	2.2	0.5	5.0	0.5	26.1	0.4
746	751	1	8.9	4.2	0.3	17.5	0.1	33.9	0.2	4.5	0.5	17.4	0.0	34.2	0.7	3.6	0.3	17.7	0.0	34.5	0.2
753	762	3	12.3	12.0	0.1	12.9	0.2	18.7	0.4	11.7	0.3	12.7	0.4	18.7	0.5	11.7	0.2	12.8	0.2	19.2	0.1
761	766	1	6.8	35.5	0.5	43.8	0.5	51.0	0.2	35.8	0.4	45.2	1.7	51.5	0.6	35.7	0.7	44.7	0.5	51.1	0.3
767	775	1	3.5	42.9	0.7	44.5	0.1	50.0	0.5	43.2	0.8	43.2	1.3	50.7	1.2	43.2	0.6	44.8	0.9	50.2	0.4
776	784	2	9.3	16.4	0.3	21.0	0.1	27.1	0.2	16.2	0.4	20.3	0.3	26.3	0.5	16.2	0.2	20.9	0.2	26.5	0.1
776	788	3	9.2	14.0	0.1	25.7	1.4	31.7	2.0	13.9	0.9	25.5	0.1	32.8	0.5	13.3	0.5	26.1	0.7	32.8	0.3
801	807	2	7.0	3.9	0.2	14.6	0.1	25.2	0.4	4.2	0.6	14.7	0.4	25.4	0.7	3.5	0.2	15.0	0.3	25.0	0.1
808	826	3	10.8	4.5	0.1	5.4	0.1	9.8	0.2	4.7	0.4	5.3	0.1	9.9	0.2	4.4	0.0	5.4	0.1	10.0	0.1
809	824	3	9.6	6.7	0.1	7.9	0.1	13.5	0.1	6.8	0.6	7.6	0.1	13.5	0.3	6.4	0.0	7.8	0.2	13.7	0.1
827	836	2	6.4	19.5	0.5	28.1	0.5	35.2	0.3	19.2	0.7	27.8	0.3	35.8	0.6	18.7	0.3	28.6	0.3	35.6	0.2
840	849	2	4.1	72.3	0.6	73.9	0.3	73.1	1.1	74.0	0.5	72.9	0.1	74.0	0.9	73.0	0.5	73.2	0.9	73.3	0.8
845	850	1	7.8	84.7	0.2	85.1	0.8	84.9	0.9	85.1	0.7	84.4	0.8	85.1	0.3	85.0	0.6	84.8	1.3	85.3	0.2
850	856	2	9.4	43.7	1.0	54.8	0.5	61.3	0.6	42.9	1.0	54.3	0.6	61.1	0.7	40.9	0.8	54.2	0.2	61.6	0.3
851	856	2	7.5	35.5	1.3	48.8	0.2	56.8	0.7	34.2	1.3	48.6	0.9	57.0	0.4	32.4	0.3	49.3	0.3	57.6	0.1
882	886	1	6.3	1.4	0.2	1.8	0.4	1.5	0.3	1.7	0.4	2.1	0.6	2.1	0.3	1.7	0.7	1.7	0.5	1.7	0.3
887	898	3	7.8	5.0	0.5	11.3	0.3	12.3	2.6	5.2	0.1	11.3	0.3	13.9	0.2	5.1	0.8	8.7	4.7	13.8	0.3
887	900	2	9.9	2.5	0.0	6.5	0.1	8.3	0.1	2.5	0.1	6.3	0.1	8.3	0.3	2.3	0.1	6.4	0.1	8.3	0.1
908	912	2	11.4	1.2	0.3	3.4	0.4	13.4	0.3	1.2	0.4	3.1	0.2	13.7	0.3	1.8	0.5	3.6	0.5	15.0	0.4
908	919	3	13.6	18.9	0.3	35.7	0.3	39.1	0.4	18.2	0.8	35.3	0.3	38.6	0.5	17.4	0.4	35.0	0.7	39.0	0.1
909	919	3	12.8	20.0	0.7	38.3	0.4	42.0	0.8	19.0	0.7	37.9	0.8	41.3	0.7	18.5	0.3	37.5	0.6	42.0	0.4
939	958	5	6.1	16.3	0.3	22.8	0.2	27.1	0.5	16.6	0.6	22.2	0.9	27.1	0.8	16.0	0.3	23.2	0.1	26.8	0.2
964	973	3	8.4	7.1	0.1	9.8	0.2	15.1	0.2	6.9	0.2	9.7	0.2	15.1	0.4	6.6	0.1	10.1	0.1	15.6	0.2
964	974	4	10.4	6.5	0.2	9.2	0.4	14.3	0.3	6.3	0.2	9.1	0.3	14.2	0.4	6.0	0.2	9.0	0.1	14.4	0.6
978	989	2	12.4	15.6	0.7	45.0	0.3	58.6	0.4	14.7	0.9	45.4	0.6	57.8	0.2	15.1	0.2	48.0	0.3	58.0	0.3
982	989	2	9.4	22.7	1.0	59.9	0.8	78.2	0.1	21.8	1.2	61.5	0.7	77.9	0.4	22.9	0.4	66.2	0.7	78.2	0.3
1003	1009	2	3.9	57.3	1.7	69.2	0.1	72.7	1.3	58.5	0.7	68.3	1.4	72.8	1.2	57.3	0.7	69.3	1.0	71.6	0.2
1010	1019	3	7.9	1.0	0.2	1.9	0.1	8.1	0.3	1.2	0.2	2.3	0.1	8.4	0.2	1.0	0.1	2.2	0.1	8.2	0.1
1023	1033	4	8.8	36.1	0.7	51.8	0.3	53.2	0.5	35.1	1.0	51.6	1.1	52.5	0.8	32.3	0.6	51.8	0.7	52.5	0.1
1024	1033	4	8.3	38.9	0.6	57.2	0.5	57.6	0.2	37.8	1.4	56.6	0.2	57.3	0.7	34.5	0.3	57.0	0.5	57.0	0.5
1024	1044	5	8.1	39.6	0.5	50.2	0.2	51.4	0.2	39.6	0.7	49.6	0.9	50.5	0.8	37.5	0.9	50.5	0.7	50.6	0.4
1034	1044	3	3.2	49.8	1.6	51.4	0.1	51.9	0.5	50.7	1.3	50.8	1.2	51.9	0.8	51.0	0.5	51.6	0.8	50.8	0.7

0 10 20 30 40 50 70 80 90

Figure 39: All HDX p110δ and p85α peptide data for experiments examining conformational changes in APDS1 N-terminal mutations under the basal state.

The charge state *(Z)*, residue start *(S)*, residue end number *(E)*, and retention time *(RT)* are displayed for every peptide. Three time-points are labelled (3, 30, 300), and the relative

level of HDX is coloured on a blue-to-red continuum. Data listed are the average of 3 independent experiments, with SDs presented. ##No coverage for the specific peptide.

p85α				WT Basal						E81K Basal						G124D Basal					
S	E	Z	RT	3	SD	30	SD	300	SD	3	SD	30	SD	300	SD	3	SD	30	SD	300	SD
8	13	2	7.6	4.4	0.2	5.3	0.0	13.8	0.6	4.3	0.7	5.7	0.2	14.3	0.3	3.8	0.4	5.9	0.1	14.4	0.2
14	21	3	2.9	23.6	2.0	32.5	1.4	30.2	4.3	25.6	1.8	32.7	2.2	32.8	0.6	25.2	1.3	33.3	1.8	30.5	3.4
22	30	2	12.6	2.5	0.1	6.8	0.2	12.0	0.3	2.4	0.5	6.8	0.2	11.5	0.1	2.2	0.2	6.8	0.4	11.8	0.2
25	37	3	9.8	25.9	0.2	26.6	0.3	26.8	0.5	26.0	0.1	26.0	0.6	26.2	0.2	25.7	0.6	26.6	0.3	26.2	0.2
38	52	2	8.5	39.2	0.4	58.0	0.3	60.9	0.7	38.7	1.4	57.0	0.3	59.5	0.3	37.7	1.0	57.6	0.1	59.8	0.3
53	60	1	11.9	10.3	0.3	21.8	0.1	25.0	0.1	10.2	0.7	21.8	0.1	24.9	0.1	9.4	0.5	21.8	0.2	24.9	0.0
53	73	3	11.9	7.0	0.2	15.5	0.1	21.0	0.3	6.7	0.6	15.2	0.2	20.5	0.2	6.1	0.3	15.4	0.1	20.8	0.1
59	72	2	7.7	8.0	0.3	17.0	0.3	24.5	0.3	7.8	1.0	16.9	0.2	24.2	0.0	7.3	0.3	17.5	0.2	24.7	0.2
73	106	5	6.5	52.1	0.3	56.3	0.5	57.0	0.4	52.3	0.8	55.2	0.9	56.7	0.4	52.0	0.7	56.2	0.1	56.4	0.3
74	107	5	6.0	53.9	0.6	57.4	0.6	58.2	0.5	54.0	0.4	56.4	0.5	57.8	0.2	54.2	0.7	57.5	0.4	57.4	0.3
77	107	5	5.2	60.1	0.7	60.7	0.1	61.3	0.6	60.8	1.0	60.6	0.4	61.0	0.6	60.6	0.9	60.9	0.2	60.6	0.2
113	118	1	11.7	25.7	0.8	60.2	0.4	72.9	0.4	26.6	1.4	60.2	0.2	72.1	0.3	22.8	0.2	60.5	0.7	72.7	0.0
119	132	2	12.6	12.6	0.5	24.3	0.2	33.0	0.1	13.4	0.6	24.5	0.1	34.0	1.1	11.4	0.2	24.5	0.2	33.4	0.2
139	146	3	4.8	15.4	1.0	38.1	0.3	57.0	0.8	15.4	0.2	34.2	2.3	57.1	1.5	13.7	0.3	37.6	0.7	55.8	0.9
149	158	2	6.3	55.1	0.6	57.9	0.3	63.6	0.6	55.8	0.2	56.9	0.6	63.4	0.6	55.5	0.9	57.8	0.5	63.3	0.5
150	157	2	3.1	67.3	2.4	68.1	0.7	69.3	1.8	68.3	1.1	67.8	1.5	68.4	1.4	69.4	0.8	68.7	1.6	68.3	1.1
168	173	1	4.7	77.7	0.6	77.9	1.1	77.8	0.3	77.4	0.3	77.6	0.7	78.5	0.4	78.2	0.2	78.3	0.6	78.2	0.1
177	185	2	9.3	10.4	0.2	11.6	0.3	13.2	0.3	10.6	0.3	11.7	0.5	14.7	1.1	10.1	0.2	11.9	0.1	13.7	0.1
177	186	2	11.9	8.7	0.2	10.0	0.0	11.9	0.2	8.5	0.3	9.9	0.3	12.6	0.8	8.2	0.1	10.1	0.1	12.0	0.1
186	202	3	11.9	11.7	0.2	12.9	0.2	15.1	0.1	12.1	0.4	13.1	0.2	15.7	0.6	11.3	0.4	13.0	0.1	15.4	0.1
186	203	3	12.3	10.9	0.3	12.2	0.1	14.9	0.1	11.5	0.3	12.3	0.3	15.5	0.6	10.4	0.1	12.3	0.1	15.2	0.1
191	202	2	11.4	18.2	0.2	19.7	0.3	23.1	0.2	19.0	1.1	20.3	0.2	24.0	1.1	17.4	0.2	20.0	0.1	23.6	0.2
207	218	1	8.6	56.2	0.4	71.1	0.3	70.7	0.5	55.8	1.6	69.3	0.7	69.6	0.3	54.7	1.3	69.9	0.2	70.0	0.1
223	237	3	8.7	7.1	0.1	8.2	0.1	15.2	0.3	7.5	0.1	8.1	0.2	16.0	0.9	7.0	0.2	8.2	0.1	15.5	0.3
238	261	4	13.5	10.4	0.2	14.3	0.1	18.2	0.3	10.7	0.1	14.2	0.2	18.5	0.6	10.1	0.1	13.9	0.4	18.3	0.1
242	261	3	10.3	13.0	0.1	17.7	0.1	22.5	0.2	13.2	0.2	17.4	0.2	22.9	0.7	12.4	0.3	17.6	0.1	22.6	0.2
262	266	1	4.5	2.0	0.1	2.2	0.5	2.3	0.7	2.9	0.4	2.3	0.8	4.0	1.6	1.8	0.3	2.1	0.6	2.9	0.4
262	268	2	11.1	2.8	0.5	2.3	0.3	2.1	0.7	2.8	0.1	2.4	0.2	3.3	0.3	2.7	0.6	2.3	0.6	2.3	0.5
262	272	2	13.0	1.2	0.1	2.2	0.1	7.8	0.1	1.9	0.0	2.6	0.1	8.9	0.7	1.3	0.1	2.5	0.2	8.4	0.2
267	272	1	12.4	1.7	0.4	4.8	0.6	20.5	0.4	3.1	0.5	5.3	0.2	23.0	1.7	1.6	0.5	5.3	0.5	21.2	0.4
273	286	2	9.4	43.1	0.4	49.9	0.4	54.8	0.2	43.0	0.5	49.0	0.3	53.6	0.4	42.4	1.1	49.0	0.3	53.9	0.3
287	291	2	6.3	0.9	0.5	1.1	0.3	0.9	0.4	1.5	0.6	1.1	0.2	2.9	1.3	1.0	0.3	0.8	0.3	1.2	0.1
294	325	4	7.8	72.0	0.3	73.3	0.3	73.6	0.2	71.9	0.4	72.4	0.2	72.6	0.4	72.0	0.6	72.7	0.3	73.0	0.2
294	326	4	8.2	71.8	0.2	72.7	0.1	72.9	0.3	71.2	0.7	71.7	0.4	72.0	0.5	71.4	0.7	72.1	0.4	72.3	0.3
299	326	4	6.9	76.7	0.6	76.9	0.5	77.5	0.3	77.4	0.3	76.8	0.4	76.8	0.7	77.3	1.2	77.1	0.2	77.2	0.2
327	332	1	5.0	2.9	0.5	3.3	0.4	7.4	1.2	2.9	0.6	3.5	0.4	7.3	0.4	3.0	0.2	3.5	0.4	7.3	0.5
333	341	2	12.0	30.6	0.5	47.5	0.4	53.4	0.4	29.8	0.5	46.7	0.3	53.0	0.2	28.9	0.2	47.0	0.7	53.3	0.5
334	341	2	9.3	36.9	0.5	55.0	0.3	62.4	0.4	36.5	0.6	54.1	0.2	61.2	0.7	35.1	0.7	54.7	0.5	61.4	0.6
342	355	3	7.9	16.7	0.2	23.2	0.2	36.6	0.6	16.8	0.3	23.2	0.5	37.3	0.4	16.5	0.1	24.0	0.5	37.8	0.4
346	355	3	6.5	16.2	0.2	18.9	0.3	28.6	0.4	16.3	0.5	19.0	0.7	29.0	1.3	16.4	0.3	19.5	0.3	28.9	0.6
356	371	4	7.0	19.7	0.4	24.5	0.2	25.5	0.6	19.7	0.2	24.2	1.0	25.6	0.8	19.4	0.2	25.1	0.5	25.4	0.5
356	372	4	9.2	16.1	0.4	20.4	0.1	21.0	0.3	16.4	0.1	20.5	0.7	21.4	0.6	15.6	0.6	20.5	0.2	21.1	0.4
373	380	2	2.9	18.2	1.1	22.0	0.1	33.3	0.4	18.9	0.8	22.4	1.1	34.8	0.9	18.4	0.3	23.0	0.6	33.8	0.4
381	398	4	10.8	18.5	0.0	23.9	0.0	26.4	0.2	18.4	0.2	23.7	0.1	26.3	0.4	17.9	0.2	23.4	0.2	26.3	0.1
381	401	4	10.9	21.8	0.1	27.5	0.2	30.3	0.1	21.5	0.4	26.9	0.3	29.5	0.3	21.1	0.3	26.9	0.3	29.8	0.2
402	413	3	8.5	22.3	0.3	25.3	0.2	25.7	0.2	21.9	0.5	25.0	0.0	25.7	0.4	21.4	0.2	25.2	0.1	25.6	0.1
405	413	3	5.8	32.1	0.7	36.5	0.3	36.9	0.4	31.9	0.9	36.2	0.3	37.2	0.7	31.0	0.4	36.7	0.2	36.8	0.3
414	420	1	6.9	78.2	0.9	83.7	0.4	83.8	0.2	77.8	0.6	83.7	0.2	83.9	0.3	77.0	0.3	83.6	0.2	83.8	0.2
414	420	2	6.9	78.1	0.7	83.2	0.3	83.6	0.5	77.7	1.0	83.0	0.5	83.9	0.4	76.7	0.3	83.6	0.4	83.6	0.1
421	435	3	9.1	36.7	0.5	47.4	0.2	50.5	0.5	36.5	0.3	46.9	0.1	50.6	0.4	35.9	0.3	47.3	0.2	50.6	0.3
421	443	4	9.5	45.7	0.7	54.0	1.1	55.6	0.5	45.2	0.5	52.6	0.4	54.6	0.3	44.4	0.5	53.1	0.3	55.0	0.4
436	443	2	5.2	57.5	0.5	65.0	1.1	64.6	1.7	57.1	0.6	64.8	1.2	65.3	2.4	56.6	1.2	65.9	0.4	65.4	0.6
444	456	2	6.8	0.9	0.2	3.3	0.4	14.7	0.5	1.2	0.3	3.7	0.5	16.2	0.8	0.9	0.2	3.8	0.4	16.6	0.5
457	466	3	5.8	1.4	0.3	2.1	0.1	6.8	0.3	1.6	0.0	2.6	0.2	7.7	0.5	1.7	0.5	2.8	0.1	9.0	0.4
467	476	2	5.5	1.6	0.2	3.1	0.2	15.1	0.5	1.6	0.1	4.2	0.2	19.2	0.4	1.7	0.3	5.7	0.3	24.2	0.5
470	476	2	3.4	3.7	0.5	6.0	0.2	21.3	0.7	3.8	0.1	7.2	0.5	26.6	0.9	4.2	0.6	9.4	0.1	30.6	0.0
477	486	3	6.2	1.1	0.3	1.4	0.1	5.0	0.3	1.0	0.0	1.7	0.1	7.3	0.4	0.9	0.4	1.4	0.3	5.1	0.3
508	520	4	4.8	39.6	1.0	50.5	0.7	51.6	0.8	39.4	1.1	49.7	1.2	51.7	0.9	39.2	0.3	51.3	1.0	50.7	0.2
538	549	4	8.1	0.9	0.2	2.0	0.1	10.7	0.3	0.8	0.0	2.0	0.2	10.7	0.2	1.0	0.1	5.8	0.2	21.9	0.3
556	570	4	7.7	1.9	0.1	4.7	0.1	10.3	0.2	1.9	0.2	5.1	0.1	12.1	1.0	1.8	0.0	6.8	0.3	18.2	0.1
556	570	5	7.7	2.3	0.7	4.7	0.2	10.3	0.3	1.5	0.4	4.9	0.2	12.4	0.7	1.0	0.2	6.8	0.2	17.7	0.5
557	570	3	7.1	2.3	0.2	5.6	0.2	11.2	0.6	2.4	0.1	6.2	0.5	13.3	0.6	2.3	0.3	8.0	0.2	18.7	0.4
571	581	4	7.0	0.2	0.3	1.3	0.3	9.7	0.3	0.2	0.2	1.6	0.3	11.2	0.4	0.3	0.3	1.5	0.3	10.5	0.3
582	596	3	7.0	25.2	1.0	47.6	0.2	52.0	0.7	25.5	0.7	47.4	0.3	51.7	0.8	23.2	0.6	48.1	0.4	51.2	0.4
610	637	4	7.4	18.1	0.3	25.8	0.2	29.1	0.3	18.0	0.6	25.3	0.5	29.0	0.3	17.4	0.5	26.0	0.2	28.8	0.3
638	646	3	4.3	14.4	0.5	15.9	0.2	21.5	0.8	14.9	0.7	15.6	0.8	22.1	0.7	14.6	0.2	16.4	0.4	21.3	0.3
647	657	3	4.9	38.5	0.6	47.8	0.3	50.8	0.3	38.8	0.6	47.4	0.8	50.9	0.5	38.5	0.3	48.2	0.4	50.4	0.2
661	680	4	7.2	20.9	0.3	28.3	0.4	33.3	0.3	20.9	0.7	27.9	0.2	33.7	0.4	20.2	0.2	28.5	0.3	33.5	0.2
661	687	4	10.4	16.4	0.2	24.5	0.0	33.9	0.2	16.1	0.4	24.1	0.3	33.6	0.4	15.7	0.2	24.2	0.1	33.9	0.2
681	687	2	10.6	23.1	0.3	33.8	0.1	52.3	1.4	24.8	0.5	34.9	0.1	52.3	2.1	24.8	4.2	34.4	0.9	52.9	1.5
694	703	3	8.3	3.6	0.2	6.7	0.1	8.9	0.2	3.6	0.3	6.6	0.1	9.1	0.4	3.3	0.1	6.8	0.1	9.0	0.2
704	710	2	4.9	19.1	0.4	31.4	0.2	33.2	0.3	19.1	0.4	31.4	0.8	33.4	0.3	18.7	0.1	32.2	0.2	33.2	0.3
704	711	2	4.0	20.8	1.2	38.8	0.1	41.0	0.4	20.8	0.9	40.8	1.0	41.3	0.3	20.0	0.4	40.0	1.4	41.5	0.2
711	719	2	11.0	2.7	0.2	4.5	0.2	13.0	0.1	2.8	0.5	4.7	0.2	13.3	0.2	2.5	0.3	4.8	0.1	13.4	0.1
711	724	3	8.5	30.7	0.0	37.5	0.0	43.4	0.2	30.8	0.1	37.2	0.2	43.5	0.4	30.4	0.2	37.6	0.1	43.4	0.2

Figure A1.1 cont.: All HDX p110δ and p85α peptide data for experiments examining conformational changes in APDS1 N-terminal mutations under the basal state.

p110δ				WT Basal						WT pY						WT Membrane + pY						G124D Basal						G124D pY						G124D Membrane + pY					
S	E	Z	RT	3	SD	30	SD	300	SD	3	SD	30	SD	300	SD	3	SD	30	SD	300	SD	3	SD	30	SD	300	SD	3	SD	30	SD	300	SD	3	SD	30	SD	300	SD
12	18	2	4.2	65.7	1.2	64.8	0.2	65.4	1.0	64.5	0.2	68.0	0.9	68.8	0.3	67.0	2.2	66.4	0.2	68.7	0.1	64.7	0.7	66.6	0.4	67.5	1.0	67.4	0.9	65.8	0.6	68.5	1.0	67.2	1.0	65.9	0.9	69.0	1.4
12	19	2	4.1	65.9	1.0	65.2	0.7	67.2	0.4	64.1	0.9	67.9	0.8	68.7	0.3	65.6	2.2	65.4	0.1	67.7	0.9	64.9	0.8	66.2	0.5	67.8	0.9	67.3	1.6	66.2	0.4	68.7	1.7	66.7	1.2	66.2	2.6	69.0	0.2
24	31	2	12.5	2.5	0.3	14.0	0.5	23.3	0.0	2.0	0.0	13.8	0.1	23.1	0.4	2.5	0.3	13.8	0.1	23.6	0.5	3.6	0.1	16.7	0.2	24.8	0.2	2.6	0.5	14.6	0.2	23.8	0.1	2.4	0.6	13.5	0.1	24.0	0.1
32	42	2	9.5	20.6	0.9	31.6	0.4	32.7	0.2	20.1	0.5	31.7	0.6	32.9	0.5	22.9	0.9	31.6	0.0	34.2	0.2	20.1	0.8	31.1	0.4	32.4	0.6	21.1	0.0	31.8	0.2	32.9	0.4	22.7	1.5	31.6	0.6	34.1	0.6
35	42	2	5.3	30.5	2.0	45.5	0.7	48.0	0.2	28.2	1.0	46.6	0.6	49.4	0.6	33.6	1.3	45.5	1.2	49.4	0.6	29.3	0.2	45.8	0.5	48.2	0.6	31.6	0.9	45.6	0.6	49.4	1.3	33.8	3.3	45.8	1.8	50.9	0.1
43	59	4	11.6	4.4	0.3	10.1	0.3	18.7	0.1	4.2	0.1	10.5	0.1	19.6	0.1	4.4	0.1	10.1	0.2	19.2	0.0	4.3	0.1	10.5	0.1	19.8	0.4	4.7	0.1	10.6	0.1	19.6	0.0	4.0	0.7	9.6	0.1	18.7	0.2
43	67	4	12.1	13.9	0.7	23.8	0.4	32.0	0.1	13.3	0.0	24.5	0.5	32.3	0.5	13.7	0.8	23.6	0.1	32.6	0.8	13.8	0.2	24.3	0.2	32.1	0.5	14.0	0.2	24.3	0.2	32.0	0.5	13.2	1.4	23.1	0.2	32.2	0.7
48	59	3	11.8	7.7	0.6	17.5	0.3	29.1	0.0	8.0	0.0	18.3	0.4	30.2	0.7	8.0	0.3	17.5	0.3	30.0	1.0	7.6	0.2	18.0	0.3	30.4	0.3	8.1	0.0	18.1	0.1	29.7	0.1	7.2	1.1	16.7	0.0	29.2	0.4
60	67	2	6.3	37.1	2.2	53.9	0.6	64.3	0.1	35.6	0.9	54.8	1.3	64.7	0.4	37.2	0.8	52.8	1.0	63.7	0.6	38.2	0.8	54.6	1.1	63.9	0.5	39.0	0.4	53.4	0.6	64.6	0.7	36.7	2.8	52.9	1.8	64.8	0.5
71	82	1	8.1	15.6	1.3	27.4	0.8	35.1	0.6	14.8	0.5	28.9	0.2	37.2	0.4	19.9	0.2	31.4	1.2	42.7	1.3	17.7	2.9	29.9	0.5	44.1	1.5	17.2	0.3	30.8	0.1	44.4	0.2	20.9	1.6	33.4	0.4	48.1	0.4
71	82	2	8.1	14.9	1.3	27.0	0.1	36.6	0.2	14.6	0.0	28.1	0.4	38.8	0.2	18.7	0.4	31.0	1.0	46.7	0.6	15.3	0.3	29.3	0.7	47.0	0.7	17.4	0.0	30.8	0.1	46.4	0.1	20.7	1.8	34.2	0.3	50.9	0.1
71	96	3	12.5	18.6	1.2	34.6	0.1	48.0	0.0	17.7	0.1	35.5	0.4	49.7	0.7	22.2	1.4	36.4	0.6	57.1	0.9	18.3	0.3	36.5	0.0	56.0	0.6	19.1	0.1	36.1	0.2	53.5	0.3	23.6	2.2	38.0	0.3	58.9	0.6
83	96	3	11.2	7.0	0.8	22.2	0.3	39.0	0.1	6.9	0.3	23.2	0.5	38.7	0.9	10.5	0.5	23.3	0.4	43.6	1.2	8.1	0.2	23.8	0.2	44.5	0.2	7.7	0.2	23.2	0.3	41.2	0.5	10.4	1.9	24.0	0.2	44.5	0.6
102	116	4	6.1	54.3	2.2	57.8	0.7	58.9	0.9	51.1	1.8	58.7	1.1	59.2	1.1	54.9	1.1	57.7	2.1	57.6	1.0	54.5	1.0	58.7	1.1	60.0	0.1	54.5	0.4	57.6	0.8	58.4	1.4	55.4	1.8	57.8	2.0	59.8	0.4
102	120	3	10.3	34.2	0.6	39.3	0.8	44.7	0.5	33.6	0.9	40.0	1.3	45.4	1.2	35.5	1.2	40.6	0.5	48.7	2.0	35.5	2.0	40.5	0.3	47.7	0.8	34.6	0.1	40.9	0.1	46.9	0.6	35.6	1.2	40.5	1.0	48.3	0.9
120	127	3	5.6	10.6	1.0	26.4	1.2	44.0	0.2	11.1	0.1	32.2	0.8	45.5	0.8	20.6	0.8	38.2	2.5	46.7	1.1	11.8	0.5	27.5	0.5	42.1	0.2	15.3	0.5	28.1	0.2	39.0	1.5	17.6	1.8	30.3	1.3	41.4	0.1
121	127	2	4.3	12.2	1.0	28.8	0.4	47.1	0.9	12.6	0.1	36.6	0.6	49.4	0.9	24.3	1.0	42.5	1.7	47.9	0.7	13.4	0.1	30.9	0.7	45.3	0.0	16.2	0.5	31.2	0.2	42.7	1.9	19.5	1.7	33.8	1.2	44.8	1.0
121	131	3	9.6	11.5	0.7	26.1	0.8	28.6	0.5	11.9	0.1	27.0	0.9	29.0	1.1	16.9	0.5	27.2	0.9	28.8	0.8	10.1	1.3	25.1	0.6	28.8	0.8	13.7	0.3	25.7	0.0	26.1	0.7	14.8	1.4	25.8	1.4	27.0	1.2
132	138	1	5.0	5.8	0.7	16.1	1.0	39.0	0.1	6.1	1.8	17.1	0.6	43.4	0.4	6.4	1.0	17.7	0.2	42.9	0.7	5.7	0.6	17.6	1.7	41.7	1.5	6.2	0.3	20.1	0.6	44.8	0.1	6.2	0.2	19.0	1.5	44.8	0.5
132	139	1	9.2	4.5	0.6	13.0	1.3	29.9	0.9	5.7	1.8	13.3	0.6	31.8	0.8	5.9	0.7	14.4	0.4	33.0	0.9	5.1	0.4	13.2	0.1	30.9	0.7	4.9	0.0	15.1	0.4	33.0	0.1	5.1	0.6	15.0	0.1	33.4	1.3
139	145	2	7.3	4.5	0.7	21.6	3.0	41.6	0.4	5.8	1.8	18.9	0.8	40.0	0.6	5.9	1.5	19.7	0.3	39.9	0.2	4.8	0.6	22.6	1.6	43.3	0.3	4.5	0.1	19.5	0.7	41.4	1.0	4.7	0.4	18.6	1.1	40.1	0.7
140	146	2	7.3	3.7	0.4	21.4	3.1	41.5	1.3	5.0	2.2	18.0	0.9	40.0	0.8	5.0	0.8	19.0	0.1	39.6	0.3	4.1	1.0	22.1	1.5	43.2	0.3	3.6	0.1	18.5	0.5	41.6	0.6	3.3	0.8	18.0	1.5	40.3	1.1
150	159	3	8.2	25.0	1.1	47.9	0.8	69.5	0.2	23.2	0.7	47.6	0.7	70.4	1.3	24.7	0.9	47.7	0.1	69.6	1.0	24.8	0.6	47.8	1.3	70.8	0.4	25.0	0.4	48.8	0.4	70.3	0.6	24.8	2.1	47.8	1.5	70.3	0.2
150	162	3	11.1	16.6	1.0	36.6	0.8	56.4	0.0	15.9	0.1	35.9	0.8	52.6	1.2	17.2	0.6	35.2	0.5	50.5	1.7	16.6	0.2	37.9	0.3	56.3	0.6	16.9	0.0	37.1	0.3	52.1	0.7	17.3	1.5	35.3	0.1	52.1	0.5
163	190	3	13.1	45.3	0.4	56.0	0.4	63.0	0.2	44.0	0.3	56.4	0.5	63.8	0.6	45.1	0.4	56.0	0.3	64.0	0.6	44.6	0.3	56.3	0.1	63.1	0.4	45.2	0.3	56.9	0.4	63.7	0.3	45.2	0.8	56.0	0.4	63.9	0.4
164	175	3	12.2	13.1	0.2	14.1	0.2	19.3	0.0	13.0	0.0	14.5	0.3	19.3	0.2	13.2	0.4	14.2	0.3	19.3	0.2	13.4	0.3	14.7	0.2	19.5	0.5	13.9	0.5	15.2	0.2	20.4	0.4	13.6	0.3	14.0	0.4	19.3	0.4
168	191	3	12.2	54.2	0.5	64.5	0.5	69.9	0.1	53.1	0.8	65.0	0.7	70.2	0.4	54.3	0.6	64.6	0.2	70.8	0.7	53.5	0.4	64.9	0.1	69.9	0.4	54.2	0.4	65.2	0.3	70.0	0.3	54.4	0.7	64.1	0.4	70.6	0.6
183	191	3	9.4	50.3	1.4	71.9	0.7	78.9	0.5	50.4	2.3	72.4	1.4	78.0	0.4	50.5	1.3	69.9	0.2	78.0	0.4	49.6	1.2	69.0	2.3	77.4	0.7	51.6	0.9	72.2	0.4	78.2	0.5	50.7	0.8	69.4	2.8	78.0	0.5
192	200	1	6.9	29.0	2.2	38.2	0.9	46.3	1.2	27.1	1.5	38.9	1.0	47.6	0.6	30.4	1.0	38.3	0.0	47.7	0.9	27.6	1.1	38.5	0.9	46.9	1.1	30.0	0.3	38.4	0.5	47.7	1.3	29.8	1.1	38.9	2.8	48.8	0.2
203	216	3	12.3	17.4	1.1	33.0	0.2	37.3	0.1	16.2	0.1	33.1	0.4	36.7	0.3	17.0	0.5	32.1	0.4	36.2	0.8	16.6	0.2	33.1	0.4	36.8	0.6	17.6	0.2	33.3	0.2	36.4	0.2	16.6	1.6	32.0	0.5	36.2	0.3
205	216	2	11.1	11.4	1.1	29.9	0.5	35.2	0.3	10.2	0.2	29.9	0.8	34.8	0.2	10.6	0.6	29.6	0.5	34.9	0.2	11.1	0.2	29.9	0.2	34.7	0.4	10.8	0.2	30.0	0.1	34.8	0.3	10.3	2.0	29.2	0.2	34.3	0.6
206	216	1	9.7	13.4	1.8	33.3	1.8	39.1	1.1	11.5	0.4	32.6	0.9	38.5	0.4	12.4	0.6	33.6	0.7	38.4	1.7	12.3	1.2	33.4	0.5	39.5	0.5	12.5	0.1	32.6	0.3	38.1	0.9	11.9	1.6	33.0	0.8	37.6	0.3
206	216	2	9.7	13.5	1.1	33.9	0.9	39.6	0.1	12.0	0.4	33.4	0.7	38.9	0.2	12.5	0.6	33.1	0.2	38.6	0.1	13.0	0.4	33.3	0.2	39.1	0.3	12.7	0.1	33.3	0.3	39.2	0.4	11.8	2.0	32.6	0.7	38.4	0.7
221	238	4	6.9	47.7	1.9	56.4	0.2	62.1	0.6	45.9	1.3	57.3	1.0	62.7	0.3	47.9	0.6	56.7	1.4	62.3	0.6	46.9	1.1	56.6	1.0	62.1	0.6	47.5	0.2	56.4	0.6	62.0	0.5	47.2	2.2	56.5	1.4	63.0	0.5
222	238	4	6.7	51.9	1.6	60.6	0.3	65.7	0.6	49.6	0.9	60.9	0.7	66.5	0.5	50.9	1.0	60.1	1.4	65.7	0.3	51.1	0.7	60.2	0.7	66.0	0.4	51.5	0.1	60.2	0.6	66.2	0.6	50.6	2.9	59.9	1.6	66.6	0.3
228	238	2	7.6	54.1	1.3	64.6	0.4	74.2	0.1	51.4	1.4	64.5	0.5	74.5	0.5	52.6	0.6	63.9	1.0	73.6	0.8	53.2	1.0	62.8	3.0	74.5	1.6	53.9	0.0	64.7	0.6	74.3	0.4	53.1	2.5	64.1	0.8	73.9	0.1
239	250	3	9.0	4.5	0.0	5.3	0.3	7.5	0.1	4.5	0.2	5.2	0.2	7.5	0.0	4.9	0.1	5.6	0.1	8.2	0.2	4.6	0.3	5.3	0.2	7.7	0.2	4.6	0.1	5.3	0.2	7.7	0.1	4.7	0.2	5.4	0.1	8.1	0.4
251	258	1	9.5	10.1	0.1	11.0	0.7	11.3	0.0	9.6	0.5	10.5	0.5	11.1	0.3	10.6	0.4	11.0	0.1	11.7	0.2	10.1	0.5	10.7	0.3	11.2	0.5	9.9	0.1	10.4	0.3	10.9	0.2	10.1	0.2	10.6	0.1	11.3	0.7
251	259	2	12.8	5.0	0.1	5.4	0.3	5.8	0.1	5.1	0.3	5.7	0.3	6.2	0.2	6.1	0.3	6.2	0.0	6.9	0.3	4.8	0.1	5.5	0.2	5.8	0.3	5.2	0.2	5.7	0.1	6.1	0.3	5.8	0.1	6.0	0.3	6.3	0.6
265	274	3	8.1	13.7	0.4	17.8	0.5	23.2	0.4	13.4	0.0	17.7	0.6	24.2	0.3	13.8	0.2	17.5	0.4	24.5	0.3	13.9	0.2	17.4	0.2	23.3	0.2	13.7	0.1	17.7	0.3	24.0	0.0	13.7	0.5	17.6	1.0	24.0	1.1
267	283	4	9.3	3.7	0.1	5.2	0.1	8.0	0.0	4.1	0.2	5.4	0.2	8.5	0.4	5.2	0.6	6.1	0.3	9.9	1.0	3.6	0.1	5.1	0.2	8.0	0.2	4.5	0.2	5.4	0.2	8.6	0.3	4.6	0.2	6.0	0.1	9.4	0.4
275	283	2	8.4	2.0	0.2	4.9	0.2	11.4	0.2	1.9	0.1	4.5	0.3	11.4	0.1	2.1	0.1	4.8	0.0	11.6	0.1	2.1	0.3	4.9	0.2	11.8	0.3	2.0	0.1	4.8	0.1	12.0	0.2	1.9	0.3	4.9	0.4	12.0	0.5
284	313	5	4.9	65.7	1.1	66.1	0.1	67.7	1.2	63.5	1.4	67.0	0.5	68.4	0.6	65.5	1.2	66.3	0.9	67.6	0.7	65.3	0.5	66.9	0.2	68.6	0.3	65.8	0.6	65.6	0.3	68.1	1.1	65.9	0.7	65.9	1.6	68.6	0.4
284	316	5	6.3	59.9	1.3	60.3	0.5	61.4	0.8	58.0	1.4	61.2	0.8	62.1	0.5	59.7	0.7	60.1	1.6	61.1	0.8	59.2	0.6	60.8	0.7	62.2	0.2	60.4	0.3	60.4	0.6	61.5	0.8	59.9	0.9	60.3	1.6	62.4	0.3
317	327	2	13.9	10.3	0.5	16.1	0.2	22.1	0.1	9.7	0.1	16.1	0.3	22.2	0.2	9.9	0.3	15.6	0.2	22.2	0.3	10.0	0.2	16.4	0.1	22.0	0.1	10.1	0.1	16.3	0.1	22.2	0.2	9.9	0.9	15.8	0.0	22.2	0.1
328	337	2	4.2	16.5	1.3	34.8	0.6	44.9	0.7	18.0	0.0	38.6	0.4	47.5	0.3	21.4	1.2	37.4	0.0	47.1	0.7	17.2	0.2	38.7	0.4	46.0	0.4	26.2	0.3	37.1	0.0	48.0	0.9	23.2	3.0	36.6	1.1	48.7	0.1
328	341	4	6.8	12.9	1.4	22.3	0.2	29.1	0.5	12.7	0.5	24.6	0.6	31.8	0.7	13.5	0.5	22.7	1.1	31.2	2.0	12.8	0.9	23.7	0.5	30.1	0.8	16.7	0.3	24.5	0.3	34.2	0.5	13.7	2.1	23.7	1.3	34.0	0.8
342	347	1	7.0	2.4	0.2	3.1	0.5	3.6	0.5	2.3	0.0	2.5	0.2	3.1	0.6	2.7	0.2	3.1	0.4	3.2	0.4	3.1	0.4	3.6	0.4	3.2	0.6	2.7	0.4	3.1	0.1	3.7	0.0	2.5	0.3	2.6	0.2	3.2	0.5
342	353	2	9.6	7.0	0.5	13.1	0.4	16.6	0.3	8.7	0.2	12.8	0.4	14.5	0.2	9.5	0.4	13.2	0.1	14.8	0.3	7.1	0.3	13.1	0.2	16.4	0.2	9.4	0.3	12.8	0.2	14.2	0.1	9.1	0.9	12.9	0.1	14.4	0.3
348	354	2	8.5	12.5	1.0	21.5	0.3	27.6	0.4	15.6	0.6	20.8	0.3	23.9	0.4	15.7	0.4	21.4	0.1	23.2	0.3	12.6	0.6	21.5	0.5	27.4	1.0	16.8	0.3	20.9	0.2	23.4	1.0	15.4	1.9	21.2	1.3	23.4	0.3
354	362	2	4.4	27.8	1.7	42.8	0.3	45.9	0.4	26.0	0.6	44.4	0.5	47.9	0.8	25.1	1.6	42.6	0.1	46.8	1.0	26.9	0.1	43.9	0.4	46.6	0.4	28.1	0.7	43.4	0.3	47.9	1.0	23.7	2.9	41.8	0.7	48.2	0.2
355	362	2	3.5	29.2	1.7	45.9	1.1	48.6	0.4	25.6	0.1	46.5	0.8	51.4	0.5	23.9	1.0	45.7	1.3	50.2	0.7	27.9	0.3	46.2	0.3	49.5	0.7	27.2	0.3	45.6	0.5	50.9	1.2	22.5	2.3	43.7	0.5	51.0	0.2
366	377	3	10.8	14.8	0.6	23.4	0.5	36.2	0.1	13.7	0.3	23.3	0.5	36.0	0.3	13.3	0.5	22.9	0.0	35.9	0.2	14.6	0.3	23.7	0.1	37.7	0.3	13.6	0.1	23.9	0.1	37.2	0.2	12.7	0.9	22.6	0.1	36.0	0.4
369	377	3	10.2	15.4	0.5	23.4	0.7	30.7	0.2	14.1	0.1	23.2	0.4	30.3	0.1	13.8	0.4	22.8	0.2	30.3	0.3	15.1	0.4	23.7	0.2	32.3	0.2	14.3	0.1	23.3	0.2	31.6	0.1	13.8	0.8	22.5	0.1	30.3	0.2
378	384	2	12.5	1.2	0.0	1.8	0.2	4.3	0.2	1.0	0.2	1.2	0.2	3.3	0.1	1.3	0.3	1.4	0.5	3.6	0.6	1.2	0.1	1.6	0.1	4.1	0.6	1.0	0.4	1.5	0.2	3.4	0.2	1.1	0.1	1.7	0.0	3.3	0.4
381	387	2	9.8	1.6	0.1	4.1	0.1	22.3	0.5	2.4	0.2	3.3	0.3	17.5	0.5	1.8	0.5	3.0	0.6	14.0	1.4	3.0	0.8	6.1	0.6	26.6	0.7	2.7	0.8	5.4	0.6	26.3	1.0	3.7	0.3	5.5	0.6	23.1	2.8
388	392	2	9.7	0.2	0.2	0.7	0.5	0.7	0.7	0.4	0.2	0.5	0.2	0.7	0.2	0.8	0.2	1.2	0.3	0.7	0.4	0.3	0.1	0.8	0.2	0.8	0.2	0.4	0.3	0.6	0.2	0.4	0.3	0.4	0.2	0.6	0.4	0.7	0.3
395	423	5	8.3	11.9	0.7	14.9	0.3	16.0	0.4	11.1	0.9	14.8	0.9	15.7	0.2	11.1	0.6	13.9	0.4	15.4	0.2	11.3	1.3	13.4	0.2	15.9	0.4	11.4	1.0	14.2	0.3	15.6	0.5	10.4	0.3	12.6	1.8	15.7	0.9
426	439	4	9.1	16.2	0.7	25.6	0.4	33.0	0.0	15.6	0.5	25.7	0.6	33.6	0.3	16.5	0.3	25.8	0.1	33.6	0.2	15.8	0.7	24.7	0.4	32.7	0.4	16.4	0.4	25.8	0.3	33.4	0.3	16.2	1.1	25.7	1.1	34.0	0.7
439	452	2	12.4	32.1	0.7	35.2	0.2	40.0	0.2	31.9	0.3	36.5	0.5	40.3	0.7	33.1	0.8	35.3	0.2	40.6	0.5	31.5	0.4	34.4	0.3	39.2	0.7	32.9	0.5	36.5	0.1	40.0	0.4	33.1	0.7	35.4	0.2	40.2	0.4
440	452	2	11.7	37.3	0.4	40.7	0.9	46.0	0.2	36.8	0.6	41.8	0.7	45.9	0.6	37.5	0.9	40.7	0.1	46.2	0.7	36.5	0.6	39.7	0.6	45.3	0.7	37.7	0.5	42.1	0.2	45.9	0.6	37.6	0.8	40.2	0.2	45.9	0.5
440	468	3	10.9	28.7	0.9	40.0	0.8	50.4	0.0	27.5	1.0	42.3	0.6	52.2	0.8	29.2	0.8	41.1	0.3	52.3	1.0	27.8	1.0	39.2	0.3	50.3	0.7	29.6	0.3	42.4	0.2	51.7	0.5	29.4	1.6	40.4	0.1	51.6	0.9
453	468	2	5.6	40.1	2.5	57.4	0.1	70.8	0.7	38.2	1.2	59.0	0.8	73.8	0.7	40.9	1.2	59.3	0.9	72.8	0.7	38.2	0.7	56.9	0.4	71.5	0.4	41.8	0.7	59.3	0.4	73.9	1.5	41.7	3.5	59.4	1.8	74.0	0.4
473	485	2	10.9	26.0	1.2	37.2	0.5	56.1	1.9	25.1	0.6	38.3	0.5	57.2	2.5	30.2	4.0	39.4	0.4	64.0	5.7	26.6	0.4	39.2	1.1	56.7	1.4	29.3	2.1	41.8	1.8	65.6	3.2	30.7	2.2	41.1	0.6	63.1	3.1
476	485	2	8.5	22.3	1.1	35.6	0.7	55.7	0.3	21.4	0.4	35.5	0.5	55.1	0.8	22.1	0.5	35.4	0.1	56.0	0.7	21.5	0.3	35.4	0.3	55.0	1.0	22.3	0.1	35.9	0.2	55.8	0.3	21.8	2.1	35.0	0.3	55.5	0.3
476	488	2	10.5	27.6	1.1	41.1	0.6	58.8	0.4	27.6	1.0	42.2	0.9	58.7	0.2	28.9	0.9	41.8	0.1	59.2	0.1	26.7	0.3	40.5	0.4	57.4	0.5	28.1	0.1	41.8	0.3	59.1	0.9	29.3	1.1	40.8	0.1	58.3	0.5
501	508	2	4.4	32.0	1.3	39.1	0.4	62.4	0.2	30.0	0.7	40.8	0.5	63.6	0.3	31.9	1.2	39.5	0.0	62.5	0.4	31.2	0.3	41.2	0.3	63.2	0.3	31.7	0.4	39.4	0.2	63.7	1.3	31.4	1.8	39.7	1.1	63.8	0.8
515	522	2	4.2	54.2	0.9	52.8	0.7	54.1	1.6	51.9	0.6	55.8	1.0	56.5	0.8	53.8	2.4	54.0	0.6	54.9	1.3	53.1	0.4	54.2	0.3	54.9	1.1	54.4	1.1	53.6	0.5	56.2	2.4	54.1	1.7	54.1	1.6	56.4	0.5
516	523	2	4.2	54.2	0.9	52.8	0.7	54.1	1.6	51.9	0.6	55.8	1.0	56.5	0.8	53.8	2.4	54.0	0.6	54.9	1.3	53.1	0.4	54.2	0.3	54.9	1.1	54.4	1.1	53.6	0.5	56.2	2.4	54.1	1.7	54.1	1.6	56.4	0.5
524	529	2	3.1	1.8	0.2	4.2	0.7	9.5	0.2	4.1	1.4	19.5	0.9	36.8	1.1	3.8	0.2	20.2	0.3	37.4	3.4	2.4	0.3	3.9	0.3	12.0	1.0	4.0	0.3	19.3	1.1	38.1	1.6	3.8	1.1	17.6	1.8	38.3	1.0
524	546	5	11.4	2.1	0.1	4.9	0.4	7.7	0.0	1.9	0.0	6.1	0.5	10.2	0.5	2.1	0.2	5.9	0.4	10.4	0.2	2.0	0.0	5.1	0.1	7.4	0.6	2.0	0.1	6.2	0.1	10.0	0.2	1.9	0.3	5.4	0.1	10.1	0.8
550	564	4	8.4	1.0	0.1	4.2	0.2	5.9	0.1	0.7	0.2	2.5	0.3	5.5	0.0	0.9	0.1	2.7	0.2	5.5	0.1	0.9	0.1	3.9	0.2	5.7	0.1	0.9	0.1	2.3	0.1	5.1	0.1	0.8	0.1	2.4	0.2	5.3	0.4
552	565	4	9.1	0.5	0.2	2.5	0.4	4.3	0.7	0.7	0.4	1.5	0.1	3.2	0.2	0.8	0.1	2.3	0.0	3.3	0.3	0.6	0.1	2.0	0.1	3.6	0.4	0.5	0.0	1.7	0.1	2.9	0.1	0.4	0.3	1.9	0.3	3.5	0.6
568	574	2	13.2	9.1	0.7	26.7	0.7	48.2	0.5	7.9	0.4	28.3	0.8	49.3	1.2	9.5	0.1	28.8	0.0	50.8	1.1	8.8	0.3	27.8	0.2	48.2	0.7	8.5	0.2	29.2	0.3	50.1	1.1	9.2	1.8	29.9	0.1	51.6	0.6
568	577	2	14.2	19.2	1.1	40.7	1.1	59.7	1.3	20.2	0.3	42.5	1.1	60.5	0.5	22.4	0.8	42.5	1.0	62.3	2.0	18.5	0.3	39.7	1.3	58.6	2.1	20.2	0.1	43.0	0.1	61.8	1.2	21.8	0.4	43.5	0.4	62.1	0.7
583	587	1	12.9	14.8	1.4	33.1	0.2	50.8	0.3	15.9	0.2	35.4	0.7	52.4	1.9	20.1	1.1	39.0	0.9	54.7	2.2	15.1	0.8	35.1	1.2	51.5	1.3	19.0	0.0	37.5	0.6	51.4	0.8	21.9	3.1	41.9	0.8	54.1	2.1
583	595	2	13.2	8.1	0.7	18.8	0.3	34.6	0.1	7.4	0.0	19.2	0.6	34.5	1.1	8.8	0.4	19.3	0.8	35.5	0.5	7.6	0.3	18.9	0.4	33.5	1.0	8.6	0.3	18.6	0.3	32.5	0.8	9.1	1.0	19.2	0.3	33.8	2.1
585	595	2	12.3	4.6	0.4	12.3	0.4	27.4	0.5	4.4	0.1	12.0	0.5	27.0	1.0	5.1	0.2	11.4	0.3	27.3	0.6	4.2	0.2	11.2	0.3	25.8	0.9	4.4	0.3	10.5	0.3	24.8	0.5	4.7	0.4	10.5	0.0	26.0	1.4
596	608	2	8.4	7.0	0.3	12.5	0.2	18.5	0.2	6.7	0.4	12.7	0.5	18.6	0.1	7.2	0.3	12.7	0.2	18.1	0.4	6.9	0.8	11.9	0.2	18.5	0.3	7.3	0.4	12.8	0.2	18.2	0.5	7.1	0.6	13.1	1.1	18.4	0.6
616	625	2	11.0	14.7	1.0	24.0	0.2	32.6	0.1	14.4	0.4	24.9	0.4	33.2	0.4	15.0	0.6	25.2	0.4	33.0	0.6	14.7	0.3	24.4	0.2	33.5	0.3	14.9	0.2	26.1	0.2	34.1	0.4	15.1	1.4	25.9	0.3	33.7	0.2
628	634	2	11.7	-0.3	0.5	0.3	0.4	1.6	0.7	-0.4	0.3	0.0	0.6	0.9	0.4	0.2	0.6	0.2	0.9	1.0	0.9	-0.4	0.4	0.4	0.1	1.0	0.5	-0.6	0.1	-0.4	0.2	2.0	0.5	-0.7	0.1	0.3	0.2	2.5	0.2
630	634	2	10.4	0.9	0.1	1.1	0.7	1.1	0.1	1.3	0.2	1.1	0.5	1.4	0.1	1.2	0.3	1.1	0.4	1.6	0.7	1.2	0.3	1.4	0.2	1.0	0.9	1.2	0.0	1.3	0.2	1.5	0.4	1.3	0.4	1.2	0.1	1.5	0.6
633	647	4	9.1	1.1	0.0	2.5	0.1	3.6	0.1	1.1	0.0	2.5	0.1	3.5	0.0	1.2	0.1	2.7	0.2	3.7	0.1	1.1	0.2	2.6	0.1	3.7	0.2	1.2	0.1	2.7	0.1	3.8	0.1	1.2	0.2	2.7	0.0	3.9	0.3
634	647	4	8.0	1.8	0.2	4.8	0.1	6.2	0.1	1.7	0.1	4.8	0.1	6.2	0.0	2.0	0.0	5.1	0.2	6.3	0.3	1.9	0.2	4.9	0.1	6.5	0.2	2.1	0.0	5.1	0.1	6.8	0.1	2.1	0.4	4.9	0.2	6.9	0.2
635	646	4	6.3	2.6	0.4	6.6	0.7	8.5	0.5	2.4	0.3	6.5	0.2	8.9	0.3	2.8	0.2	6.8	0.7	9.1	0.4	2.7	0.2	7.0	0.5	8.9	0.2	3.0	0.1	6.7	0.1	9.3	0.2	2.8	0.6	6.7	0.1	9.6	0.1
636	646	4	5.5	2.2	0.2	5.2	0.3	7.2	0.3	1.6	0.1	5.4	0.4	7.6	0.1	2.2	0.2	6.0	0.5	8.0	0.3	2.0	0.3	5.6	0.6	8.3	0.1	2.1	0.1	5.0	0.3	8.2	0.1	2.1	0.5	5.9	0.4	8.0	0.3
647	651	2	12.9	1.1	0.1	1.4	0.1	1.8	0.3	1.1	0.1	1.3	0.2	1.6	0.4	1.3	0.0	1.4	0.0	1.7	0.5	1.1	0.1	1.5	0.0	1.7	0.1	1.1	0.1	1.5	0.1	1.6	0.3	1.2	0.1	1.4	0.0	1.8	0.3
648	655	3	10.0	0.5	0.5	0.7	0.2	1.1	0.5	0.5	0.3	0.6	0.5	1.5	0.1	0.7	0.1	0.8	0.1	1.4	0.5	0.2	0.1	0.6	0.4	1.1	0.3	0.6	0.1	0.9	0.1	1.4	0.1	0.3	0.3	1.0	0.5	1.3	0.5
662	668	2	13.2	0.8	0.0	1.1	0.1	1.2	0.1	0.9	0.1	1.1	0.1	1.4	0.1	0.9	0.1	1.2	0.1	1.6	0.2	1.0	0.1	1.1	0.1	1.5	0.1	1.0	0.1	1.2	0.1	1.8	0.1	1.0	0.1	1.1	0.1	1.6	0.0
671	683	4	6.0	3.3	0.4	6.7	0.3	12.2	0.3	2.8	0.2	6.9	0.3	12.2	0.4	3.3	0.3	7.1	0.1	12.1	0.0	3.4	0.4	7.8	0.4	12.6	0.2	3.2	0.1	7.0	0.1	12.6	0.3	3.6	0.6	7.4	0.4	12.9	0.2
683	689	2	5.7	2.3	0.5	3.7	0.8	5.3	0.5	2.2	0.1	2.9	0.5	5.2	0.6	2.6	0.4	3.2	0.3	6.3	1.1	3.1	0.8	4.3	0.5	5.9	1.1	3.3	0.5	3.8	0.2	6.8	0.5	2.2	0.4	3.5	0.1	7.0	1.1
698	713	5	5.0	28.0	1.9	42.6	0.5	48.9	0.8	25.9	0.7	43.3	0.7	49.8	1.0	25.3	1.2	41.6	1.0	48.5	0.7	27.5	0.4	43.6	0.4	49.9	0.5	28.7	0.6	42.6	0.4	50.4	1.4	25.1	2.3	41.2	1.6	50.5	0.3
698	715	4	6.8	20.3	1.5	31.2	0.2	38.6	0.1	19.1	0.8	31.8	0.8	39.1	0.2	18.6	0.4	30.5	0.9	38.2	0.7	19.7	0.9	31.5	0.7	39.7	0.4	20.7	0.2	32.1	0.6	40.3	0.7	18.3	1.7	30.7	1.3	40.5	0.5
714	719	2	10.6	1.5	0.0	1.9	0.2	2.6	0.1	1.1	0.0	1.7	0.1	3.0	0.3	1.4	0.1	1.8	0.1	3.0	0.2	1.9	0.2	2.5	0.3	3.8	0.1	1.9	0.2	2.5	0.2	4.9	0.2	1.6	0.8	1.9	0.1	3.5	0.5
726	740	2	10.5	3.9	0.3	16.2	0.7	24.1	0.3	3.6	0.0	16.1	0.3	24.3	0.2	4.1	0.2	16.8	0.3	24.2	0.1	4.0	0.1	16.7	0.2	24.2	0.1	4.3	0.1	17.0	0.2	24.9	0.0	4.3	0.6	17.2	0.2	24.6	0.4
726	741	2	11.9	3.3	0.2	14.6	0.5	22.3	0.0	3.6	0.2	15.1	0.3	22.6	0.1	4.1	0.3	16.0	0.1	22.8	0.2	3.5	0.2	15.4	0.3	22.2	0.1	3.8	0.3	15.7	0.2	23.1	0.1	4.2	0.4	15.9	0.1	23.1	0.5
728	740	2	10.1	4.5	0.4	19.6	0.8	29.4	0.2	4.3	0.1	19.4	0.4	29.5	0.1	4.8	0.2	20.5	0.6	29.4	0.1	5.0	0.2	20.3	0.1	29.4	0.2	5.1	0.2	20.4	0.2	30.1	0.2	5.1	0.8	21.0	0.4	29.7	0.4
741	745	1	6.7	2.1	0.2	4.7	0.5	26.2	0.6	2.0	0.3	4.6	0.2	25.1	1.0	2.3	0.3	4.4	0.0	24.8	1.9	2.7	0.5	5.7	0.4	26.7	0.2	3.1	0.1	5.9	0.5	27.7	0.4	2.8	0.4	4.9	0.1	25.8	1.8
746	751	1	8.9	2.7	0.4	16.6	0.6	34.3	0.2	3.0	0.1	16.7	0.4	34.2	0.6	2.7	0.3	14.3	0.3	34.2	0.5	3.0	0.3	17.1	0.2	34.1	0.1	3.9	0.4	17.4	0.4	35.1	0.2	2.7	0.7	11.8	0.3	33.5	0.7
752	760	3	10.2	19.4	0.3	21.2	0.7	27.8	0.0	19.7	0.8	21.6	0.6	27.5	0.4	20.0	0.4	21.2	0.1	27.3	0.0	20.1	0.9	21.7	0.2	28.0	0.5	20.6	0.2	22.4	0.2	29.0	0.2	20.1	0.3	20.9	0.2	27.5	0.6
752	762	3	12.3	12.6	0.3	13.6	0.2	18.7	0.0	12.8	0.2	14.1	0.4	18.8	0.2	13.0	0.4	13.9	0.3	19.0	0.1	12.9	0.2	14.4	0.2	19.0	0.3	13.6	0.4	14.9	0.1	20.0	0.2	13.3	0.2	13.9	0.1	19.0	0.3
753	760	3	10.1	19.1	0.4	20.9	0.4	29.0	0.5	19.1	1.0	21.0	0.2	28.9	0.5	19.3	0.7	20.7	0.8	29.1	0.7	19.4	0.4	21.9	0.3	29.4	0.7	19.8	0.3	22.0	0.3	31.3	0.5	19.1	0.7	20.3	0.2	29.8	1.4
753	762	3	12.3	11.8	0.4	13.1	0.3	18.7	0.2	11.9	0.2	13.4	0.6	19.0	0.1	11.9	0.2	13.2	0.2	18.9	0.6	12.3	0.2	13.9	0.2	19.2	0.3	12.5	0.4	14.2	0.1	20.1	0.6	12.1	0.4	13.4	0.3	19.1	0.7
761	766	1	6.4	34.4	1.5	45.2	1.9	57.0	1.1	32.4	1.0	42.9	1.0	55.5	0.9	33.7	0.8	41.9	0.2	55.6	1.4	34.3	1.1	46.4	0.5	56.5	1.6	35.6	0.5	43.8	1.1	59.9	0.8	34.6	1.7	42.4	2.1	56.7	2.1
763	775	2	5.2	47.9	2.4	48.9	0.8	53.8	0.2	45.3	1.1	50.6	0.5	55.2	0.9	47.7	0.9	47.8	2.3	53.1	1.8	46.7	1.0	48.4	0.3	54.7	1.3	49.5	0.0	50.1	0.3	55.0	1.6	48.2	1.0	48.8	2.4	54.4	0.5
767	775	1	3.6	42.9	0.5	43.0	1.5	50.4	0.0	41.8	0.4	45.3	0.6	51.6	0.2	42.6	1.6	43.4	1.1	50.1	1.2	41.7	0.2	43.3	1.8	50.9	0.7	44.1	0.5	44.3	0.2	51.7	1.2	43.1	0.6	42.9	0.7	50.3	0.2
776	784	2	9.3	13.8	1.0	19.4	0.2	24.8	0.2	13.6	0.2	19.2	0.3	24.9	0.4	11.9	0.5	18.5	0.3	24.6	0.4	14.1	0.7	18.7	0.3	24.9	0.4	15.4	0.2	19.8	0.3	25.2	0.6	10.9	1.5	19.1	0.5	25.3	0.9
776	788	3	9.2	12.5	1.6	26.1	0.7	33.8	0.4	11.6	0.1	26.6	0.9	34.3	0.6	10.4	0.6	24.8	0.3	33.8	0.4	12.6	0.6	25.8	0.3	33.3	0.6	14.3	0.1	27.0	0.3	34.7	0.7	8.9	2.1	24.3	1.5	33.5	1.5

Figure 40: All HDX p110δ and p85α peptide data for experiments examining conformational changes in APDS1 mutations under basal, pY-activated, and membrane-bound states.

The charge state *(Z)*, residue start *(S)*, residue end number *(E)*, and retention time *(RT)* are displayed for every peptide. Three time-points are labelled (3, 30, 300 seconds), and the relative level of HDX is coloured on a blue-to-red continuum (% deuterium incorporation).

Data listed are the average of 3 independent experiments, with SDs presented. ##No coverage for the specific peptide.

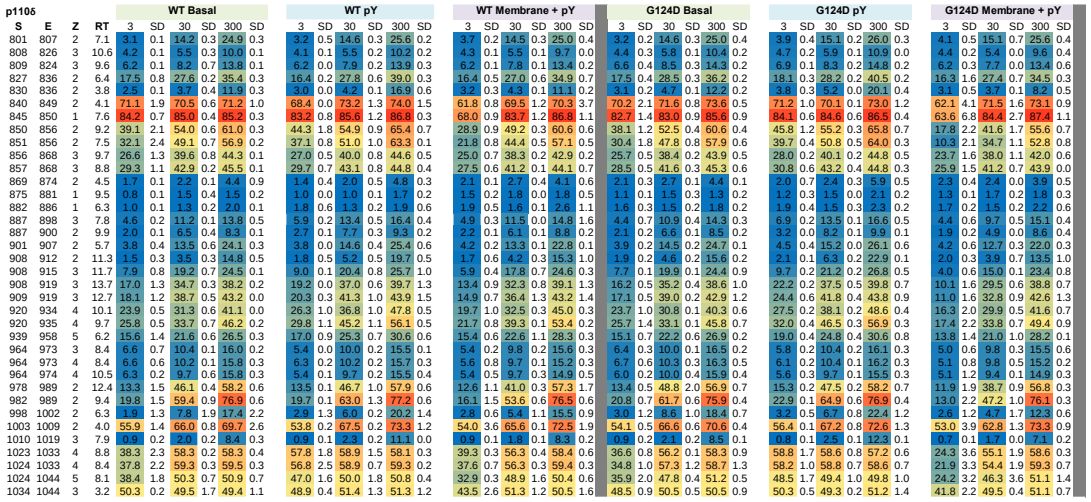

Figure A1.2 cont.: All HDX p110δ and p85α peptide data for experiments examining conformational changes in APDS1 mutations under basal, pY-activated, and membrane-bound states.

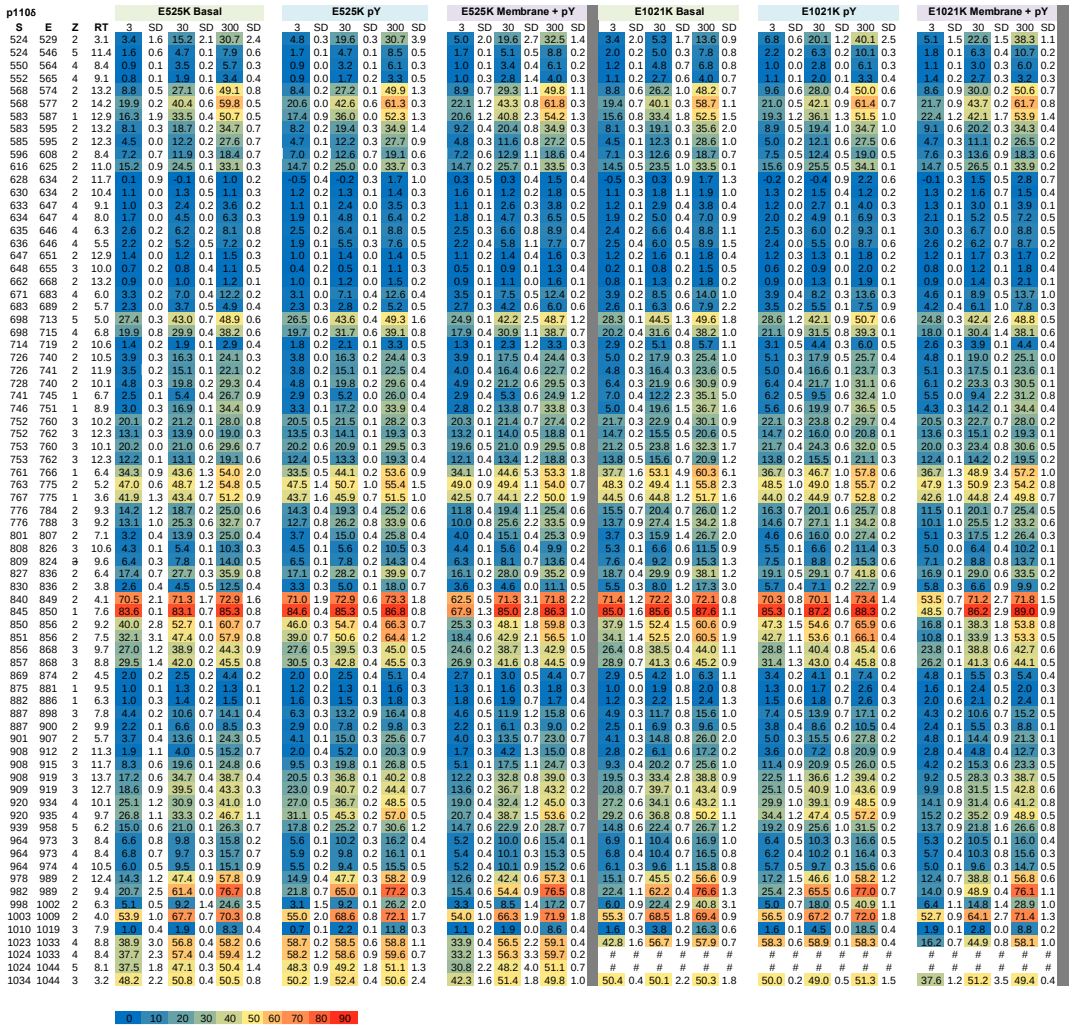

Figure A1.2 cont.: All HDX p110δ and p85α peptide data for experiments examining conformational changes in APDS1 mutations under basal, pY-activated, and membrane-bound states.

p85α				WT Basal						WT pY						WT Membrane + pY						G124D Basal						G124D pY						G124D Membrane + pY					
S	E	Z	RT	3	SD	30	SD	300	SD	3	SD	30	SD	300	SD	3	SD	30	SD	300	SD	3	SD	30	SD	300	SD	3	SD	30	SD	300	SD	3	SD	30	SD	300	SD
8	13	2	7.6	3.1	0.2	5.4	0.5	14.3	0.4	3.0	0.2	5.2	0.1	15.1	0.4	3.6	0.2	5.4	0.1	14.1	0.3	3.2	0.5	5.4	0.2	14.7	0.6	3.4	0.0	5.2	0.0	15.1	0.2	3.0	0.3	5.3	0.1	14.2	0.7
14	21	3	3.0	28.7	0.6	35.8	2.1	36.9	0.9	26.4	0.9	37.8	1.1	39.5	0.8	26.1	1.6	37.3	0.3	38.8	1.1	27.5	0.7	36.7	1.4	37.8	0.5	27.6	0.8	35.8	0.3	38.8	1.0	25.3	0.6	35.7	0.2	39.0	0.7
22	30	2	12.6	1.9	0.1	6.1	0.3	11.6	0.0	2.8	0.5	6.5	0.2	11.6	0.3	3.5	0.6	7.1	0.1	12.1	0.3	1.9	0.2	6.5	0.2	11.5	0.1	2.5	0.1	6.6	0.1	11.5	0.3	3.0	0.4	6.9	0.2	11.7	0.4
25	37	3	9.7	23.8	0.1	24.8	0.2	25.0	0.3	23.6	1.3	25.1	0.4	25.2	0.8	23.6	0.3	24.4	0.2	25.1	0.8	23.7	0.9	24.6	0.1	25.2	0.4	24.6	0.2	25.0	0.2	25.1	0.3	23.1	0.3	24.0	1.3	25.2	0.7
38	52	2	8.5	36.8	1.6	55.2	1.1	59.2	0.4	31.8	0.9	56.2	0.8	59.6	0.6	33.4	0.2	53.7	2.5	60.0	0.8	35.5	1.5	53.7	1.2	59.5	0.6	34.4	0.3	55.8	0.4	58.7	0.5	32.4	2.5	53.4	1.0	59.8	0.9
53	60	1	11.8	9.0	0.6	21.8	0.5	24.9	0.3	8.6	0.5	21.7	0.5	24.5	0.7	8.7	0.3	21.5	0.5	24.3	0.7	8.6	0.1	21.8	0.4	24.9	0.3	8.6	0.2	21.6	0.1	24.4	0.3	8.0	1.2	21.3	0.1	24.2	0.1
53	73	3	11.9	5.8	0.4	15.0	0.4	20.6	0.1	5.4	0.1	15.3	0.3	20.7	0.5	5.7	0.2	15.3	0.2	21.3	0.4	5.5	0.2	15.2	0.2	20.7	0.2	5.8	0.1	15.4	0.1	20.2	0.2	5.2	0.8	15.0	0.4	21.0	0.5
59	72	2	7.7	6.7	0.6	16.6	0.4	24.5	0.1	6.0	0.1	16.9	0.4	24.3	0.1	6.4	0.1	17.0	0.8	24.5	0.1	6.5	0.3	16.5	0.6	24.7	0.2	6.8	0.4	17.0	0.2	24.2	0.1	5.8	0.9	16.9	0.0	24.9	0.4
73	106	5	6.5	51.4	1.4	54.8	0.4	55.4	0.8	49.5	1.2	55.2	0.8	55.9	0.4	51.1	0.8	54.4	1.5	55.2	0.6	50.8	0.7	55.1	0.8	56.1	0.1	51.5	0.1	54.4	0.6	55.3	0.7	51.0	1.3	54.2	1.6	56.3	0.2
74	107	5	6.1	53.1	1.5	56.1	0.8	57.2	0.7	51.2	1.2	56.5	0.7	57.5	0.7	52.7	1.2	55.8	1.6	56.8	0.5	52.6	0.6	56.5	0.8	57.8	0.1	53.2	0.7	55.5	0.5	57.3	1.1	52.6	1.1	55.2	1.7	58.1	0.3
77	106	5	5.3	59.0	1.3	58.9	0.4	59.8	0.9	57.0	1.6	59.8	0.6	60.3	0.7	59.0	0.9	59.2	1.3	59.6	0.5	58.6	0.3	60.1	0.3	60.2	0.1	59.8	0.8	58.8	0.3	60.1	0.9	59.0	0.7	58.9	1.4	60.6	0.1
77	107	5	5.3	58.7	1.4	58.5	0.4	59.2	0.8	56.6	1.8	59.5	0.7	60.0	0.6	58.4	1.0	58.6	1.4	59.2	0.4	58.1	0.3	59.6	0.5	60.0	0.1	59.3	0.7	58.5	0.2	59.7	1.0	58.9	0.5	58.5	1.4	60.1	0.1
113	118	1	11.9	22.7	1.7	58.3	0.9	71.3	0.4	19.6	0.1	57.8	0.6	70.0	0.7	20.0	1.1	56.0	0.3	70.2	0.4	20.9	0.4	59.0	0.5	70.9	0.9	20.6	0.4	57.9	0.3	70.5	0.8	18.8	3.8	54.0	0.1	69.7	0.2
119	132	2	12.6	11.6	1.1	24.6	0.5	34.5	0.1	10.6	0.1	24.9	0.4	34.4	0.2	11.0	0.6	25.1	0.1	34.5	0.2	10.8	0.2	24.6	0.1	34.2	0.1	11.2	0.1	24.9	0.3	34.4	0.2	10.4	1.8	24.3	0.0	33.9	0.2
122	132	2	12.6	13.8	1.3	25.4	0.7	37.8	0.0	15.1	0.5	28.4	0.9	39.7	2.2	15.3	0.5	27.4	0.3	40.4	3.3	12.7	0.9	25.5	2.1	37.6	1.1	15.2	1.1	27.6	0.5	38.7	0.4	14.1	2.0	28.2	3.4	39.1	0.4
133	138	2	7.3	1.0	0.1	1.5	0.1	1.9	0.5	1.5	0.1	1.5	0.3	2.1	0.4	1.9	0.2	2.5	0.1	2.4	0.7	1.2	0.3	1.5	0.1	1.6	0.2	1.4	0.3	1.8	0.2	2.2	0.2	1.7	0.2	2.0	0.5	2.3	0.2
139	146	3	4.9	18.8	0.9	44.1	1.0	58.3	1.0	17.5	0.1	44.7	1.0	59.2	0.5	18.5	0.5	44.4	0.0	58.2	0.6	18.5	0.1	45.3	0.1	58.8	0.9	18.8	0.2	43.7	0.5	59.0	0.9	18.9	1.9	43.8	1.8	59.0	0.4
149	158	2	6.3	53.7	1.6	56.6	0.4	62.6	0.6	51.7	2.0	58.0	1.0	63.8	0.5	54.5	0.6	57.9	1.5	62.5	1.0	52.7	1.2	58.0	1.4	63.8	0.6	55.2	0.9	57.2	0.7	62.5	1.4	54.4	1.8	57.2	2.4	64.3	0.2
150	157	2	3.2	67.4	1.2	67.8	1.7	67.8	1.7	66.8	1.6	71.1	2.3	71.3	0.4	70.0	3.1	70.5	0.6	71.0	2.1	66.3	1.3	67.4	1.1	69.7	1.4	67.7	1.3	67.7	0.7	70.6	2.2	68.4	1.2	68.8	1.1	72.1	0.3
150	160	2	5.2	56.5	2.0	63.2	0.2	63.6	1.3	53.5	1.8	65.7	1.2	66.8	0.7	57.0	1.4	64.3	1.8	66.1	1.7	56.0	1.5	64.7	1.5	65.4	0.8	57.8	0.9	63.6	0.3	65.5	1.5	57.0	2.1	64.3	2.7	67.6	0.1
168	173	1	4.7	77.1	1.2	76.3	1.4	78.8	0.1	74.8	0.5	79.0	0.8	79.8	0.5	77.4	1.1	76.3	2.0	79.6	0.8	76.2	0.6	77.0	1.2	78.7	0.6	77.5	1.1	77.4	0.4	79.7	0.4	77.8	1.1	76.8	1.8	79.7	0.2
177	185	2	9.2	10.3	0.3	12.6	0.2	14.4	0.1	10.0	0.5	12.8	0.3	14.6	0.3	10.5	0.2	13.0	0.0	14.8	0.6	10.3	0.4	12.6	0.2	13.9	0.2	10.5	0.0	12.9	0.1	14.4	0.1	10.2	0.4	12.6	0.3	14.5	0.2
177	186	2	11.9	8.2	0.4	10.3	0.4	12.3	0.3	8.7	0.6	11.0	0.6	12.5	0.1	9.1	0.2	11.1	0.3	12.9	0.1	8.1	0.2	10.4	0.0	11.7	0.2	8.4	0.4	11.0	0.1	12.4	0.2	8.7	0.8	10.8	0.1	12.5	0.5
186	202	3	11.8	10.9	0.3	13.0	0.1	15.7	0.1	10.8	0.1	13.3	0.3	15.7	0.2	11.0	0.3	13.1	0.2	15.7	0.1	10.6	0.3	12.7	0.3	15.5	0.3	10.9	0.1	13.2	0.1	15.7	0.3	10.7	0.7	12.9	0.1	15.4	0.2
186	203	3	12.3	10.0	0.3	12.2	0.2	15.4	0.1	10.0	0.0	12.4	0.4	15.2	0.1	10.1	0.3	12.1	0.2	15.2	0.1	9.8	0.2	12.0	0.1	15.0	0.3	10.1	0.1	12.2	0.0	15.3	0.5	9.8	0.6	11.9	0.1	14.8	0.2
191	202	2	11.4	16.8	0.7	20.3	0.5	24.4	0.5	16.9	0.0	20.9	0.2	24.2	0.3	17.5	1.0	20.6	0.2	24.2	0.4	16.2	0.4	19.5	0.6	23.8	0.4	17.1	0.3	20.9	0.4	24.1	0.3	16.7	1.1	20.6	0.6	23.7	0.6
207	218	1	8.6	52.9	2.8	67.9	1.0	70.1	0.1	43.6	1.5	68.9	0.7	71.0	0.1	48.2	0.6	67.7	2.4	71.3	0.8	50.6	2.0	65.1	2.0	70.3	0.2	48.5	0.5	68.9	0.4	70.4	0.3	48.6	4.5	68.4	0.5	71.1	1.1
207	218	2	8.6	48.4	2.4	64.8	1.6	68.2	0.1	40.7	2.3	66.7	1.5	69.2	0.1	45.6	0.4	65.1	4.2	69.4	0.7	46.5	1.9	63.0	1.8	67.9	0.6	46.6	0.8	66.4	0.6	68.4	0.3	46.1	2.9	65.1	0.4	69.4	0.8
220	237	4	10.3	5.6	0.1	7.1	0.3	16.7	0.2	6.0	0.2	7.7	0.3	17.7	0.6	5.8	0.1	7.3	0.4	19.1	2.4	5.5	0.5	7.0	0.2	16.8	0.4	5.8	0.3	7.8	0.1	17.2	0.3	5.7	0.2	7.6	0.1	18.6	0.2
223	237	3	8.7	6.5	0.2	7.8	0.1	15.5	0.1	6.4	0.1	7.7	0.3	14.9	0.2	6.6	0.1	7.9	0.0	15.7	0.1	6.5	0.3	7.6	0.1	15.5	0.2	6.5	0.3	7.7	0.1	14.8	0.3	6.4	0.1	7.8	0.4	16.1	0.5
238	261	4	13.6	9.7	0.2	13.6	0.1	17.3	0.3	9.1	0.3	14.0	0.4	17.4	0.8	9.5	0.3	13.5	0.5	17.6	0.5	9.3	0.3	13.9	0.1	17.5	0.4	9.4	0.3	14.1	0.1	17.2	0.4	9.5	0.4	13.5	0.2	17.6	0.4
242	261	3	10.3	12.6	0.2	18.1	0.4	22.8	0.1	12.1	0.4	18.3	0.5	23.0	0.5	12.6	0.5	18.3	0.1	23.2	0.3	12.5	0.7	17.8	0.2	22.8	0.3	12.4	0.0	18.3	0.0	22.6	0.2	12.5	0.8	17.8	0.4	23.1	0.5
262	266	1	4.6	2.5	0.3	3.4	0.5	4.2	1.1	2.4	0.5	3.7	0.5	3.8	0.6	2.9	0.7	3.9	0.9	3.5	0.3	2.6	0.6	3.5	0.4	3.4	0.6	2.8	0.3	3.9	0.3	4.0	0.1	2.6	0.5	2.8	0.1	3.7	0.4
262	268	2	10.9	1.2	0.0	1.3	0.1	2.1	0.2	1.3	0.4	1.6	0.5	2.6	0.1	1.8	0.4	2.6	0.1	2.8	0.2	0.9	0.5	1.1	0.6	1.9	0.4	1.4	0.4	2.1	0.4	2.7	0.7	1.4	0.6	2.3	0.8	2.3	0.2
262	272	2	13.0	0.9	0.1	1.7	0.1	7.5	0.1	1.2	0.1	2.2	0.1	7.9	0.1	1.6	0.1	2.9	0.1	8.3	0.2	0.8	0.1	1.8	0.0	7.5	0.1	1.3	0.1	2.3	0.1	7.9	0.1	1.3	0.1	2.6	0.1	8.0	0.1
267	272	1	12.1	1.7	0.2	4.2	0.3	20.4	0.3	2.6	0.2	4.7	0.3	21.0	0.5	2.6	0.4	4.9	0.3	20.5	0.2	1.8	0.1	4.1	0.1	20.2	0.1	2.4	0.3	4.8	0.2	20.7	0.4	2.6	0.3	4.8	0.2	20.5	0.8
273	286	2	9.4	44.1	0.4	51.6	0.5	56.2	0.5	43.9	0.9	52.1	1.1	56.9	1.0	45.3	0.9	51.5	0.3	57.5	0.8	44.1	2.1	50.5	0.4	56.6	0.8	44.6	0.6	51.7	0.4	55.8	0.6	44.6	0.4	50.9	1.3	57.2	0.8
287	291	2	7.0	1.3	0.1	1.5	0.1	1.9	0.2	1.5	0.3	1.4	0.3	1.9	0.2	1.5	0.3	1.9	0.2	2.3	0.8	1.3	0.1	1.5	0.5	1.7	0.3	1.3	0.6	1.8	0.3	2.1	0.2	1.3	0.6	1.3	0.1	2.1	0.2
294	325	4	7.8	72.0	0.5	72.8	0.1	72.6	0.7	70.7	1.5	73.2	1.0	73.1	0.2	72.2	0.2	73.0	0.9	73.0	0.6	71.1	0.7	71.7	0.4	73.1	0.3	72.0	0.9	72.7	0.7	72.4	0.5	71.8	0.6	72.6	1.9	73.2	0.5
294	326	4	8.2	71.8	0.4	72.9	0.2	72.8	0.6	70.5	1.6	73.0	1.1	73.2	0.3	72.1	0.2	73.0	0.7	73.3	0.6	71.0	1.0	71.7	0.3	73.2	0.2	71.8	0.5	72.7	0.6	72.7	0.4	71.6	0.7	72.7	1.9	73.3	0.5
299	325	4	6.2	77.1	0.9	76.6	0.2	77.1	0.8	75.3	1.8	77.6	0.8	77.7	0.3	77.4	0.9	76.9	0.9	77.0	0.4	76.4	0.3	76.5	0.7	77.4	0.2	77.8	0.0	76.7	0.5	77.3	0.8	77.5	0.8	76.5	1.8	77.9	0.3
299	326	4	7.0	76.4	0.7	76.5	0.1	76.7	0.3	75.3	1.6	77.2	0.9	77.3	0.1	77.0	0.7	76.9	1.0	76.8	0.4	75.9	0.7	75.8	0.8	77.1	0.4	76.8	0.5	76.2	0.8	76.9	0.3	76.7	0.4	76.3	1.7	77.1	0.1
327	332	1	5.0	47.9	2.2	65.2	0.9	71.0	1.1	45.4	0.3	67.1	0.6	72.7	0.6	48.2	2.3	65.3	0.7	72.5	0.6	47.1	0.5	65.0	0.4	71.4	1.2	48.3	1.4	64.9	0.3	72.9	1.2	47.0	4.3	63.7	1.3	72.6	0.2
329	333	1	9.0	25.9	0.3	38.7	0.2	44.7	0.3	25.7	0.2	41.7	0.7	46.5	0.5	27.8	0.6	40.8	0.9	47.1	0.8	25.6	1.1	37.9	0.2	44.3	0.5	27.0	0.3	41.2	0.2	46.1	0.6	26.9	1.3	40.5	1.4	46.2	0.7
333	341	2	12.0	28.3	1.2	45.7	0.7	52.8	0.3	19.9	0.0	34.7	0.8	49.3	1.2	19.9	0.5	29.7	0.0	47.2	1.4	27.4	0.7	45.9	0.5	52.6	0.7	19.5	0.0	29.9	0.4	46.3	0.6	19.4	0.4	26.5	0.2	44.9	0.6
334	341	2	9.3	34.5	1.1	54.0	0.1	61.5	0.3	26.1	0.9	41.5	1.1	57.3	1.0	26.2	0.4	36.6	0.3	54.9	0.6	33.9	1.2	53.1	0.3	61.4	0.5	26.0	0.3	36.4	0.3	54.1	0.4	25.4	0.6	33.0	1.1	52.6	0.8
342	349	2	4.5	17.6	1.7	33.2	1.0	54.2	1.4	9.1	0.5	26.7	0.6	48.0	0.7	9.6	0.4	24.3	0.1	44.2	0.6	17.7	0.4	33.9	1.6	55.6	1.1	9.8	1.0	23.5	0.2	46.2	1.0	8.8	1.4	22.6	0.9	43.6	0.4
342	355	3	7.9	15.6	0.6	22.5	0.1	36.4	0.6	12.4	0.3	19.6	0.6	30.9	0.2	12.4	0.0	18.7	0.8	29.1	0.4	15.2	0.8	21.9	0.5	37.4	0.4	12.8	0.4	18.8	0.3	29.3	0.5	11.6	1.0	17.9	0.8	28.4	0.6
346	355	3	6.6	16.5	1.0	18.7	0.2	29.3	0.3	13.6	0.5	17.5	0.6	24.9	0.4	14.2	0.6	17.2	0.9	23.2	0.3	16.2	0.9	19.2	0.9	30.1	0.2	14.7	0.2	17.2	0.3	23.9	0.6	13.8	1.4	16.8	0.8	23.5	0.2
356	369	4	5.3	26.1	1.6	31.4	0.4	33.8	0.2	18.6	0.8	26.0	0.4	33.2	1.4	18.7	1.4	23.3	1.1	29.9	0.4	25.6	0.2	32.9	0.5	34.5	0.5	19.3	0.4	22.9	0.3	30.6	1.0	17.9	1.1	21.8	1.1	28.2	0.1
356	371	4	6.9	19.7	1.4	25.1	0.1	25.8	0.4	14.5	1.0	20.1	0.5	25.3	0.2	14.9	0.7	18.8	0.8	23.7	0.0	19.4	1.1	25.0	1.0	26.4	0.2	14.6	0.1	18.2	0.3	23.3	0.7	13.8	1.0	17.2	1.0	22.1	0.3
356	372	4	9.3	15.4	0.6	20.9	0.3	21.2	0.5	12.1	0.7	16.5	0.7	20.8	0.5	12.0	0.1	15.5	0.0	20.2	0.2	15.7	1.4	19.8	0.4	21.1	0.5	11.8	0.4	15.2	0.2	19.1	0.4	11.0	0.4	14.0	0.7	18.3	0.4
372	380	3	3.5	17.9	0.2	21.5	1.0	36.7	1.4	16.8	0.1	21.6	0.7	29.8	0.8	17.3	1.4	21.9	1.2	27.9	1.2	17.2	0.3	23.3	0.2	38.8	0.4	17.7	0.4	20.6	0.3	28.6	1.6	17.5	0.8	20.4	0.7	28.1	0.4
373	380	2	3.1	19.1	0.3	22.9	1.3	34.9	1.6	18.6	0.4	22.9	0.6	27.7	0.6	18.9	1.3	22.9	1.5	25.6	1.6	18.3	0.5	23.9	0.5	37.7	0.9	19.7	0.5	21.3	0.2	26.2	1.5	18.9	0.6	21.3	0.8	25.7	0.2
373	380	3	3.1	19.1	0.4	22.3	1.2	33.5	1.6	18.2	0.5	21.9	1.3	26.3	1.0	18.5	1.7	22.7	1.9	24.7	1.5	18.4	0.6	23.3	0.8	36.4	0.8	18.3	0.7	20.4	0.2	24.8	1.4	18.5	1.3	20.4	0.3	24.4	0.5
381	398	4	10.9	18.3	0.4	24.1	0.5	27.1	0.2	12.9	0.3	20.4	0.5	26.2	0.4	12.9	0.6	19.8	0.2	26.3	0.3	18.1	0.4	24.1	0.0	26.9	0.5	12.8	0.1	19.7	0.2	25.8	0.2	12.5	1.0	18.8	0.1	25.6	0.4
381	401	4	10.8	21.3	0.4	27.7	0.6	30.8	0.1	17.1	0.4	25.1	0.6	30.2	0.2	17.5	0.5	24.8	0.3	30.5	0.1	21.2	0.4	27.8	0.1	30.6	0.4	17.2	0.1	24.7	0.1	29.8	0.1	17.1	1.0	23.7	0.2	29.9	0.6
402	413	3	8.5	21.1	0.9	25.1	0.1	25.5	0.1	8.7	0.3	21.7	0.6	25.0	0.2	8.2	0.3	18.0	0.1	24.5	0.1	20.4	0.4	24.3	0.2	25.5	0.2	8.0	0.2	17.1	0.1	24.4	0.3	7.4	1.0	13.8	0.8	21.8	0.4
405	413	3	5.9	31.4	2.0	36.1	0.3	37.0	0.6	12.8	0.5	31.6	0.5	36.8	0.6	12.4	0.6	26.1	0.7	35.3	0.3	30.4	0.6	36.8	0.7	37.5	0.2	12.4	0.2	25.1	0.1	36.2	0.8	11.4	1.9	20.3	0.6	32.2	0.2
414	420	1	7.0	76.9	2.5	83.0	0.6	82.7	1.0	20.3	0.9	70.3	1.0	83.2	0.4	11.4	0.5	51.4	0.0	79.2	0.8	74.9	1.0	82.1	1.3	82.9	0.6	10.5	0.2	50.7	0.7	80.6	0.3	5.3	0.9	25.3	0.6	65.0	0.5
414	420	2	7.0	77.0	2.3	83.7	0.2	84.3	0.3	20.9	0.1	71.0	1.1	84.5	0.2	10.5	0.8	51.7	0.1	80.4	0.8	75.2	0.6	82.3	0.9	84.4	0.3	10.4	0.2	51.0	0.7	82.4	0.4	5.0	0.9	25.5	1.2	66.5	0.2
421	435	3	9.1	34.0	0.7	46.6	0.2	50.0	0.1	31.4	0.5	43.6	0.6	47.8	0.3	31.2	0.7	42.4	0.3	47.5	0.2	33.8	0.7	45.8	0.1	50.3	0.5	31.7	0.4	42.7	0.3	47.1	0.5	30.1	1.5	41.2	1.0	46.9	0.4
421	443	4	9.5	42.4	0.6	51.7	0.3	53.5	0.4	41.1	1.6	50.2	0.8	52.2	0.5	41.4	0.8	49.4	0.4	52.2	0.4	41.7	1.2	50.7	0.5	53.3	0.2	42.1	0.6	49.6	0.4	51.5	0.4	40.4	1.0	48.2	1.1	51.9	0.6
435	443	2	5.7	59.9	2.3	68.1	0.8	69.4	0.5	61.6	1.4	68.2	1.0	70.6	0.4	63.0	2.5	68.0	0.9	69.5	0.7	58.7	1.1	68.9	0.5	68.9	1.7	65.1	0.7	67.7	0.7	70.2	1.5	62.7	2.2	66.5	3.1	69.9	0.6
436	443	2	5.1	58.2	2.6	66.4	0.6	66.8	2.4	58.5	1.3	65.9	0.8	68.9	0.7	60.3	2.3	65.0	1.3	66.9	1.4	56.9	0.8	67.5	1.2	68.3	1.9	61.7	0.5	64.8	0.3	67.6	1.3	59.8	2.8	65.3	3.2	68.4	0.4
444	456	2	6.8	0.8	0.1	3.3	0.2	14.5	0.1	4.7	0.0	22.7	0.6	41.4	0.1	4.1	0.2	21.5	0.2	41.2	0.6	0.9	0.3	3.7	0.0	16.9	0.3	4.5	0.1	22.7	0.3	41.9	0.7	3.3	1.2	19.3	1.0	42.3	0.5
457	466	3	5.7	0.9	0.3	1.7	0.0	6.3	0.2	1.2	0.2	2.5	0.1	11.2	0.2	1.6	0.1	3.5	0.3	15.5	0.1	1.2	0.2	2.4	0.3	9.6	0.2	1.3	0.1	3.7	0.1	18.0	0.9	1.3	0.2	3.8	0.3	19.2	0.2
467	476	2	5.6	1.0	0.1	2.7	0.1	13.5	0.0	1.3	0.0	4.9	0.2	22.9	0.7	2.1	0.2	10.2	0.0	33.9	0.3	1.6	0.6	5.4	0.5	24.1	0.5	2.1	0.1	9.8	0.1	35.1	0.5	2.3	0.7	12.6	0.7	41.6	2.6
470	476	2	3.5	3.4	0.5	5.6	0.7	18.9	0.2	3.6	0.1	8.8	0.4	31.5	0.6	4.5	0.4	17.2	1.0	47.3	0.7	3.9	0.7	9.1	0.7	30.5	1.0	4.5	0.2	15.9	0.1	47.8	1.2	5.1	0.7	20.8	0.3	54.3	0.1
477	486	3	6.2	0.5	0.2	1.3	0.1	5.1	0.3	0.5	0.1	1.4	0.2	7.1	0.1	1.0	0.1	2.7	0.0	12.7	0.3	0.7	0.3	1.3	0.2	4.9	0.2	0.9	0.2	2.2	0.2	11.7	0.2	0.9	0.1	3.3	0.3	16.1	0.3
508	520	4	4.8	39.2	2.3	48.7	0.5	50.9	1.1	35.2	1.0	50.8	0.6	51.9	1.4	36.9	2.6	49.6	0.8	50.5	0.9	38.4	0.7	50.2	1.3	51.5	0.4	38.1	1.2	48.4	0.8	51.7	1.7	36.7	2.5	48.5	2.4	52.2	0.2
508	531	5	9.2	11.6	0.6	25.5	0.4	36.9	0.5	10.8	0.4	25.0	1.1	36.7	0.7	10.8	0.2	24.6	0.1	35.8	0.1	11.8	0.9	25.6	0.1	39.3	0.6	11.2	0.6	24.8	0.3	36.6	0.5	10.0	1.3	23.5	1.9	35.7	1.4
522	538	4	6.9	3.0	0.7	8.6	0.3	23.5	0.2	2.6	0.0	8.4	0.4	23.1	0.4	2.7	0.3	8.1	0.3	21.0	0.1	3.0	0.2	10.6	0.3	28.4	0.3	2.6	0.3	8.4	0.1	23.3	0.6	2.2	0.7	7.4	0.8	20.9	0.2
538	549	4	8.1	0.7	0.2	1.7	0.4	9.1	0.2	0.5	0.3	1.9	0.1	9.6	0.2	0.7	0.1	2.3	0.2	11.0	0.3	1.2	0.3	5.4	0.2	22.7	0.1	0.8	0.1	3.3	0.0	16.1	0.4	0.7	0.1	2.5	0.4	13.2	0.7
556	570	4	7.7	1.9	0.2	5.1	0.2	10.6	0.1	1.7	0.1	7.2	0.3	19.5	0.4	2.5	0.1	12.0	0.0	31.7	0.4	2.0	0.2	7.9	0.1	21.4	0.1	2.7	0.0	13.1	0.1	35.9	0.6	2.9	0.6	14.0	1.1	38.1	0.7
556	570	5	7.7	2.3	0.1	5.1	0.5	11.5	0.1	2.2	0.6	7.8	0.1	20.4	0.2	2.8	0.2	12.6	0.5	32.4	0.1	2.2	0.5	8.6	0.5	22.3	0.2	2.8	0.1	13.6	0.2	36.5	0.6	3.2	0.9	14.4	1.2	38.6	0.5
557	570	3	7.2	2.4	0.2	6.3	0.3	11.8	0.3	2.3	0.4	8.6	0.3	20.5	0.3	3.0	0.2	13.4	0.4	32.9	0.3	2.7	0.0	9.1	0.5	21.9	0.2	3.5	0.4	14.3	0.2	36.7	0.7	3.4	0.9	15.4	1.2	39.7	0.8
571	581	4	7.1	0.5	0.4	2.1	0.1	11.3	0.2	0.3	0.0	4.8	0.2	26.3	0.2	0.6	0.2	5.5	0.4	28.2	0.2	0.5	0.4	2.2	0.1	11.5	0.1	0.8	0.3	6.0	0.0	31.6	0.6	0.6	0.3	5.7	0.6	30.7	0.8
582	596	3	7.1	21.9	2.8	44.9	0.3	49.5	0.4	38.8	0.9	50.7	1.2	57.9	0.3	36.2	1.3	49.6	1.2	55.6	0.5	21.2	1.2	45.0	0.9	50.2	0.3	38.2	0.5	49.4	0.9	56.6	0.8	32.8	3.8	48.4	2.6	56.2	0.6
582	596	5	7.0	22.4	2.4	45.8	0.6	50.5	0.7	39.8	1.4	51.7	1.2	58.5	0.4	36.8	1.5	50.6	1.4	56.7	0.2	21.5	1.3	45.6	1.1	50.9	0.1	39.0	0.7	50.0	1.0	57.2	0.8	33.7	3.7	49.0	2.2	57.1	0.5
610	637	4	7.3	17.3	0.9	25.4	0.2	28.8	0.3	11.5	0.1	17.0	0.4	21.2	0.3	12.1	0.4	17.0	0.6	20.0	0.1	16.7	0.8	25.1	0.6	29.2	0.1	12.2	0.2	16.6	0.2	19.9	0.3	11.7	1.2	16.3	0.8	19.6	0.3
638	646	3	4.4	14.8	0.6	15.3	0.4	21.4	0.4	13.1	0.3	16.6	0.5	22.1	0.9	14.5	0.9	16.1	0.3	21.0	0.2	14.8	0.2	17.1	0.5	22.5	0.3	14.5	0.8	15.6	0.3	22.0	1.0	14.3	0.9	15.6	0.3	22.1	0.3
647	656	3	3.6	47.8	0.4	50.4	1.1	54.3	1.2	30.4	0.0	38.8	0.7	53.6	0.4	30.9	1.6	38.7	0.7	52.0	1.4	46.2	0.5	51.9	0.8	56.0	0.5	31.0	1.0	37.5	0.2	52.3	1.4	30.5	1.3	36.9	0.6	51.6	0.0
647	657	3	5.0	38.0	1.5	46.7	0.4	50.3	0.9	22.7	0.6	29.9	0.5	44.3	0.3	23.6	0.8	29.2	0.5	42.5	0.7	37.9	0.0	48.4	0.5	51.3	0.6	23.9	0.7	28.8	0.2	43.0	1.1	23.4	1.1	28.3	1.0	42.6	0.2
661	666	1	5.4	7.7	0.9	19.2	2.3	37.1	0.5	8.1	0.1	17.3	0.4	36.7	1.3	9.0	0.8	17.2	2.2	35.1	1.8	8.5	0.8	19.4	0.7	37.7	1.1	8.6	2.1	18.0	0.0	37.9	0.1	8.4	1.3	16.0	0.1	37.0	0.7
661	680	4	7.3	19.6	0.7	27.7	0.3	33.1	0.1	12.7	0.1	23.6	0.3	31.4	0.2	13.5	0.2	23.6	0.3	30.1	0.0	19.1	0.5	27.5	0.5	33.6	0.1	13.3	0.1	23.3	0.2	29.8	0.4	13.0	0.9	22.6	0.7	28.9	0.2
661	687	4	10.4	15.2	0.4	24.0	0.5	34.1	0.1	15.1	0.3	28.3	0.5	36.6	0.4	15.6	0.4	27.8	0.2	36.2	0.6	15.0	0.4	24.3	0.2	34.3	0.3	15.6	0.0	28.1	0.2	35.5	0.3	15.3	1.0	27.0	0.6	35.3	0.6
681	687	2	10.6	21.7	0.4	36.8	0.6	56.2	0.0	40.0	1.3	62.4	0.9	69.9	0.1	40.8	1.3	62.4	0.6	70.5	0.6	21.5	0.3	37.7	0.3	55.9	0.6	41.5	0.8	62.6	0.2	69.2	0.3	40.8	1.3	61.5	1.8	69.3	0.3
694	703	3	8.4	2.8	0.2	6.2	0.1	8.2	0.3	4.1	0.3	5.9	0.2	7.0	0.0	4.4	0.1	6.0	0.3	7.3	0.1	2.6	0.2	5.8	0.1	8.4	0.2	4.4	0.2	5.9	0.1	6.9	0.2	4.2	0.4	6.0	0.4	7.2	0.3
697	703	2	5.0	5.1	0.6	10.8	0.1	14.5	0.6	7.4	0.3	11.0	0.2	13.2	0.5	8.1	0.5	10.8	0.5	12.6	0.2	5.0	0.2	11.7	0.3	15.4	0.2	8.4	0.2	10.4	0.1	12.8	0.9	8.3	1.0	10.6	0.6	13.4	0.2
704	710	2	5.1	18.3	0.9	30.9	0.1	32.5	0.7	2.1	0.1	9.4	0.2	17.2	0.1	2.2	0.3	7.6	0.2	16.1	0.1	18.1	0.1	31.6	0.3	33.2	0.4	2.2	0.2	7.3	0.1	16.2	0.6	1.9	0.3	5.7	0.0	15.5	0.1
704	711	2	4.1	19.1	0.7	37.0	0.4	39.5	0.7	6.5	0.3	20.7	0.1	27.7	0.2	6.4	0.8	18.7	0.8	26.4	0.8	18.4	0.5	38.1	0.3	40.7	0.2	6.9	0.3	18.4	0.2	26.8	0.6	5.7	0.8	16.6	0.1	26.3	0.3
711	719	2	11.0	2.2	0.0	4.8	0.4	13.9	0.1	2.6	0.1	5.9	0.1	14.7	0.2	2.7	0.1	5.8	0.1	14.0	0.1	2.2	0.1	4.9	0.2	13.9	0.1	2.5	0.1	6.4	0.1	14.5	0.3	2.4	0.3	5.4	0.3	13.9	0.2
711	724	3	8.6	29.7	0.2	37.0	0.1	43.0	0.3	28.8	0.5	37.0	0.5	43.5	0.4	28.8	0.2	36.4	0.4	43.3	0.6	29.3	0.7	36.3	0.3	43.3	0.4	29.2	0.4	37.2	0.2	43.2	0.3	28.1	0.6	35.3	1.2	43.0	0.5

Figure A1.2 cont.: All HDX p110δ and p85α peptide data for experiments examining conformational changes in APDS1 mutations under basal, pY-activated, and membrane-bound states.

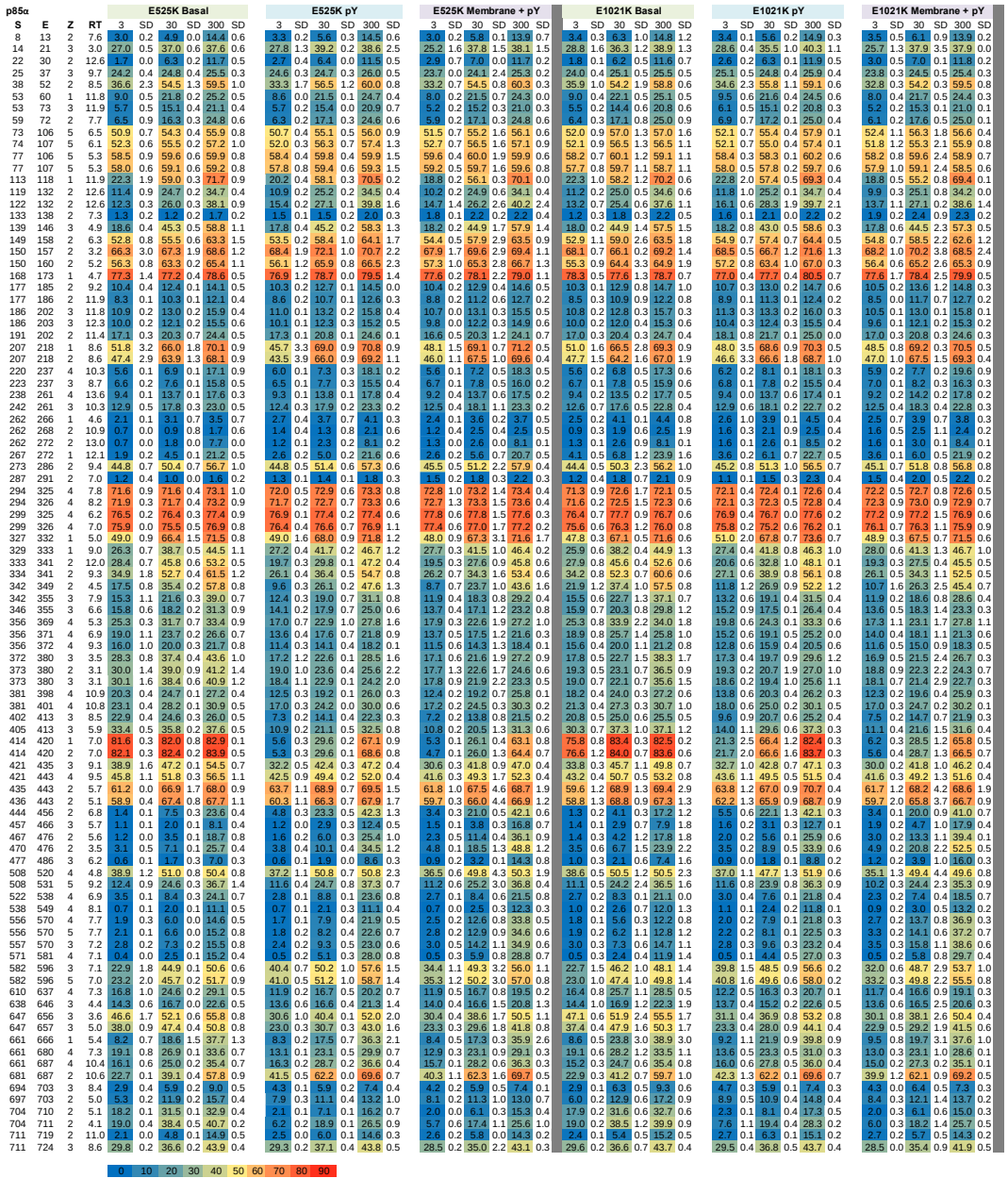

Figure A1.2 cont.: All HDX p110δ and p85α peptide data for experiments examining conformational changes in APDS1 mutations under basal, pY-activated, and membrane-bound states.

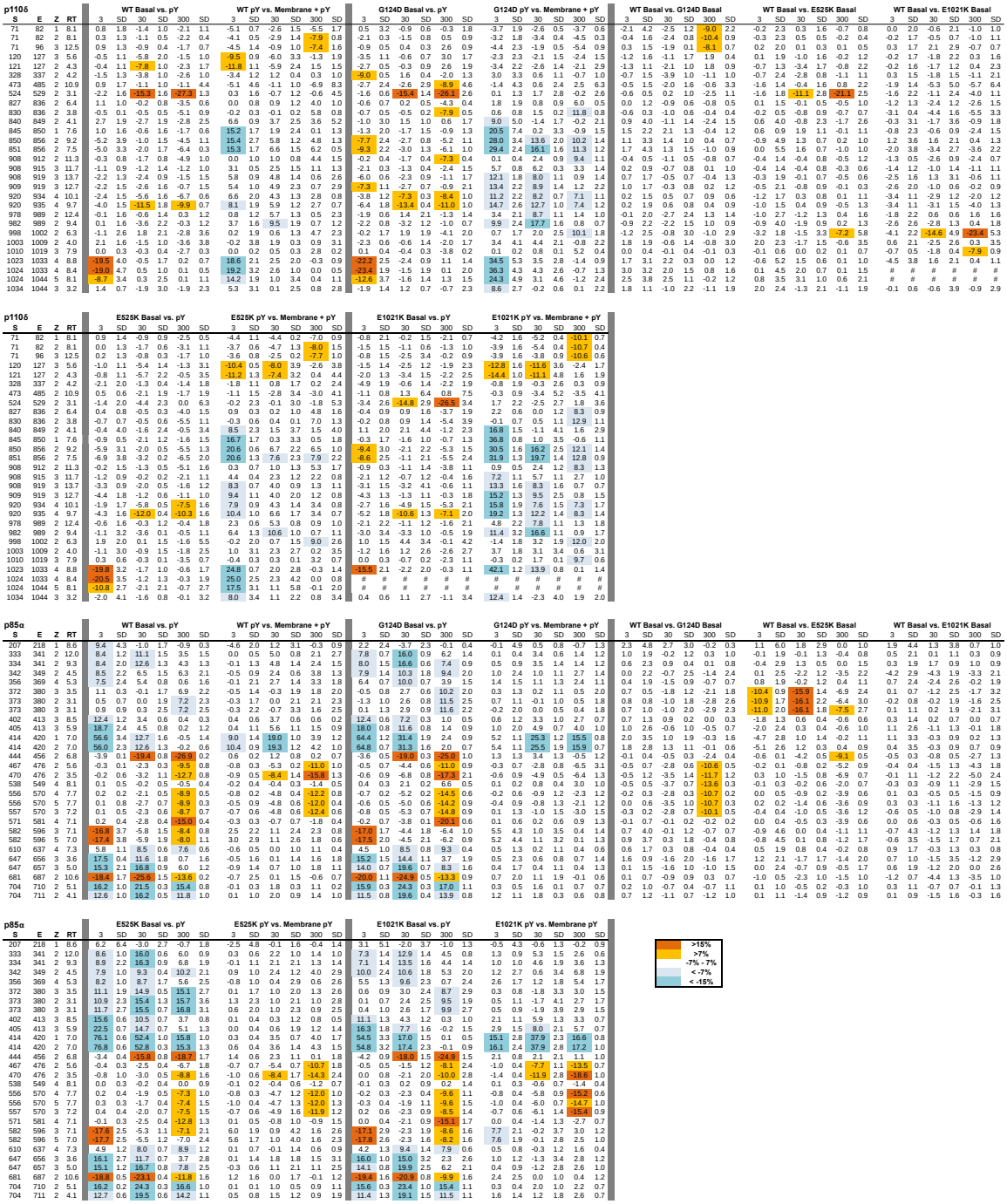

Figure 41: HDX differences in APDS1 mutations and under different activation states (pY-bound, and membrane bound).

Differences in exchange at all time points for a selected set of peptides (some overlapping peptides have been removed), but all data can be found in Fig. 40) that undergo decreases (positive values) / increases (negative values) in exchange between conditions (WT and APDS1 mutations, pY-activated, membrane-bound) are shown. The specific conditions being compared are labelled above the selected columns. Increases/decreases greater than 0.7 Da and 7% are coloured according to the legend.

p110δ				>30%	8-15%	PI3K WT				PI3K deletion			
Start	End	Z	RT	Sequence	15-30%	<8%	3.0	SD	300	SD	3.0	SD	300	SD
12	18	2	4.2	WTKEENQ			69.9	1.7	69.4	0.1	70.2	1.9	69.2	0.6
12	19	2	4.2	WTKEENQS			72.2	1.0	72.8	0.2	67.5	4.3	69.6	0.4
24	31	2	12.6	FLLPTGVY			7.2	0.6	31.2	0.5	9.7	0.3	36.2	0.8
32	42	2	9.6	LNFPVSRNANL			31.1	0.7	38.7	0.2	36.5	0.1	46.0	0.2
35	42	2	5.4	PVSRNANL			44.8	0.6	55.8	0.1	49.2	0.9	60.3	0.4
43	59	4	11.8	STIKQLLWHRAQYEPLF			7.4	0.1	25.4	0.2	8.9	0.3	27.1	0.0
43	67	4	12.2	STIKQLLWHRAQYEPLFHMLSGPEA			20.1	0.6	36.6	0.4	22.2	0.3	39.3	0.4
48	59	3	11.9	LLWHRAQYEPLF			11.4	0.3	34.1	0.4	13.8	0.3	34.9	0.5
60	67	2	6.3	HMLSGPEA			49.0	0.4	68.0	0.6	49.5	0.6	67.6	0.4
71	82	2	8.2	TCINQTAEQQEL			25.2	0.5	51.0	0.7	34.3	1.2	72.7	0.2
71	96	3	12.6	TCINQTAEQQELEDEQRRLCDVQPFL			29.9	0.5	61.9	0.1	34.4	0.4	73.2	0.3
83	96	3	11.3	EDEQRRLCDVQPFL			15.2	0.6	52.1	0.4	20.4	0.8	58.3	0.2
102	116	4	6.2	VAREGDRVKKLINSQ			59.6	0.2	63.2	0.7	59.0	0.6	62.4	0.2
102	120	3	10.4	VAREGDRVKKLINSQISLL			37.9	0.2	48.3	0.2	39.8	0.2	58.2	0.4
120	127	3	5.7	LIGKGLHE			17.1	0.9	50.0	1.9	40.9	0.6	54.7	0.1
121	127	2	4.3	IGKGLHE			20.5	1.3	53.1	0.7	43.4	1.1	50.0	0.9
121	131	3	9.7	IGKGLHEFDSL			20.1	0.5	31.2	0.7	29.8	0.6	31.7	0.1
150	162	3	11.3	AAARRQQLGWEAW			24.4	0.6	61.6	0.3	30.2	0.2	64.8	1.0
163	190	3	13.2	LQYSFPLQLEPSAQTWGPGTLRLPNRAL			53.9	0.3	70.6	0.4	56.3	0.4	75.0	0.2
164	175	3	12.3	QYSFPLQLEPSA			15.1	0.1	25.2	0.1	17.6	0.5	30.8	0.3
168	191	3	12.2	PLQLEPSAQTWGPGTLRLPNRALL			62.4	0.7	76.4	0.2	64.1	1.0	77.9	0.1
183	191	3	9.5	LRLPNRALL			60.1	0.5	82.8	0.4	55.4	2.2	80.1	1.5
192	200	1	7.0	VNVKFEGSE			32.5	0.2	44.2	0.1	35.9	1.3	48.6	0.8
203	216	3	12.4	FTFQVSTKDVPLAL			24.4	0.7	41.0	0.4	24.6	1.4	47.1	1.9
205	216	2	11.1	FQVSTKDVPLAL			19.9	0.6	40.0	0.2	20.5	0.8	45.6	0.5
206	216	2	9.8	QVSTKDVPLAL			20.6	0.9	42.6	0.1	22.8	0.9	49.3	0.7
221	238	4	6.9	LRKKATVFRQPLVEQPED			55.8	0.4	66.7	0.3	54.9	0.4	65.5	1.5
228	238	2	7.7	FRQPLVEQPED			60.9	0.2	78.7	0.5	56.5	1.8	73.6	3.1
239	250	3	9.1	YTLQVNGRHEYL			5.5	0.2	10.2	0.1	7.1	0.3	17.8	0.1
251	258	1	9.6	YGSYPLCQ			11.0	1.1	14.0	0.8	16.9	2.1	28.9	0.3
251	259	2	12.9	YGSYPLCQF			6.6	0.2	7.6	0.1	8.3	0.4	13.0	0.2
265	274	3	8.2	CLHSGLTPHL			13.8	0.2	25.0	0.0	14.6	0.2	27.1	0.2
267	283	4	9.4	HSGLTPHLTMVHSSSIL			3.3	0.3	8.7	0.0	6.5	0.7	15.2	2.0
275	283	2	8.5	TMVHSSSIL			3.6	0.2	16.9	0.1	8.5	0.5	29.0	0.0
284	313	5	5.0	AMRDEQSNPAPQVQKPRAKPPPIPAKKPSS			70.8	0.3	73.3	0.4	70.7	1.6	72.6	0.0
284	316	5	6.3	AMRDEQSNPAPQVQKPRAKPPPIPAKKPSSVSL			65.1	0.2	66.9	0.1	64.9	1.0	66.5	0.2
317	327	2	13.9	WSLEQPFRIEL			12.6	0.1	24.3	0.1	14.8	0.1	28.0	0.2
328	337	2	4.2	IQGSKVNADE			26.9	0.6	51.9	0.2	38.3	0.7	60.5	0.6
328	341	4	6.9	IQGSKVNADERMKL			18.7	0.4	34.5	0.1	26.8	1.0	44.0	0.2
342	347	1	7.1	VVQAGL			3.7	0.7	4.2	0.7	6.7	1.3	6.3	0.1
342	353	2	9.7	VVQAGLFHGNEM			12.1	0.7	20.7	0.1	15.7	0.5	21.3	1.0
348	354	2	8.6	FHGNEML			18.2	0.1	31.3	0.0	23.7	1.3	28.1	0.7
355	362	2	3.5	CKTVSSSE			39.7	0.9	53.7	0.0	40.1	0.7	57.7	1.3
366	377	3	10.9	CSEPVWKQRLEF			19.7	0.5	43.8	0.0	20.3	0.1	48.2	0.2
369	377	3	10.3	PVWKQRLEF			19.3	0.4	36.6	0.5	21.2	1.2	42.9	0.3
378	384	2	12.5	DINICDL			1.1	0.3	4.6	0.0	3.4	1.4	7.3	1.2
381	387	2	9.9	ICDLPRM			-2.4	0.2	16.7	0.5	2.2	2.0	18.6	0.4
388	392	2	9.7	ARLCF			1.7	0.3	2.4	0.9	1.6	2.5	5.4	1.6
426	439	4	9.1	FDYKDQLKTGERCL			20.8	0.1	35.5	0.2	23.8	1.1	39.8	0.2
439	452	2	12.5	LYMWPSVPDEKGEL			36.8	0.4	43.8	0.4	38.4	0.4	44.4	0.8
440	452	2	11.7	YMWPSVPDEKGEL			42.6	0.7	50.8	0.1	43.6	0.7	51.0	0.4
440	468	3	11.0	YMWPSVPDEKGELLNPTGTVRSNPNTDSA			37.7	0.5	56.0	0.4	40.1	0.2	59.5	0.3
453	468	2	5.6	LNPTGTVRSNPNTDSA			51.5	0.7	79.1	0.2	55.7	0.8	80.6	0.6
476	488	2	10.6	PEVAPHPVYYPAL			34.9	0.6	64.0	0.2	39.0	1.0	65.6	0.4
501	508	2	4.4	VHVTEEEQ			42.1	1.1	66.0	2.1	51.1	0.8	66.7	1.6
515	522	2	4.3	LERRGSGE			58.5	0.7	58.6	0.3	56.6	1.4	57.4	0.1
516	523	2	4.3	ERRGSGEL			58.5	0.7	58.6	0.3	56.6	1.4	57.4	0.1
524	529	2	3.2	YEHEKD			5.6	0.5	18.3	2.3	15.7	2.5	37.2	0.5
524	546	5	11.5	YEHEKDLVWKLRHEVQEHFPEAL			3.6	0.2	9.7	0.4	4.3	0.1	14.0	0.0
550	564	4	8.5	LLVTKWNKHEDVAQM			2.1	0.0	7.4	0.3	2.3	0.4	9.8	0.4
568	574	2	13.3	LCSWPEL			19.4	1.0	59.8	1.9	25.5	0.6	62.9	0.4
583	587	1	12.9	LDFSF			26.6	0.6	58.8	0.6	36.5	0.2	63.4	0.9
583	595	2	13.3	LDFSFPDCHVGSF			12.7	0.3	38.7	0.0	15.3	0.3	36.5	1.1
585	595	2	12.4	FSFPDCHVGSF			6.3	0.3	30.8	0.1	7.4	0.6	29.5	0.7
596	608	2	8.4	AIKSLRKLTDDEL			11.2	0.3	22.1	0.5	12.2	0.3	24.4	0.2
616	625	2	11.0	VQVLKYESYL			18.2	0.6	33.0	0.0	21.6	0.2	40.2	0.8
628	634	2	11.0	ELTKFLL			0.6	1.0	2.1	1.0	1.1	0.3	2.4	2.0
633	647	4	9.2	LLDRALANRKIGHFL			1.4	0.2	4.1	0.0	3.3	0.2	10.3	0.2

PI3K % Relative Deuterium Incorporation: 0, 10, 20, 30, 40, 50, 60, 70, 80, 90

Figure 42: All HDX p110δ and p85α peptide data for experiments examining conformational changes in APDS2 mutation in the basal state.

The charge state *(Z)*, residue start *(S)*, residue end number *(E)*, and retention time *(RT)* are displayed for every peptide. Two time-points are labelled (3 & 300 seconds), and the relative level of HDX is coloured on a blue-to-red continuum (% deuterium incorporation). Peptides with differences in exchange have the sequence colour according to the legend. The data listed are the average of three independent experiments, with SD shown next to all HDX values.

p110δ					PI3K WT				PI3K deletion			
Start	End	Z	RT	Sequence	3.0	SD	300	SD	3.0	SD	300	SD
634	647	4	8.0	LDRALANRKIGHFL	2.6	0.1	7.5	0.3	5.1	1.0	17.3	0.2
635	646	4	6.4	DRALANRKIGHF	3.7	0.4	9.8	0.3	6.8	0.8	21.0	0.1
636	646	4	5.6	RALANRKIGHF	3.8	0.8	10.3	0.9	6.6	1.8	21.8	2.5
647	651	2	13.0	LFWHL	0.3	0.4	1.1	0.6	2.9	0.6	9.6	0.2
648	655	3	10.1	FWHLRSEM	1.2	0.5	1.5	0.3	4.7	0.3	7.7	0.9
662	668	2	13.3	LRFGLIL	1.3	0.3	1.8	0.1	3.6	0.2	10.5	0.2
683	689	2	5.9	MKQGEAL	1.9	0.8	4.5	0.2	11.0	1.2	23.9	4.9
698	713	5	5.0	FVKLSSQKTPKPQTKE	39.2	0.7	58.1	0.6	42.9	1.1	60.1	0.3
698	715	4	6.9	FVKLSSQKTPKPQTKELM	28.6	0.6	46.8	0.0	32.3	0.3	50.5	1.0
726	740	2	10.6	EALSHLQSPLDPSTL	7.6	0.5	27.0	0.5	12.6	0.8	35.6	0.3
726	741	2	12.1	EALSHLQSPLDPSTLL	5.9	0.3	24.1	0.5	11.7	1.8	33.9	0.6
728	740	2	10.2	LSHLQSPLDPSTL	8.4	0.5	31.3	0.2	15.7	0.0	42.1	0.4
746	751	1	9.0	VEQCTF	4.9	0.4	37.1	0.1	9.2	1.7	47.0	2.3
752	760	3	10.3	MDSKMKPLW	22.1	0.5	34.7	0.3	24.3	0.3	39.4	0.4
752	762	3	12.3	MDSKMKPLWIM	13.3	0.4	22.6	0.0	16.4	0.1	28.6	0.2
753	760	3	10.2	DSKMKPLW	23.3	0.5	38.4	0.8	32.8	0.9	46.3	0.2
753	762	3	12.4	DSKMKPLWIM	12.8	0.4	23.3	0.3	15.3	0.3	32.0	0.8
767	775	1	3.7	EAGSGGSVG	45.0	1.1	56.5	0.2	45.5	2.0	56.2	1.5
776	784	2	9.4	IIFKNGDDL	19.5	0.4	28.7	0.2	21.6	0.3	33.3	0.6
801	807	2	7.2	WKQEGLD	4.5	0.4	27.0	0.7	9.6	0.6	33.9	0.1
808	826	3	10.7	LRMTPYGCLPTGDRTGLIE	5.2	0.4	13.3	0.2	8.4	0.1	22.2	0.0
809	824	3	9.7	RMTPYGCLPTGDRTGL	5.5	0.6	16.4	0.2	11.6	2.3	30.4	1.5
827	836	2	6.5	VVLRSDTIAN	23.7	0.2	41.6	0.0	27.8	0.5	55.2	1.6
830	836	2	3.8	RSDTIAN	0.6	0.2	15.8	0.5	9.5	1.4	44.4	1.1
850	856	2	9.4	FNKDALL	57.5	5.7	69.7	0.5	61.7	1.8	73.4	1.7
851	856	2	7.6	NKDALL	46.4	0.5	65.4	0.1	46.5	1.4	67.7	0.8
856	868	3	9.8	LNWLKSKNPGEAL	35.1	0.3	49.4	0.0	37.7	0.4	51.3	0.1
857	868	3	9.0	NWLKSKNPGEAL	38.5	0.3	49.5	0.4	40.3	0.1	51.7	0.2
869	874	2	4.5	DRAIEE	2.3	0.4	6.5	0.2	7.0	0.8	14.8	1.4
875	881	1	9.6	FTLSCAG	-1.7	0.3	-1.3	0.1	1.9	0.6	3.0	0.6
882	886	1	6.4	YCVAT	-0.6	0.0	-0.1	0.3	1.9	0.8	2.6	0.3
887	898	3	7.9	YVLGIGDRHSDN	6.5	0.4	15.9	0.1	13.2	2.6	24.8	0.2
887	900	2	10.0	YVLGIGDRHSDNIM	3.0	0.2	9.2	0.2	7.4	0.2	16.3	0.1
901	907	2	5.8	IRESGQL	6.1	0.2	26.8	0.3	11.8	0.3	33.3	0.4
908	912	2	11.5	FHIDF	1.9	0.4	17.8	1.6	6.5	3.2	32.5	0.6
908	915	3	11.8	FHIDFGHF	13.1	0.9	28.7	0.6	18.9	0.2	34.1	0.2
908	919	3	13.8	FHIDFGHFLGNF	25.5	0.7	43.5	0.1	33.8	0.3	44.9	0.8
909	919	3	12.8	HIDFGHFLGNF	29.5	1.0	47.9	0.3	36.9	1.2	47.1	0.6
920	934	4	10.2	KTKFGINRERVPFIL	30.7	0.6	46.9	0.1	35.0	0.8	53.4	0.7
920	935	4	9.8	KTKFGINRERVPFILT	31.9	0.5	53.9	0.3	40.4	0.3	60.5	0.1
939	958	5	6.3	VHVIQQGKTNNSEKFERFRG	20.0	0.4	30.5	0.2	24.3	0.4	33.6	0.4
964	973	3	8.5	YTILRRHGLL	8.2	0.0	17.1	0.4	9.0	0.5	20.2	1.3
964	973	4	8.5	YTILRRHGLL	9.8	0.8	17.8	0.4	8.6	1.0	19.8	2.0
964	974	4	10.6	YTILRRHGLLF	6.9	0.3	15.7	0.3	7.5	0.2	18.9	0.6
978	989	2	12.5	FALMRAAGLPEL	22.1	0.5	59.8	0.2	32.4	1.9	62.4	0.2
982	989	2	9.5	RAAGLPEL	32.8	1.0	80.3	0.6	48.7	1.3	82.1	0.3
1010	1019	3	8.0	EALKHFRVKF	0.5	0.1	10.8	0.2	2.9	0.3	21.5	1.4
1024	1033	4	8.5	RESWKTKVNW	50.8	0.7	61.4	0.7	61.0	1.6	61.5	0.4
1024	1044	5	8.2	RESWKTKVNWLAHNVSKDNRQ	48.7	1.0	54.4	1.2	52.9	0.9	53.2	0.5
1034	1044	3	3.3	LAHNVSKDNRQ	55.2	1.2	55.4	0.0	53.3	0.8	54.6	0.6

Figure A1.4 cont.: All HDX p110δ and p85α peptide data for experiments examining conformational changes in APDS2 mutation in the basal state.

p85α					>30%	8-15%	PI3K WT				PI3K deletion			
S	E	Z	RT	Sequence	15-30%	<8%	3.0	SD	300.0	SD	3.0	SD	300.0	SD
8	13	2	7.7	YRALYD			6.1	1.0	19.4	0.6	5.6	0.6	19.2	0.6
14	21	3	3.0	YKKEREED			29.7	2.9	36.8	3.6	23.9	2.9	32.9	4.0
22	30	2	12.7	IDLHLGDIL			4.5	0.3	14.9	0.6	4.8	0.3	15.7	0.7
38	52	2	8.7	VALGFSDGQEARPEE			52.4	0.8	65.9	0.3	50.9	0.1	65.5	0.8
53	60	1	11.9	IGWLNGYN			16.0	0.8	27.6	0.2	16.6	1.0	28.1	0.5
59	72	2	7.8	YNETTGERGDFPGT			13.3	0.3	30.4	1.0	12.6	0.8	30.2	1.0
73	106	5	6.5	YVEYIGRKKISPPTPKPRPPRPLPVAPGSSKTEA			56.3	0.1	59.8	0.0	56.4	0.7	60.2	0.3
77	106	5	5.4	IGRKKISPPTPKPRPPRPLPVAPGSSKTEA			65.2	0.5	65.1	0.3	64.7	0.9	64.8	0.5
77	107	5	5.4	IGRKKISPPTPKPRPPRPLPVAPGSSKTEAD			65.7	0.6	65.8	0.2	64.8	0.9	64.1	0.1
113	118	1	12.0	LTLPDL			41.4	1.1	77.4	0.2	40.6	1.6	75.9	0.0
119	132	2	12.7	AEQFAPPDIAPPLL			19.8	0.5	38.6	0.4	19.5	0.4	38.5	0.1
122	132	2	12.7	FAPPDIAPPLL			20.1	0.5	41.4	1.3	22.8	0.3	44.7	1.7
133	138	2	7.4	IKLVEA			2.0	0.2	2.2	0.3	2.7	0.7	3.0	0.0
139	146	3	5.0	IEKKGLEC			22.7	0.2	58.8	0.5	27.6	0.4	60.7	1.2
149	158	2	6.4	LYRTQSSSNL			58.5	0.5	66.8	0.1	61.2	0.3	69.9	1.0
168	173	1	4.8	DTPSVD			81.7	0.5	81.8	0.4	81.4	1.6	81.3	0.0
177	185	2	9.3	IDVHVLADA			11.5	0.3	15.0	0.1	11.7	0.3	15.4	0.3
177	186	2	12.0	IDVHVLADAF			8.1	0.4	11.7	0.2	9.1	0.3	13.4	0.3
186	202	3	12.0	FKRYLLDLPNPVIPAAV			13.2	0.0	18.6	0.5	12.9	0.2	18.5	0.1
186	203	3	12.4	FKRYLLDLPNPVIPAAVY			12.1	0.2	18.2	0.3	11.8	0.4	18.1	0.1
207	218	1	8.7	ISLAPEVQSSEE			68.7	0.8	74.1	0.1	65.0	3.2	71.2	4.9
207	218	2	8.7	ISLAPEVQSSEE			68.5	0.9	74.0	0.1	66.2	0.4	70.6	0.0
220	237	4	10.4	IQLLKKLIRSPSIPHQYW			7.8	0.6	30.3	0.4	7.7	0.2	33.1	1.1
223	237	3	8.8	LKKLIRSPSIPHQYW			8.0	0.1	21.6	0.1	8.3	0.3	21.7	0.3
238	261	4	13.6	LTLQYLLKHFFKLSQTSSKNLLNA			13.0	0.0	22.2	0.3	13.1	0.2	22.3	0.6
242	261	3	10.4	YLLKHFFKLSQTSSKNLLNA			16.5	0.3	27.7	0.6	17.6	0.6	28.7	1.1
262	266	1	4.7	RVLSE			2.1	0.8	3.4	0.6	3.4	1.1	5.6	2.0
262	268	2	11.0	RVLSEIF			0.8	0.9	2.1	1.3	1.7	0.4	2.2	1.6
262	272	2	13.1	RVLSEIFSPML			1.3	0.2	10.9	0.0	1.4	0.1	10.7	0.1
267	272	1	12.2	IFSPML			0.0	0.2	28.5	0.2	3.5	1.2	31.7	0.9
273	286	2	9.5	FRFSAASSDNTENL			50.4	0.9	61.0	0.2	50.5	0.6	61.4	1.1
287	291	2	7.1	IKVIE			0.7	0.8	0.8	0.7	1.9	1.1	4.5	0.3
294	325	4	7.8	ISTEWNERQPAPALPPKPPKPTTVANNGMNNN			76.9	0.6	76.9	0.7	76.3	1.4	75.9	1.0
294	326	4	8.2	ISTEWNERQPAPALPPKPPKPTTVANNGMNNNM			77.2	0.6	77.0	0.7	77.7	1.0	77.6	0.9
299	325	4	6.3	NERQPAPALPPKPPKPTTVANNGMNNN			80.5	0.2	80.8	0.3	80.4	0.6	82.6	1.0
299	326	4	7.1	NERQPAPALPPKPPKPTTVANNGMNNNM			79.3	1.3	78.9	0.7	79.3	2.0	80.9	0.0
329	333	1	9.0	QDAEW			30.9	0.8	47.9	0.4	35.7	1.5	58.8	1.9
333	341	2	12.1	WYWGDISRE			38.8	0.8	56.7	0.1	33.5	1.0	59.8	0.2
334	341	2	9.4	YWGDISRE			47.2	0.9	66.6	0.1	41.2	0.6	66.4	0.6
342	349	2	4.6	EVNEKLRD			25.5	0.7	63.7	0.3	29.4	3.9	67.2	1.2
342	355	3	7.9	EVNEKLRDTADGTF			20.1	0.0	43.2	0.5	18.9	0.5	52.9	0.8
346	355	3	6.7	KLRDTADGTF			18.0	0.3	31.8	0.5	17.9	1.2	43.7	1.2
356	371	4	7.1	LVRDASTKMHGDYTLT			23.6	0.2	27.7	0.3	20.3	0.4	35.9	0.7
356	372	4	9.4	LVRDASTKMHGDYTLTL			19.1	0.5	22.9	0.4	16.2	0.3	30.9	1.3
372	380	3	3.5	LRKGGNNKL			21.6	0.6	43.9	0.3	31.4	0.2	49.6	0.6
373	380	2	3.1	RKGGNNKL			22.4	0.8	41.9	1.0	32.3	0.6	47.9	0.5
381	398	4	11.0	IKIFHRDGKYGFSDPLTF			21.8	0.4	29.3	0.2	22.5	0.3	32.0	0.4
381	401	4	10.9	IKIFHRDGKYGFSDPLTFSSV			25.1	0.7	33.3	0.1	25.6	0.4	35.7	0.6
402	413	3	8.6	VELINHYRNESL			26.2	0.2	27.4	0.0	23.7	0.3	28.6	0.2
405	413	3	6.0	INHYRNESL			36.8	0.2	38.8	0.0	33.5	0.6	39.8	0.4
414	420	1	7.1	AQYNPKL			85.4	0.2	86.3	0.6	80.0	0.7	85.8	0.9
414	420	2	7.1	AQYNPKL			87.0	0.3	89.9	0.2	80.4	1.1	88.3	0.4
421	437	3	0.0	DVKLLYPVSKYQQEIQM							48.1	0.5	66.8	0.2
480	487	2	8.0	KRTAIEAF			3.1	0.8	5.9	0.5	25.1	0.8	65.0	0.3
508	520	4	4.8	YIEKFKREGNEKE			47.6	0.9	53.9	1.0	48.0	0.9	54.1	0.8
522	538	4	7.0	QRIMHNYDKLKSRISEI			5.2	0.1	30.4	0.3	7.9	0.5	29.4	2.1
538	549	4	8.1	IIDSRRRLEEDL			1.1	0.2	20.5	0.4	10.4	0.9	51.3	0.5
556	570	4	7.8	YREIDKRMNSIKPDL			3.4	0.1	17.0	0.4	59.5	1.1	59.4	0.3
557	570	3	7.3	REIDKRMNSIKPDL			3.8	0.2	18.3	0.5	60.9	1.1	62.2	0.2
571	581	4	7.2	IQLRKTRDQYL			1.4	0.2	18.2	0.2	55.2	0.5	56.2	0.9
582	596	3	7.1	MWLTQKGVRQKKLNE			40.3	0.6	58.6	0.4	66.7	0.7	66.8	0.2
582	596	5	7.2	MWLTQKGVRQKKLNE			36.5	0.3	54.4	0.7	64.1	0.7	64.6	0.8
610	637	4	7.4	VEDDEDLPHHDEKTWNVGSSNRNKAENL			21.6	0.1	30.2	0.2	23.4	1.0	37.1	0.0
638	646	3	4.5	LRGKRDGTF			17.7	0.4	25.4	0.7	19.2	1.1	36.0	0.9
647	656	3	3.6	LVRESSKQGC			53.5	0.7	60.4	0.1	54.8	1.1	65.2	0.3
647	657	3	5.1	LVRESSKQGCY			44.5	0.7	54.9	0.2	45.4	0.4	56.5	0.7
661	680	4	7.4	VVVDGEVKHCVINKTATGYG			26.0	0.2	37.4	0.3	28.7	1.4	50.4	0.2
661	687	4	10.4	VVVDGEVKHCVINKTATGYGFAEPYNL			21.1	0.5	39.6	0.1	30.5	0.5	50.3	0.1
681	687	2	10.7	FAEPYNL			29.1	0.8	67.9	0.1	63.3	1.6	76.0	0.3
694	703	3	8.5	LVLHYQHTSL			4.9	0.1	10.6	0.3	9.8	1.0	26.9	0.3
697	703	2	5.1	HYQHTSL			8.6	0.4	18.2	0.4	15.5	0.6	33.4	0.1
704	710	2	5.1	VQHNDSL			23.4	0.3	36.1	0.1	25.1	0.7	35.5	0.2
711	719	2	11.0	NVTLAYPVY			3.9	0.3	17.6	0.2	6.3	1.5	50.9	0.5
711	724	3	8.7	NVTLAYPVYAQQRR			33.8	0.1	46.7	0.2	35.9	2.4	65.6	0.9

PI3K % Relative Deuterium Incorporation: 0, 10, 20, 30, 40, 50, 60, 70, 80, 90

Figure A1.4 cont.: All HDX p110δ and p85α peptide data for experiments examining conformational changes in APDS2 mutation in the basal state.

p110α				>30%	8-15%	PI3K WT				PI3K deletion			
S	E	Z	RT	Sequence	15-30% <8%	3.0	SD	300.0	SD	3.0	SD	300.0	SD
11	20	3	11.7	WGIHLMPPRI		37.6	0.2	56.2	0.3	41.9	0.4	61.4	0.9
11	23	3	12.4	WGIHLMPPRILVE		27.1	0.1	46.9	0.6	30.0	0.2	49.2	0.5
24	30	2	10.9	CLLPNGM		1.8	0.2	18.0	0.2	3.7	0.7	24.0	0.5
37	42	2	7.2	LREATL		0.7	0.3	15.6	0.1	1.8	0.4	24.3	0.1
43	62	5	9.4	ITIKHELFKEARKYPLHQLL		8.0	0.2	26.7	0.1	8.6	0.6	25.9	0.4
50	64	4	8.5	FKEARKYPLHQLLQD		17.3	0.0	42.5	0.3	20.3	2.3	42.6	0.4
71	76	1	5.4	VSVTQE		7.1	0.4	29.3	0.4	15.3	0.7	39.9	0.4
77	82	2	7.1	AEREEF		11.9	0.3	32.1	0.7	16.5	1.2	34.3	1.5
83	91	3	7.1	FDETRRLCD		3.3	0.1	14.2	0.9	4.3	0.2	20.2	0.5
83	92	3	10.0	FDETRRLCDL		1.7	0.1	11.0	0.4	2.5	0.2	18.8	0.2
92	99	2	14.0	LRLFQPFL		1.0	0.1	5.3	0.4	2.5	0.2	13.3	0.1
93	99	2	12.8	RLFQPFL		0.9	0.1	1.5	0.4	2.9	0.5	4.0	0.3
100	116	4	6.9	KVIEPVGNREEKILNRE		30.4	0.1	57.5	0.7	51.7	0.4	61.2	0.8
100	119	4	9.8	KVIEPVGNREEKILNREIGF		20.3	0.9	47.3	0.4	46.0	0.5	59.5	0.2
114	119	2	8.8	NREIGF		9.5	0.3	22.6	3.2	39.2	3.4	70.9	1.9
120	127	1	9.6	AIGMPVCE		20.9	0.1	48.4	2.2	50.7	0.3	75.7	2.5
129	138	2	6.9	DMVKDPEVQD		30.4	0.3	49.3	1.4	45.9	1.2	55.4	0.5
131	138	2	5.1	VKDPEVQD		34.8	0.2	46.7	0.0	53.4	0.9	59.5	0.5
153	164	4	5.6	LRDLNSPHSRAM		25.8	0.2	44.4	2.0	33.5	0.2	50.0	1.5
154	164	3	4.6	RDLNSPHSRAM		29.7	0.1	47.4	2.4	36.7	2.4	49.6	3.5
165	192	3	10.2	YVYPPNVESSPELPKHIYNKLDKGQIIV		29.0	0.2	47.9	0.2	29.9	1.3	50.6	2.5
165	192	4	10.2	YVYPPNVESSPELPKHIYNKLDKGQIIV		29.3	0.2	48.2	0.0	30.9	0.4	50.0	1.1
193	209	3	11.7	VIWVIVSPNNDKQKYTL		29.3	0.1	43.6	0.8	32.0	0.7	44.9	1.2
196	209	3	8.2	VIVSPNNDKQKYTL		41.6	0.9	53.0	0.8	42.5	0.4	54.0	1.8
224	233	2	4.5	AIRKKTRSML		36.6	0.1	45.2	0.8	36.1	0.9	45.7	1.6
234	238	1	3.8	LSSEQ		71.9	2.3	72.8	1.0	70.9	2.7	72.0	5.0
261	269	2	9.3	FLEKYPLSQ		13.6	0.4	27.4	0.8	20.2	0.8	33.2	2.7
261	275	4	9.6	FLEKYPLSQYKYIRS		13.4	0.2	21.0	0.7	15.9	0.6	23.7	0.9
279	287	2	12.0	LGRMPNLML		18.3	0.3	31.6	0.7	20.8	0.4	31.1	1.9
280	287	2	11.4	GRMPNLML		20.5	0.1	33.2	0.3	22.0	0.4	35.3	0.7
288	293	2	6.2	MAKESL		44.0	1.8	72.0	6.0	49.5	2.1	75.4	1.0
294	301	2	10.2	YSQLPMDC		56.5	0.1	72.4	1.2	58.4	0.4	74.4	2.6
308	327	3	7.8	SRRISTATPYMNGETSTKSL		56.2	0.8	62.5	0.9	55.6	1.3	64.0	1.1
321	327	2	5.0	ETSTKSL		44.7	1.2	63.9	0.7	46.8	1.2	65.9	0.7
328	334	1	12.2	WVINSAL		39.0	0.4	50.5	0.2	38.4	0.5	51.7	1.0
335	342	2	8.1	RIKILCAT		2.2	0.4	24.2	0.1	2.7	1.0	26.3	0.2
343	350	2	7.7	YVNVNIRD		77.9	0.2	83.8	0.3	82.2	0.5	86.7	1.8
347	355	3	9.0	NIRDIDKIY		33.9	0.0	45.4	0.3	41.8	0.3	48.7	0.7
356	369	2	8.1	VRTGIYHGGEPLCD		5.9	0.1	9.5	0.6	8.8	1.3	15.5	2.2
356	369	3	8.1	VRTGIYHGGEPLCD		7.1	0.1	10.6	0.8	9.6	0.5	13.6	0.4
370	386	3	10.6	NVNTQRVPCSNPRWNEW		23.4	0.1	48.8	0.3	26.0	0.2	51.8	0.6
390	402	3	11.5	DIYIPDLPRAARL		4.4	0.1	13.2	0.4	6.1	0.4	16.8	1.4
391	402	3	11.0	IYIPDLPRAARL		2.9	0.3	3.8	0.3	5.0	0.1	6.8	0.3
408	429	5	10.6	SVKGRKGAKEEHCPLAWGNINL		5.0	0.5	8.5	0.4	5.2	0.4	9.8	0.4
430	436	1	10.9	FDYTDTL		4.3	0.5	25.9	0.3	7.4	0.6	33.0	1.0
437	443	2	7.8	VSGKMAL		34.5	0.2	44.3	0.8	36.4	1.2	46.7	0.8
444	455	2	13.1	NLWPVPHGLEDL		23.9	0.3	46.0	0.1	41.6	0.4	45.4	0.1
444	473	3	14.0	NLWPVPHGLEDLLNPIGVTGSNPNKETPCL		16.3	0.1	45.1	0.3	26.3	0.5	49.3	0.2
455	473	3	10.8	LLNPIGVTGSNPNKETPCL		18.0	0.1	51.8	0.3	22.9	0.8	55.6	0.2
456	474	2	9.4	LNPIGVTGSNPNKETPCLE		18.4	0.2	54.2	0.5	24.3	0.7	57.0	0.7
483	491	2	10.8	VVKFPDMSV		28.4	0.0	47.0	0.1	32.2	0.9	52.7	1.0
484	491	2	10.4	VKFPDMSV		36.0	0.8	57.6	0.5	44.9	0.6	65.6	0.5
492	498	2	8.3	IEEHANW		30.6	0.3	44.1	0.0	35.3	0.8	56.9	1.8
499	506	2	7.3	SVSREAGF		72.3	0.1	74.1	0.3	74.5	1.2	76.7	3.4
507	523	3	7.8	SYSHAGLSNRLARDNEL		44.9	0.6	45.8	1.4	45.8	1.0	45.3	1.0
523	533	4	4.9	LRENDKEQLKA		27.9	2.1	56.1	3.2	31.3	1.8	57.0	3.9
524	531	2	5.0	RENDKEQL		32.0	0.5	51.8	1.2	35.2	0.8	54.6	3.0
524	533	2	4.3	RENDKEQLKA		24.4	0.2	56.1	0.8	28.8	2.7	59.6	0.6
524	533	3	4.3	RENDKEQLKA		24.9	0.6	56.4	0.3	28.7	0.7	57.7	0.4
532	542	2	7.1	KAISTRDPLSE		17.7	0.2	48.0	0.1	23.6	2.3	48.5	0.9
532	542	3	7.1	KAISTRDPLSE		16.9	1.2	46.5	1.0	23.6	0.2	46.5	0.6
534	542	2	7.9	ISTRDPLSE		22.0	0.4	55.5	2.5	26.3	0.2	55.6	1.7
543	551	2	10.1	ITEQEKDFL		7.8	0.4	22.9	0.6	19.7	0.2	33.2	0.3
552	565	4	11.3	WSHRHYCVTIPEIL		2.3	0.2	23.3	0.5	5.4	2.9	26.1	1.9
552	570	4	13.0	WSHRHYCVTIPEILPKLLL		2.8	0.1	16.4	0.4	4.0	0.3	18.3	0.4
566	570	2	10.2	PKLLL		1.8	0.5	2.8	1.1	4.2	2.5	7.3	1.7
571	583	3	8.6	SVKWNSRDEVAQM		2.0	0.2	15.5	0.5	3.3	0.3	13.6	0.2
584	598	2	10.6	YCLVKDWPPIKPEQA		7.5	0.1	32.0	0.7	13.6	1.9	38.2	1.2
587	598	2	8.2	VKDWPPIKPEQA		8.9	0.1	38.6	0.1	14.0	2.2	48.4	3.2
602	613	2	9.8	LDCNYPDPMVRG		4.1	0.1	23.6	0.1	6.6	0.5	29.9	0.7
619	632	3	11.2	LEKYLTDDKLSQYL		6.7	0.0	33.1	0.5	9.1	1.0	37.1	1.2
636	648	2	12.3	VQVLKYEQYLDNL		7.3	0.1	18.7	0.1	9.6	0.2	21.6	0.8
649	666	5	10.0	LVRFLLKKALTNQRIGHF		1.2	0.4	2.9	0.3	2.7	0.7	4.1	0.7

PI3K % Relative Deuterium Incorporation: 0, 10, 20, 30, 40, 50, 60, 70, 80, 90

Figure 43: All HDX p110α and p85α peptide data for experiments examining conformational changes in APDS2 mutation in the basal state.

The charge state *(Z)*, residue start *(S)*, residue end number *(E)*, and retention time *(RT)* are displayed for every peptide. Three time-points are labelled (3, 30, 300 seconds), and the relative level of HDX is coloured on a blue-to-red continuum (% deuterium incorporation). Data listed are the average of 3 independent experiments, with SDs presented. ##No coverage for the specific peptide.

p110α					WT				deletion			
S	E	Z	RT	Sequence	3.0	SD	300.0	SD	3.0	SD	300.0	SD
653	666	3	7.4	LLKKALTNQRIGHF	1.6	0.6	3.9	0.1	3.3	0.4	6.2	0.3
667	671	2	13.7	FFWHL	1.8	0.1	3.1	0.7	3.0	0.3	6.4	0.1
672	687	4	9.2	KSEMHNKTVSQRFGLL	6.7	0.3	24.6	0.6	10.1	0.8	27.6	0.6
691	697	2	7.1	YCRACGM	28.2	0.1	34.3	0.0	31.3	0.1	41.3	1.1
698	709	3	6.8	YLKHLNRQVEAM	2.4	0.3	5.0	0.1	4.2	0.4	13.3	1.2
713	734	5	10.7	INLTDILKQEKKDETQKVQMKF	47.3	0.1	60.0	0.7	49.4	0.2	65.9	3.3
720	734	5	6.7	KQEKKDETQKVQMKF	48.7	0.9	51.3	0.8	49.0	1.0	51.0	0.8
735	744	3	8.7	LVEQMRRPDF	18.8	0.5	68.7	0.7	35.6	1.5	72.3	2.1
745	764	3	14.1	MDALQGFLSPLNPAHQLGNL	2.0	0.1	11.7	1.0	5.0	1.6	14.2	1.7
745	766	3	14.0	MDALQGFLSPLNPAHQLGNLRL	7.3	0.2	16.0	0.0	8.9	0.8	16.8	0.9
746	764	2	13.7	DALQGFLSPLNPAHQLGNL	2.8	0.1	12.1	0.3	4.3	0.5	14.4	0.2
746	766	3	13.7	DALQGFLSPLNPAHQLGNLRL	8.1	0.1	16.5	0.3	8.8	0.1	18.4	0.5
751	764	2	11.7	FLSPLNPAHQLGNL	4.4	0.0	16.7	0.4	7.3	0.2	22.3	1.3
751	766	3	12.0	FLSPLNPAHQLGNLRL	11.3	0.1	20.9	0.3	12.8	0.3	24.2	1.2
769	781	4	10.4	CRIMSSAKRPLWL	17.4	0.2	32.4	0.4	20.1	0.6	33.7	2.4
782	789	1	11.2	NWENPDIM	33.7	0.2	61.1	0.3	36.1	0.9	64.0	0.2
799	807	2	9.6	IIFKNGDDL	19.8	0.2	29.9	0.5	24.2	1.9	35.1	1.6
799	811	3	9.5	IIFKNGDDLRQDM	11.7	0.1	30.5	2.5	14.6	0.6	28.4	1.3
815	821	2	9.6	QIIRIME	-1.4	0.0	-0.5	0.3	2.4	0.3	6.0	0.0
816	821	2	9.2	IIRIME	-0.5	0.3	-0.6	0.3	2.8	2.4	4.8	1.7
822	830	1	10.7	NIWQNQGLD	16.1	0.1	36.7	1.2	22.5	1.7	42.1	2.9
822	831	2	12.7	NIWQNQGLDL	11.8	0.1	31.3	0.6	14.1	0.2	32.3	0.6
831	839	2	12.5	LRMLPYGCL	3.7	0.1	17.1	0.5	6.0	0.0	21.0	0.5
832	839	2	11.5	RMLPYGCL	4.9	0.4	21.3	0.1	7.1	0.8	26.4	1.4
850	858	3	5.9	VVRNSHTIM	14.6	0.7	26.1	0.4	17.8	0.6	39.1	1.1
859	872	3	10.1	QIQCKGGLKGALQF	62.3	0.1	69.0	0.0	59.5	1.9	68.9	1.4
873	879	2	3.7	NSHTLHQ	11.1	0.5	37.3	0.4	12.9	2.5	35.1	1.3
880	893	4	7.8	WLKDKNKGEIYDAA	24.1	0.4	36.2	0.9	24.2	0.2	39.9	1.1
904	908	1	6.7	YCVAT	-2.2	0.1	-0.8	0.6	-0.7	0.9	5.9	1.5
909	920	3	9.5	FILGIGDRHNSN	7.4	0.3	16.9	0.8	10.5	0.5	22.9	1.4
909	921	3	10.4	FILGIGDRHNSNI	4.5	0.1	12.5	0.7	6.1	0.9	15.0	0.4
922	929	2	6.7	MVKDDGQL	2.8	0.7	10.5	1.0	4.5	0.3	12.9	0.9
930	934	2	11.7	FHIDF	4.3	0.4	24.3	1.3	7.7	0.9	29.5	3.2
930	937	3	12.0	FHIDFGHF	7.2	0.3	28.4	0.7	13.2	0.7	28.9	0.8
961	976	4	7.0	LIVISKGAQECTKTRE	29.4	0.8	44.0	0.4	28.6	2.2	48.9	1.1
962	970	2	5.7	IVISKGAQE	22.8	0.3	35.0	1.5	23.4	0.5	37.1	0.4
962	976	3	5.7	IVISKGAQECTKTRE	32.2	0.4	48.1	0.4	31.6	0.8	45.5	0.6
984	989	2	9.1	CYKAYL	-5.1	1.2	-3.3	1.5	-2.3	1.9	4.3	2.9
985	989	2	8.7	YKAYL	-1.8	0.2	-0.2	1.0	0.6	2.2	5.5	2.5
990	997	2	5.1	AIRQHANL	11.1	0.3	36.4	1.8	12.8	0.6	36.7	0.4
1002	1006	1	13.3	FSMML	2.9	0.5	24.3	0.2	6.9	0.5	36.8	1.6
1006	1013	1	10.9	LGSGMPEL	26.4	0.4	51.0	0.6	38.9	0.5	64.0	1.4
1006	1015	2	9.0	LGSGMPELQS	22.9	0.4	57.4	2.5	15.5	0.5	59.1	2.6
1039	1055	4	8.0	FMKQMNDAHHGGWTTKM	22.5	0.5	27.2	0.6	23.3	1.1	29.2	0.8
1039	1055	5	7.9	FMKQMNDAHHGGWTTKM	21.9	0.2	26.3	0.3	23.0	1.3	27.3	0.8
1040	1055	4	7.1	MKQMNDAHHGGWTTKM	23.9	0.2	28.3	0.4	25.6	0.3	31.6	1.0
1060	1068	2	4.0	HTIKQHALN	55.2	0.2	57.4	1.6	53.2	1.0	57.2	1.3
1060	1068	3	4.0	HTIKQHALN	57.1	0.8	58.5	0.9	54.0	0.1	58.0	1.6

Figure A1.5 cont.: All HDX p110α and p85α peptide data for experiments examining conformational changes in APDS2 mutation in the basal state.

p85α					>30%	8-15%	PI3K WT				PI3K Deletion			
Start	End	Z	RT	Sequence	15-30%	<8%	3.0	SD	300.0	SD	3.0	SD	300.0	SD
8	13	2	7.56	YRALYD			3.6	0.1	16.0	0.6	4.4	0.5	17.7	0.1
38	52	2	8.52	VALGFSDGQEARPEE			46.3	0.1	64.1	0.6	44.6	0.2	63.1	0.9
53	60	1	11.85	IGWLNGYN			13.6	0.1	26.8	0.5	15.0	0.5	28.7	0.7
73	106	5	6.5	YVEYIGRKKISPPTPKPRPPRPLPVAPGSSKTEA			55.2	0.0	59.5	0.0	55.8	0.4	60.1	1.0
77	106	5	5.23	IGRKKISPPTPKPRPPRPLPVAPGSSKTEA			64.2	0.1	64.9	0.6	64.1	0.1	65.1	0.7
77	107	5	5.19	IGRKKISPPTPKPRPPRPLPVAPGSSKTEAD			63.4	0.0	63.9	0.6	63.5	0.5	64.1	0.6
113	118	1	11.7	LTLPDL			37.8	0.1	77.4	0.8	36.8	0.8	76.3	0.6
119	132	2	12.63	AEQFAPPDIAPPLL			18.2	0.2	38.4	0.5	18.3	0.3	38.4	0.4
139	146	3	4.82	IEKKGLEC			28.7	1.5	62.9	0.7	31.2	2.4	64.1	1.7
149	158	2	6.33	LYRTQSSSNL			55.8	0.2	64.6	0.9	56.9	1.7	67.6	1.8
168	173	1	4.66	DTPSVD			80.2	0.3	81.2	0.7	81.3	0.7	81.2	0.3
177	186	2	11.91	IDVHVLADAF			8.6	0.2	11.9	0.8	11.5	0.9	17.2	2.0
186	202	3	11.85	FKRYLLDLPNPVIPAAV			12.9	0.2	18.3	0.1	12.9	0.1	18.2	0.3
186	203	3	12.32	FKRYLLDLPNPVIPAAVY			11.6	0.2	17.6	0.0	11.7	0.1	17.8	0.5
207	218	1	8.63	ISLAPEVQSSEE			66.0	1.3	74.8	0.1	62.1	2.8	67.7	1.7
220	237	4	10.27	IQLLKKLIRSPSIPHQYW			4.4	0.1	18.6	0.1	7.7	0.4	23.3	2.2
223	237	3	8.68	LKKLIRSPSIPHQYW			7.2	0.2	20.4	0.3	7.5	0.1	20.9	0.4
238	261	4	13.53	LTLQYLLKHFFKLSQTSSKNLLNA			11.9	0.2	21.0	0.2	11.9	0.1	21.3	0.1
242	261	3	10.27	YLLKHFFKLSQTSSKNLLNA			14.7	0.2	26.2	0.0	16.1	0.1	27.7	0.9
262	268	2	11.12	RVLSEIF			0.1	0.3	1.4	0.9	1.8	0.5	2.3	1.8
262	272	2	13	RVLSEIFSPML			0.0	0.1	9.9	0.2	2.0	0.4	13.6	2.3
267	272	1	12.42	IFSPML			2.3	0.3	27.2	0.4	2.6	0.8	31.9	2.2
273	286	2	9.37	FRFSAASSDNTENL			48.8	0.2	60.5	0.5	49.7	0.3	61.6	0.6
287	291	2	6.31	IKVIE			-3.1	0.6	0.4	1.5	-1.7	1.0	2.4	0.9
294	325	4	7.78	ISTEWNERQPAPALPPKPPKPTTVANNGMNNN			76.8	0.2	77.3	0.3	77.1	0.4	77.8	0.9
294	326	4	8.19	ISTEWNERQPAPALPPKPPKPTTVANNGMNNNM			76.5	0.1	77.2	0.0	77.3	0.4	78.1	1.0
299	325	4	6.18	NERQPAPALPPKPPKPTTVANNGMNNN			80.3	0.2	81.1	0.5	79.8	0.4	82.3	0.4
333	341	2	12.01	WYWGDISRE			29.9	0.0	55.8	0.3	29.3	0.1	57.8	0.5
334	341	2	9.32	YWGDISRE			37.3	0.1	65.9	1.0	37.8	0.4	66.5	1.0
342	349	2	4.46	EVNEKLRD			14.2	0.4	49.8	2.3	22.0	0.3	59.7	0.6
342	355	3	7.88	EVNEKLRDTADGTF			15.2	0.4	33.4	0.8	16.7	0.2	43.7	0.8
356	371	4	6.98	LVRDASTKMHGDYTLT			19.4	0.3	27.1	0.3	18.6	0.1	30.7	0.5
356	372	4	9.22	LVRDASTKMHGDYTLTL			15.0	0.1	21.5	0.3	15.4	0.1	26.8	0.1
372	380	3	3.33	LRKGGNNKL			19.3	0.6	39.3	0.6	27.4	1.0	44.3	0.6
373	380	2	2.92	RKGGNNKL			20.4	0.5	37.0	0.7	27.7	0.7	43.5	0.6
381	398	4	10.8	IKIFHRDGKYGFSDPLTF			20.1	0.1	27.8	0.2	21.2	0.0	29.6	0.4
402	413	3	8.52	VELINHYRNESL			21.1	0.3	27.1	0.3	19.8	0.2	25.1	0.3
405	413	3	5.8	INHYRNESL			30.0	0.4	38.1	0.5	31.3	0.4	39.3	0.2
414	420	1	6.92	AQYNPKL			72.3	0.7	86.3	0.0	75.4	1.3	86.8	0.5
414	420	2	6.92	AQYNPKL			72.4	1.0	86.9	0.2	74.7	0.4	85.9	0.2
508	520	4	4.76	YIEKFKREGNEKE			35.7	0.1	50.5	2.0	35.8	0.7	51.2	0.6
538	549	4	8.09	IIDSRRRLEEDL			0.0	0.5	10.0	0.1	3.3	0.1	32.2	0.5
556	570	4	7.67	YREIDKRMNSIKPDL			0.9	0.1	19.3	0.7	58.6	0.6	59.5	0.9
582	596	3	6.98	MWLTQKGVRQKKLNE			38.0	0.0	56.8	0.8	62.4	0.7	64.5	0.9
610	637	4	7.4	VEDDEDLPHHDEKTWNVGSSNRNKAENL			21.0	0.3	34.7	0.4	21.9	0.1	35.5	0.5
638	646	3	4.34	LRGKRDGTF			16.1	0.4	29.3	1.0	17.7	0.6	30.6	0.8
647	656	3	3.53	LVRESSKQGC			50.5	0.7	60.1	1.0	51.7	1.2	61.5	1.8
647	657	3	4.92	LVRESSKQGCY			41.2	0.2	53.3	0.8	41.9	0.5	54.6	0.6
661	680	4	7.24	VVVDGEVKHCVINKTATGYG			24.6	0.2	45.4	0.8	25.7	0.5	46.4	0.6
661	687	4	10.43	VVVDGEVKHCVINKTATGYGFAEPYNL			28.1	0.0	47.4	0.1	28.5	0.3	48.3	0.7
681	687	2	10.64	FAEPYNL			63.0	0.6	77.7	1.5	63.3	0.6	75.3	0.8
694	703	3	8.33	LVLHYQHTSL			7.3	0.1	21.7	0.3	9.9	0.4	23.9	0.4
697	703	2	4.98	HYQHTSL			12.7	0.2	30.9	0.3	14.5	0.3	31.6	0.3
704	710	2	4.94	VQHNDSL			21.6	0.0	33.8	0.3	24.5	0.8	36.4	0.6
711	724	3	8.48	NVTLAYPVYAQQRR			31.7	0.0	57.2	0.1	37.7	0.9	60.3	0.5

PI3K % Relative Deuterium Incorporation: 0, 10, 20, 30, 40, 50, 60, 70, 80, 90

Figure A1.5 cont.: All HDX p110α and p85α peptide data for experiments examining conformational changes in APDS2 mutation in the basal state.

p110α				WT						p85α(Q572*)					
S	E	Z	RT	3	SD	30	SD	300	SD	3	SD	30	SD	300	SD
10	19	3	11.8	23.4	1.5	34.9	1.2	44.4	1.1	33.1	1.0	38.1	0.6	48.6	0.4
11	23	3	12.4	16.2	1.3	30.1	0.4	38.6	0.6	22.3	0.5	32.4	0.1	41.5	0.4
24	30	1	10.8	2.9	0.5	4.3	0.2	12.6	0.1	2.7	0.6	4.1	0.4	11.3	0.1
31	36	1	9.8	42.0	1.7	42.4	0.6	41.8	0.8	42.9	0.7	43.3	2.7	41.8	1.1
37	42	2	7.18	1.2	0.2	1.9	0.3	6.3	0.3	1.3	0.5	2.5	0.3	9.7	0.3
43	62	4	9.4	5.0	0.3	14.3	0.3	23.3	0.3	4.8	0.3	14.0	0.3	22.2	0.2
43	64	3	9.62	7.6	0.9	18.3	0.1	27.9	0.7	7.4	0.2	18.5	0.2	27.2	0.3
50	64	3	8.47	11.9	0.2	27.1	0.9	38.2	1.2	11.6	0.0	27.5	0.2	38.1	1.1
50	67	3	8.61	10.8	0.6	26.5	0.5	39.5	1.8	10.3	0.6	26.9	1.2	37.1	0.7
63	68	1	5.36	12.2	1.3	28.2	1.2	39.8	0.6	13.4	1.4	28.3	1.8	40.1	1.4
69	76	1	9.16	1.0	0.6	5.7	0.2	13.2	0.3	3.0	0.4	11.9	0.4	15.3	0.9
69	82	2	10.9	4.1	0.4	12.7	0.7	18.3	1.0	5.9	0.7	14.4	0.4	19.6	0.6
71	82	2	9.29	4.1	0.5	13.9	0.3	22.5	0.4	5.4	0.4	16.4	0.3	24.7	0.4
77	82	2	7.07	6.8	0.5	21.5	0.6	28.9	1.0	7.5	0.6	17.8	0.1	27.5	0.5
83	91	2	7.07	1.4	0.1	2.7	0.4	7.3	0.2	1.6	0.4	3.1	0.5	10.1	0.1
92	99	2	14.1	0.6	0.1	0.7	0.2	1.4	0.1	0.8	0.4	0.9	0.1	3.8	0.3
93	99	2	12.9	0.5	0.2	0.5	0.0	0.7	0.2	0.5	0.5	0.7	0.1	1.1	0.1
95	99	1	13.2	2.0	0.6	1.7	0.6	1.2	1.2	2.2	2.3	1.4	0.3	2.2	0.4
100	109	2	5.31	44.6	1.1	57.2	0.9	60.5	0.2	49.4	1.3	58.4	1.3	61.8	1.2
100	116	4	6.82	20.3	1.0	30.4	1.0	48.1	1.4	28.9	1.5	51.7	0.9	57.6	1.0
100	119	5	9.8	11.7	1.1	19.5	1.1	34.3	0.3	19.2	0.6	37.7	0.7	45.6	0.4
120	127	1	9.65	8.0	0.8	22.3	0.1	32.1	0.7	16.4	0.8	30.8	0.1	47.9	0.5
120	128	1	12.9	8.4	1.4	26.1	0.8	37.1	1.4	14.5	2.0	31.4	0.1	49.1	1.2
128	138	2	8.79	17.1	1.0	30.0	0.5	38.0	1.3	14.5	0.5	28.3	0.8	37.1	0.3
128	139	2	11	13.0	1.0	25.4	0.6	30.6	1.1	11.4	0.6	22.5	0.1	30.0	0.6
153	163	3	4.61	26.5	1.3	32.6	0.7	43.0	0.9	24.0	0.6	30.8	0.4	44.0	1.8
153	164	3	5.62	17.3	0.7	24.6	0.5	37.1	0.2	20.1	1.6	25.7	0.0	38.7	0.5
154	164	3	4.55	19.9	1.3	27.5	0.3	39.9	0.9	20.6	0.6	27.0	1.1	41.0	0.5
165	191	4	10.1	23.4	2.1	31.2	0.5	41.1	0.3	22.3	0.8	30.7	0.5	40.4	1.5
165	192	5	10.3	21.2	1.2	28.3	0.1	38.1	0.2	21.0	0.2	28.2	0.4	37.2	0.7
165	193	5	10.3	19.9	1.4	26.4	0.2	35.9	0.6	19.7	0.3	26.4	0.1	34.6	0.8
193	209	3	11.7	21.0	1.3	33.3	0.4	38.3	0.5	20.4	0.6	32.2	0.7	38.4	0.4
196	209	3	8.13	28.6	1.2	41.5	0.5	44.7	1.4	28.4	0.6	41.8	1.2	43.9	0.1
210	222	3	8.13	9.2	0.4	9.8	0.3	12.9	0.7	8.1	0.2	8.6	0.2	11.6	0.2
223	233	3	5.12	42.1	2.0	49.1	0.4	55.3	0.4	42.3	1.9	46.7	0.6	54.5	1.7
244	252	1	10.7	42.1	1.6	47.2	0.8	49.3	0.7	42.6	1.7	47.8	0.1	49.0	1.6
245	252	1	10	36.2	1.8	42.3	0.9	43.0	1.3	33.4	1.5	39.4	0.2	38.8	1.2
253	260	1	7.15	1.8	0.9	5.2	0.5	6.6	0.2	2.7	0.6	5.5	0.4	6.5	0.6
260	269	2	11	10.8	0.6	12.2	0.4	19.6	0.2	11.0	0.8	12.0	0.0	19.0	0.4
261	269	2	9.29	12.6	0.7	13.9	0.3	21.2	0.3	13.0	0.3	13.9	0.4	20.6	0.5
261	270	2	10.6	10.8	0.7	12.5	0.7	19.8	0.3	10.7	0.8	11.9	0.3	19.1	0.7
261	275	4	9.55	11.9	0.4	12.7	0.3	16.9	0.3	12.3	0.3	13.0	0.5	16.6	0.3
262	269	2	7.64	15.0	0.3	15.7	1.0	17.3	0.3	15.2	1.1	14.9	1.0	17.5	0.2
279	287	2	12	14.1	0.3	19.9	0.3	25.1	0.5	14.2	0.5	19.6	0.0	24.5	0.5
280	287	1	11.4	14.6	1.2	21.3	0.1	26.6	0.1	15.3	0.7	21.7	0.3	26.4	0.6
288	293	1	6.17	35.9	1.3	41.4	0.5	58.4	1.5	36.9	2.2	41.0	0.1	57.8	0.9
294	301	2	10.1	36.5	1.3	52.3	0.5	57.5	1.0	36.6	0.8	52.2	0.6	57.2	0.7
302	327	4	9.75	41.7	1.2	44.2	0.5	46.8	0.2	41.7	0.9	44.8	1.3	45.9	0.9
308	327	4	7.63	46.0	1.5	51.4	1.1	54.3	1.3	46.9	1.9	51.6	1.0	54.2	0.7
328	334	1	12.2	31.3	1.0	37.6	0.7	39.6	0.8	31.6	0.8	37.2	0.0	39.4	0.4
335	342	2	8.04	1.0	0.5	6.2	0.1	17.9	0.4	0.6	0.1	4.1	0.1	16.3	0.1
343	350	2	7.64	63.5	2.1	77.0	1.2	79.4	1.8	78.1	1.5	76.8	1.8	78.5	0.4
343	355	2	10.8	36.0	2.0	44.8	0.3	49.0	0.3	43.0	0.3	48.3	0.2	49.0	0.9
347	355	2	9	29.2	1.5	35.9	0.6	44.3	1.8	32.6	0.5	42.8	2.1	44.5	0.3
355	369	2	8.6	4.5	0.7	6.9	1.0	7.2	0.5	3.1	0.0	6.2	0.3	6.6	0.5
356	369	2	8	3.7	0.5	6.4	0.3	7.3	0.2	3.6	0.1	6.5	0.5	7.1	0.2
356	373	3	8.26	5.4	0.5	11.1	0.5	12.0	0.9	5.7	0.4	10.9	0.2	11.5	0.0
370	385	3	7.73	16.2	1.2	31.3	0.8	43.0	0.9	16.5	0.5	30.1	0.8	42.3	0.7
370	386	3	10.5	13.7	1.1	29.6	0.4	39.8	0.3	13.8	0.1	28.1	0.3	39.1	0.4
370	387	3	12	11.3	0.9	26.2	0.4	35.2	0.1	11.0	0.3	24.8	0.1	34.5	0.2
390	402	3	11.4	1.3	0.3	5.0	0.1	9.5	0.1	1.1	0.4	4.1	0.0	9.5	0.2
391	402	3	10.9	0.8	0.1	0.8	0.0	0.9	0.2	0.8	0.2	0.9	0.0	1.0	0.1
408	429	5	10.7	4.6	0.6	4.8	0.1	6.4	0.1	4.7	0.2	5.0	0.1	6.7	0.4
430	436	1	10.8	1.0	0.4	1.9	0.2	10.5	0.3	0.1	0.4	1.2	0.1	9.4	0.6
430	443	2	12.1	10.6	1.0	17.2	0.0	25.4	0.1	9.4	0.4	17.0	0.2	25.0	0.3
432	443	2	10.6	11.8	0.3	19.6	0.3	24.2	0.3	10.8	0.4	18.9	0.3	24.2	0.7
444	454	2	11.5	14.0	1.0	28.7	0.5	35.0	0.8	21.3	0.6	34.1	0.0	34.9	0.6
444	455	2	13.4	13.3	0.9	32.7	0.8	40.5	1.1	21.2	0.8	39.3	0.0	40.6	0.6
444	473	3	14	9.3	0.5	20.9	0.1	34.0	0.7	11.9	0.4	25.3	0.3	35.4	0.6
455	473	3	10.8	11.3	0.6	19.8	0.3	36.2	0.8	11.8	0.3	24.1	0.1	39.3	0.6
456	473	2	9.9	12.8	0.6	22.7	0.4	43.0	0.5	13.6	0.2	28.3	0.2	46.6	0.5
456	474	2	9.3	12.4	0.6	21.2	0.5	40.3	0.6	13.3	0.3	26.2	0.3	42.9	0.7
474	478	1	10.1	1.9	0.9	1.4	0.4	3.0	1.2	1.2	0.2	1.2	0.3	2.3	0.2
481	491	2	11	22.8	0.3	26.0	0.5	32.7	0.7	20.9	0.8	26.3	0.6	32.5	0.7
487	491	1	7.64	46.7	1.6	58.1	1.1	74.6	1.3	47.9	1.6	56.8	0.2	74.0	0.3
492	506	3	9.81	41.3	1.7	43.9	0.4	46.7	0.3	41.6	0.5	45.4	0.9	46.6	1.0
495	506	3	9.3	39.3	1.0	41.3	0.6	42.0	0.8	39.8	0.2	42.2	0.7	41.8	0.9
495	507	3	8.9	52.4	1.6	53.1	1.4	56.5	2.1	52.8	0.9	53.5	4.6	56.3	0.5
499	506	2	7.28	62.1	1.0	63.4	1.2	65.4	1.7	63.4	2.5	61.9	1.1	63.9	0.2
499	507	2	6.46	66.7	1.7	67.6	1.2	69.7	1.3	71.3	2.2	69.3	0.7	72.4	1.1
506	517	3	8.96	39.3	1.2	37.5	1.8	39.5	1.7	38.3	2.5	38.1	2.6	38.1	0.9
507	520	3	6.25	44.4	1.0	45.6	0.7	45.5	1.2	45.1	2.4	43.9	1.9	46.4	1.2
507	522	3	6.32	40.7	0.8	42.5	0.8	43.7	1.1	42.7	1.7	42.9	0.4	43.1	1.3
507	523	4	7.79	41.6	0.8	41.5	0.9	43.3	1.4	43.2	1.8	42.4	1.4	43.0	0.6
508	523	4	7.84	44.0	1.8	42.9	0.2	44.9	1.3	44.5	1.2	43.6	1.7	44.4	0.3

0 10 20 30 40 50 60 70 80 90

Figure 44: All HDX p110α and p85α peptide data for experiments examining conformational changes in the oncogenic p85α-Q572* mutant in the basal state.
The charge state *(Z)*, residue start *(S)*, residue end number *(E)*, and retention time *(RT)* are displayed for every peptide. Three time-points are labelled (3, 30, 300 seconds), and the relative level of HDX is coloured on a blue-to-red continuum (% deuterium incorporation). Data listed are the average of 3 independent experiments, with SDs presented. ##No coverage for the specific peptide.

p110α				WT						p85α[Q572*]β					
S	E	Z	RT	3	SD	30	SD	300	SD	3	SD	30	SD	300	SD
524	531	2	4.91	20.1	1.7	40.1	0.7	47.4	0.2	19.1	0.6	39.8	0.9	46.4	1.0
524	533	2	4.28	15.7	2.0	31.6	0.0	46.6	0.8	15.4	0.6	31.8	0.3	45.0	0.9
532	542	2	7.02	11.3	1.2	18.5	1.9	32.6	0.9	11.2	1.3	17.9	0.2	30.0	0.5
534	542	2	7.88	13.2	0.3	21.7	0.2	39.3	1.2	13.1	0.4	20.6	0.6	35.4	0.2
543	551	1	9.97	3.6	1.2	10.4	0.5	15.2	0.5	8.9	0.1	13.3	0.2	15.8	0.6
550	565	4	12.6	2.2	0.5	8.0	0.3	16.6	0.2	2.1	0.5	7.4	0.3	15.9	0.4
552	565	4	11.4	1.3	0.3	9.3	0.1	19.7	0.2	1.3	0.1	8.7	0.0	19.0	0.4
552	570	4	13.1	1.1	0.2	5.9	0.1	12.5	0.1	1.0	0.1	5.4	0.0	11.8	0.1
561	570	2	13.8	0.6	0.2	2.5	0.2	6.5	0.2	0.7	0.4	2.2	0.2	6.0	0.2
571	583	2	8.59	0.7	0.2	2.3	0.1	8.4	0.4	0.7	0.1	2.0	0.1	7.3	0.1
584	598	3	10.6	3.8	0.7	13.2	0.3	23.5	0.2	3.5	0.5	12.3	0.1	22.6	0.6
585	598	3	9.82	3.2	0.5	12.6	0.7	23.4	0.4	3.0	0.6	13.1	1.2	22.2	0.2
587	598	2	8.18	4.9	0.6	16.0	0.9	31.3	0.6	4.2	0.3	15.0	0.7	28.9	0.3
601	614	2	12.5	1.9	0.9	5.7	0.4	13.1	0.8	2.3	0.4	6.2	1.0	12.3	0.2
602	613	2	9.55	2.5	0.7	7.7	0.5	17.5	0.2	2.9	0.4	8.1	0.3	17.7	0.6
602	615	3	11.6	1.5	0.4	6.1	0.9	11.7	0.3	1.3	0.4	6.4	1.5	11.6	0.7
602	628	5	13.8	6.7	0.7	11.2	0.5	20.7	0.9	6.7	0.3	11.4	0.3	20.0	0.6
602	630	5	13.6	5.6	1.0	10.1	0.5	20.8	0.3	4.7	0.8	10.5	0.4	20.7	0.2
614	628	4	11.8	8.7	1.2	15.4	1.3	27.5	0.2	8.5	1.0	15.6	0.8	27.6	1.3
615	632	3	11.6	6.8	0.2	13.1	0.4	26.9	0.3	6.9	0.8	12.9	0.2	27.3	0.2
619	632	3	11.1	5.5	0.4	11.4	0.2	27.5	0.4	5.4	0.4	11.5	0.4	27.1	0.4
631	635	1	12.6	-0.2	0.8	-0.3	1.7	0.3	1.0	0.2	0.3	0.1	0.6	0.8	0.3
636	648	2	12.4	3.6	0.6	10.6	0.2	16.0	0.3	3.2	0.3	10.8	0.1	15.9	0.1
636	649	2	13.9	3.4	0.7	10.1	0.3	15.5	0.4	3.1	0.1	10.5	0.3	15.3	0.2
649	666	4	9.75	0.4	0.1	0.4	0.0	0.6	0.1	0.4	0.2	0.5	0.0	0.7	0.2
653	666	3	7.33	0.3	0.3	0.7	0.3	0.8	0.2	0.5	0.3	0.5	0.2	1.6	0.1
667	671	2	13.7	0.5	0.1	0.5	0.2	0.6	0.2	0.7	0.2	0.9	0.1	0.7	0.1
672	687	4	9.29	6.2	0.3	9.4	0.2	19.3	0.3	6.6	0.0	10.1	0.5	20.2	0.6
676	687	2	9.61	7.1	1.4	11.0	0.6	23.6	0.5	7.7	0.8	11.8	0.6	25.2	0.0
688	692	1	7.87	1.3	0.7	0.2	1.7	1.3	1.2	1.0	1.6	1.2	1.4	1.5	1.0
691	697	2	7.06	21.3	1.1	27.9	0.6	30.3	0.7	21.5	0.7	28.1	0.6	29.6	0.1
698	708	2	5.63	0.8	0.6	3.0	0.7	4.7	0.5	0.6	0.3	2.6	0.7	4.3	0.7
698	709	3	6.91	0.3	0.1	1.5	0.1	2.2	0.1	0.3	0.2	1.3	0.2	2.3	0.1
713	717	1	7.54	2.9	1.2	3.3	1.6	6.8	0.5	2.3	0.7	4.6	0.1	11.5	0.2
714	735	4	10.7	40.3	2.0	47.9	0.5	53.7	0.6	43.9	0.4	48.8	0.2	57.1	1.3
716	734	3	7.99	42.4	0.4	49.1	0.5	57.0	1.4	45.0	0.4	50.8	0.8	57.7	0.8
720	734	4	6.61	43.1	1.3	49.7	1.9	51.0	1.1	46.7	1.7	49.6	0.6	50.1	0.3
735	744	2	8.56	9.2	1.1	36.9	0.8	60.8	0.8	13.5	1.5	43.9	0.5	60.3	0.4
745	764	3	14.1	1.1	0.1	1.9	0.3	5.1	0.3	1.1	0.3	2.0	0.2	5.3	0.2
745	766	3	14.1	4.8	0.2	6.2	0.1	9.4	0.2	4.7	0.2	6.3	0.1	9.3	0.1
746	764	3	13.6	1.2	0.2	1.4	0.1	4.8	0.2	1.0	0.1	1.5	0.1	4.7	0.2
746	766	3	13.7	4.9	0.4	6.2	0.1	9.4	0.1	4.7	0.2	6.2	0.1	9.2	0.1
751	764	2	11.7	1.3	0.3	1.8	0.2	6.0	0.2	1.4	0.3	1.9	0.0	6.1	0.1
751	766	3	11.9	6.5	0.5	8.2	0.1	11.6	0.1	6.3	0.3	8.2	0.0	11.5	0.1
767	781	4	10.9	15.3	0.9	22.7	0.6	29.1	0.4	15.4	0.4	23.5	0.3	28.6	1.0
769	781	3	10.4	13.6	0.9	21.6	0.5	26.9	0.2	13.9	0.3	22.2	0.3	26.7	0.5
782	789	1	11.2	20.0	1.1	38.3	0.7	46.6	2.5	20.1	1.0	37.6	0.4	46.7	0.9
782	791	1	10.8	26.6	2.2	42.5	1.0	45.7	3.2	26.0	0.6	41.4	0.4	46.9	0.5
793	797	1	6.66	45.7	2.8	58.4	0.8	60.6	2.0	45.7	1.8	58.3	0.4	60.4	1.3
793	798	1	7.13	29.4	1.3	44.7	0.6	55.7	2.0	29.7	1.4	43.9	2.1	55.7	0.2
798	811	3	9.96	6.3	0.8	14.4	0.6	24.0	0.5	6.1	0.5	14.7	0.4	24.4	0.9
812	816	1	11.4	1.3	0.5	1.0	0.3	1.5	0.3	0.8	1.1	0.5	0.7	0.8	0.3
815	821	2	9.5	0.3	0.2	0.4	0.1	0.6	0.1	0.4	0.0	0.5	0.0	0.7	0.1
822	830	1	10.6	11.9	1.1	15.5	0.5	25.2	0.8	11.9	0.7	15.4	0.0	24.4	0.5
822	831	1	12.7	7.6	0.6	10.2	0.3	18.1	1.1	7.3	0.7	10.0	0.6	17.4	0.5
831	839	2	12.4	1.7	0.2	6.5	0.2	12.0	0.1	1.8	0.3	6.4	0.1	12.0	0.2
832	839	2	11.5	2.5	0.2	8.0	0.1	15.2	0.1	2.1	0.6	7.5	0.4	15.0	0.2
840	847	1	11	3.3	0.8	5.7	0.4	7.9	0.3	3.5	0.6	5.5	0.1	7.7	0.5
848	858	3	7.68	11.8	0.8	20.0	0.4	25.8	0.7	13.2	0.6	21.3	0.4	26.4	1.1
848	859	2	7.19	11.3	1.3	19.3	1.3	27.7	0.9	11.2	0.6	19.5	0.2	28.8	1.8
859	872	3	10.1	56.3	0.5	58.7	0.5	62.4	0.1	58.4	0.7	58.9	1.0	63.1	0.5
873	893	2	8.17	11.5	0.7	22.2	0.2	25.5	1.2	10.8	0.6	22.1	1.3	24.4	0.8
880	893	2	7.84	15.1	1.0	29.7	0.7	32.5	1.0	14.1	0.5	29.3	1.6	32.2	0.3
892	896	1	9.71	0.4	0.8	1.4	0.5	2.7	0.9	0.9	0.5	1.5	1.1	1.5	0.9
904	908	1	6.62	0.9	0.5	1.6	0.1	1.7	0.2	0.9	0.5	1.2	0.1	1.2	0.2
909	920	2	9.51	3.5	1.3	9.8	2.2	13.3	0.9	5.9	0.6	10.3	2.3	12.8	1.2
909	921	2	10.4	2.2	0.5	6.5	0.6	9.1	0.1	3.1	0.4	7.8	0.3	10.0	0.4
921	929	1	8.04	0.3	0.3	2.5	0.5	8.1	0.6	0.3	0.4	2.7	1.1	8.3	1.0
923	929	1	5.64	1.9	0.2	3.6	0.4	9.0	0.6	2.2	0.5	3.4	0.5	8.8	0.8
930	956	5	10.4	7.4	0.6	10.9	0.1	18.9	0.6	8.3	0.1	13.6	0.2	21.1	0.4
961	976	4	7.25	27.1	1.0	33.1	1.2	42.1	0.8	28.2	1.5	32.1	0.7	41.8	0.1
961	980	4	9.13	14.6	1.3	17.4	0.9	26.7	0.8	14.6	0.7	18.3	1.1	25.7	0.8
962	976	4	5.62	29.2	0.9	36.5	0.4	45.8	0.9	30.1	0.8	35.3	0.4	45.9	0.7
962	980	4	8.34	13.1	1.1	17.0	0.9	26.8	1.0	13.0	0.5	16.6	1.4	25.7	1.1
985	989	1	8.61	-0.5	1.0	0.3	2.6	0.2	2.1	-0.3	0.2	-1.6	0.1	0.0	0.5
990	997	2	5.06	8.8	0.9	21.2	0.6	35.6	0.2	9.0	0.3	20.8	0.3	35.5	0.5
1002	1006	1	13.2	1.0	0.6	2.1	0.2	11.8	0.6	1.0	0.8	2.1	0.2	13.7	0.3
1005	1013	1	11.9	18.3	2.7	32.2	0.5	42.5	2.2	19.3	0.8	34.6	1.1	45.0	1.4
1017	1021	1	7.94	10.0	1.3	22.9	0.3	25.1	0.4	7.6	0.6	22.8	0.0	25.7	0.5
1022	1028	2	7.58	0.4	0.2	0.3	0.1	1.1	0.3	0.3	0.1	0.1	0.2	1.3	0.5
1029	1036	1	6.35	16.2	1.6	29.9	0.5	41.4	0.7	17.1	2.1	29.4	0.2	42.5	1.5
1034	1038	1	8.6	0.8	0.9	0.9	0.8	1.9	0.5	0.0	0.5	0.4	0.2	1.5	0.1
1039	1055	4	7.89	18.9	0.7	21.8	0.4	24.5	0.5	19.3	0.5	22.3	0.5	24.0	0.3
1060	1068	2	4.22	56.7	2.4	57.4	0.2	58.6	0.8	57.7	1.7	56.8	0.5	59.9	0.7

0 10 20 30 40 50 60 70 80 90

Figure A1.6 cont.: All HDX p110α and p85α peptide data for experiments examining conformational changes in the oncogenic p85α-Q572* mutant in the basal state.

p85α				WT						p85α (Q572*)					
S	E	Z	RT	3	SD	30	SD	300	SD	3	SD	30	SD	300	SD
8	13	1	7.9	1.9	0.1	2.8	0.2	9.9	0.9	1.1	0.3	2.4	0.4	9.2	0.1
12	21	3	4.7	23.1	1.6	37.4	1.3	38.3	0.4	22.3	0.3	36.8	1.0	38.9	0.6
22	30	1	13	3.7	0.8	6.8	1.5	12.4	1.2	2.2	0.4	5.3	0.6	11.3	0.5
25	30	1	10	0.5	0.3	1.1	0.3	2.7	0.4	0.6	0.1	1.1	0.0	2.3	0.2
25	37	3	10	21.0	1.6	22.3	0.9	21.9	1.3	22.2	1.5	21.6	0.9	22.2	1.2
31	37	1	5.5	70.1	1.1	72.9	0.3	74.0	0.4	72.4	1.3	71.8	0.8	74.0	1.4
38	52	2	8.9	28.9	1.5	47.4	0.6	52.2	1.7	27.9	0.4	48.0	0.5	52.0	0.4
43	52	2	4.3	22.5	2.5	55.5	0.4	64.9	1.5	20.1	0.7	55.2	0.2	67.4	3.1
53	58	1	12	7.6	0.9	24.1	0.3	29.3	0.6	6.7	0.3	23.0	0.2	29.0	0.5
53	60	1	12	5.9	0.6	17.4	0.2	21.7	0.4	5.2	0.2	16.5	0.0	21.5	0.4
53	72	2	12	4.1	0.5	13.5	0.2	18.5	0.7	3.7	0.0	13.0	0.1	18.3	0.2
53	73	2	12	3.8	0.5	12.2	0.3	17.0	0.5	3.4	0.1	11.8	0.0	16.8	0.2
59	72	2	7.9	4.5	0.6	13.8	0.3	20.0	0.4	4.0	0.2	13.6	0.1	19.4	0.3
59	73	2	9	4.0	0.5	11.2	0.3	16.3	0.2	3.6	0.4	11.1	0.6	15.7	0.1
60	72	2	7.5	4.8	1.1	14.2	0.2	18.1	0.7	4.2	0.2	14.4	0.3	18.7	0.3
61	72	2	7.4	5.1	0.7	15.2	0.5	17.5	0.8	4.6	0.2	15.3	0.2	17.1	0.2
73	106	5	6.7	50.0	0.7	55.1	0.6	56.4	1.1	51.7	1.8	54.5	0.7	55.7	0.7
74	106	5	6.3	51.8	0.8	56.7	0.7	57.7	1.1	53.5	1.9	56.3	0.1	57.3	1.0
77	106	5	5.9	59.2	1.0	61.2	0.2	61.2	0.3	61.0	1.6	60.8	0.1	61.1	1.2
77	107	5	5.6	58.6	1.0	60.7	0.5	60.3	0.6	60.8	1.6	60.5	1.1	60.8	1.2
107	112	1	4.7	75.7	2.4	74.1	0.8	76.9	1.7	78.2	2.0	75.0	0.9	77.3	1.1
108	118	2	12	47.6	1.3	61.1	0.7	66.5	1.3	48.6	1.9	60.5	0.0	67.3	0.9
111	118	1	12	43.4	3.1	63.9	0.5	74.5	1.4	44.2	2.5	62.6	0.5	74.2	1.1
113	118	1	12	18.2	2.4	51.5	0.8	67.3	1.4	16.7	1.7	49.3	0.1	67.0	0.9
119	132	1	13	9.5	1.0	22.3	0.4	30.8	0.9	8.8	0.7	22.1	0.2	30.2	0.4
133	149	2	11	13.5	0.9	25.5	1.9	37.4	0.9	14.0	0.6	24.4	1.8	36.7	0.2
136	146	2	6.9	9.0	1.2	22.3	1.4	31.8	0.4	9.0	0.7	21.3	0.3	31.9	1.2
138	146	1	5.8	12.8	1.2	31.4	1.0	46.7	1.2	12.8	1.0	31.1	0.4	45.4	0.9
138	149	2	7.9	17.4	0.9	31.7	1.6	48.0	0.6	15.5	0.3	31.0	0.9	45.6	1.5
149	158	2	6.7	48.1	1.8	52.1	1.5	58.1	1.6	49.4	2.1	51.3	0.6	57.4	1.8
149	160	2	6.4	45.6	0.9	56.1	1.7	59.3	0.3	46.3	0.9	53.6	1.9	58.5	1.6
150	158	2	6	58.9	1.3	61.6	0.6	61.5	0.8	61.1	1.7	61.0	0.7	61.9	1.5
150	160	2	5.5	53.0	1.2	61.9	0.4	62.1	0.4	55.0	0.8	62.3	2.7	62.9	1.0
161	167	1	9.7	20.3	2.6	33.9	2.2	45.4	2.1	23.9	3.0	38.2	3.0	49.6	1.7
162	173	2	9.1	35.4	1.7	39.9	0.7	45.8	3.5	36.3	1.4	40.0	1.1	46.8	1.8
168	173	1	5	74.8	1.2	75.2	0.3	76.6	0.6	77.7	1.7	75.4	0.5	77.6	0.3
168	174	1	9	70.5	2.4	70.8	1.6	72.1	4.5	71.4	2.0	71.9	1.3	73.0	2.2
177	186	2	12	7.5	0.7	9.4	0.3	10.7	0.6	7.5	0.4	9.6	0.1	10.9	0.8
186	202	3	12	10.1	0.5	12.4	0.1	14.3	0.2	10.1	0.5	12.4	0.1	14.0	0.2
186	203	3	13	10.0	0.5	12.1	0.2	14.3	0.2	9.8	0.5	11.8	0.1	13.7	0.3
187	202	2	12	11.4	0.8	13.9	0.1	16.0	0.5	11.9	1.0	14.2	0.2	15.7	0.5
207	218	1	8.9	45.7	2.8	63.1	1.1	63.2	3.7	44.5	1.7	63.1	1.3	63.9	1.2
207	219	1	10	42.1	2.4	58.4	0.4	62.3	0.7	40.8	0.9	57.8	0.5	61.8	0.7
220	237	3	11	4.2	0.5	5.5	0.7	11.3	0.3	4.2	0.6	5.1	0.2	10.3	0.2
223	237	3	9	6.5	0.2	7.3	0.1	13.5	0.2	6.6	0.3	7.4	0.1	12.7	0.2
238	259	5	14	5.3	0.2	9.0	0.6	12.7	0.5	5.4	0.9	9.2	0.1	12.5	0.4
242	261	4	11	12.0	0.8	16.8	0.2	21.5	0.2	12.2	0.4	16.8	0.1	21.5	0.6
260	272	2	14	1.4	0.5	2.4	1.0	8.0	0.5	1.6	1.1	2.4	0.2	7.1	0.8
262	272	2	13	0.9	0.2	1.6	0.1	6.2	0.1	1.0	0.2	1.5	0.1	5.7	0.3
267	272	1	13	1.2	0.5	3.6	0.2	16.8	0.6	1.4	0.8	2.6	0.1	15.4	0.6
273	285	2	8.1	49.3	2.1	51.7	2.1	55.3	1.5	50.4	1.4	52.5	2.2	55.6	1.3
273	286	2	9.7	37.4	1.6	42.4	0.8	48.7	0.8	38.3	1.0	42.1	0.8	48.8	0.7
278	286	1	6.5	44.4	0.5	50.4	1.0	56.4	1.4	47.5	0.5	48.7	0.3	57.4	2.3
282	286	1	6.1	46.8	1.7	58.8	1.8	75.7	0.7	49.5	1.0	58.7	4.0	76.1	1.5

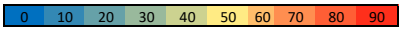

Figure A1.6 cont.: All HDX p110α and p85α peptide data for experiments examining conformational changes in the oncogenic p85α-Q572* mutant in the basal state.

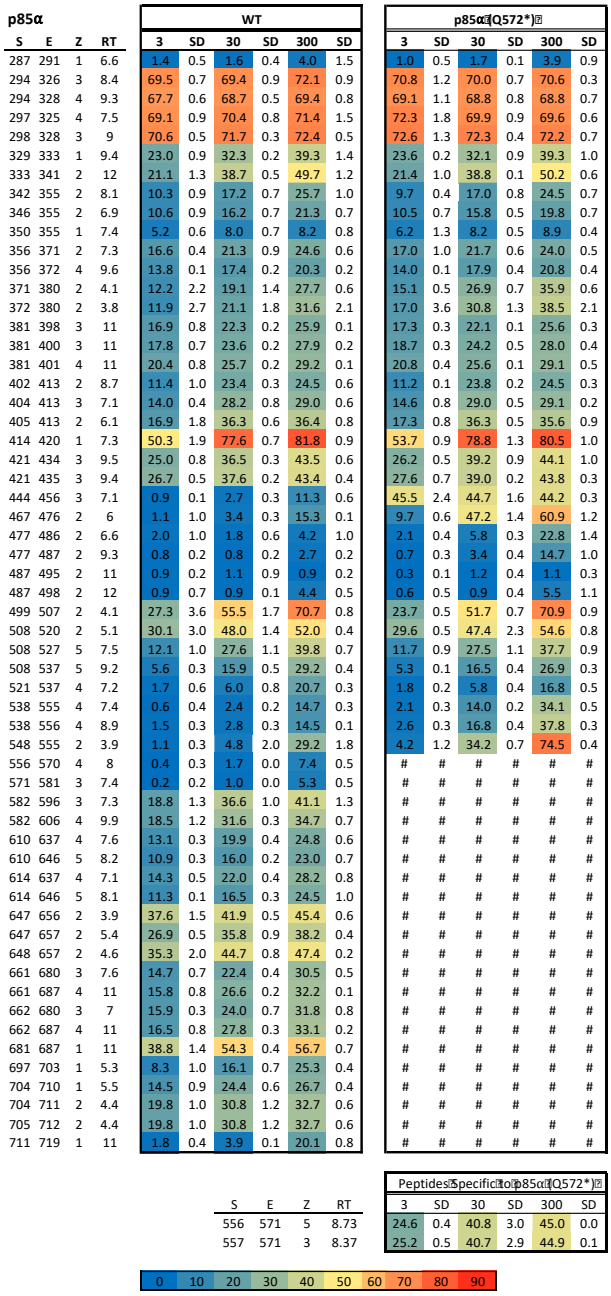

p85α				WT						p85α (Q572*)					
S	E	Z	RT	3	SD	30	SD	300	SD	3	SD	30	SD	300	SD
287	291	1	6.6	1.4	0.5	1.6	0.4	4.0	1.5	1.0	0.5	1.7	0.1	3.9	0.9
294	326	3	8.4	69.5	0.7	69.4	0.9	72.1	0.9	70.8	1.2	70.0	0.7	70.6	0.3
294	328	4	9.3	67.7	0.6	68.7	0.5	69.4	0.8	69.1	1.1	68.8	0.8	68.8	0.7
297	325	4	7.5	69.1	0.9	70.4	0.8	71.4	1.5	72.3	1.8	69.9	0.9	69.6	0.6
298	328	3	9	70.6	0.5	71.7	0.3	72.4	0.5	72.6	1.3	72.3	0.4	72.2	0.7
329	333	1	9.4	23.0	0.9	32.3	0.2	39.3	1.4	23.6	0.2	32.1	0.9	39.3	1.0
333	341	2	12	21.1	1.3	38.7	0.5	49.7	1.2	21.4	1.0	38.8	0.1	50.2	0.6
342	355	2	8.1	10.3	0.9	17.2	0.7	25.7	1.0	9.7	0.4	17.0	0.8	24.5	0.7
346	355	2	6.9	10.6	0.9	16.2	0.7	21.3	0.7	10.5	0.7	15.8	0.5	19.8	0.7
350	355	1	7.4	5.2	0.6	8.0	0.7	8.2	0.8	6.2	1.3	8.2	0.5	8.9	0.4
356	371	2	7.3	16.6	0.4	21.3	0.9	24.6	0.6	17.0	1.0	21.7	0.6	24.0	0.5
356	372	4	9.6	13.8	0.1	17.4	0.2	20.3	0.2	14.0	0.1	17.9	0.4	20.8	0.4
371	380	2	4.1	12.2	2.2	19.1	1.4	27.7	0.6	15.1	0.5	26.9	0.7	35.9	0.6
372	380	2	3.8	11.9	2.7	21.1	1.8	31.6	2.1	17.0	3.6	30.8	1.3	38.5	2.1
381	398	3	11	16.9	0.8	22.3	0.2	25.9	0.1	17.3	0.3	22.1	0.1	25.6	0.3
381	400	3	11	17.8	0.7	23.6	0.2	27.9	0.2	18.7	0.3	24.2	0.5	28.0	0.4
381	401	4	11	20.4	0.8	25.7	0.2	29.2	0.1	20.8	0.4	25.6	0.1	29.1	0.5
402	413	2	8.7	11.4	1.0	23.4	0.3	24.5	0.6	11.2	0.1	23.8	0.2	24.5	0.3
404	413	3	7.1	14.0	0.4	28.2	0.8	29.0	0.6	14.6	0.8	29.0	0.5	29.1	0.2
405	413	2	6.1	16.9	1.8	36.3	0.6	36.4	0.8	17.3	0.8	36.3	0.5	35.6	0.9
414	420	1	7.3	50.3	1.9	77.6	0.7	81.8	0.9	53.7	0.9	78.8	1.3	80.5	1.0
421	434	3	9.5	25.0	0.8	36.5	0.3	43.5	0.6	26.2	0.5	39.2	0.9	44.1	1.0
421	435	3	9.4	26.7	0.5	37.6	0.2	43.4	0.4	27.6	0.7	39.0	0.2	43.8	0.3
444	456	3	7.1	0.9	0.1	2.7	0.3	11.3	0.6	45.5	2.4	44.7	1.6	44.2	0.3
467	476	2	6	1.1	1.0	3.4	0.3	15.3	0.1	9.7	0.6	47.2	1.4	60.9	1.2
477	486	2	6.6	2.0	1.0	1.8	0.6	4.2	1.0	2.1	0.4	5.8	0.3	22.8	1.4
477	487	2	9.3	0.8	0.2	0.8	0.2	2.7	0.2	0.7	0.3	3.4	0.4	14.7	1.0
487	495	2	11	0.9	0.2	1.1	0.9	0.9	0.2	0.3	0.1	1.2	0.4	1.1	0.3
487	498	2	12	0.9	0.7	0.9	0.1	4.4	0.5	0.6	0.5	0.9	0.4	5.5	1.1
499	507	2	4.1	27.3	3.6	55.5	1.7	70.7	0.8	23.7	0.5	51.7	0.7	70.9	0.9
508	520	2	5.1	30.1	3.0	48.0	1.4	52.0	0.4	29.6	0.5	47.4	2.3	54.6	0.8
508	527	5	7.5	12.1	1.0	27.6	1.1	39.8	0.7	11.7	0.9	27.5	1.1	37.7	0.9
508	537	5	9.2	5.6	0.3	15.9	0.5	29.2	0.4	5.3	0.1	16.5	0.4	26.9	0.3
521	537	4	7.2	1.7	0.6	6.0	0.8	20.7	0.3	1.8	0.2	5.8	0.4	16.8	0.5
538	555	4	7.4	0.6	0.4	2.4	0.2	14.7	0.3	2.1	0.3	14.0	0.2	34.1	0.5
538	556	4	8.9	1.5	0.3	2.8	0.3	14.5	0.1	2.6	0.3	16.8	0.4	37.8	0.3
548	555	2	3.9	1.1	0.3	4.8	2.0	29.2	1.8	4.2	1.2	34.2	0.7	74.5	0.4
556	570	4	8	0.4	0.3	1.7	0.0	7.4	0.5	#	#	#	#	#	#
571	581	3	7.4	0.2	0.2	1.0	0.0	5.3	0.5	#	#	#	#	#	#
582	596	3	7.3	18.8	1.3	36.6	1.0	41.1	1.3	#	#	#	#	#	#
582	606	4	9.9	18.5	1.2	31.6	0.3	34.7	0.7	#	#	#	#	#	#
610	637	4	7.6	13.1	0.3	19.9	0.4	24.8	0.6	#	#	#	#	#	#
610	646	5	8.2	10.9	0.3	16.0	0.2	23.0	0.7	#	#	#	#	#	#
614	637	4	7.1	14.3	0.5	22.0	0.4	28.2	0.8	#	#	#	#	#	#
614	646	5	8.1	11.3	0.1	16.5	0.3	24.5	1.0	#	#	#	#	#	#
647	656	2	3.9	37.6	1.5	41.9	0.5	45.4	0.6	#	#	#	#	#	#
647	657	2	5.4	26.9	0.5	35.8	0.9	38.2	0.4	#	#	#	#	#	#
648	657	2	4.6	35.3	2.0	44.7	0.8	47.4	0.2	#	#	#	#	#	#
661	680	3	7.6	14.7	0.7	22.4	0.4	30.5	0.5	#	#	#	#	#	#
661	687	4	11	15.8	0.8	26.6	0.2	32.2	0.1	#	#	#	#	#	#
662	680	3	7	15.9	0.3	24.0	0.7	31.8	0.8	#	#	#	#	#	#
662	687	4	11	16.5	0.8	27.8	0.3	33.1	0.2	#	#	#	#	#	#
681	687	1	11	38.8	1.4	54.3	0.4	56.7	0.7	#	#	#	#	#	#
697	703	1	5.3	8.3	1.0	16.1	0.7	25.3	0.4	#	#	#	#	#	#
704	710	1	5.5	14.5	0.9	24.4	0.6	26.7	0.4	#	#	#	#	#	#
704	711	2	4.4	19.8	1.0	30.8	1.2	32.7	0.6	#	#	#	#	#	#
705	712	2	4.4	19.8	1.0	30.8	1.2	32.7	0.6	#	#	#	#	#	#
711	719	1	11	1.8	0.4	3.9	0.1	20.1	0.8	#	#	#	#	#	#

S	E	Z	RT
556	571	5	8.73
557	571	3	8.37

Peptides specific to p85α (Q572*)					
3	SD	30	SD	300	SD
24.6	0.4	40.8	3.0	45.0	0.0
25.2	0.5	40.7	2.9	44.9	0.1

Figure A1.6 cont.: All HDX p110α and p85α peptide data for experiments examining conformational changes in the oncogenic p85α-Q572* mutant in the basal state.

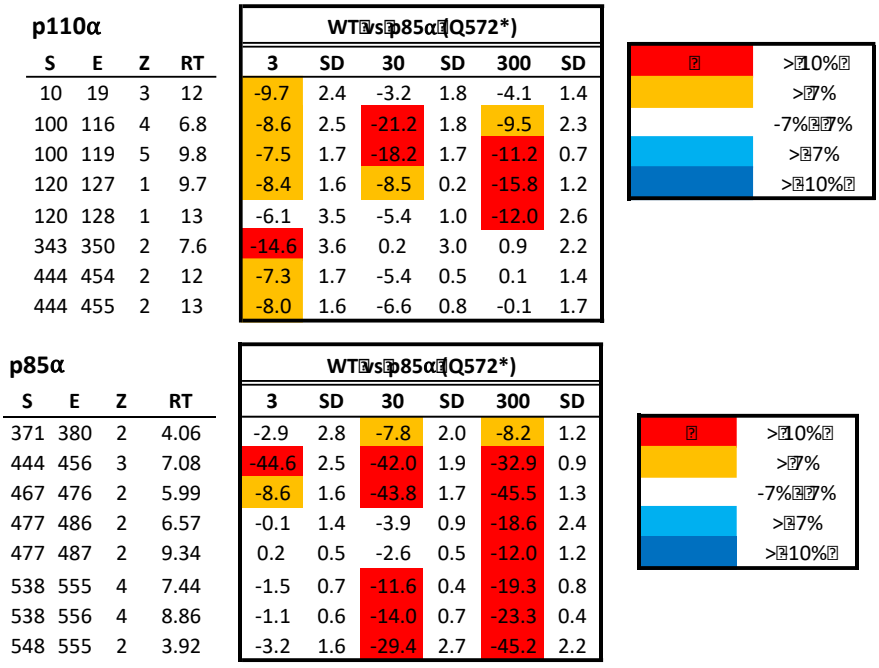

Figure 45: HDX differences in oncogenic p85α-Q572* mutant in the basal state. Differences in exchange at all time points for a selected set of peptides (some overlapping peptides have been removed, but all data can be found in Fig. 40) that undergo decreases (positive values) / increases (negative values) in exchange between WT and p85α-Q572* mutant are shown. The specific conditions being compared are labelled above the selected columns. Increases/decreases greater than 0.5 Da and 7% are coloured according to the legend.

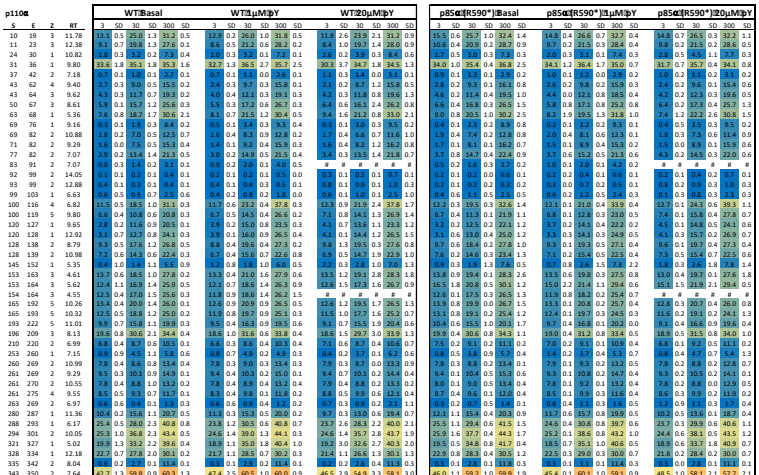

Figure 46: All HDX p110α and p85α peptide data for experiments examining conformational changes in the C-terminal p85α-iSH2 mutants in the basal, 1 uM PDGFR pY, and 20 uM PDGFR pY states.

The charge state *(Z)*, residue start *(S)*, residue end number *(E)*, and retention time *(RT)* are displayed for every peptide. Three time-points are labelled (3, 30, 300 seconds), and the relative level of HDX is coloured on a blue-to-red continuum (% deuterium incorporation).

Data listed are the average of 3 independent experiments, with SDs presented. ##No coverage for the specific peptide.

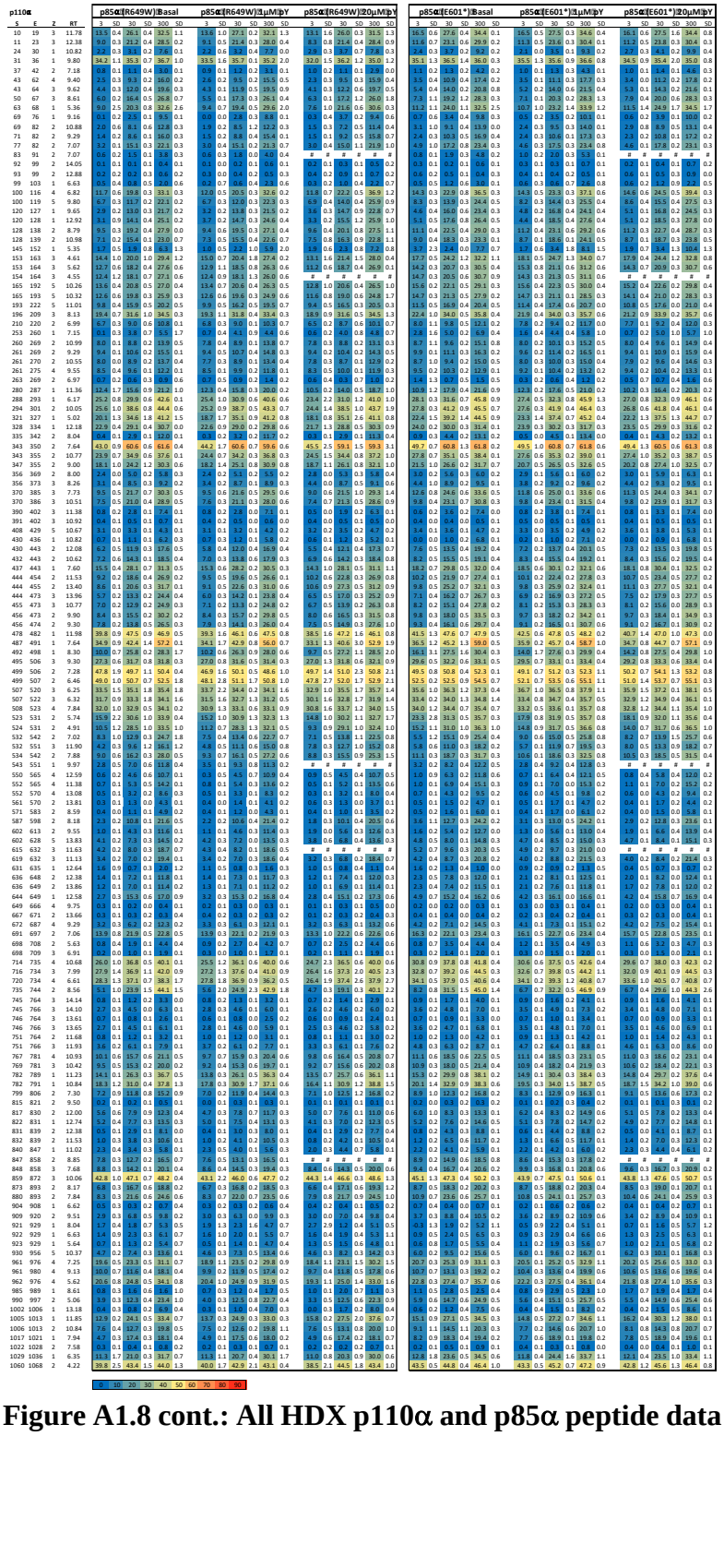

Figure A1.8 cont.: All HDX p110α and p85α peptide data for experiments examining

conformational changes in the C-terminal p85α-iSH2 mutants in the basal, 1 uM PDGFR pY, and 20 uM PDGFR pY states.

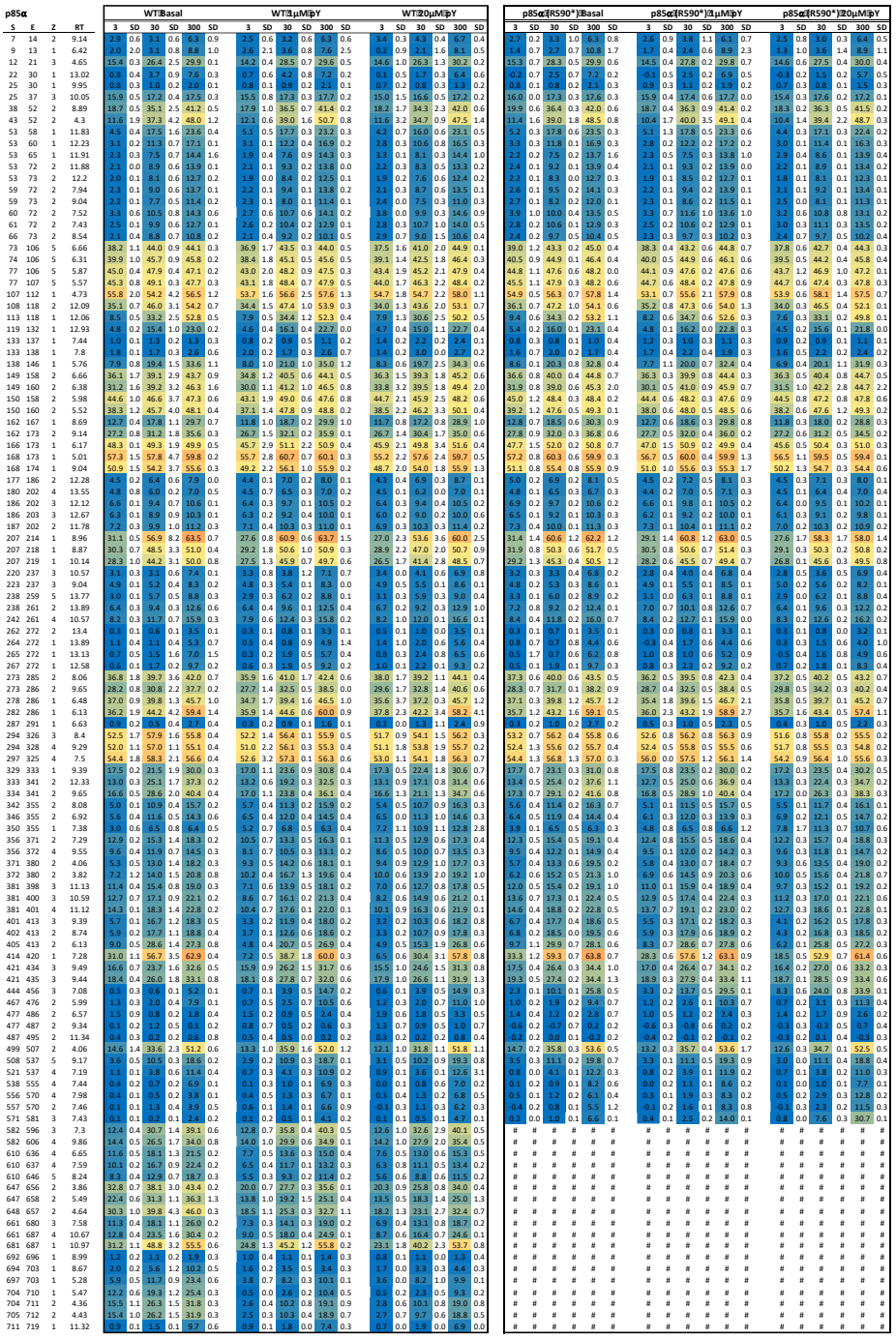

Figure A1.8 cont.: All HDX p110α and p85α peptide data for experiments examining conformational changes in the C-terminal p85α-iSH2 mutants in the basal, 1 uM PDGFR pY, and 20 uM PDGFR pY states.

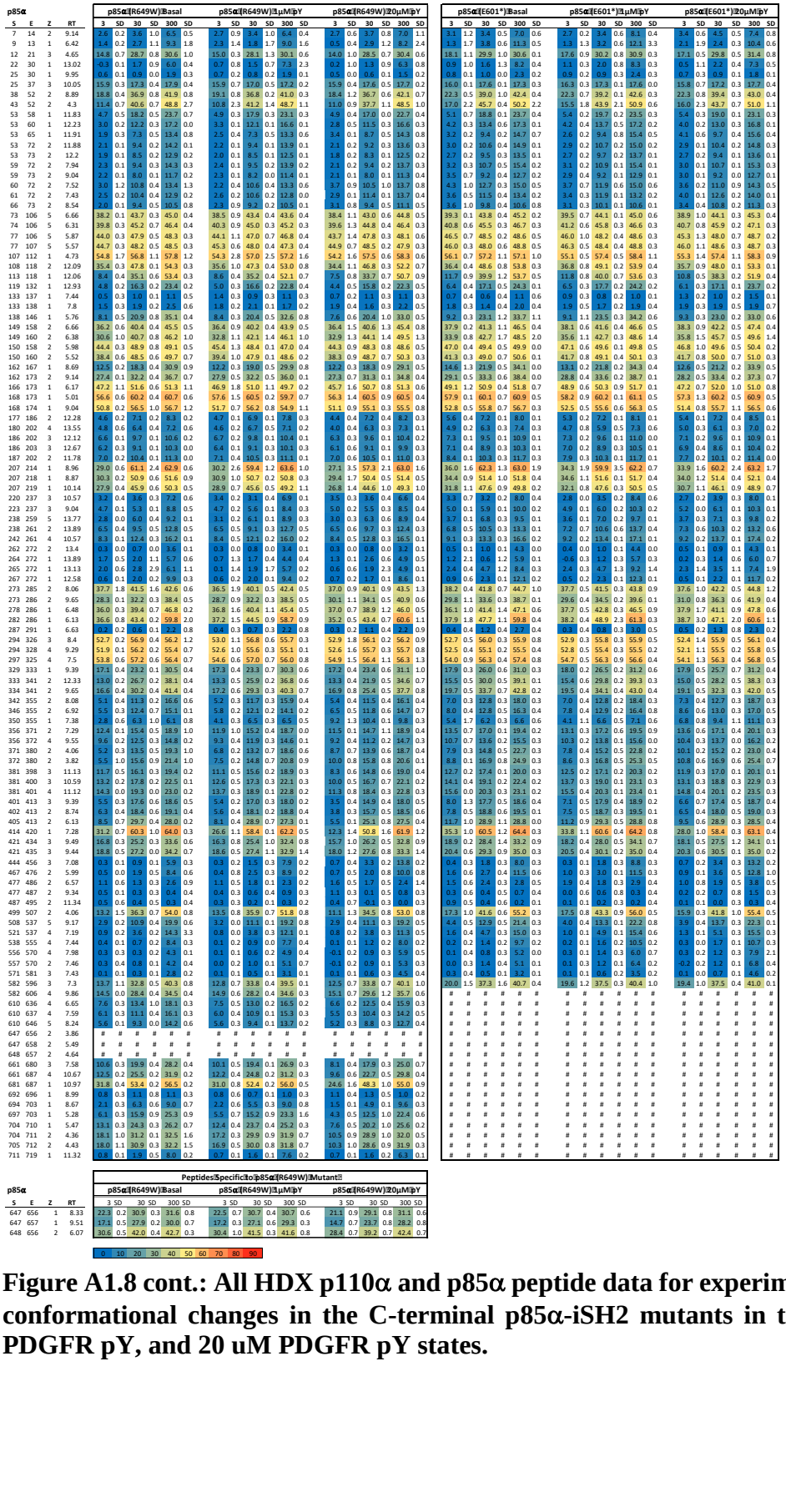

Figure A1.8 cont.: All HDX p110α and p85α peptide data for experiments examining conformational changes in the C-terminal p85α-iSH2 mutants in the basal, 1 uM PDGFR pY, and 20 uM PDGFR pY states.

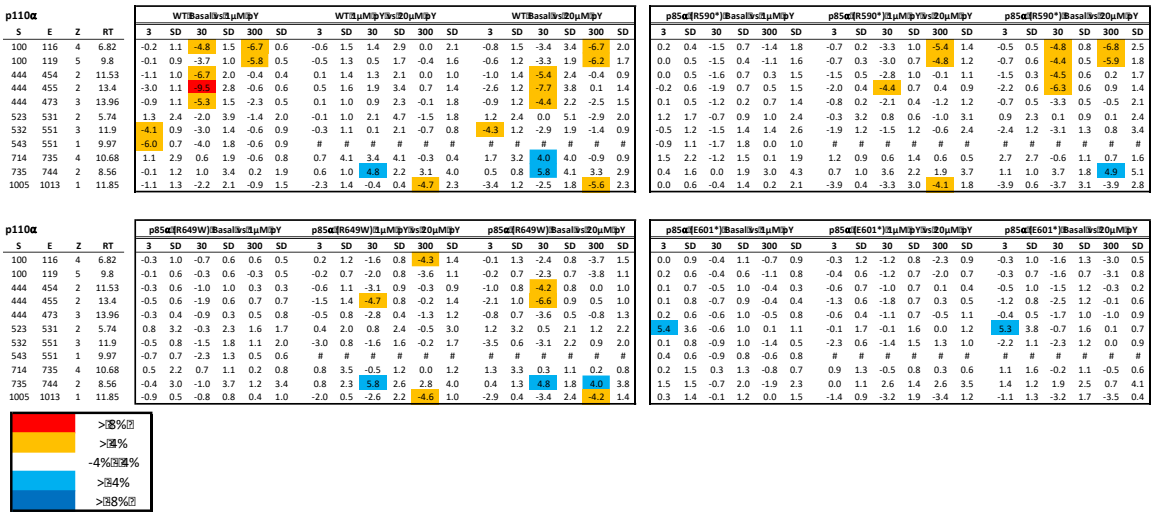

Figure 47: HDX differences in C-terminal p85α-iSH2 mutants and under different concentrations of PDGFR pY (basal or 0 uM, 1 uM, and 20 uM PDGFR pY).
Differences in exchange at all time points for a selected set of peptides (some overlapping peptides have been removed, but all data can be found in Fig. 40) that undergo decreases (positive values) / increases (negative values) in exchange between WT and p85α-Q572* mutant are shown. The specific conditions being compared are labelled above the selected columns. Increases/decreases greater than 0.5 Da and 7% are coloured according to the legend.

p85α				WT Basal vs 1 μM pY						WT 1 μM pY vs 20 μM pY						WT Basal vs 20 μM pY						p85α (R590*) Basal vs 1 μM pY						p85α (R590*) 1 μM pY vs 20 μM pY						p85α (R590*) Basal vs 20 μM pY					
S	E	Z	RT	3	SD	30	SD	300	SD	3	SD	30	SD	300	SD	3	SD	30	SD	300	SD	3	SD	30	SD	300	SD	3	SD	30	SD	300	SD	3	SD	30	SD	300	SD
297	325	4	7.5	1.8	4.9	0.9	2.1	0.3	1.0	-0.4	4.2	3.2	1.8	0.0	1.3	1.4	2.8	4.1	3.9	0.2	1.1	-1.6	1.4	-0.7	2.5	0.9	1.7	1.8	0.9	1.1	2.1	0.5	1.6	0.2	2.2	0.4	2.3	1.4	0.5
333	341	2	12.33	-0.2	0.9	5.9	2.0	4.8	0.5	0.1	1.6	2.1	1.0	1.1	0.9	-0.2	1.2	8.0	2.5	5.9	0.8	0.7	1.0	0.4	0.8	0.7	1.5	-0.7	0.8	2.6	0.9	2.2	0.6	0.0	0.8	3.0	0.5	2.9	1.3
334	341	2	9.65	-0.5	1.6	4.8	2.5	4.3	0.9	0.4	2.4	2.7	1.7	1.3	1.0	-0.1	1.8	7.5	3.3	5.7	1.1	0.4	1.1	0.2	1.2	1.2	1.2	-0.4	0.5	2.6	1.3	2.1	0.7	0.1	0.7	2.8	0.5	3.3	1.1
350	355	1	7.38	-2.2	1.3	-0.3	1.3	0.1	0.9	-1.9	1.9	-4.1	1.6	-6.5	3.2	-4.1	1.7	-4.4	1.9	-6.4	3.3	-1.0	0.9	-0.1	1.3	-0.3	1.5	-2.9	2.5	-4.8	1.5	-4.1	1.8	-3.9	1.8	-4.8	1.2	-4.4	0.8
371	380	2	4.06	-4.0	1.0	-1.2	2.1	0.1	0.4	-0.1	1.3	1.3	1.7	0.4	0.3	-4.1	1.4	0.1	2.4	0.5	0.5	-0.1	0.9	0.3	1.3	1.0	1.0	-3.5	1.0	-0.5	1.1	-0.6	1.0	-3.6	1.0	-0.2	1.0	0.4	0.5
372	380	2	3.82	-3.0	1.6	-2.7	2.9	1.2	1.3	0.2	0.9	2.8	3.3	0.4	1.5	-2.9	1.8	0.1	3.5	1.6	1.9	-0.8	1.2	0.7	1.4	1.0	1.6	-3.1	1.1	-1.1	1.3	-1.5	1.3	-3.9	1.0	-0.3	0.9	-0.5	1.7
381	398	3	11.13	4.2	0.9	1.5	1.4	1.0	0.5	0.2	1.2	1.2	1.4	0.2	0.7	4.4	0.9	2.7	1.7	1.2	0.8	1.0	0.6	-0.5	0.6	0.2	1.4	1.3	0.4	0.7	0.5	-0.3	0.6	2.3	0.8	0.3	0.3	-0.1	1.2
381	400	3	10.59	4.1	1.4	1.0	1.1	0.7	0.5	0.5	1.3	1.2	0.8	0.2	0.4	4.6	1.3	2.2	1.5	0.9	0.2	0.7	1.2	-0.1	0.4	0.0	0.8	1.7	0.8	0.4	0.5	0.2	0.9	2.4	0.9	0.3	0.2	0.2	1.1
381	401	4	11.12	3.9	0.9	0.7	1.5	0.8	0.3	0.3	1.6	1.4	0.7	0.0	0.2	4.3	1.0	2.1	2.0	0.9	0.2	0.8	1.1	-0.3	0.4	-0.2	0.7	1.0	1.0	0.5	0.2	0.2	0.3	1.9	0.7	0.3	0.3	0.0	0.6
401	413	3	9.39	2.4	0.3	4.8	1.6	0.3	0.7	0.2	0.4	1.6	1.0	-0.1	1.0	2.5	0.3	6.4	1.8	0.1	1.3	1.2	0.7	0.5	0.5	0.4	0.8	1.4	0.5	0.9	0.7	0.5	0.6	2.6	0.7	1.4	0.9	0.8	0.8
402	413	2	8.74	2.3	0.4	5.1	1.6	0.2	0.6	0.4	0.3	1.9	1.5	0.8	0.5	2.6	0.4	7.0	2.0	1.0	0.7	1.0	0.5	0.6	0.6	0.6	0.8	1.5	0.5	1.1	0.9	0.5	0.3	2.5	0.5	1.7	0.3	1.0	0.7
405	413	2	6.13	4.1	0.9	8.0	1.9	0.4	1.2	-0.1	1.0	5.3	2.4	0.1	1.0	4.1	1.0	13.3	3.3	0.5	1.4	1.4	1.7	1.3	1.4	0.2	1.2	2.0	0.7	2.8	1.2	0.6	0.9	3.4	1.1	4.1	1.1	0.9	0.9
414	420	1	7.28	23.8	1.5	18.0	5.3	2.9	0.6	0.7	1.0	8.3	4.8	2.2	1.0	24.5	1.6	26.3	6.6	5.1	1.1	5.0	1.8	1.7	1.9	0.7	1.6	9.8	1.1	4.7	1.8	1.7	1.4	14.8	1.7	6.4	1.4	2.5	1.3
444	456	3	7.08	-0.2	0.4	-3.2	0.6	-9.5	0.3	0.1	0.2	-0.1	1.0	-0.3	0.5	-0.1	0.3	-3.3	0.7	-9.7	0.5	-1.1	0.3	-3.6	0.5	-3.7	0.6	-4.9	0.7	-10.3	1.2	-4.3	0.2	-6.0	0.7	-13.9	0.9	-8.0	0.6
556	570	4	7.98	-0.1	0.6	-0.8	0.5	-2.9	0.3	0.1	0.9	0.0	0.5	-0.1	0.6	0.1	0.6	-0.7	0.4	-3.0	0.6	0.2	0.2	-0.7	0.5	-2.2	0.6	-0.2	0.3	-1.0	0.6	-4.5	0.4	0.0	0.2	-1.7	0.5	-6.7	0.6
557	570	2	7.46	-0.5	0.1	-0.1	0.5	-2.7	1.4	0.8	0.3	0.2	0.4	0.4	1.2	0.3	0.4	0.2	0.7	-2.3	0.7	-0.3	0.4	-0.8	0.3	-2.8	1.9	0.0	0.5	-0.7	0.4	-3.3	1.1	-0.3	0.5	-1.5	0.4	-6.1	1.5
571	581	3	7.43	0.0	0.3	-0.3	0.2	-1.7	0.3	0.0	0.3	0.0	0.2	-0.6	0.3	0.0	0.2	-0.3	0.2	-2.3	0.2	-0.2	0.2	-1.6	0.3	-7.3	0.3	-0.4	0.2	-5.1	0.5	-16.7	0.2	-0.6	0.1	-6.6	0.4	-24.0	0.2
582	596	3	7.3	-0.4	1.2	-5.1	1.8	-1.2	1.1	0.2	1.7	3.3	3.2	0.2	1.0	-0.2	1.4	-1.8	4.3	-1.0	1.0	#	#	#	#	#	#	#	#	#	#	#	#	#	#	#	#	#	#
610	636	4	6.65	3.9	1.0	4.4	1.6	6.5	0.6	0.1	1.0	0.6	0.9	-0.3	0.9	4.0	1.0	5.1	1.9	6.2	0.7	#	#	#	#	#	#	#	#	#	#	#	#	#	#	#	#	#	#
610	637	4	7.59	3.6	0.6	5.0	0.9	9.2	0.4	0.2	1.1	0.7	0.5	-0.2	0.5	3.8	1.0	5.6	1.3	9.0	0.4	#	#	#	#	#	#	#	#	#	#	#	#	#	#	#	#	#	#
610	646	5	8.24	2.7	0.7	3.6	0.9	7.3	0.5	0.0	0.9	0.5	0.7	-0.1	0.4	2.7	0.9	4.1	1.3	7.2	0.5	#	#	#	#	#	#	#	#	#	#	#	#	#	#	#	#	#	#
647	656	2	3.86	12.9	1.4	10.4	3.3	7.8	0.3	-0.3	1.6	1.9	1.1	1.5	0.5	12.6	1.6	12.3	3.8	9.4	0.6	#	#	#	#	#	#	#	#	#	#	#	#	#	#	#	#	#	#
647	658	2	5.49	8.6	1.6	12.1	2.5	11.2	1.7	0.3	1.5	0.9	2.8	0.1	1.7	8.9	1.1	13.0	2.4	11.3	2.5	#	#	#	#	#	#	#	#	#	#	#	#	#	#	#	#	#	#
648	657	2	4.64	11.8	2.1	14.5	4.6	13.4	1.3	0.3	2.4	2.2	3.0	0.3	1.8	12.1	2.3	16.6	7.0	13.7	1.0	#	#	#	#	#	#	#	#	#	#	#	#	#	#	#	#	#	#
661	680	3	7.58	4.0	0.7	4.0	1.4	7.0	0.4	0.3	0.7	1.0	1.1	0.3	0.4	4.3	0.8	5.0	1.9	7.3	0.4	#	#	#	#	#	#	#	#	#	#	#	#	#	#	#	#	#	#
661	687	4	10.67	3.8	0.9	5.5	2.0	5.5	0.3	0.3	1.1	1.6	1.1	0.3	0.3	4.1	1.0	7.1	2.3	5.8	0.3	#	#	#	#	#	#	#	#	#	#	#	#	#	#	#	#	#	#
681	687	1	10.97	6.4	2.4	3.6	4.4	-0.3	0.8	1.7	3.1	5.0	3.4	2.1	1.0	8.0	2.9	8.6	5.5	1.7	1.4	#	#	#	#	#	#	#	#	#	#	#	#	#	#	#	#	#	#
694	703	1	8.67	0.4	0.5	2.1	1.7	6.8	0.8	-0.1	0.3	0.2	0.9	-0.9	0.6	0.3	0.2	2.3	1.5	5.8	0.8	#	#	#	#	#	#	#	#	#	#	#	#	#	#	#	#	#	#
697	703	1	5.28	2.1	1.2	3.5	1.2	13.3	0.6	0.2	0.7	0.1	1.2	0.3	0.2	2.3	0.5	3.6	1.9	13.6	0.7	#	#	#	#	#	#	#	#	#	#	#	#	#	#	#	#	#	#
704	710	1	5.47	11.7	0.7	16.7	1.4	15.0	0.8	0.0	0.2	0.4	0.7	1.0	0.7	11.7	0.8	17.1	1.7	16.1	0.5	#	#	#	#	#	#	#	#	#	#	#	#	#	#	#	#	#	#
704	711	2	4.36	12.9	1.5	16.0	2.4	12.7	1.2	-0.3	1.0	0.2	1.7	0.1	1.7	12.7	1.7	16.2	2.4	12.7	1.1	#	#	#	#	#	#	#	#	#	#	#	#	#	#	#	#	#	#
705	712	2	4.43	12.9	1.3	15.9	2.0	13.0	1.0	-0.2	1.0	0.6	1.1	0.1	1.2	12.7	1.7	16.5	2.2	13.1	0.8	#	#	#	#	#	#	#	#	#	#	#	#	#	#	#	#	#	#

p85α				p85α (R649W) Basal vs 1 μM pY						p85α (R649W) 1 μM pY vs 20 μM pY						p85α (R649W) Basal vs 20 μM pY						p85α (E601*) Basal vs 1 μM pY						p85α (E601*) 1 μM pY vs 20 μM pY						p85α (E601*) Basal vs 20 μM pY					
S	E	Z	RT	3	SD	30	SD	300	SD	3	SD	30	SD	300	SD	3	SD	30	SD	300	SD	3	SD	30	SD	300	SD	3	SD	30	SD	300	SD	3	SD	30	SD	300	SD
297	325	4	7.5	-0.8	1.1	0.2	1.4	0.4	1.6	-0.2	2.0	0.6	1.8	-0.3	2.2	-1.1	2.0	0.8	1.7	0.1	2.1	-0.7	1.4	0.0	1.3	0.8	1.2	0.6	1.8	0.0	1.3	-0.2	0.8	-0.1	2.2	0.0	0.7	0.6	1.3
333	341	2	12.33	-0.3	0.7	0.8	0.5	1.3	1.0	0.0	1.0	3.9	0.7	2.2	1.3	-0.3	0.6	4.7	0.8	3.5	1.1	0.1	1.1	0.2	0.7	-0.2	0.4	0.4	1.1	1.6	0.7	1.0	0.6	0.5	1.0	1.8	1.0	0.8	0.4
334	341	2	9.65	-0.6	1.1	0.9	0.6	1.1	1.0	0.2	1.4	3.9	0.8	2.5	1.5	-0.3	1.2	4.8	0.9	3.6	1.1	0.2	1.0	-0.5	1.0	-0.2	0.6	0.4	1.0	1.9	0.6	1.0	0.9	0.6	1.1	1.4	0.9	0.7	0.7
350	355	1	7.38	-1.4	0.9	-0.2	1.2	-0.4	1.3	-5.0	1.7	-4.0	0.3	-3.3	0.9	-6.4	1.9	-4.2	1.0	-3.7	1.1	1.3	2.8	-0.3	0.8	-0.5	1.2	-2.7	1.9	-2.9	1.6	-4.0	0.9	-1.4	2.5	-3.2	1.4	-4.5	0.9
371	380	2	4.06	-1.7	0.5	0.2	1.2	0.6	1.6	-1.9	0.9	-0.6	1.2	-0.1	1.0	-3.6	1.0	-0.4	1.0	0.6	1.4	0.1	0.6	-0.4	1.1	-0.1	0.5	-2.4	0.6	0.0	0.8	-0.2	0.6	-2.2	0.5	-0.4	0.7	-0.3	0.7
372	380	2	3.82	-2.0	1.2	0.8	1.6	0.6	1.8	-2.6	1.1	-1.0	1.5	0.2	0.9	-4.5	1.8	-0.1	1.6	0.8	1.0	0.2	0.4	0.0	1.3	-0.4	0.8	-2.2	0.9	-0.1	1.1	-0.1	1.2	-2.0	0.7	-0.1	1.4	-0.5	1.1
381	398	3	11.13	0.6	1.0	0.6	0.4	0.5	0.5	2.8	1.2	0.7	0.8	-0.1	0.7	3.4	1.1	1.3	0.9	0.4	0.5	0.1	0.4	0.3	0.3	-0.3	0.6	0.6	0.4	0.1	0.4	0.2	0.3	0.8	0.4	0.4	0.3	0.0	0.4
381	400	3	10.59	0.7	0.7	0.5	0.5	0.4	0.4	2.5	1.1	0.7	1.0	0.0	0.5	3.2	0.8	1.2	0.9	0.4	0.3	0.4	0.7	0.2	0.4	-0.7	0.5	0.7	0.6	0.1	0.4	0.2	0.6	1.1	0.7	0.3	0.5	-0.5	0.5
381	401	4	11.12	0.6	0.3	0.4	0.1	0.2	0.3	2.4	1.1	0.5	0.3	0.0	0.4	3.0	0.9	0.9	0.3	0.2	0.4	0.1	0.4	0.1	0.5	-0.3	0.3	0.6	0.8	0.1	0.3	-0.1	0.4	0.8	0.5	0.2	0.5	-0.4	0.5
401	413	3	9.39	0.2	0.5	0.6	0.9	0.6	0.7	1.9	0.6	2.1	0.7	0.0	0.7	2.1	0.8	2.7	0.9	0.6	1.0	0.8	1.8	-0.2	0.9	-0.2	0.6	0.5	1.2	0.4	0.9	0.2	0.6	1.3	2.0	0.3	1.0	0.0	0.8
402	413	2	8.74	0.6	0.7	0.3	0.7	0.3	0.8	1.9	0.6	2.5	0.7	0.3	1.0	2.5	0.6	2.7	1.1	0.6	1.0	0.3	1.0	0.1	0.9	0.0	0.2	1.0	0.9	0.7	0.8	0.5	0.4	1.3	1.0	0.7	1.1	0.5	0.4
405	413	2	6.13	0.5	1.1	0.9	1.1	0.7	0.3	2.5	0.5	3.8	1.5	-0.1	0.5	3.0	0.8	4.6	1.2	0.5	0.6	0.6	1.9	-0.4	1.5	0.0	0.8	1.7	1.5	0.4	0.7	0.3	1.2	2.3	1.5	0.0	1.3	0.3	0.4
414	420	1	7.28	4.6	1.8	1.9	1.1	1.8	0.8	14.3	2.5	7.6	1.7	0.3	1.7	18.9	2.1	9.5	2.5	2.1	1.5	1.5	2.1	0.0	1.6	0.2	1.1	5.8	2.2	2.2	0.7	1.1	1.1	7.3	2.0	2.1	1.5	1.3	0.7
444	456	3	7.08	0.0	0.4	-0.5	0.3	-2.0	0.5	-0.4	0.6	-1.8	0.4	-5.9	0.4	-0.4	0.6	-2.3	0.3	-7.9	0.5	0.1	0.4	0.1	0.6	-0.8	0.6	-0.4	0.2	-1.7	0.6	-4.3	0.5	-0.3	0.5	-1.6	0.6	-5.1	0.5
556	570	4	7.98	0.2	0.4	-0.3	0.4	-0.6	0.5	0.2	0.3	-0.3	0.5	-1.0	0.9	0.4	0.4	-0.6	0.5	-1.6	0.5	-0.2	0.5	-0.6	0.6	-0.9	0.8	0.0	0.4	0.1	0.6	-1.9	2.9	-0.2	0.7	-0.4	0.5	-2.8	2.2
557	570	2	7.46	0.3	0.6	-0.2	0.2	-0.9	1.2	0.2	0.4	0.0	0.3	-0.2	1.1	0.4	0.6	-0.1	0.2	-1.1	0.7	-0.1	0.6	0.1	0.5	-1.4	0.4	0.2	0.4	0.1	0.2	-0.4	0.7	0.1	0.4	0.2	0.5	-1.8	0.5
571	581	3	7.43	0.0	0.1	-0.2	0.2	-0.3	0.3	0.0	0.2	-0.1	0.3	-1.5	0.5	0.0	0.1	-0.3	0.4	-1.8	0.5	0.2	0.5	-0.1	0.2	-0.3	0.3	0.0	0.2	-0.1	0.3	-1.1	0.4	0.2	0.4	-0.2	0.1	-1.4	0.4
582	596	3	7.3	0.9	1.9	-1.0	0.9	0.8	0.9	0.3	1.4	0.0	1.1	-0.6	1.1	1.2	1.8	-1.0	1.3	0.2	1.8	0.4	2.7	-0.2	1.9	0.4	1.4	0.1	2.2	0.0	0.7	-0.7	1.1	0.6	2.5	-0.2	2.0	-0.3	0.5
610	636	4	6.65	0.0	0.8	0.4	1.2	1.6	0.5	0.9	0.7	0.5	0.6	0.6	0.5	0.9	0.5	0.9	1.4	2.2	0.6	#	#	#	#	#	#	#	#	#	#	#	#	#	#	#	#	#	#
610	637	4	7.59	0.0	0.6	0.2	0.4	0.8	0.6	0.6	0.7	0.5	0.4	1.1	0.7	0.6	0.6	0.7	0.7	1.9	0.8	#	#	#	#	#	#	#	#	#	#	#	#	#	#	#	#	#	#
610	646	5	8.24	0.0	0.4	0.0	0.1	0.5	0.8	0.4	0.6	0.5	0.4	1.0	0.6	0.5	0.5	0.5	0.3	1.5	1.0	#	#	#	#	#	#	#	#	#	#	#	#	#	#	#	#	#	#
647	656	2	3.86	#	#	#	#	#	#	#	#	#	#	#	#	#	#	#	#	#	#	#	#	#	#	#	#	#	#	#	#	#	#	#	#	#	#	#	#
647	658	2	5.49	#	#	#	#	#	#	#	#	#	#	#	#	#	#	#	#	#	#	#	#	#	#	#	#	#	#	#	#	#	#	#	#	#	#	#	#
648	657	2	4.64	#	#	#	#	#	#	#	#	#	#	#	#	#	#	#	#	#	#	#	#	#	#	#	#	#	#	#	#	#	#	#	#	#	#	#	#
661	680	3	7.58	0.4	0.8	0.5	0.5	1.3	0.7	2.0	0.9	1.6	0.5	2.0	1.0	2.5	0.7	2.0	0.7	3.2	1.1	#	#	#	#	#	#	#	#	#	#	#	#	#	#	#	#	#	#
661	687	4	10.67	0.3	0.5	0.7	0.4	0.7	0.5	2.6	1.0	2.1	0.7	1.4	0.7	2.9	0.8	2.8	0.6	2.0	0.5	#	#	#	#	#	#	#	#	#	#	#	#	#	#	#	#	#	#
681	687	1	10.97	0.8	1.2	1.0	0.4	0.6	0.6	6.4	2.4	4.1	1.2	1.0	1.4	7.2	2.0	5.2	1.2	1.5	1.1	#	#	#	#	#	#	#	#	#	#	#	#	#	#	#	#	#	#
694	703	1	8.67	-0.1	0.9	0.8	1.0	0.0	1.5	0.6	0.7	0.5	0.4	-0.6	1.1	0.5	0.4	1.3	0.7	-0.6	0.9	#	#	#	#	#	#	#	#	#	#	#	#	#	#	#	#	#	#
697	703	1	5.28	0.6	1.0	0.8	1.8	2.0	2.5	1.2	1.2	2.7	1.9	0.9	2.2	1.8	0.9	3.5	1.9	2.9	1.5	#	#	#	#	#	#	#	#	#	#	#	#	#	#	#	#	#	#
704	710	1	5.47	0.7	0.6	0.6	0.7	1.0	1.0	4.8	0.8	3.5	1.4	-0.4	0.5	5.5	0.7	4.1	1.2	0.6	1.0	#	#	#	#	#	#	#	#	#	#	#	#	#	#	#	#	#	#
704	711	2	4.36	0.9	1.3	1.3	1.1	0.6	2.3	6.7	1.2	1.0	1.9	-0.1	1.2	7.5	1.9	2.3	1.1	0.5	2.0	#	#	#	#	#	#	#	#	#	#	#	#	#	#	#	#	#	#
705	712	2	4.43	1.2	1.6	0.8	1.1	0.3	2.2	6.6	1.5	1.4	1.7	0.0	1.0	7.8	2.1	2.2	1.1	0.3	1.8	#	#	#	#	#	#	#	#	#	#	#	#	#	#	#	#	#	#

Figure A1.9 cont.: HDX differences in C-terminal p85α-iSH2 mutants and under different concentrations of PDGFR pY (basal or 0 uM, 1 uM, and 20 uM PDGFR pY).

A.2 Supplementary Tables

Table 1: Mutations in PIK3CD, PIK3R1, PIK3R2, and PIK3CA that lead to APDS, SHORT, Agammaglobulinemia, and Overgrowth syndromes.

PIK3CD				
Mutation Residue	**Disease**	**Inheritance**	**Mutation**	**Paper**
81	APDS 1	Dominant	E81K	Takeda et al., 2017; Heurtier et al., 2017
124	APDS 1	Dominant	G124D	Takeda et al., 2017; Heurtier et al., 2018; Edwards et al., 2019
334	APDS 1	Dominant	N334K	Dulau Florea et al., 2017; Lucas et al., 2014a; Edwards et al., 2019
405	APDS 1	Dominant	R405C	Rae et al., 2017
416	APDS 1	Dominant	C416R	Crank et al., 2014
525	APDS 1	Dominant	E525A	Tsujita et al., 2016
525	APDS 1	Dominant	E525K	Coulter et al., 2017; Dulau Florea et al., 2017; Lucas et al., 2014a; Teranishi et al., 2017; Tsujita et al., 2016; Edwards et al., 2019
929	APDS 1	Dominant	R929C	Wentink et al., 2017
1021	APDS 1	Dominant	E1021K	Angulo et al., 2013; Coulter et al., 2017; Crank et al., 2014; Dulau Florea et al., 2017; Hartman et al., 2016; Elgizouli et al., 2016; Liu et al., 2016; Lucas et al., 2014a; Pham & Cunningham-Rundles 2018; Saettini et al., 2017; Tang et al., 2017; Tsujita et al., 2016; Wentink et al., 2017; Edwards et al., 2019
1025	APDS 1	Dominant	E1025G	Dulau Florea et al., 2017
1025	APDS 1	Dominant	E1025K	Edwards et al., 2019
PIK3R1				
Mutation Residue	**Disease**	**Inheritance**	**Mutation**	**Paper**
298	Agammaglobulinemia	Recessive	W298*	Conley et al., 2012
301	Agammaglobulinemia	Recessive	R301*	Tang et al., 2017
434-475	APDS 2	Dominant	del 434-475	Deau et al., 2015; Hauck et al., 2017; Kuhlen et al., 2016; Lucas et al., 2014b; Petrovski et al., 2016; Sugiyama et al., 2017; Wentink et al., 2017
434-475	APDS 2-SHORT	Dominant	del 434-475	Bravo Garcia-Morato et al., 2017; Petrovski et al., 2016; Sugiyama et al., 2017
489	SHORT	Dominant	E489K	Thauvin-Robinet et al., 2013
564	APDS 2	Dominant	N564K	Wentink et al., 2017
631	SHORT	Dominant	R631Q	Thauvin-Robinet et al., 2013
636-653*	SHORT	Dominant	653* (N636Tfs*18)	Dyment et al., 2013
643-651*	SHORT	Dominant	651* (D643Dfs*8)	Barcena et al., 2014
649	SHORT	Dominant	R649W	Bárcena et al., 2014; Chudasama et al., 2013; Dyment et al., 2013; Huang-Doran et al., 2016; Klatka et al., 2017; Schroeder et al., 2014; Thauvin-Robinet et al., 2013
539	SHORT	Dominant	I539del	Thauvin-Robinet et al., 2013
653	SHORT	Dominant	K653*	Klatka et al., 2017
657	SHORT	Dominant	Y657*	Dyment et al., 2013; Huang-Doran et al., 2016

PROS = PIK3CA Related Overgrowth Syndromes; Dominant = refers to the expected inheritance. Mutations also occur *de novo*. # = mixture of possible inheritance. Mutations are either *de novo* germline, postzygotic somatic mosaic, or inherited from a parent with germline mosaic mutation; * = nonsense mutation; del = deletion of nucleotides composing stated residue; G106_R108delinsI = deletion of 8 nucleotides, insertion of 2 nucleotides resulting in the loss of three amino acid residues in exchange for one (106GNR->106I)

Table A2.1 cont.: Mutations in PIK3CD, PIK3R1, PIK3R2, and PIK3CA that lead to APDS, SHORT, Agammaglobulinemia, and Overgrowth syndromes.

PIK3R2				
Mutation Residue	**Disease**	**Inheritance**	**Mutation**	**Paper**
373	Overgrowth Syndrome	#	G373R	Mirzaa et al., 2015; Rivière et al., 2012
376	Overgrowth Syndrome	#	L376G	Mirzaa et al., 2015
401	Overgrowth Syndrome	*De novo*	L401P	Nakamura et al., 2013
557	Overgrowth Syndrome	*De novo*	D557H	Terrone et al., 2016
PIK3CA				
Mutation Residue	**Disease**	**Inheritance**	**Mutation**	**Paper**
81	Overgrowth Syndrome	#	E81K	Kuentz et al., 2017; Rivière et al., 2012
88	Overgrowth Syndrome	#	R88Q	Rivière et al., 2012
104	Overgrowth Syndrome	#	P104L	Kuentz et al., 2017
106	Overgrowth Syndrome	#	G106V	Kuentz et al., 2017
106,108	Overgrowth Syndrome	#	G106_R108Idelins	Kuentz et al., 2017
110	Overgrowth Syndrome	#	E110del	Kuentz et al., 2017
115	Overgrowth Syndrome	#	R115P	Kuentz et al., 2017
118	Overgrowth Syndrome	#	G118D	Kuentz et al., 2017
364	Overgrowth Syndrome	#	R364R	Kuentz et al., 2017; Rivière et al., 2012
365	Overgrowth Syndrome	#	E365K	Kuentz et al., 2017; Rivière et al., 2012
378	Overgrowth Syndrome	#	C378Y	Kuentz et al., 2017; Rivière et al., 2012
418	Overgrowth Syndrome	#	E418K	Kuentz et al., 2017
420	Overgrowth Syndrome	#	C420R	Kuentz et al., 2017
449	Overgrowth Syndrome	#	P449T	Kuentz et al., 2017
452	Overgrowth Syndrome	#	E453K	Kuentz et al., 2017
453	Overgrowth Syndrome	#	E453del	Rivière et al., 2012
471	Overgrowth Syndrome	#	P471L	Kuentz et al., 2017
542	Overgrowth Syndrome	#	E542K	Kuentz et al., 2017
542	Overgrowth Syndrome	#	E542G	Kuentz et al., 2017
544	Overgrowth Syndrome	#	T544N	Jansen et al., 2015;
545	Overgrowth Syndrome	#	E545K	Kuentz et al., 2017; Rivière et al., 2012
546	Overgrowth Syndrome	#	E546K	Kuentz et al., 2017
546	Overgrowth Syndrome	#	E546R	Kuentz et al., 2017
546	Overgrowth Syndrome	#	E546H	Kuentz et al., 2017
726	Overgrowth Syndrome	#	E726K	Kuentz et al., 2017; Rivière et al., 2012
901	Overgrowth Syndrome	#	C901F	Kuentz et al., 2017
909	Overgrowth Syndrome	#	F909L	Kuentz et al., 2017
914	Overgrowth Syndrome	#	G914A	Kuentz et al., 2017
914	Overgrowth Syndrome	#	G914R	Kuentz et al., 2017; Rivière et al., 2012
1021	Overgrowth Syndrome	#	Y1021C	Kuentz et al., 2017; Rivière et al., 2012
1021	Overgrowth Syndrome	#	Y1021H	Kuentz et al., 2017
1025	Overgrowth Syndrome	#	T1025N	Kuentz et al., 2017
1025	Overgrowth Syndrome	#	T1025A	Rivière et al., 2012
1035	Overgrowth Syndrome	#	A1035V	Kuentz et al., 2017; Rivière et al., 2012
1043	Overgrowth Syndrome	#	M1043I	Kuentz et al., 2017; Rivière et al., 2012
1043	Overgrowth Syndrome	#	M1043V	Kuentz et al., 2017
1044	Overgrowth Syndrome	#	N1044K	Kuentz et al., 2017
1047	Overgrowth Syndrome	#	H1047L	Lindhurst et al., 2012
1047	Overgrowth Syndrome	#	H1047Q	Kuentz et al., 2017
1047	Overgrowth Syndrome	#	H1047R	Lindhurst et al., 2012
1047	Overgrowth Syndrome	#	H1047Y	Kuentz et al., 2017; Rivière et al., 2012
1049	Overgrowth Syndrome	#	G1049S	Rivière et al., 2012
1050	Overgrowth Syndrome	#	G1050S	Kuentz et al., 2017

PROS = PIK3CA Related Overgrowth Syndromes; Dominant = refers to the expected inheritance. Mutations also occur *de novo*. # = mixture of possible inheritance. Mutations are either *de novo* germline, postzygotic somatic mosaic, or inherited from a parent with germline mosaic mutation; * = nonsense mutation; del = deletion of nucleotides composing stated residue; G106_R108delinsI = deletion of 8 nucleotides, insertion of 2 nucleotides resulting in the loss of three amino acid residues in exchange for one (106GNR->106I)

A.3 Copyright Permissions

For manuscripts adapted in this dissertation:

(A) **Dornan, G.L.,** & Burke, J.E. (2018). Molecular Mechanisms of Human Disease Mediated by Oncogenic and Primary Immunodeficiency Mutations in Class IA Phosphoinositide 3-Kinases. Front. Immunol. 9. *575*.

-Open access journal (no permission required)

(B) **Dornan, G.L.,** Siempelkamp, B.D., Jenkins, M.L., Vadas, O., Lucas, C.L., & Burke, J.E. (2017). Conformational disruption of PI3Kδ regulation by immunodeficiency mutations in PIK3CD and PIK3R1. *Proc Natl Acad Sci*. 114: 1982–1987.

- No permission required from PNAS. From their website (https://www.pnas.org/page/about/rights-permissions) it clearly states that "authors need not obtain permission for the following cases:

1. to use their original figures or tables in their future works;
2. to make copies of their articles for their own personal use, including classroom use, or for the personal use of colleagues, provided those copies are not for sale and are not distributed in a systematic way;
3. to include their articles as part of their dissertations; or
4. to use all or part of their articles in printed compilations of their own works. The full journal reference must be cited and, for articles published in volumes 90–105 (1993–2008), "Copyright (copyright year) National Academy of Sciences."

(C) Vadas, O., Jenkins, M.L., **Dornan, G.L.**, & Burke, J.E. (2017). Chapter Seven - Using Hydrogen–Deuterium Exchange Mass Spectrometry to Examine Protein–Membrane Interactions. Methods Enzymol. M.H. Gelb, ed. (Academic Press), pp. 143–172.

- From Elseviers website (https://www.elsevier.com/about/policies/copyright/permissions) on copyright permissions: "Authors can include their articles in full or in part in a thesis or dissertation for non-commercial purposes."

(D) Takeda, A.J., Zhang, Y., **Dornan, G.L.**, Siempelkamp, B.D., Jenkins, M.L., Matthews, H.F., McElwee, J.J., Bi, W., Seeborg, F.O., Su, H.C., Burke, J.E., & Lucas, C.L. (2017). Novel PIK3CD mutations affecting N-terminal residues of p110δ cause activated PI3Kδ syndrome (APDS) in humans. J Allergy Clin Immunol. 140: 1152-1156.

- From Elsevier website (https://www.elsevier.com/about/policies/copyright/permissions) on copyright permissions: “Authors can include their articles in full or in part in a thesis or dissertation for non-commercial purposes.”